Strategies to inhibit O -methylguanine-DNA-methyltransferase (MGMT) for combination chemotherapy of temozolomide-resistant gliomas

Jaime Franco Pinto

Thèse de doctorat

NNT : 2021UPASF052

université PARIS-SACLAY

Strategies to inhibit O^6-methylguanine-DNA-methyltransferase (MGMT) for combination chemotherapy of temozolomide-resistant gliomas

Stratégies d'inhibition de la O^6-méthylguanine-ADN-méthyltransférase (MGMT) pour la chimiothérapie combinée des gliomes résistants au témozolomide

Thèse de doctorat de l'université Paris-Saclay

École doctorale n° 571 : molécules, matériaux, instrumentation et biosystèmes (2MIB)
Spécialité de doctorat : Chimie
Graduate School : Chimie. Référent : Faculté des sciences d'Orsay

Thèse préparée dans l'unité de recherche **Chimie et modélisation pour la biologie du cancer (Université Paris-Saclay, CNRS, Inserm)**, sous la direction de **Anton GRANZHAN**, Chargé de recherche et la co-direction de **Sophie BOMBARD**, Directrice de recherche.

Thèse soutenue à Paris-Saclay, le 15 Décembre 2021, par

Jaime FRANCO PINTO

Composition du Jury

Boris VAUZEILLES Directeur de recherche, CNRS, UPR2301, Université Paris Saclay	Président
Jean-François CONSTANT Chargé de recherche (HDR), CNRS, UMR5250,Université Grenoble Alpes	Rapporteur & Examinateur
Marcel HOLLENSTEIN Chargé de Recherche (HDR), Institut Pasteur, UMR3523, Institut Pasteur	Rapporteur & Examinateur
Paola ARIMONDO Directrice de recherche, CNRS, UMR3523, Institut Pasteur	Examinatrice
Anton GRANZHAN Chargé de recherche, CNRS, UMR9187, Institut Curie	Directeur de thèse

université PARIS-SACLAY

ÉCOLE DOCTORALE
Sciences Chimiques : Molécules, Matériaux, Instrumentation et Biosystèmes (2MIB)

Titre : Stratégies d'inhibition de la O^6-méthylguanine-ADN-méthyltransférase (MGMT) pour la chimiothérapie combinée des gliomes résistants au témozolomide

Mots clés : Glioblastome, résistance, témozolomide, méthyltransférase, inhibiteurs

Résumé : Le gliome est un nom d'un vaste groupe de cancers primitifs du système nerveux central (SNC). Ce type des cancers du cerveau est une tumeur très maligne et invasive, qui se caractérise par un très mauvais pronostic et une espérance de vie très courte. Aucun remède n'a été trouvé jusqu'à présent, et le traitement palliatif consiste en une approche multimodale qui comprend la chirurgie, la radiothérapie et la chimiothérapie avec le Temozolomide (TMZ). Le TMZ est un promédicament qui libère un cation diazométhyle alkylant les bases nucléiques de l'ADN, notamment en position O^6 de la guanine en produisant l'adduit O6-méthylguanine (O^6MeG). La formation d'O6MeG conduit à la mort cellulaire suite à l'échec de la réparation de l'ADN. Cependant, plus de 50% des patients montrent une réfractivité envers ce médicament en raison de la surexpression de la O6-méthylguanine-ADN-méthyltransférase (MGMT), une enzyme suicide qui élimine le groupement méthyle de la O^6MeG en restaurant la guanine.

Dans le cadre de cette thèse, nous avons exploré trois stratégies originales pour surmonter la chimiorésistance MGMT-dépendante, afin d'augmenter l'efficacité du TMZ. La première stratégie consistait à développer des ligands pouvant interagir avec les résidus O^6MeG dans l'ADN par des liaisons hydrogènes, en masquant ainsi ces derniers de l'action de la MGMT. Ici, la capacité de 11 nouveaux composés (ainsi que 18 autres molécules synthétisées précédemment) à stabiliser les duplexes de l'ADN contenant les résidus d'O^6MeG a été évaluée in vitro, ainsi que leur cytotoxicité intrinsèque ou en combinaison avec le TMZ, dans la lignée cellulaire multirésistante T98G. Cependant, aucun des composés n'était capable de stabiliser sélectivement l'ADN contenant la O^6MeG, ni de générer de cytotoxicité (seul ou en combinaison avec la TMZ) dans cette lignée, cette stratégie a donc été abandonnée.

La seconde stratégie était basée sur les molécules hybrides comportant une unité interagissant avec l'ADN (l'acridine) liée à un inhibiteur bien connu de la MGMT, O^6-benzylguanine (O^6BG), dans le but d'obtenir des composés qui interagissent avec l'ADN et inhibent également la MGMT. Deux séries d'hybrides de trois composés chaque ont été obtenues, en variant le site d'attache (N^9 de la guanine vs. le groupement benzyle) et la longueur et la nature chimique du linker. Il a été démontré que tous les hybrides interagissent avec l'ADN double-brin, quoique sans l'intercalation du résidu de l'acridine, et inhibent la MGMT irréversiblement in vitro avec une efficacité variable mais comparable à celle de la O^6BG. Parmi ces composés, deux hybrides N^9-conjugués ont montré one cytotoxicité synergique en combinaison avec les doses sous-toxiques du TMZ. L'un des composés a été démontré à inactiver la MGMT cellulaire ; toutefois, contrairement au O^6BG, ce composé ne produit pas de dommage à l'ADN ni seul ni en combinaison avec la O^6BG, selon les résultats d'immunomarquage γH2AX. Enfin, il a été démontré que ce composé induit l'apoptose dans les cellules, non pas en générant des cassures d'ADN double-brin mais en activant les caspases 3 et 7.

La troisième approche consistait à synthétiser un inhibiteur de MGMT photo-activable, notamment le derivé de la O^6BG portant un groupement photo-clivable qui, suite à l' irradiation, pourrait libérer l'inhibiteur de MGMT actif. Malheureusement, le derivé portant le groupement photo-clivable s'est avéré plus cytotoxique que la O^6BG même, cette stratégie a donc été abandonnée

Title : Strategies to inhibit O^6-methylguanine-DNA-methyltransferase (MGMT) for combination chemotherapy of temozolomide-resistant gliomas

Keywords : Glioblastoma, resistance, temozolomide, methyltransferase, inhibitors

Abstract : Glioma is the term coined for describing a vast group of primary cancers in the Central Nervous System (CNS), whitin this group, we can find glioblastoma or glioblastoma multiforme (GBM) as the source of 60% of brain cancer in adults, having a peak in patients between 55 and 60 years. This type of brain cancer is a highly malignant and invasive tumor (Grade IV), that is characterized by a very poor prognosis, a very short life expectancy. In clinics, no cure has been found so far, and the first line palliative treatment consists on a multimodal approach that contains surgery, radiotherapy and chemotherapy with the drug Temozolomide (TMZ).

TMZ, is a prodrug that releases a methyl cation that alkylates DNA nucleobases, specially in the position O^6 of the guanine creating the O^6methylguanine adduct (O^6MeG). The formation of O^6MeG leads to the cell death by generating a plethora of effects related with cell replication. However, more than 50% of the patients show a refractivity towards this drug because they over express O^6-methylguanine-DNA-methyltransferase (MGMT) enzyme, which is a suicide enzyme that removes the methyl group from O^6MeG restoring the original guanine.

In the context of this Thesis, we developed three different strategies to overcome this MGMT resistance by inhibiting the action of this enzyme to increase TMZ's action. The first strategy consisted on the development of small ligands that could interact with O^6MeG by hydrogen bonds, therefore masking the latter from MGMT action. Here, the capacity of stabilization of DNA surrogates containing O^6MeG of eleven novel compounds plus another previously eighteen synthesized molecules was evaluated *in vitro* as well their cytotoxicity alone or in combination with TMZ in the multidrug resistant cell line T98G. Unfortunately for this strategy, none of the compounds was able to selectively discriminate O^6MeG containing DNA nor to generate cytotoxicity (alone or in combination) in T98G cell lines therefore this strategy was abandoned.

The second strategy was based on the synthesis of hybrid molecules containing a DNA interacting scaffold (acridine) and a well-known MGMT inhibitor (O^6-benzylguanine, O^6BG). The synthesis of these molecules aimed to generate compounds that interact with DNA and also inhibit MGMT. The purpose of choosing the acridine core was sustained by the fact that the scaffold showed interesting biological properties in cancerous cells that for example increase the pro-apoptotic cascade. Here, we demonstrate one molecule was able to interact with DNA, inhibit MGMT *in vitro* and in cellulo, to be active in T98G cells alone (GI_{50} = 1.1 µM) and synergic when combined with TMZ. Finally, it was demonstrated that this compound created apoptosis in cells, not by generating double strand DNA breaks (DSB) but by enhancing caspases 3 and 7.

The third approach was to synthesize caged (unactive and less toxic) MGMT inhibitor (O^6BG) which, upon irradiation with light, could release the uncaged or active MGMT inhibitor in a controlled way. Unfortunatelly, the construction of this caged inhibitor turned out to be more toxic *in cellulo* than the parental contro O^6BG therefore the strategy was discarded.

Acknowledgments

To be honest I cant't do this. Not because I don't know what to say, but actually because I don't know how or where to start. Frankly, if both me and you manage to reach the bottom of this page, we should congratulate ourselves. Either because I managed to write something sufficiently long enough to fill this void or because you were patient enough to "tolerate" what I am trying to achieve here. To start with, I would like to say that life is, almost by definition, a whirlwind of (dis)organized thoughts, ideas and feelings. Mine, by practical extension, is not alien to this definition. The issue within me, myself and I has always reside in the fact that I (we if you consider the three of us) have been always searching for what I should search for and in me. Having doubts, questioning things, researching and trying to satisfy my curiosity have always seemed normal to me, since I believe these are the things that move someone forward. And in this quest, I came here to France trying to better understand where I should look at.

As an answer, or more actually as an acknowledgment to this, is why Anton and Sophie should receive the initial words. First, because they allow me to satisfy my curiosity regarding research in such an interesting topic. From them, I learned a lot of things related to science (just wait a little bit more, I'll tell you in a few pages) and I want to state that I have always been supported by them. Second, and most important, because they gave me the opportunity to live abroad and this has been so far one of my best experiences in my life. Therefore: GRACIAS.

Not less important, I want to take the chance to thank the whole UMR9187/U1196 unit. Since I am afraid to forget somebody, I won't write all your names. I just wanted to say that if you think I should have mentioned you, you're probably right…you're part of this as well…thanks…for everything.

Those that for sure I will mention belong to my "parisian" family. First, because they are less to name and is easier to remember them, and second…because it is less likely for them to read this so if I forget someone no one will get offended. They won't notice it... So: Dani, Paula, Javi, Pato, Lautaro, Gonzalo, Gaston, Anita, Charline, Chino, Xavi, Gonçalo, Claudia, Deep and Charlotte; thanks a lot for being my daily support during this time. In addition to the heart-chosen family, I would like to thanks my Uruguayan friends. Guys we will meet soon to eat tons of "asado", say the same stupid and immature things as usual, watch as many football matches as possible (we need to admit we can't run anymore so I will avoid the phrase "play some football matches") and maybe, but just maybe…we will share some beers together.

Y finalmente dejando lo mas importante para lo último, y de corazón se los digo, Papá, mamá, Javi, Joaquín, abuela Mary y tata Cacho: no sé qué hubiera hecho sin su apoyo, muchas gracias por estar siempre del lado correcto del mostrador. Los quiero hasta el cielo, ida y vuelta… pasando por el Yi.

This project has received funding from the European Union's Horizon 2020 research and Innovation programme under the Marie Sklodowska-Curie Grant Agreement No 666003

“No te olvidés del pago
si te vas pa’ la ciudad
cuanti más lejos te vayas
más te tenés que acordar.
Cierto que hay muchas cosas
que se pueden olvidar,
pero algunas son olvido y otras son cosas nomas”

Pal que se va

Alfredo Zitarrosa

Contents

List of abreviations

A	Adenine
AAG	Alkyladenine glycosilase
ACNU	Nimustine
ADP	Adenosine diphosphate
AP	Apurininc apyrimidinic site
APE1	Apurininc apyrimidinic endonuclease 1
ATP	Adenosine triphosphate
ATR	Ataxia telangiectasia and Rad3-related protein
BAIB	Bis-acetoxy iodobenzuene
BBB	Blood-brain barrier
BCNU	Carmustine
BER	Base excision repair system
Boc	tert-Butyloxycarbonyl
Bsp119I	Restriction enzyme Bsp119I
C	Cytosine
CCNU	Lomustine
CI	Combination index
CNS	Central nervous system
CT DNA	Calf-thymus DNA
DCM	Dichloromethane
DIPEA	Di-isopropyl ethyl amine
DM	Muscular distrophy
DMF	Dimethyl formamide
DMNB	Dimethoxy nitrobenzyl
DMSO	Dimethyl sulfoxide
DNA	Desoxyribonucleic acid
ds	Double strand
DSB	Double strand break
EDCI	1-Ethyl-3-(3-dimethylaminopropyl)carbodiimide
EGFR	Epithelial growth receptor factor
ER	Rethiculum endoplasmatic
EtOH	Ethanol
FAM	5-Carboxyfluorescein
FRET	Forster resonance energy transfer
G	Guanine
GBM	Glioblastoma multiforme
GI_{50}	Growth inhibition 50%
GSC	Glioblastoma stem cell
Gy	Gray
HBTU	2-(1H-benzotriazol-1-yl)-1,1,3,3-tetramethyluronium hexafluorophosphate
HDMS	Hexamethyl disilazane
HMBC	Heteronuclear Multiple Bond Coherence
HOBt	Hydroxybenzo triazol
HR	Homologous recombination

ICL	Intrastrand cross link
IDH	Isocitrate deshydrogenase
LCMS	Liquid cromatography mass spectrometry
LE	Locally excited state
LG	Lomeguatrib
MeCN	Acetonitrile
MGMT	O^6-methylguanine-DNA-methyltransferase
MMEJ	Microhomology mediated end joining
MMR	Mismatch repair system
***N*^{3}MeA**	N^3 methyladenine
***N*^{7}MeG**	N^7 methylguanine
NHEJ	Non-homologous end joining
NMR	Nuclear magnetic resonance
NPOM	Nitropyperonyloxymethoxyl
O^{6}BG	O^6 benzylguanine
O^{6}MeG	O^6 methylguanine
ONB	Ortho nitrobenzyl
OS	Overal survival
p53	Protein 53
PARP-1	poly(ADP-ribose) polymerase 1
PCL	Protein cross link
PD	Pharmacodynamics
PFS	Progresion free survival
PK	Pharmacokinetics
Pol	Polymerase
PPG	Photoprotected group
pRB	Retinoblastoma protein
PTEN	Phosphatase and tensine homologue
RNA	Ribonucleic acid
RT	Radiotherapy
RT	Radiotherapy
rt	room temperature
ss	Single strand
SSB	Single strand break
T	Thymine
TAMRA	5-Carboxytetramethylrhodamine
TEMPO	(2,2,6,6-Tetramethylpiperidin-1-yl)oxyl
TERT	Telomerase reverse transcriptase
THF	Tehtrahydrofurane
TICT	Twisted intramolecular charge transfer
TLC	Thin layer cromatography
TLS	Translesion synthesis
TMZ	Temozolomide
TTF	Tumour treating fields
VEGF	Vascuar endothelial growth factor
XRCC1	X-ray cross-complementing protein

Résumé

I) Introduction

I.I) Gliome, glioblastome, pertinence clinique et traitement

Le gliome est le terme inventé pour décrire un vaste groupe de cancers primitifs du système nerveux central (SNC) qui englobe environ 80 % des tumeurs cérébrales qui incluent l'astrocytome, l'astrocytome anaplasique, l'épendyome, l'oligodendrogliome ou le glioblastome. Au sein de ce groupe, nous pouvons trouver le glioblastome ou le glioblastome multiforme (GBM) comme source de 60% des cancers du cerveau chez les adultes, avec un pic chez les patients entre 55 et 60 ans, avec une légère préférence de genre masculin.[1–3]

Ce type de cancer du cerveau est une tumeur très maligne et invasive (Grade IV), qui se caractérise par un très mauvais pronostic, une espérance de vie très courte de 15 mois qui est inversement proportionnelle à l'âge du patient, et une espérance de vie maximale de 5 années pour seulement 0,47 % des patients.1 Malgré une faible incidence mondiale de moins de 10 pour 100 000 personnes, il a été souligné comme un problème de santé important.[1,2]

Aucune association entre le glioblastome et des facteurs environnementaux tels que le tabagisme, les risques alimentaires, l'exposition aux pesticides, les téléphones portables des champs électromagnétiques n'a été trouvée. Étonnamment, une prédisposition génétique à développer cette maladie n'a été rencontrée que chez 5 à 10 % des patients. Jusqu'à présent, une exposition à de fortes doses de rayonnement a été le seul risque confirmé de développer cette maladie mortelle.2 Selon la littérature,1–4 ce type de tumeur peut être sous-classé en deux catégories si elles sont considérées comme de novo ou dérivées d'autre cancer astrocytome. Une distinction qui peut être faite par les mutations de l'isocitrate déshydrogénase 1 (IDH-1), à savoir le glioblastome de type sauvage IDH pour les cancers primitifs ou de novo ou les tumeurs du glioblastome IDH-mutant pour les cancers secondaires ou métastatiques. Comme caractéristiques génétiques, on peut trouver une amplification sur le récepteur du facteur de croissance épidermique (EGFR), une mutation dans le promoteur de la transcriptase inverse de la télomérase (TERT), une délétion sur le gène homologue de la phosphatase et de la tensine (PTEN), IDH-1 ou Mutations IDH-2, une mutation sur la protéine p53 ou dans la protéine du rétinoblastome (pRB). Ces caractéristiques génétiques et d'autres contribuent à la prolifération cellulaire incontrôlée, à l'instabilité génomique, à la résistance à l'apoptose et à l'infiltration diffuse des cellules malignes.[1–5]

En clinique, aucun remède n'a été trouvé à ce jour, et le traitement palliatif de première intention consiste en une approche multimodale qui comprend la chirurgie, la radiothérapie et la chimiothérapie. La première et la plus importante étape consiste à retirer la tumeur. Cette stratégie

dépend de la taille et de la zone impliquée et il a été observé que les patients ayant subi une résection totale de la tumeur avaient une survie globale (SG) et une survie sans progression (SSP) plus longues que les patients ayant subi une résection partielle de la tumeur.[1,2] Cette tumeur étant considérée comme très invasive, la chirurgie est complétée par une radiothérapie (RT, 60 Gy fractionnés sur six semaines en fractions de 2 Gy) pour éliminer les cellules cancéreuses restantes qui n'ont pu être enlevées par chirurgie. Enfin, le médicament disponible par voie orale Temozolomide (TMZ) est utilisé à une dose de 75 mg/m^2 pendant la radiothérapie et suivi de six cycles tous les 1 à 5 jours pour un total de 28 jours à une dose de 150 à 200 mg/m^2, ce qui confère une prolongation de la durée de survie de 12,1 à 14,6 mois si l'on compare les thérapies sans et avec chimiothérapie.[3]

I.II) Temozolomide comme traitement de chimiothérapie de première intention

Mécanisme d'action du TMZ

Le témozolomide (TMZ) ou Temodar® est une prodrogue dont l'utilisation principale est le traitement du GBM, mais qui est également utilisé pour le traitement d'autres types de tumeurs cérébrales telles que l'épendymome, l'astrocytome, l'astrocytome pilocytique ou le gliome pointin intrinsèque diffus.6 Est petite molécule lipophile capable de traverser la barrière hémato-encéphalique (BHE) et permettant une administration orale. Il est stable à pH acide mais se décompose à pH supérieur à 7. Il a une demi-vie de 1,8 h à pH 7,4 et ses principaux métabolites sont excrétés par l'urine.
La décomposition du TMZ par l'intermédiaire de monométhyltriazène (MTIC) conduit à la formation du cation méthyldiazonium hautement réactif, qui agit comme un agent alkylant monofonctionnel qui réagit avec des macromolécules telles que des protéines ou de l'ADN. Dans l'ADN, TMZ méthyle les nucléobases conduisant à la formation de *N*^{7}MeGuanine (*N*^{7}MeG, 70% de formation), *N*^{3}MeAdénine (*N*^{3}MeA, 9%) et O^{6}MeGuanine (O^{6}MeG, 5%, **Figure 1**, page 4).[5,7]

Étant donné que l'ADN joue un rôle central dans le stockage des informations nécessaires au développement, à la survie et à la reproduction d'un organisme, son maintien par la machinerie cellulaire est vital.[8,9] En raison des différentes modifications de l'ADN créées par l'action TMZ, les cellules répondre pour les réparer par deux voies principales.

Toxicité induite par l'O^6MeG

Avec ces raisons prises en compte, l'augmentation de la lipophilie et le nouveau modèle de formation d'HB, on pourrait expliquer pourquoi lors de la réplication de l'ADN, une polymérase basse fidélité appelée polymérase de synthèse trans-lésionnelle (TLS) insère un thymine (T) face la nucléobase O^6MeG créant un mésappariement O^6MeG:T. En utilisant une polymérase haute fidélité comme le grand fragment d'ADN polymérase I de *Bacillus stearothermophilus*, les chercheurs ont pu cristalliser la paire de bases O^6Me:T dans le site actif de la polymérase. Ici, ils ont observé que dans cette paire de bases, le groupe méthyle pointe vers l'oxygène et qu'une faible interaction électrostatique existe entre les protons O-méthyle et le groupe carbonyle de la thymine. Cette interaction ressemble à une paire de bases Watson-Crick canonique (Figure 2D)12 qui est thermodynamiquement légèrement moins stable que la paire O^6MeG:C de 0,6 kcal/mol (**Figure 2**, page 6).[11,13] Cette inadéquation moins stable (O^6MeG:T vs. G:C, + 5,1 kcal/mol) ressemble au mésappariement G:T, une raison pour laquelle il est reconnu par le complexe hétérodimère MUTSα, composé des protéines MSH2 et MSH6 du système MMR. Une fois le mésappariement trouvé par l'hétérodimère, une coupure sur l'ADN a lieu, suivie du recrutement d'une exonucléase Exo 1 qui supprime environ 150 nucléotides (nt) entourant la lésion. L'espace est alors rempli par la polymérase Pol δ et l'entaille scellée par l'ADN Lig I.[14,15] Cependant, Pol δ insère à nouveau un T opposé au résidu O^6MeG persistant, et ce cycle futile de retrait/insertion se répète et bloque cycle de réplication dans la phase G^2/M (**Figure 3**, page 7).[5,15] Une fois qu'il y a un blocage dans la fourche de réplication, l'apoptose via l'ataxie télangiectasie et la signalisation de la protéine associée à Rad3 (ATR) peut être déclenchée et aboutir à la mort cellulaire. Aussi, une cassure de l'ADN double brin (DSB) pourrait se produire ayant deux possibilités : soit l'apoptose et la mort cellulaire, soit la réparation de la DSB avec des mutations sur le contenu en ADN (**Figure 5**, page 11). De plus, TMZ peut avoir un effet qui ne peut pas conduire directement à la mort, c'est-à-dire la survie via le dépassement du TLS au détriment de la modification du contenu de l'ADN.[15]

N^3MeA, N^7MeA et le système de réparation par excision de base (BER)

Le système BER agit en conséquence des modifications créées par les agents alkylants sur les bases nucléiques à l'exception de O^6MeG. Dans ce cas, les adduits N^7MeG et N^3MeA sont réparés avec les enzymes impliquées (**Figure 4**, page 9). La première modification n'est pas mutagène ou cytotoxique en soi, mais elle se dépurine rapidement et spontanément pour donner un site apurinique d'ADN (site AP), qui est également le même produit de la réaction entre la nucléobase N3MeA et l'enzyme alkyladénineglycosilase (AAG) qui clive le liaison entre la position N9 de l'adénine et le carbone C-1 du sucre désoxyribose (**Figure 4A**). Ce site AP est reconnu par l'endonucléase apurinique-apyrimidinique 1 (APE1), qui crée une entaille sur le squelette de l'ADN en clivant la liaison sucre-phosphate.
Cette cassure simple brin (SSB) est réparée de deux manières similaires différant par le nombre de nucléotides impliqués. Dans les deux sens, la lésion est d'abord reconnue par le complexe poly(ADP-ribose)polymérase 1 (PARP-1). Dans le patch court BER, Pol-β supprime la fraction désoxysucre en laissant un groupe phosphate à l'extrémité 5' de l'espace, qui est le substrat de la même enzyme qui réinsère un nouveau nucléotide. Pour sceller l'entaille, l'action conjointe du complexe protéine de complémentation croisée des rayons X (XRCC1)/ADN Lig III a lieu pour rétablir l'ADNdb. Pour le long patch BER, l'ADN peut être le substrat de deux ADN polymérases différentes comme la Pol ε ou la Pol γ qui éliminent les nucléotides (2-10 nt) dans le brin endommagé en laissant un espace, qui est ensuite rempli par de nouveaux nucléotides création d'un support à rabat unique. Pour conclure, le lambeau est excisé par l'action de la cellule proliférante antigénique nucléaire (PCNA). [9,14,16]

Comme on peut l'observer, cette voie de réparation implique plusieurs enzymes et intermédiaires dans le processus pour parvenir à un ADNdb entièrement réparé. Il a été démontré que les intermédiaires qui appartiennent à cette cascade peuvent être plus toxiques que les produits originaux comme le N^7MeG ou le N^3MeA. C'est pourquoi une régulation stricte de la cascade est nécessaire. Par exemple, le site AP, s'il n'est pas résolu rapidement, peut bloquer la fourche de réplication de l'ADN ou il peut réagir avec une protéine créant une réticulation de protéine d'ADN qui conduit au même effet. [9,14,16] Ce blocage peut être dépassé (s'il n'y a pas de réticulation) par l'utilisation de la polymérase TLS qui permet à la cellule de s'échapper du blocage en insérant des nucléotides avec moins de précision que les normales. Dans ce cas, la cellule survit mais au prix de l'incorporation de mauvais nucléotides qui peuvent muter le contenu d'ADN dans la lésion endommagée. Dans le cas où l'action TLS n'a pas lieu, la fourche peut s'effondrer, entraînant la lésion de l'ADN la plus toxique, le DSB (**Figure 4B**).

Une fois qu'un DSB s'est formé parmi l'ADN, les kinases de la voie de signalisation des dommages à l'ADN (ATM, ATR) sont recrutées sur le site des dommages, puis phosphorylent une histone appelée H2AX en γH2AX, ce qui aide au recrutement de nombreux facteurs de réponse aux dommages à l'ADN. Le DSB peut être réparé de trois manières différentes selon la littérature (**Figure 5**, page 11).[3-5] Dans le système de jonction d'extrémité non homologue (NHEJ), les extrémités clivées sont stabilisées par le complexe Ku70/Ku80 qui lie et stabilise le DSB, empêchant une résection dans les extrémités de l'ADN. Selon que les extrémités sont compatibles ou non, elles peuvent être ligaturées par action de la Pol γ ou de l'ADN Lig IV. Dans la jonction d'extrémité médiée par microhomologie (MMEJ), le système utilise des séquences de microhomologie (2-50 nt) pour recuire les brins complémentaires. Pour être recuit, l'action conjointe du complexe MRE11-RAD50-NBS1 (MRN) plus PARP-1 conduit à la résection des régions flanquantes à côté de la lésion dans ce qu'on appelle un lambeau parage. Puis des nucléotides sont ajoutés par action de la Pol θ et l'entaille est scellée par l'action du complexe (XRCC1)/DNA Lig III. Dans le cas de la recombinaison homologue (HR), le terme « résolution sans cicatrice » a été inventé car la cellule utilise la chromatide sœur comme matrice pour réparer l'ADN endommagé. Ici, l'ADN clivé est stabilisé par le complexe MRN, qui amplifie la signalisation γH2AX. Après cela, une suppression d'environ 300 nt est effectuée dans une direction 3' à 5', suivie d'une invasion de la chromatide sœur qui est utilisée comme modèle pour synthétiser le nouvel ADN ss. Dans les deux premiers cas (MMEJ et NHEJ), la cellule peut survivre mais comme il y a une réduction de la longueur de l'ADN, la perte d'information peut conduire à des mutations si les loci endommagés contiennent des informations pertinentes. Pour la recombinaison HR, il n'y a pas de raccourcissement de la longueur mais l'information d'origine peut être mutée puisque la matrice utilisée est la chromatide sœur et le fragment d'ADN nouvellement synthétisé pourrait contenir des informations de l'autre allèle. Enfin, il existe un autre chemin de non-résolution pour le DSB, et cela se produit une fois que les dommages causés sont élevés et que la cellule ne peut pas faire face à un tel événement. Ici, la cellule meurt soit par la mort cellulaire programmée appelée apoptose, soit par simple nécrose (**Figure 4B**).[14,17,18]

I.III) Résistance à TMZ dans GBM

Comme cela a été mentionné, O^6MeG est le produit TMZ le plus toxique car ses effets hautement cytotoxiques peuvent conduire à la mort cellulaire et à la réduction du gliome. Cependant, près de 50% des patients qui reçoivent du TMZ présentent une réfractivité envers ce traitement, en particulier lors d'un traitement prolongé. Pour comprendre les causes, les mécanismes de résistance peuvent être classés selon s'ils sont MGMT-dépendants ou indépendants.

Résistance dépendante de la MGMT

Le groupe méthyle de la nucléobase O^6MeG est éliminé par l'enzyme O^6-méthylguanine-ADN méthyltransférase (MGMT) qui est une protéine nucléaire omniprésente de 21 kDa.[19] On pense que le complexe MSHα recrute sur le site de la lésion l'enzyme MGMT qui lie l'ADN de manière coopérative et scanne l'ADN dans une direction 5 'à 3' pour trouver le mésappariement. Le mécanisme a été suggéré comme un événement en quatre étapes (**Figure 6A**, page 13).[20] Premièrement, l'enzyme se lie à l'ADN où un motif hélice tour hélice (HTH) interagit avec le petit sillon de l'ADN. Deuxièmement, le résidu Tyr114 interagit avec le phosphate 3' du nucléotide modifié, poussant le phosphate vers l'intérieur du brin, tandis que l'Arg135 s'empile entre les bases. Ces deux actions aident à extraire l'O^6MeG de l'ADN, dont la place est occupée par l'Arg135 qui forme des liaisons hydrogène avec le C opposé. Par ce mécanisme, le résidu O6MeG est placé dans le site actif de MGMT. Une fois en place, les groupements carbonyle Cys145 et Val148 acceptent les hydrogènes de l'amine exocyclique (position 2 de la guanine) alors que l'OH de Tyr114 et le NH de Ser135 donnent respectivement des hydrogènes au N^3 et à l'O^6 de la guanine. Une fois stabilisée, une triade catalytique est formée par les résidus Glu172, His146 et Cys145 pour former un thiolate en présence d'eau. L'anion attaque ensuite le groupe méthyle de l'O^6MeG à partir de son site opposé via un mécanisme S_N2, en supprimant de manière irréversible le CH_3 et en restaurant le G d'origine dans la troisième étape (**Figure 6B**). Enfin, le complexe MGMT.DNA se dissocie et la protéine MGMT alkylée est dégradée par protéolyse. Une caractéristique importante à souligner à propos de cette enzyme est qu'il s'agit d'un système unique « one-shot » ou « suicide » utilisé pour réparer les dommages à l'ADN dans la cellule. En fait, MGMT reconnaît, lie et retourne également les résidus G de l'ADN, mais la sélectivité de MGMT envers son substrat (O^6MeG) n'est pas basée sur la forme complémentaire mais sur la réactivité spécifique du groupe Cys avec le substrat méthyle. [5,7,15,21,22]

Il a été montré que l'expression de MGMT change selon l'organe, le tissu, le type de cancer (tumeur cérébrale incluse) et même au sein d'une même tumeur et que cette expression est régulée par plusieurs facteurs.[7,23-25]

Considérant que l'élimination du groupe méthyle dans le O^6MeG restaure le G d'origine médié par MGMT, il n'est pas surprenant d'observer que les patients présentant une activité élevée de MGMT dans la tumeur ne répondent pas au traitement par TMZ.

Le gène MGMT se trouve sur le chromosome 10, région q26.3 et le mécanisme de régulation épigénétique le plus important correspond à la méthylation sur les îlots CpG de la région promotrice. D'une part la méthylation de ces îlots, en particulier dans les clusters -249 à -103 et +107 à +196, altère le tassement de l'ADN empêchant l'accès à la machinerie de transcription donc pour l'expression de MGMT obtenant des cellules sensibles à TMZ. D'autre part, une faible méthylation du promoteur peut conduire à l'expression de MGMT et à la résistance à la TMZ, ce qui explique pourquoi la stratification des patients en fonction du niveau de méthylation du promoteur est actuellement suggérée pour le traitement par TMZ.

Il a été constaté que dans les groupes récurrents de patients atteints de GBM traités par RT + TMZ (ou les agents alkylants de deuxième ligne ACNU, BCNU ou CCNU, voir Section 1.5.2 page 22) l'activité MGMT des cellules était plus élevée que dans les cancers primitifs à GBM dans contrairement aux patients qui n'ont reçu que la RT.25 Mais il a également été observé que l'exposition au TMZ ne modifie pas le niveau de méthylation du promoteur chez les patients. De ce fait, la résistance ou les niveaux plus élevés d'expression de MGMT peuvent être attribués soit à d'autres facteurs qui régulent l'expression du gène MGMT en plus de la méthylation du promoteur, soit à une sélection chimio de cellules de gliome naturelles résistantes à la TMZ au détriment des cellules sensibles.[25]

En plus de la méthylation du promoteur, l'expression de MGMT peut être modulée par plusieurs facteurs comme les différents niveaux d'expression des facteurs de transcription ou encore à cause du microenvironnement tumoral, tous pouvant conduire à une forte plasticité sur l'expression des protéines.[22] Parmi les facteurs de transcription pouvant interagir avec le promoteur MGMT, on retrouve NF-kB, CEBP, AP-1 ou le Sp1 dont il a été montré qu'il est associé à la protéine p53.[24,26] Dans le cas du microenvironnement, un facteur important à considérer est la quantité d'O2 présente dans le cancer. Étant donné que les cancers sont connus pour se développer dans des conditions hypoxiques, la régulation à la hausse du facteur 1α inductible par l'hypoxie (HIF-1α) pourrait réguler l'expression du promoteur MGMT, ce qui pourrait expliquer pourquoi dans le noyau interne de la tumeur où il y a moins d'expression de l'oxygène MGMT est plus élevée que dans le noyau externe chez les patients atteints de gliome.[24] Une autre voie pour réguler l'expression des gènes est la modification des lysines dans les histones H3 et H4 par acétylation, un événement qui décompresse l'ADN permettant la transcription MGMT. De plus, les résidus peuvent être méthylés dans l'histone H3, un processus qui conduit à l'extinction des gènes.[22,24]

Concernant les cellules cancéreuses naturellement résistantes, le concept de cellules souches de glioblastome (CGC) apparaît. Ce sont des cellules qui, à l'intérieur du microenvironnement tumoral, peuvent s'auto-répliquer, se différencier et acquérir une radio et une chimiorésistance en ayant, par

exemple, des niveaux plus élevés de protéine MGMT. Dans ce cas, les cellules résistantes au TMZ sont sélectionnées par chimiothérapie, ce qui rend le TMZ inefficace.[22,27]

Résistance non dépendante de la MGMT

Compte tenu du fait que TMZ a besoin d'un système MMR actif pour générer des dommages à l'ADN par la formation d'O^6MeG (**Figure 3**, page 7), l'hypothèse d'un système MMR dysfonctionnel qui pourrait conduire à une résistance à TMZ a été analysée dans d'autres types de cancer tels que : gastrique, endométriale ou colorectale.[5,15] Néanmoins, il a été noté que la survie des patientes avec un glioblastome ou des astrocytomes qui présentaient une expression plus faible de la protéine MSH6 était inchangée par rapport aux patientes avec une expression normale de MSH6. Une explication formulée à ce manque de résistance vis-à-vis du TMZ peut être le fait que même si un dysfonctionnement du système MMR conduit à une résistance ou à une inactivité du TMZ, le même manque de MMR peut également conduire à des mutations qui peuvent être délétères pour la cellule (**Figure 3**)[28]. En outre, la résistance intrinsèque pourrait être associée à la GSC avec différents niveaux d'expression de l'efflux de pompes médicamenteuses qui peuvent expulser le médicament hors de la cellule.[29,30]

Il a été démontré que TMZ peut déclencher l'autophagie dans les cellules GBM via la voie ATM/AMPK après des dommages à l'ADN. Par définition, l'autophagie est un mécanisme cytoprotecteur que la cellule utilise pour réguler l'homéostasie dans des conditions sévères telles que l'hypoxie, le manque de nutriments ou les dommages à l'ADN. Dans ce scénario, la cellule cible et dégrade les organites endommagés ou aberrants afin de maintenir son équilibre interne.

Dans le GBM, l'importance de ce phénomène a été démontrée lorsque plusieurs modulateurs de l'autophagie ont été utilisés qui, par exemple, augmentaient l'apoptose induite par le TMZ.[31] Néanmoins, les experts ont mis en doute le rôle de l'autophagie dans les cellules cancéreuses car selon eux, il existe une fine ligne entre les voies qui favorisent l'apoptose et l'autophagie, puisqu'une voie conduit à la mort cellulaire tandis que l'autre conduit à la survie.

Il existe une autre voie clé liée à la résistance à la TMZ qui est associée à la mutation du récepteur tyrosine kinase (RTK), en particulier le récepteur EFGR qui est surexprimé dans le GBM.[22,24,27] Une fois la cascade EFGR activée, deux sous-voies apparaissent, l'une liée à la voie PI3K/Akt et l'autre à la voie MAPK/Erk. En résumé, ces processus conduisent à l'inhibition de la pyruvate déshydrogénase kinase 1 (PDK1) modifiant ainsi l'obtention d'énergie à partir d'une voie glycolytique au lieu de la phosphorylation oxydative dans un processus connu sous le nom d'effet Warburg. De plus, il peut

activer HIF-α et les protéines de choc thermique qui activent le facteur de croissance endothélial vasculaire (VEGF) augmentant l'angiogenèse dans des conditions hypoxiques ou, par exemple, stimulant la production de NF-κB augmentant les propriétés de survie.[31]

Enfin, un autre mécanisme de résistance très important dans le cancer et notamment dans le glioblastome est lié à la protéine p53. Cette macromolécule est un facteur suppresseur de tumeur très important qui joue un rôle clé dans les processus cellulaires comme l'apoptose, le métabolisme cellulaire, l'intégrité du génome ou l'angiogenèse. Le gène p53 est l'un des gènes les plus dérégulés dans le cancer et cette dérégulation est retrouvée chez 84 % des patients atteints de GBM. L'absence de protéine p53, que ce soit par délétion, mutation ou expression inférieure du gène, interdit aux cellules d'arrêter le cycle cellulaire, d'entrer en apoptose ou en sénescence, permettant la croissance tumorale et la propagation de la maladie.[32]

I.V) Objectifs de la thèse

À la lumière des paragraphes susmentionnés et malgré les énormes efforts déployés par la communauté scientifique internationale, aucune nouvelle approche n'a été considérée comme réussie à ce jour. Les multiples facteurs de résistance, le déclin progressif des fonctions neurologiques dû à l'agressivité du traitement, le microenvironnement tumoral entre autres rendent le traitement du GBM assez difficile. Par conséquent, de nouvelles chimiothérapies ou immunothérapies, la stratification des patients en fonction de marqueurs biologiques tels que le statut de méthylation du promoteur pour une thérapie ciblée et personnalisée pourraient être utilisées pour rendre un meilleur pronostic de la maladie qui peut améliorer la durée de vie et la qualité des patients.

Dans cette thèse, nous explorons la conception de trois nouvelles stratégies pour inhiber l'activité MGMT en combinaison avec le TMZ pour le traitement des gliomes selon les prochaines étapes. La première repose sur la stratégie d'inhibition indirecte qui consiste à concevoir des molécules capables d'interagir avec le substrat MGMT en le masquant de l'action du MGMT. Le second est l'inhibition de la MGMT par l'utilisation de molécules hybrides ciblant à la fois le site actif de la MGMT et l'ADN. Enfin, la stratégie photocaged repose sur le principe de la conception d'une molécule en cage et inactive qui, lors d'une irradiation lumineuse, libère un inhibiteur de la MGMT pour désactiver l'enzyme de manière contrôlée.

Afin de poursuivre ces stratégies, les approches expérimentales suivantes seront réalisées. Ces approches, seront présentées plus en détail dans les chapitres suivants :

A) Synthèse des inhibiteurs de la MGMT
B) Caractérisation in vitro de l'interaction Ligand ADN
C) Etudes de leurs propriétés photophysiques
D) Essais d'inhibition de la MGMT
E) Évaluation *in cellulo* en tant qu'agents uniques contre les cellules T98G
F) Évaluation *in cellulo* en combinaison avec TMZ

II) Stratégie indirecte pour inhiber la MGMT

Principe et état de l'art

La stratégie d'inhibition « classique » d'une enzyme (E) correspond à l'utilisation d'un ligand ou inhibiteur (L) qui inhibe l'enzyme réduisant son activité soit pour rivaliser par l'accès au site actif avec le substrat naturel (S), soit en interagissant avec l'état de transition enzyme-substrat (ES).[62,63] Dans la stratégie d'inhibition indirecte (IIS), également appelée « ciblage du substrat » ou « masquage du substrat », l'accès de E à S est limité par ligand L avec le substrat S qui « masque » la transformation de S en produit (P). Il convient de mentionner que ce concept est du point de vue de la cinétique de réaction, indiscernable de l'inhibition compétitive décrite par l'équation de Michaelis-Menten. L'idée a d'abord été décrite par le groupe Kodadek où ils ont conçu des molécules pour cibler des peptides impliqués dans la modification post-traduction (PTM) et suivi par le groupe Kukar où la cible correspondait à interagir avec les modulateurs de la -sécrétase impliqués dans l'anti- processus inflammatoire dans la maladie d'Alzheimer (**Figure 8**, page 27).[62,64]

Objectifs du travail

Sur la base de l'IIS, nous avons suggéré la synthèse de petites molécules avec un motif de liaisons hydrogène qui pourraient être complémentaires de celles présentes dans la base O^6MeG. Considérant que l'O^6MeG peut, en principe, former trois liaisons hydrogène à la manière d'un Aceptor Aceptor Donor (AAD), nous proposons que nos molécules puissent avoir la possibilité de former au moins deux liaisons hydrogène à la manière d'un Donor Donor Aceptor (DDA) (**Figure 10**, page xxx) . Nous avons émis l'hypothèse que la liaison de ces molécules aux résidus O^6MeG dans l'ADNdb stabiliserait la conformation intrahélicoïdale de ce dernier, la masquant de la MGMT, entraînant un effet d'inhibition indirect.

Résultats

Dans cette partie de la thèse, nous avons systématiquement exploré la stratégie d'inhibition indirecte ciblant la MGMT. Ici, onze composés hétérocycliques ont été synthétisés en faisant varier son modèle donneur/accepteur de liaisons hydrogène, ainsi que leur taille, leur hydrophobie et leur surface, en

tant que ligands potentiels qui pourraient se lier aux résidus O^6MeG dans l'ADN. La capacité de ces molécules à stabiliser un ADNdb portant un site O6MeG:C ou un site O^6MeG:Φ substitut d'un site AP a été étudiée par des expériences de fusion UV en essayant d'obtenir des composés qui se lient et stabilisent les structures d'ADNdb contenant O^6MeG. Malheureusement, aucun des composés n'a été capable de stabiliser les substituts dans une mesure significative, de manière similaire à ce qui a été observé pour les molécules précédemment synthétisées dans notre laboratoire.

Il est intéressant de souligner que le composé Benzi, précédemment décrit comme un partenaire O^6MeG sélectif (lorsqu'il est incorporé dans le brin d'ADN opposé) n'a pas stabilisé les substituts d'ADN utilisés dans nos mains. Des facteurs tels que la séquence d'ADN, la longueur, la concentration d'ADN et de ligand, le type de tampon ou la concentration ionique peuvent être responsables de ces différences. Cependant, la plus grande différence entre les méthodologies est la façon dont le ligand est trouvé en solution. Dans les articles de Sturla, Benzi est incorporé comme nucléobase devant la base O6MeG et non librement en solution comme dans nos modèles. De cette façon, le facteur entropique est également considérablement réduit. Parce qu'il a également été prouvé que la conformation de Benzi de la liaison glycosidique entre N^9 de la nucléobase et C'1 du sucre est anti, les probabilités de créer les liaisons nécessaires avec O^6MeG pour stabiliser l'ADN sont augmentées. Dans notre cas, le ligand est libre en solution, où les probabilités d'interactions sont réduites même si les concentrations de ligands sont 10 à 30 fois supérieures à celles de l'ADN. Pour la liaison opposée au résidu O^6MeG, le ligand doit retourner le C opposé (ou s'adapter au site AP face à O^6MeG), se positionner devant la base et établir les liaisons hydrogène appropriées. En d'autres termes, la stabilité de l'interaction ligand:nucléobase modifiée doit être suffisamment élevée pour être la force motrice qui surpasse et compense tous les événements mentionnés ci-dessus.

En comparant cette stratégie avec le processus naturel de détection de O^6MeG par MGMT, le processus semble assez peu susceptible d'être réalisé par de petites molécules. Il convient de rappeler que la cellule a développé une enzyme suicide unique le long du fil de l'évolution pour détecter sélectivement un seul type de modification de l'ADN. MGMT scanne l'ADN de manière coopérative et possède de multiples points d'interaction avec l'ADN, ce qui ne se produit pas dans notre modèle. Plus important encore, MGMT se lie également aux résidus G (ce qui signifie qu'il n'a pas de sélectivité de liaison) mais il ne réagit pas avec eux car la reconnaissance est basée principalement sur la réactivité spécifique de la Cys envers le groupe méthyle dans O^6MeG. Par conséquent et compte tenu de nos résultats, la reconnaissance de cette lésion de l'ADN par de petits ligands semble assez improbable au moins *in vitro*.

Certaines 8-azaquinolones ayant été décrites comme des ligands du site AP, la capacité de ces dérivés à stabiliser sélectivement ce type de lésion a été évaluée. Ici, nous avons constaté que le composé **15** stabilise sélectivement le site A:Φ dans des expériences de fusion UV et avait également un effet «éclairant» lors de la liaison à l'ADN, bien que sans sélectivité envers les duplex contenant A:Φ.

Ces résultats nous ont encouragés à tester **15** avec tous les composés précédemment synthétisés dans la lignée cellulaire T98G pour étudier la possibilité de lier les sites AP créés par TMZ dans la cellule. Malheureusement, aucun des composés n'a montré une grande cytotoxicité contre cette lignée cellulaire, que ce soit seul ou en combinaison avec le TMZ, indiquant qu'ils n'interfèrent pas avec les voies liées à la résistance au TMZ. Parce que ni la stratégie *in vitro* ni *in cellulo* pour développer des médicaments à utiliser en combinaison avec TMZ n'a fonctionné pour l'IIS, cette approche a été abandonnée et deux nouvelles stratégies ont été explorées.

III) Stratégie d'inhibition de la MGMT avec des médicaments hybrides

Principe et état de l'art

Comme expliqué dans l'introduction, la surexpression de MGMT est la principale cause de résistance à TMZ dans le GBM mais pas la seule. En effet, les maladies (cancer inclus) sont généralement une combinaison de dysfonctionnements de la machinerie cellulaire qui rend difficile leur traitement par un seul médicament. Dans cette partie de cette thèse, nous proposons l'inhibition de la MGMT par des médicaments hybrides comme approche pour surmonter les multiples mécanismes de résistance que contient la cellule GBM qui confère une résistance au traitement actuel.

Objectifs du travail

Sur la base de la stratégie hybride, nous proposons de synthétiser des molécules contenant le noyau O6BG associé à l'échafaudage Acr dans le but d'obtenir une molécule capable d'inhiber la MGMT qui pourrait conférer les propriétés biologiques du noyau Acr. Puisqu'il a été discuté que les modifications d'O^{6}BG dans le groupe Bn et l'atome *N*^{9} maintenaient la capacité d'inactiver la MGMT par rapport à O^{6}BG, deux types d'hybrides (hybrides Bn et hybrides *N*^{9}) ont été conçus (**Chart 12A**, page 76). L'idée de cette stratégie consiste à utiliser le noyau (Acr) qui sera lié à l'O^{6}BG dans une conformation empilée ou inactive. Après le dépilage, la conformation ouverte ou active pourrait interagir avec l'ADN via Acr exposant l'O^{6}BG pour inactiver la MGMT. En raison des mécanismes MGMT, selon le type d'hybride

utilisé ; deux produits MGMT d'inactivation différents ont pu être obtenus (**Graphique 12B**).

Résultats

Le concept de molécule hybride peut être défini comme la combinaison de deux entités chimiques pour améliorer ou amplifier l'activité de l'autre, moduler l'une ou l'autre activité ou exercer une double activité à l'intérieur d'une cellule.[129] Il existe au moins trois méthodes pour combiner chaque molécule individuelle. La méthode choisie dépend de la chimie des échafaudages correspondants et de la capacité de ce nouvel hybride à rester (ou non) biologiquement inchangé. La première méthode consiste en l'utilisation d'une fonction hydrolysable en cellule telle qu'un ester, un amide ou un carbamate. La deuxième option, est l'union par l'intermédiaire d'un linker non clivable tel qu'une chaîne alkyle, un groupe polyamino, un linker polyéthylèneglycol ou enfin, par l'intermédiaire d'un linker triazole. La troisième option, peut-être la plus difficile, consiste à superposer les entités chimiques ou pharmacophores dans une seule molécule fusionnée. Ces stratégies sont passées en revue dans Decker *et al*.[129] La stratégie hybride présente plusieurs avantages tels que s'attaquer à deux cibles avec une seule molécule, ou avoir une nouvelle entité chimique avec un seul profil pharmacocinétique et pharmacodynamique (PK/PD). Pour l'hybride, aucune interaction médicament-médicament ne doit être observée, une formulation plus facile peut être obtenue ou une toxicité plus faible peut être obtenue. Cependant, ce même avantage pourrait se transformer en inconvénient puisqu'un équilibre dans la conception doit être pris en compte pour les composés qui ont individuellement une plage de concentration d'activité très inégale. Malgré ces défis, cette stratégie a été appliquée pour la conception de ligands de récepteurs/inhibiteurs d'enzymes, pour lutter contre les maladies parasitaires tropicales, la maladie d'Alzheimer, le cancer ou dans la conception de molécules pour contrôler le stress oxydatif.[129]

Conclusions

Dans cette partie de la thèse, l'approche pour cibler la MGMT à l'aide de molécules hybrides composées de deux échafaudages tels que Acr et O^6BG a été explorée. L'objectif d'attacher à l'inhibiteur de MGMT O^6BG un noyau Acr était justifié par les différents effets que ce dernier peut provoquer dans les cellules cancéreuses, avec l'objectif de donner à l'hybride une valeur ajoutée

pharmacologique capable de surmonter les multiples facteurs t qui génèrent une résistance dans le GBM cellules.

Au total, six hybrides ont été synthétisés différant par la longueur et la nature du linker et en modifiant la manière de les attacher, notamment via le cycle benzylique ou le N^9 de l'échafaudage O^6BG. Lors de la synthèse de cet ensemble de composés, l'objectif était d'avoir des molécules dans une conformation intra-empilée (ou inactive) qui lors du changement d'environnement (par interaction du noyau Acr à l'ADN), l'échafaudage O^6BG serait exposé pour inactiver MGMT, augmentant la cytotoxicité de TMZ. Les équilibres et la modulation de cette propriété ont été atteints avec succès avec deux tendances opposées, étant les hybrides N^9 plus intra-empilés lorsque la longueur du lieur était plus courte et pour les hybrides Bn moins intra-empilés lorsque la longueur du lieur était augmentée. Deux autres effets ont été démontrés pour cette stratégie. Tout d'abord, il a été montré, contrairement à notre modèle initial, que les hybrides étaient capables d'interagir mais pas de s'intercaler avec l'ADN par rapport au témoin intercalant Acr. Et deuxièmement, les hybrides étaient également capables d'inactiver la MGMT dans des tests sur gel, avec différentes capacités d'inhibition selon le test utilisé. En règle générale, les hybrides Bn sont d'aussi bons inhibiteurs in vitro que O^6BG alors que les hybrides N^9 étaient moins efficaces que le témoin. Les effets *in cellulo* des six hybrides, ainsi que de cinq autres composés, ont été étudiés et nous avons observé que la cytotoxicité de l'Acr peut être modulée en fonction des points d'attache. Les hybrides Bn ont montré une puissance micromolaire ($15 < GI_{50} < 25$ µM), alors que lorsque l'attachement a été modifié pour le N^9, la cytotoxicité a été augmentée à des valeurs micromolaires faibles pour les composés **62** et **64** ($GI_{50} < 3$ µM). Fait intéressant, ces deux composés ont montré une synergie lorsqu'ils sont combinés avec le TMZ à des concentrations sous-toxiques à la fois de l'hybride et du TMZ (valeurs de 1/8 GI_{50} de chaque composé)

Nous avons pu observer que le composé **62** était capable d'inactiver la MGMT cellulaire, validant notre hypothèse et nous avons également remarqué que la molécule est capable de générer l'apoptose seule ou en combinaison avec le TMZ dans les cellules T98G. Cependant, cette apoptose n'est pas générée par la création de DSB comme on le voit pour O^6BG avec TMZ. Le processus apoptotique a été expliqué par l'activation de la cascade pro-apoptotique puisqu'il a été observé par l'activation de l'expression de la caspase 3/7, qui peut être une conséquence de l'activation de la protéine p53. Il est à noter et comme cela a été observé pour l'effet synergique de **62** plus TMZ n'a pas été attribué à une augmentation synergique de la cascade d'apoptose.

Étonnamment également, Acr a été capable d'inhiber la MGMT dans nos tests et également de générer une synergie en combinaison avec TMZ, des propriétés intéressantes pour les futures approches de découverte de médicaments pour traiter le GBM.

Selon les prédictions *in silico*, le composé **62** et l'Acr pourraient être capables de traverser la BHE et également de respecter les règles de Lipinksi pour les médicaments disponibles par voie orale qui, conjointement avec ses propriétés biologiques, en font de bons candidats pour poursuivre le processus de développement de médicaments.

IV) Inhibition de la MGMT par des molécules photocagées

Principe et état de l'art

Le problème de la sélectivité tumorale est un problème récurrent dans le traitement du cancer. L'une des stratégies employées par les chercheurs pour pallier cet inconvénient est l'utilisation d'une molécule active conjuguée à un groupe protecteur photolabile (PPG). L'idée de cette approche consiste en ce que l'ajout du PPG rend le composé inactif, qui une fois irradié avec une certaine longueur d'onde libère l'échafaudage actif dans l'environnement en raison de l'élimination du PPG. Étant donné que le temps et l'amplitude de l'excitation de la longueur d'onde peuvent être contrôlés par des sources disponibles dans le commerce, la biodisponibilité et la pharmacodynamique d'une certaine molécule peut également être régulées spatio-temporellement (**Schéma 14**, page xxx). Idéalement, cette stratégie doit remplir certains critères pour réussir. Tout d'abord, l'ajout d'un PPG doit conduire à une molécule cage inactive (ou moins active) par rapport au composé parental. Deuxièmement, afin d'éviter la cytotoxicité lumineuse, les groupes PPG doivent pouvoir être éliminés rapidement et avec des longueurs d'onde de faible énergie. Troisièmement, la libération du PPG (ou de ses sous-produits) ne devrait pas être toxique pour le système étudié.[213-217]

Résultats

Les molécules de photocage sont une stratégie élégante pour masquer un médicament actif afin de le rendre moins actif vis-à-vis de cibles non spécifiques, qui une fois irradié dans des conditions spécifiques, il ne devient actif que dans un locus souhaité. Dans ce chapitre, nous présentons comme preuve de concept la mise en cage d'O^6BG en utilisant ONB comme PPG.

La partie synthétique a consisté en l'obtention des deux régioisomères **66** et **67** en deux étapes et son évaluation biologique. Malheureusement, les deux composés se sont avérés plus toxiques que le

composé parental. Considérant que l'isomère N^7 (**66**), qui est supposé être la molécule en cage et inactive puisque le MGMT ne devrait pas être capable d'éliminer le groupe benzyle, est deux ordres de grandeur plus cytotoxique que O^6BG, l'utilisation de l'O^6BG photocage a été abandonnée. A noter, et en raison des derniers résultats observés dans la littérature, le choix du PPG semble être la clé du succès de la stratégie; par conséquent, d'autres PPG devraient être étudiés en profondeur.

V) Conclusions généraux

Le cancer est une maladie avec une distribution mondiale qui ne fait aucune distinction d'âge, de sexe ou de statut économique. Parmi les cancers, le GBM est un type particulier de cancer du cerveau qui est le plus fréquent dans la population adulte. Malheureusement, il s'agit d'une maladie mortelle sans remède, qui implique une durée de vie très courte pour le patient. Le traitement palliatif consiste en des méthodes agressives qui diminuent fortement la qualité de vie des patients. Comme indiqué dans l'introduction, ce type de cancer n'a pas seulement la caractéristique biologique d'être une tumeur très agressive, infiltrante et récurrente avec de nombreuses caractéristiques biologiques exacerbées telles que la surexpression de MGMT, l'efflux de pompe pour la désintoxication médicamenteuse, la présence de GSC, etc. De plus, d'un point de vue physique, il a la particularité d'être situé dans une zone où des actes chirurgicaux plus complexes doivent être effectués pour accéder à cette partie du corps humain. Bien entendu, la modification chirurgicale de cet organe très important peut également entraîner une perte des capacités cognitives et de motilité du patient. De même, une autre barrière physique comme la BHE constitue un obstacle indéniable et compliqué à surmonter lorsque nous parlons de dosage de médicaments, car toutes les molécules, utilisées pour un traitement non cérébral ou d'immunothérapie, ne peuvent pas être utilisées. Compte tenu des facteurs physiques et biologiques, la communauté scientifique a consacré d'énormes efforts pour améliorer la qualité de vie, augmenter l'espérance de vie ou, dans le meilleur des cas, guérir les patients souffrant de GBM. Les stratégies consistent souvent en des approches multimodales qui tentent de surmonter toutes ces difficultés décrites ci-dessus. Dans cette thèse, seuls les essais pré ou cliniques portant sur des approches chimiothérapeutiques ont été mentionnés. Néanmoins, il est important de mentionner que d'autres modalités ont été utilisées afin d'améliorer la qualité de vie en : développant de meilleurs outils de diagnostic tels que l'imagerie par résonance magnétique (IRM) ou des techniques de fluorescence pour mieux localiser la niche tumorale. Une stratification des patients en fonction des expressions de biomarqueurs pour améliorer le pronostic de la thérapie actuelle a également été réalisée. De plus, l'immunothérapie ou les méthodes acoustiques basées sur les champs de traitement

des tumeurs (TTF) ont atteint des essais cliniques dans ce but. [2,3,226] Malgré les efforts énormes, aucune de ces méthodes n'a été en mesure d'améliorer avec succès le traitement du GBM.

Dans cette thèse, nous avons exploré trois nouvelles stratégies qui pourraient être potentiellement appliquées d'un point de vue thérapeutique. La première approche était basée sur le postulat de concevoir de petites molécules variant leur taille, leurs capacités d'empilement, leur charge, leur hydrophobie et plus important leur capacité de formation de liaisons hydrogène, vers une éventuelle interaction avec O6MeG afin de masquer ce dernier de l'action MGMT, améliorant ainsi sa pertinence biologique dans les cellules de glioblastome. Dans cette partie, onze molécules ont été synthétisées et avec dix-huit composés précédemment conçus, leur capacité à stabiliser l'ADNdb portant des nucléobases O^6MeG a été étudiée par des méthodes biophysiques. De plus, leurs propriétés cytotoxiques dans la lignée cellulaire de glioblastome multirésistant et surexprimant MGMT T98G ont été testées seules ou en combinaison avec TMZ. Malheureusement, aucun des composés étudiés n'a été capable de stabiliser sélectivement l'ADNdb contenant des résidus O^6MeG, ni dans une paire de bases O^6MeG:C ni dans un substrat O6MeG:Φ simplifié. De plus, les molécules n'ont pas montré de cytotoxicité intéressante par rapport à la T98G seule ou combinée avec TMZ. Cependant, une 8-azaquinolone, la molécule **15**, a été capable de discriminer sélectivement un substitut AP qui faisait face à une adénine (A:Φ) dans le brin opposé. Ce composé a montré une sélectivité en comparaison avec d'autres types de paires de bases dans l'ADN (A: Φ > T: Φ > C: Φ > G: Φ > O6MeG:Φ >>AT) et s'est également avéré être le plus composé cytotoxique de cette série. Même si aucune augmentation des propriétés cytotoxiques du TMZ n'a été observée dans cette lignée cellulaire, une éventuelle utilisation de ce composé dans d'autres types de lignées cellulaires ne doit pas être exclue.

Dans la seconde stratégie, l'inhibition de la MGMT par des molécules hybrides a été explorée par la conjugaison de l'ogive O^6BG avec la fraction Acr en raison des propriétés démontrées de cette dernière pour activer les voies cytotoxiques dans les cellules cancéreuses. L'intention était d'attribuer une valeur ajoutée à l'échafaudage O^6BG pour exploiter plusieurs voies cytotoxiques dans les cellules de glioblastome. Notre concept, résidait sur la conception de molécules qui différaient sur leurs points d'attache entre O^6BG et Acr (anneau N^9 et Bn) en variant également la longueur et la nature du linker. Cette idée nous aurait permis d'obtenir des composés sous deux conformations (empilées intramoléculairement ou inactives, et ouvertes ou actives) pour moduler leurs propriétés d'interaction avec l'ADN et l'inactivation de MGMT *in cellulo*, augmentant ainsi l'action de TMZ. En portant cette approche, nous avons observé que pour les hybrides les équilibres pouvaient être altérés ainsi que leurs propriétés d'inhibition de la MGMT et leurs propriétés cytotoxiques. Plus intéressant encore,

nous avons constaté que les hybrides **62** et **64** étaient capables de générer un effet synergique lorsqu'ils étaient combinés avec le TMZ lorsqu'ils étaient utilisés à des concentrations sous-toxiques, de la même manière mais à des concentrations beaucoup plus faibles que O^6BG. L'inhibition de la MGMT a été démontrée avec succès pendant **62** dans des expériences cellulaires où nous avons pu valider notre hypothèse. De plus, le bénéfice de la fusion du noyau Acr dans l'hybride a été démontré par l'activation du processus d'apoptose (comme en témoignent les tests d'Annexine V) par l'activation des caspases pro-apoptotiques 3 et 7 rendant une molécule avec au moins deux effets biologiques dans le T98G. La première, l'inhibition de la MGMT, et la seconde, l'activation des réponses pro-apoptotiques qui sont généralement régulées à la baisse dans le cancer. D'un point de vue clinique, la démonstration que ces molécules sont synergiques avec le TMZ à des concentrations sous-toxiques, et avoir un effet multi-cibles pourrait ouvrir la porte à d'autres études dans le pipeline de développement de médicaments, car cela pourrait signifier qu'une sélectivité pourrait être atteint pour les cellules qui surexpriment MGMT et qui sont également résistantes à TMZ par d'autres moyens en plus de cette surexpression de protéine.

Enfin, sur la base du manque de sélectivité spatio de l'échafaudage O6BG, la stratégie de photocage a été réalisée sur le principe d'obtenir une molécule inactive qui, lors d'une irradiation lumineuse, libérerait la molécule O6BG. Malheureusement, les produits photocagés se sont avérés plus toxiques que le composé parental *in cellulo*, par conséquent, aucun essai in vitro sur l'inhibition de la MGMT n'a été réalisé. Cependant et en raison des données de la littérature, la clé du succès de la stratégie peut résider dans le type de groupe PPG, donc l'utilisation de différents groupes peut être reconsidérée.

En résumé des trois stratégies menées dans cette thèse, une conception rationnelle des molécules combinée à leur synthèse a été réalisée. Au total, trente-trois molécules finales ont été synthétisées par des techniques classiques de synthèse organique. Pour ces molécules, leurs propriétés in vitro telles que la liaison à l'ADN, la fluorescence, l'empilement intramoléculaire ou les propriétés d'inhibition de la MGMT ont été étudiées. De plus, leur effet cytotoxique seul ou en combinaison avec le TMZ a également été analysé dans une lignée cellulaire de glioblastome. De plus, d'autres techniques telles que la microscopie à fluorescence, la cytométrie en flux ou les dosages enzymatiques ont été menées pour mieux comprendre leur mécanisme d'actions. Au total, cela représente, même à très petite échelle, une manière qui pourrait nous aider à comprendre les causes et plus important encore, les outils qui pourraient être employés à l'avenir pour traiter cette maladie d'un point de vue chimiothérapeutique.

Chapter 1
Introduction

1. Introduction

1.1 Glioma, glioblastoma, clinical relevance and treatment

Glioma is the term coined for describing a vast group of primary cancers in the Central Nervous System (CNS) that compels about 80% of brain tumors that include astrocytoma, anaplastic astrocytoma, ependyomoma, oligodendroglioma or glioblastoma. Within this group, we can find glioblastoma or glioblastoma multiforme (GBM) as the source of 60% of brain cancer in adults, having a peak in patients between 55 and 60 years, with an slight male gender preference.[1–3]

This type of brain cancer is a highly malignant and invasive tumor (Grade IV), that is characterized by a very poor prognosis, a very short life expectancy of 15 months which is inversely proportional to the patient's age, and a maximum life expectancy of 5 years rate for only 0.47% of patients.[1] Despite having a low worldwide incidence of less than 10 per 100000 persons, it has been highlighted as an important health issue.[1,2]

No association between glioblastoma and environmental factors such as smoking, dietary risks, pesticides exposure, cell phones of electromagnetic fields has been found. Surprisingly, genetic predisposition to develop this disease has been encountered in only 5-10% of the patients. So far, an exposure to high radiation doses has been the sole confirmed risk to develop this fatal disease.[2] According to the literature,[1–4] this type of tumor can be subclassified in two categories if they are considered as *de novo* or derived from other astrocytoma cancer. A distinction that can be made by the isocitrate dehydrogenase 1 (IDH-1) mutations, namely IDH-wild type glioblastoma for primary or *de novo* cancers or IDH-mutant glioblastoma tumors for secondary or metastatic cancers. As genetic hallmarks, we can find an amplification on the epidermal growth factor receptor (EGFR), a mutation in the promoter of the telomerase reverse transcriptase (TERT), a deletion on the phosphatase and tensin homologue (PTEN) gene, IDH-1 or IDH-2 mutations, a mutation on the p53 protein or in the retinoblastoma protein (pRB). These and other genetic hallmarks contribute to uncontrolled cellular proliferation, genomic instability, resistance to apoptosis and diffuse infiltration of the malignant cells.[1–5]

In clinics, no cure has been found so far, and the first line palliative treatment consists on a multimodal approach that contains surgery, radiotherapy and chemotherapy. The first and most important step consists on the removal of the tumor. This strategy depends on the size and area implicated and it has been observed that patients with total resection of the tumor had longer overall survival (OS) and progression-free survival (PFS) in comparison with patients that received partial tumor resection.[1,2] Since this tumor is considered as very invasive, the surgery is complemented with radiotherapy (RT,

60 Gy fractioned over six weeks in 2 Gy fractions) to eliminate the remaining cancerous cells that could not be removed by surgery. Finally, the orally available drug Temozolomide (TMZ) is used at a 75 mg/m^2 dose during radiotherapy and followed by six cycles every 1 to 5 days for a total of 28 days on a 150 to 200 mg/m^2 dose, which confers an extension on the survival time from 12.1 to 14.6 months if we compare therapy without and with chemotherapy.[3]

1.2 Temozolomide as the first-line chemotherapy treatment

1.2.1 Mechanism of action of TMZ

Temozolomide (TMZ) or Temodar® is a prodrug whose major use is for GBM treatment, but which is also used for the treatment of other types of brain tumors such as ependymoma, astrocytoma, pilocytic astrocytoma or diffuse intrinsic pointine glioma.[6] It is a small lipophilic molecule that is able to penetrate the blood-brain barrier (BBB) and that allows oral administration. It is stable at acidic pH but it decomposes at pH higher than 7. It has half-life of 1.8 h at pH 7.4 and its major metabolites are excreted via urine.

The decomposing of TMZ through monomethyl triazene intermediate (MTIC) leads to the formation of the highly reactive methyl diazonium cation, which acts as a monofunctional alkylating agent that reacts with macromolecules such as proteins or DNA. In DNA, TMZ methylates nucleobases leading to the formation of *N*^{7}MeGuanine (*N*^{7}MeG, 70% of formation), *N*^{3}MeAdenine (*N*^{3}MeA, 9%) and O^{6}MeGuanine (O^{6}MeG, 5%, **Figure 1**).[5,7]

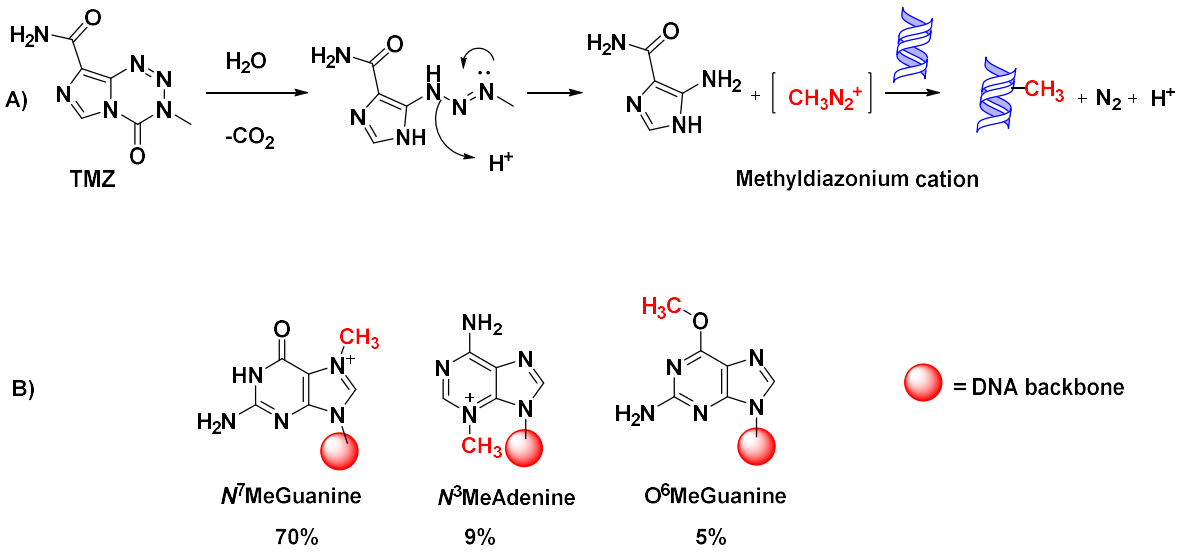

Figure 1A) Temozolomide (TMZ) structure, activation and reaction with DNA together B) most relevant DNA adducts formed.

Since DNA plays a pivotal role in storing the necessary information for an organism to develop, survive and reproduce, its maintenance by the cellular machinery is vital.[8,9] Due to the different modifications in the DNA that are created by the TMZ action, cells respond to repair them by two major pathways.

1.2.2 O^6MeG-induced toxicity

Even if N^7MeG and N^3MeA are formed in the higher amounts, it has been shown that these adducts are not responsible for the major toxicity generated by TMZ. In fact, the primarily damage arises from the O^6MeG modified nucleobase through a failure of a DNA repair pathway called mismatch repair system (MMR), a system that is normally responsible for recognition and repair of base mismatches (chiefly G:T) in DNA. In order to analyze the critical role played by the MMR system it is necessary to understand the chemical modifications induced by the methylation in the oxygen of the position 6 of the Guanine (G), in particular the changes that this carry both in the polarity of the base and in the hydrogen bond pattern between G and its complementary nucleobase Cytosine (C). The first point is that this alkylation modifies the distance of the bonds in the heterocycle of the former G and also makes it more lipophilic, producing a modified nucleobase that resembles Adenine (A).[10] The second point is related with the modification of hydrogen bond pattern in the G:C base pair (**Figure 2A**). It has been observed that in the free nucleobase the methoxy group is coplanar with the purine ring, it points in the opposite direction of the imidazole ring and in the same direction as the exocyclic amino group (**Figure 2B**). This (slight) preference for *syn* conformation is maintained in DNA (-2.7 kcal/mol *vs.* the *anti* conformation), and the position of the methyl group creates a steric clash that destabilizes the double stranded DNA (dsDNA). This destabilization is compensated by a wobble in the base pair giving a O^6MeG:C base pair with two hydrogen bonds (**Figure 2C**).[10]

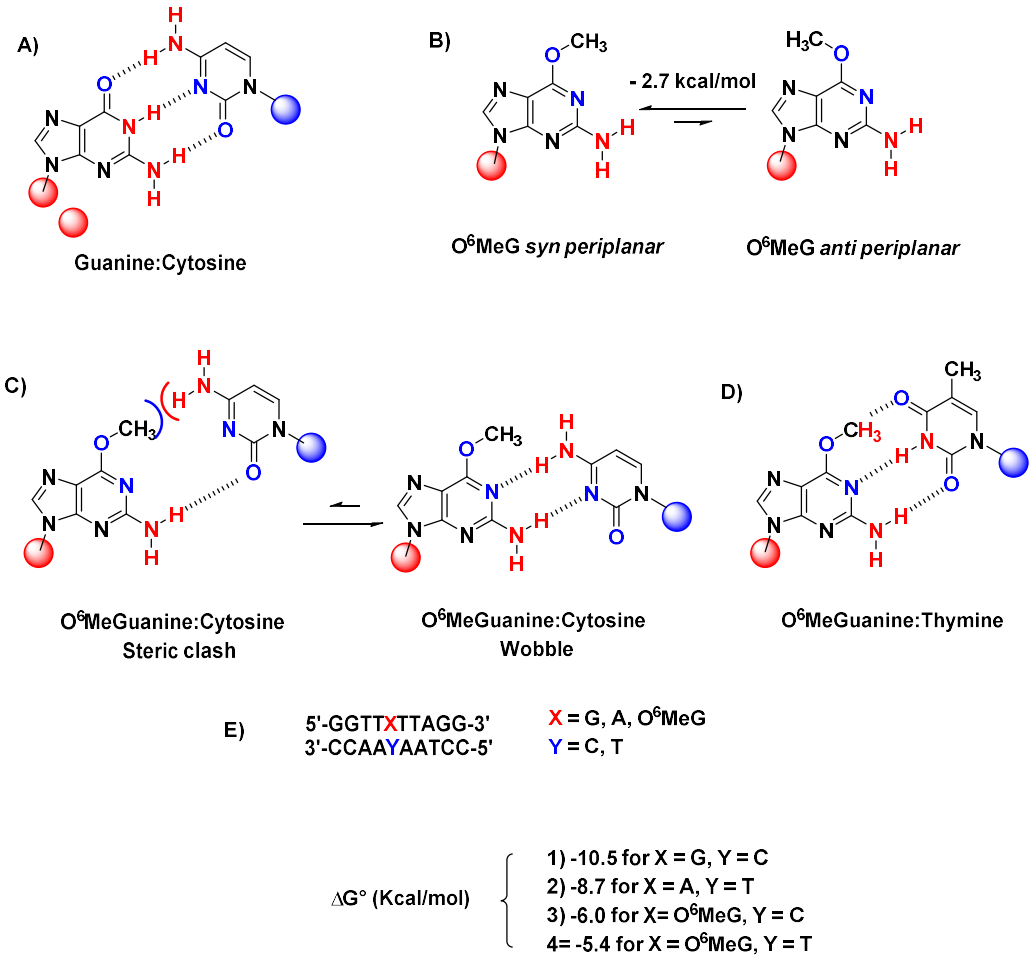

Figure 2 Implications of the formation of O^{6}MeGuanine by TMZ in the DNA nucleobases **A)** Hydrogen bond pattern for Guanine:Cytosine **B)** Conformers after addition of the methyl group at position 6 of Guanine, hydrogen bond formation for **C)** O^{6}MeGuanine:Cytosine and **D)** O^{6}MeGuanine:Thymine pairs. Colors in blue and red depict groups that can act as hydrogen bond acceptors and donors respectively **E)** sequence and ΔG° values for the DNA surrogate in 10 mM sodium phosphate, 0.1 mM Na_2EDTA, and 0.1 M NaCl buffer, pH 7.0 [11]

With these reasons taken into account, the increase in lipophillicity and the new HB formation pattern, it could be explained why during replication of the DNA, a low-fidelity polymerase called trans-lesion synthesis polymerase (TLS) inserts a Thymine (T) facing the O^{6}MeG nucleobase creating an O^{6}MeG:T mismatch. By the employment of a high-fidelity polymerase like the *Bacillus stearothermophillus* DNA polymerase I large fragment, researchers have been able to crystallize the O^{6}Me:T base pair in the active site of the polymerase. Here they observed that in this base pair the methyl group points towards the oxygen and that a weak electrostatic interaction exists between the O-methyl protons and the carbonyl group of the thymine. This interaction resembles a canonical Watson-Crick base pair (**Figure 2D**)[12] that is thermodynamically slightly less stable than the O^{6}MeG:C pair by 0.6 kcal/mol

(**Figure 2E**).[11,13] This less stable mismatch (O^6MeG:T *vs.* G:C, + 5.1 kcal/mol) resembles the G:T mismatch, a reason why is recognized by the heterodimeric complex MUTSα, comprised by the MSH2 and MSH6 proteins of the MMR system. Once the mismatch is found by the heterodimer, a nick on the DNA takes place, followed by the recruitment of an exonuclease Exo 1 which removes around 150 nucleotides (nt) surrounding the lesion. The gap is then filled by the polymerase Pol δ and the nick sealed by DNA Lig I.[14,15] However, Pol δ inserts once again a T opposite to the persisting O^6MeG residue, and this futile removal/insertion cycle is repeated and stalls the replication cycle in the G_2/M phase (**Figure 3**).[5,15] Once there is a block in the replication fork, apoptosis *via* ataxia telangiectasia and Rad3-related protein (ATR) signaling can be triggered ending up in cell death. Also, a double strand DNA break (DSB) could occur having two possibilities: either apoptosis and cell death or the repair of the DSB with mutations on the DNA content (**Figure 5,** page 11). As well, TMZ can have an effect that cannot lead directly to death that is the survival via the TLS surpassing at expenses of DNA content's modification.[15]

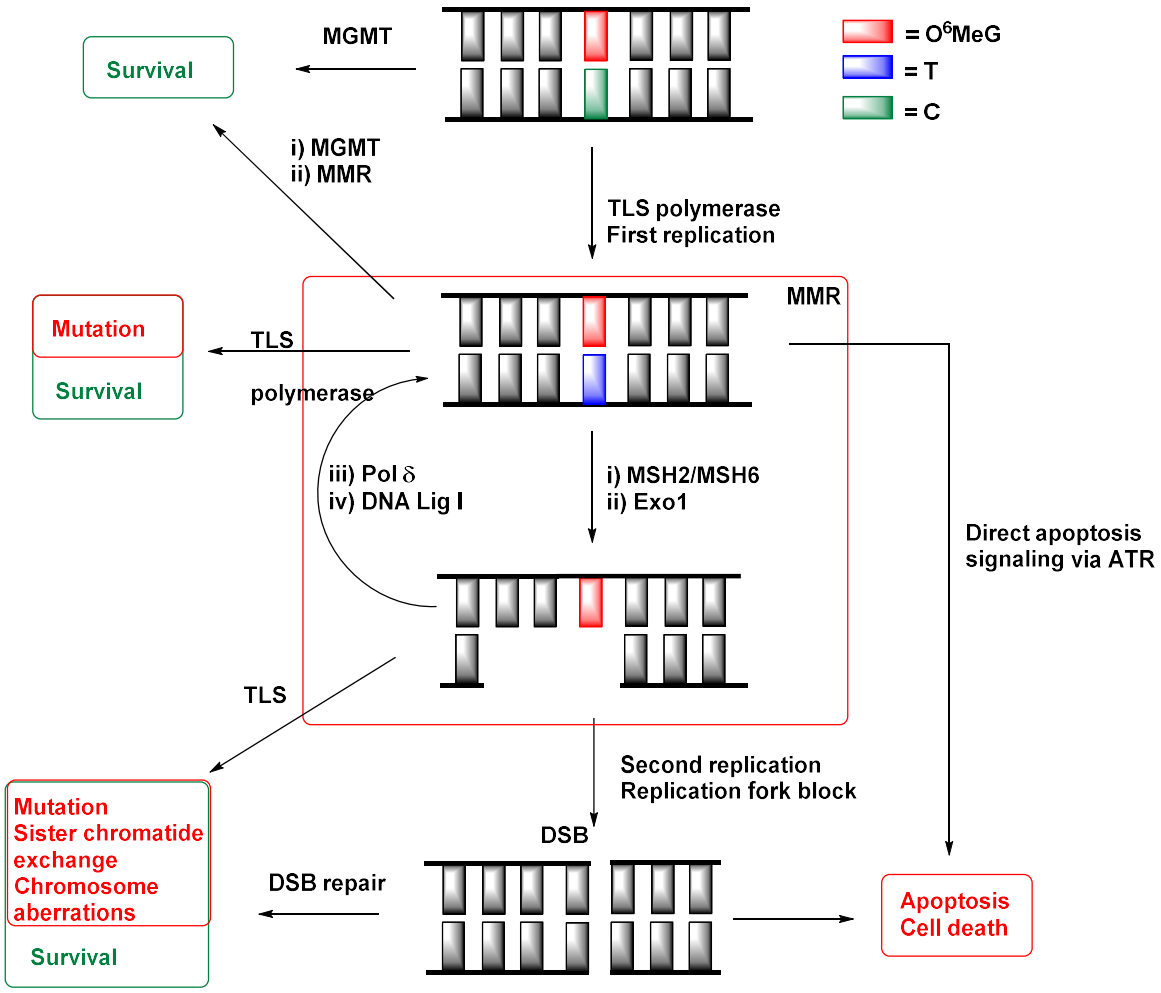

Figure 3 Representative scheme of the MMR and MGMT repair

1.2.3 N^3MeA, N^7MeA and the Base Excision Repair (BER) system

The BER system acts in consequence of the modifications created by the alkylating agents on the nucleobases with the exception of O^6MeG. In this case, N^7MeG and N^3MeA adducts are repaired with the enzymes involved in it (**Figure 4**). The former modification is not mutagenic or cytotoxic by itself but it rapidly and spontaneously depurinates to give a DNA apurinic site (AP site), which is also the same product of the reaction between the N^3MeA nucleobase and the alkyladenineglycosilase (AAG) enzyme that cleaves the bond between the N^9 position of the adenine and the C-1 carbon of the deoxyribose sugar (**Figure 4A**). This AP site is recognized by the apurinic-apyrimidinic endonuclease 1 (APE1), which creates a nick on the DNA backbone by cleaving the sugar-phosphate bond.

This single strand break (SSB) is repaired by two similar ways differing by the number of nucleotides involved. In both ways, the lesion is first recognized by the poly(ADP-ribose)polymerase 1 (PARP-1) complex. In the short patch BER, Pol-β removes the deoxysugar moiety leaving a phosphate group on the 5' end of the gap, which is the substrate of the same enzyme that re-inserts a new nucleotide. To seal the nick, the joint action of the X-ray cross-complementing protein (XRCC1)/DNA Lig III complex takes place to re-establish the dsDNA. For the long patch BER, the DNA can be the substrate of two different DNA polymerases like the Pol ε or the Pol γ that remove the nucleotides (2-10 nt) in the damaged strand leaving a gap, which then is filled by new nucleotides creating a single flap stand. To conclude, the flap is excised by the action of the proliferating cell nuclear antigenic (PCNA), flap endonuclease (FEN1) and DNA Lig I complex action seal the nick and restore the dsDNA (**Figure 4B**). [9,14,16]

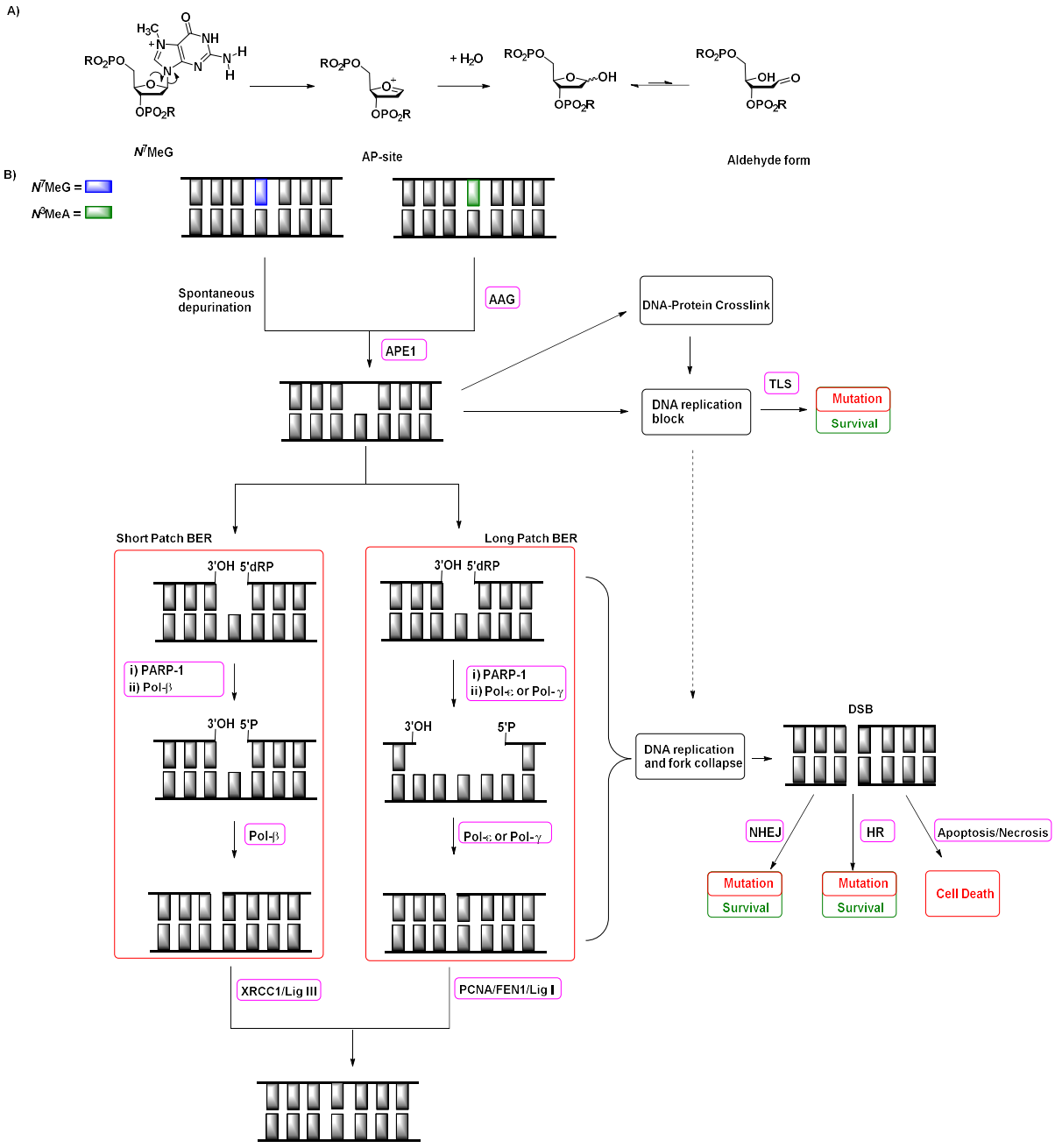

Figure 4A) Spontaneous depurination of N^7MeG and formation of the AP site and **B)** Base Excision Repair pathway in DNA monoalkylated nucleobases

As it can be observed this repair pathway involves several enzymes and intermediates in the process to achieve to a fully repaired dsDNA. It has been demonstrated that the intermediates that belong to this cascade can be more toxic than the original products like N^7MeG or N^3MeA. That is why a tight regulation of the cascade is needed. For example, the AP site, if not rapidly resolved, can block the DNA replication fork or it can react with a protein creating a DNA protein crosslink that leads to the same effect. [9,14,16] This blockage can be surpassed (if there is no crosslink) by the use of TLS polymerase that allow the cell to escape from the blockage by inserting nucleotides with less accuracy than normal

ones. In this case, the cell survives but at expenses of incorporating wrong nucleotides that may mutate the DNA content in the damaged lesion. In the case that TLS action does not take place, the fork can collapse leading to the most toxic DNA lesion, the DSB (**Figure 4B**).

Once a DSB formed among the DNA, kinases from the DNA damage signaling pathway (ATM, ATR) are recruited at the damage site and then phosphorylate an histone called H2AX into γH2AX, which helps to the recruitiment of many DNA damage response factors. The DSB can be repaired by three different ways according to the literature (**Figure 5**).[3–5] In the non homologous end joining (NHEJ) system, the cleaved ends are stabilized by the Ku70/Ku80 complex that binds and stabilizes the DSB, preventing a resection in the DNA ends. According to whether the ends are compatible or not, they can be ligated by the action of the Pol γ or DNA Lig IV. In the microhomology mediated end joining (MMEJ), the system uses sequences of microhomology (2-50 nt) to anneal the complementary strands. To be annealed the conjoint action of the MRE11-RAD50-NBS1 (MRN) plus PARP-1 complex leads to the resection of the flanking regions next to the lesion in what is called a flap trimming. Then nucleotides are added by action of the Pol θ and the nick is sealed by the action of the (XRCC1)/DNA Lig III complex. In the case of the homologous recombination (HR), the term "scarless resolution" has been coined since the cell uses the sister chromatid as a template to repair the damaged DNA. Here, the cleaved DNA is stabilized by the MRN complex, which amplifies γH2AX signaling. After that, a removal of about 300 nt is done in a 3' to 5' direction, followed by an invasion of the sister chromatid which is used as a template for synthesizing the new ssDNA. In the first two cases (MMEJ and NHEJ), the cell can survive but since there is a trimming on the DNA length, the information loss can lead to mutations if the damaged *loci* contain relevant information. For the HR recombination, there is not shortening on the length but the original information can be mutated since the template used is the sister chromatid and the newly synthesized DNA fragment could contain information from the other allele. Finally, another non-resolving path for the DSB exists, and it happens once the caused damage is high and the cell cannot cope with such event. Here the cell dies either via the programmed cell death called apoptosis or by simple necrosis (**Figure 4B**).[14,17,18]

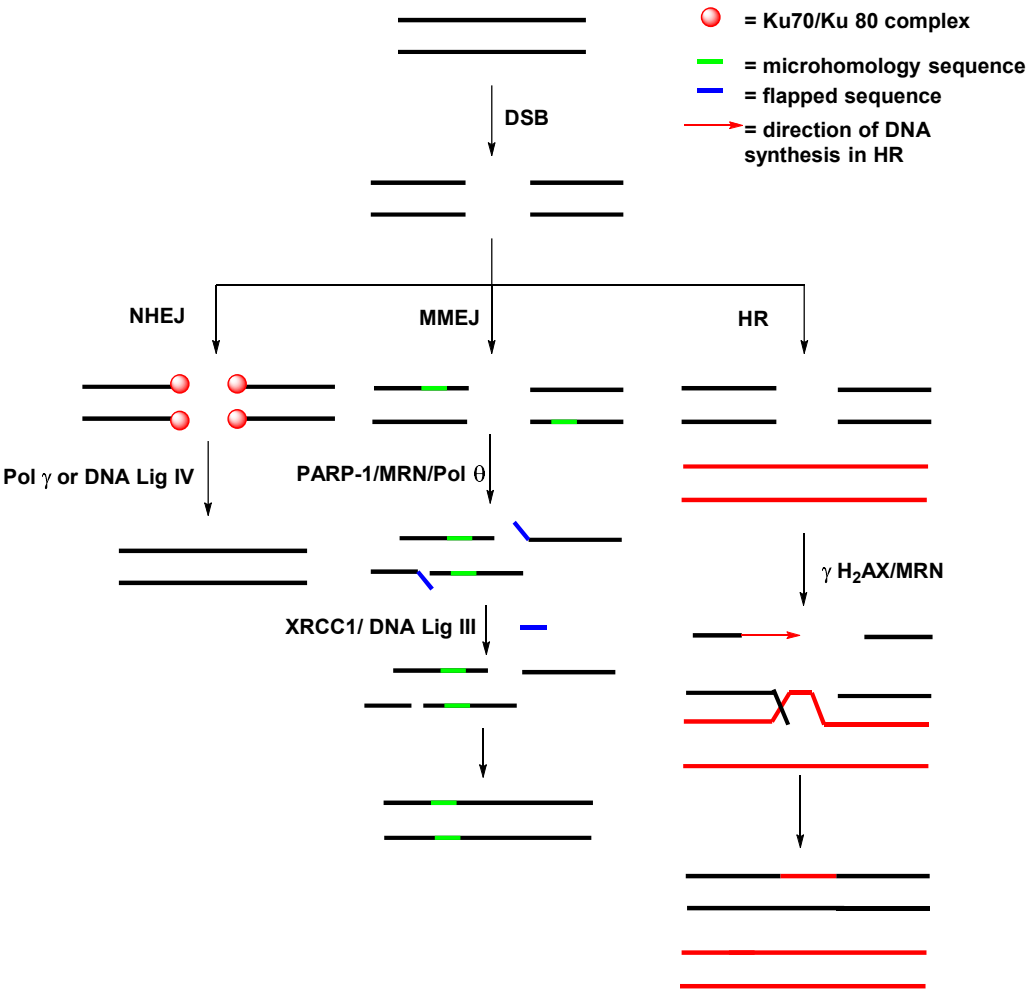

Figure 5 Simplified repair pathways of a DSB by the NHEJ, MMEJ or HR

1.3 Chemotherapy using other alkylating agents

There is no currently second-line treatment for recurrent GBM patients developped so far. One of the alternatives to TMZ has been the use of nitrosourea-derived chloroethylating agents like Nimustine (ACNU), Carmustine (BCNU) or Lomustine (CCNU) which have been used in other cancers like lymphoma or melanoma (**Chart 1A**).[15] These nitrosourea derivatives act also as monoalkylating agents but in this case transferring a chlorethyl moiety to the O^6 of the G nucleobase. This adducts rapidly reacts with the N^1 of the G that reacts with the N^4 of the opposite C forming a very toxic intrastrand crosslink (ICL) with DNA or with a protein (PCL) leading to similar effects than TMZ (**Chart 1B**).

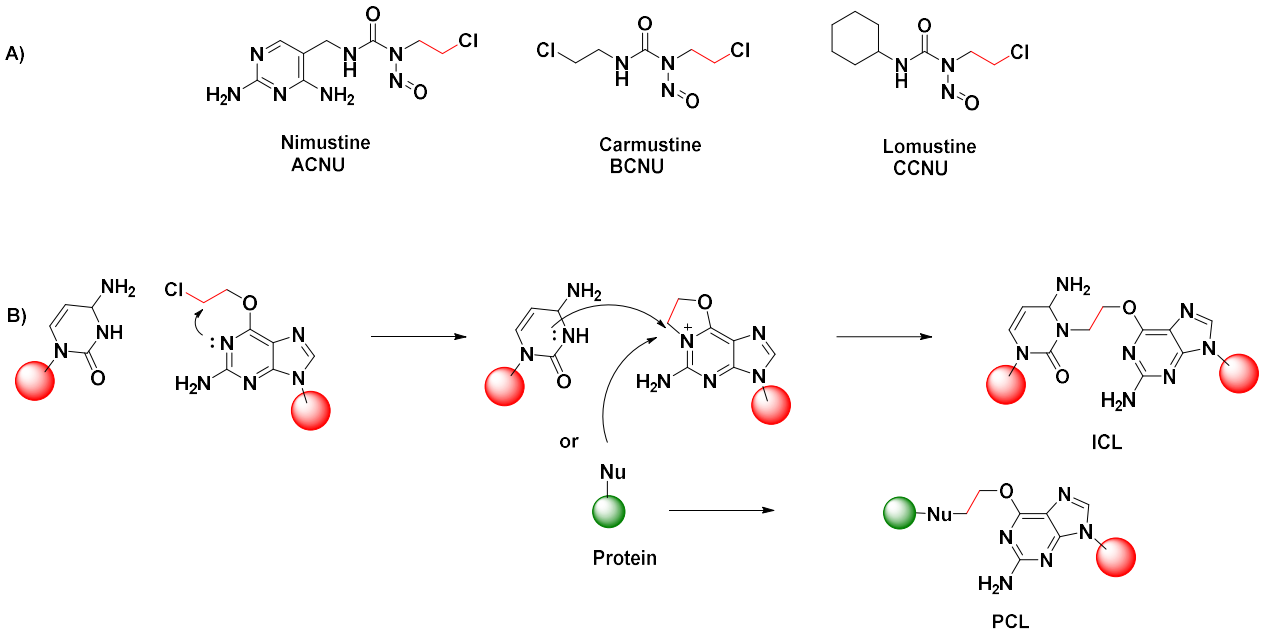

Chart 1 Structure of alternative alkylating agents **A)** Nimustine, Carbmustine and Lomustine and **B)** Mechanism of DNA interstrand cross-linking (ICL) or protein cross-linking (PCL)

1.4 Resistance to TMZ in GBM

As it has been mentioned, O^6MeG is the most toxic TMZ product since its highly cytotoxic effects can lead to cell death and to the reduction of the glioma. However, almost 50% of the patients that receive TMZ show refractivity towards this treatment, especially upon prolonged treatment. To understand the causes, the resistance mechanisms can be classified according to if they are MGMT-dependent or independent.

1.4.1 MGMT dependent resistance

The methyl group from the O^6MeG nucleobase is removed by the O^6-methylguanine-DNA methyltransferase (MGMT) enzyme which is an ubiquitous 21 kDa nuclear protein.[19] It is thought that the MSHα complex recruits to the lesion site the MGMT enzyme that then binds DNA cooperatively and scans DNA in a 5' to 3' direction to find the mispair. The mechanism has been suggested as a four step event (**Figure 6A**)[20] First, the enzyme binds the DNA where an helix turn helix (HTH) motif interacts with the minor groove of the DNA. Second, the residue Tyr114 interacts with the 3' phosphate of the modified nucleotide, pushing the phosphate inwards the strand, whereas the Arg135, stacks in between the bases. These two actions help to flip out the O^6MeG from the DNA, whose place is occupied by the Arg135 that forms hydrogen bonds with the opposite C. By this mechanism, the O^6MeG residue is placed in the active site of MGMT. Once in place, the Cys145 and

Val148 carbonyl group accept the hydrogens from the exocyclic amine (position 2 of the guanine) whereas the OH of Tyr114 and the *NH* of Ser135 donate hydrogens to the N^3 and the O^6 of the guanine respectively. Once stabilized, a catalytic triad is formed by the Glu172, His146 and Cys145 residues to form a thiolate in the presence of water. The anion then attacks methyl group of the O^6MeG from its opposite site through a S_N2 mechanism, removing irreversibly the CH_3 and restoring the original G in the third step (**Figure 6B**). Finally, the MGMT.DNA complex dissociates and the alkylated MGMT protein is degradated by proteolysis. An important feature to highlight about this enzyme is that is an unique "one-shot" or "suicide" system used to repair DNA damage within the cell. In fact, MGMT also recognizes, binds and flips out G residues from DNA, but the selectivity of MGMT towards its substrate (O^6MeG) is based not on shape complementary but on the specific reactivity of the Cys group with the methyl substrate. [5,7,15,21,22]

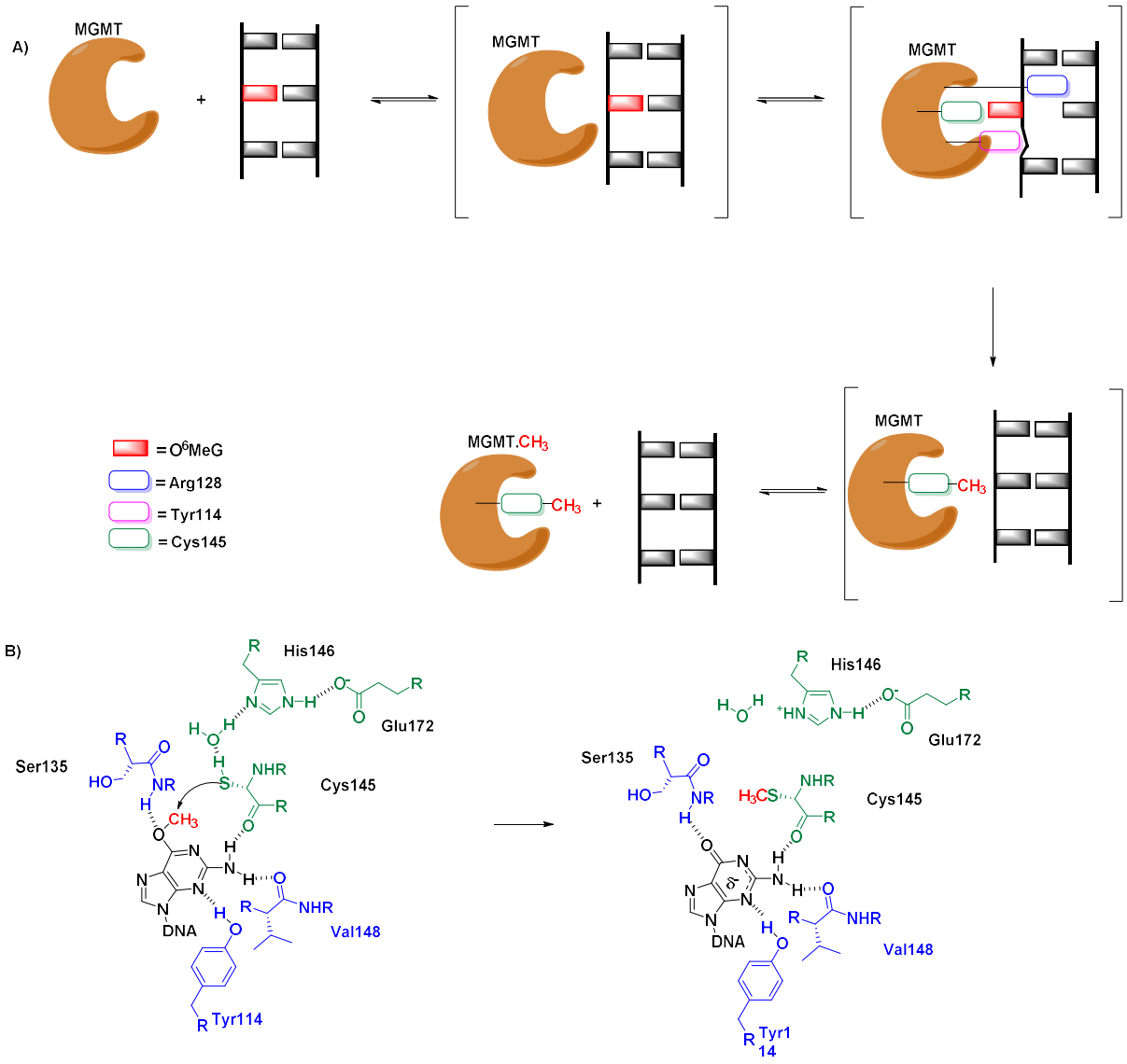

Figure 6A) Four-step reaction for and **B)** Representation of the MGMT active site

It has been shown that MGMT expression changes according to the organ, the tissue, the type of cancer (brain tumour included) and even within the same tumour and that this expression is regulated by several factors.[7,23–25]

Considering that the removal of the methyl group in the O^6MeG restores the original G mediated by MGMT, it is not unexpected to observe that patients with elevated activity of MGMT in tumor do not respond to TMZ treatment.

The MGMT gene is found on the chromosome 10, q26.3 region and the most important epigenetic regulation mechanism corresponds to methylation on the CpG islands of the promoter region. On one hand the methylation of these islands, especially in the -249 to -103 and +107 to +196 clusters, alters the packing of the DNA impeding the access to the transcription machinery therefore for the MGMT expression obtaining cells sensitive to TMZ. On the other hand, low methylation of the promoter can lead to MGMT expression and TMZ resistance, being this the explanation why stratification of patients according to the level of promoter methylation is currently being suggested for TMZ treatment.

It has been found that in recurrent groups of GBM patients treated with RT + TMZ (or the second line alkylating agents ACNU, BCNU or CCNU, see **Section 1.5.2** page 22) the MGMT activity of cells was higher than in primary GBM cancers in contrast to patients that only received RT.[25] But it also has been observed that the exposure to TMZ does not changes the level of promoter methylation in patients. Due to this, the resistance or the higher levels of MGMT expression can be attributed either to other factors that regulate the expression of the MGMT gene besides promoter methylation or because there is a chemo selection of natural TMZ-resistant glioma cells in detriment of sensitive ones.[25]

In addition to promoter methylation, MGMT expression can be modulated by several factors like the different expression levels of transcription factors or also because of the tumor microenvironment, all of them that can lead to a high plasticity on the protein expression.[22] Among the transcription factors that can interact with the MGMT promoter, we find NF-kB, CEBP, AP-1 or the Sp1 which it has been shown to be associated with the p53 protein. [24,26] In the case of microenvironment, one important factor to consider is the amount of O_2 present in the cancer. Since cancers are known to develop in hypoxic conditions, the upregulation of the hypoxia inducible factor 1α (HIF-1α) could regulate promoter MGMT expression, and this could explain why in the inner core of the tumor where there is less oxygen MGMT expression is higher than in the outside core in glioma patients.[24] Another pathways to regulate the gene expression are the modification of the lysines in the histones H3 and H4 by acetylation, an event that unpacks DNA allowing MGMT transcription. In addition the residues can be methylated in the H3 histone, a process that leads to gene silencing.[22,24]

Regarding the naturally resistant cancer cells the concept of glioblastoma stem cells (GSC) appears. These are cells that inside the tumor microenvironment can self-replicate, differentiate and acquire radio and chemoresistance by having, for example, higher levels of MGMT protein. In this case the TMZ-resistant cells are chemo-selected rendering TMZ ineffective.[22,27]

1.4.2 Non-MGMT-dependent resistance

Taking into account the fact that TMZ needs an active MMR system to generate DNA damage through O^6MeG formation (**Figure 3,** page 7), the hypothesis of a dysfunctional MMR system that could lead to TMZ resistance has been analyzed in other types of cancer such as: gastric, endometrial or colorectal.[5,15] Nevertheless, it has been noted that the survival of patients with glioblastoma or astrocytomas that presented a lower expression of MSH6 protein was unchanged in comparison with patients with normal MSH6 expression. An explanation formulated to this lack of resistance towards TMZ may be the fact that even if a dysfunction on MMR system will lead to resistance or TMZ inactivity, the very same lack of MMR can also lead to mutations that can be deleterious for the cell (**Figure 3**).[28] Besides, intrinsic resistance could be associated with GSC with different levels of expressions of drug pumps efflux that can expel the drug out of the cell.[29,30]

It has been demonstrated that TMZ can trigger autophagy in GBM cells *via* ATM/AMPK pathway after DNA damage. By definition autophagy is a cytoprotective mechanism that the cell uses to regulate homeostasis in severe conditions such as hypoxia, lack of nutrients or DNA damage. In this scenario, the cell targets and degrades damaged or aberrant organelles in order to maintain its internal balance. In GBM the importance of this phenomena has been demonstrated when several autophagy modulators were used that for example increased TMZ-induced apoptosis.[31] Nevertheless experts have cast doubt on the role of autophagy in cancerous cells because according to them, there is a thin line between the pathways that promote apoptosis and autophagy, since one pathway leads to cell death whereas the other one leads to survival.

There is another key pathway related with TMZ resistance that is associated with the mutation in the receptor tyrosine kinases (RTK) especially the EFGR receptor which is overexpressed in GBM.[22,24,27] Once EFGR cascade is activated two sub pathways appear, one related to PI3K/Akt pathway and the other to the MAPK/Erk pathway. In summary, these processes leads to the inhibition of the pyruvate dehydrogenase kinase 1 (PDK1) therefore modifying the obtention of energy from a glycolytic pathway instead of the oxidative phosphorylation in a process that is known as Warburg Effect. As well, it can activate HIF-α and heat shock proteins that activate the vascular endothelial growth factor (VEGF)

increasing the angiogenesis in hypoxic conditions or for example stimulating the NF-κB production increasing the survival properties.[31]

Finally, another very important mechanism of resistance in cancer and especially in glioblastoma is related with the protein p53. This macromolecule is a very important tumor suppressor factor that plays a key role regarding cellular processes like apoptosis, cell metabolism, genome integrity or angiogenesis. The p53 gene is one of the most de-regulated genes in cancer and this de-regulation is found in 84% of GBM patients. The absence of p53 protein, either by deletion, mutation or lower expression of the gene forbids cells to arrest cell cycle, go into apoptosis or into senescence, enabling tumor growth and disease propagation.[32]

1.5 Overcoming-TMZ resistance using auxiliary chemotherapy in GBM

1.5.1 Chemotherapy targeting DNA repair systems

As stated in the previous paragraphs, the difficulties presented by the GBM tumor itself like multiple resistance factors, rapid proliferation, high infiltration and the fact that the tumor is located in a highly sensitive area like the brain make the tratment of this disease rather difficult. Nevertheless, many attempts that go from early stage drug discoveries to clinical trials have been performed as mono or combined therapy (**Figure 7**).

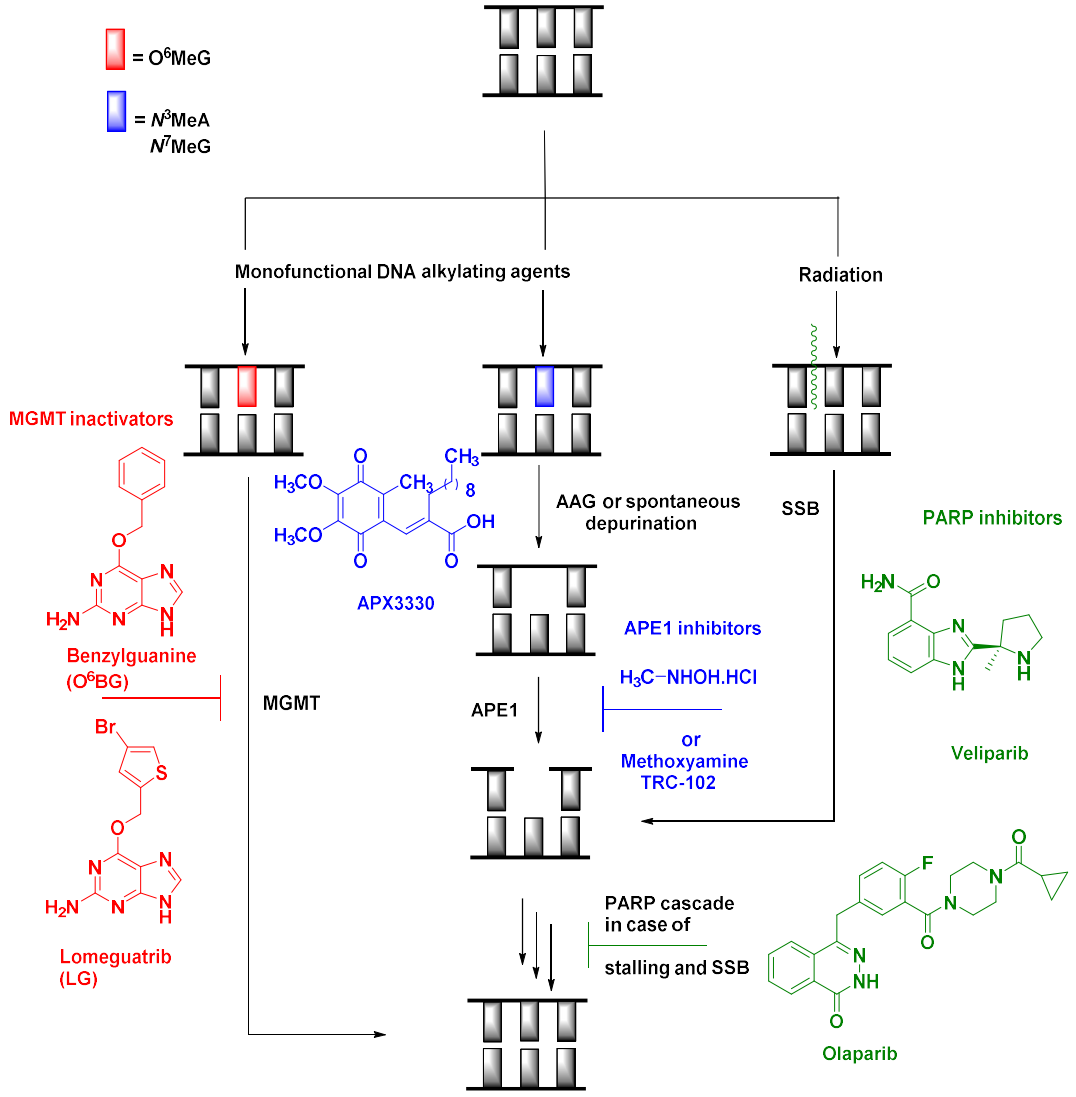

Figure 7 Schematic representation of the DNA repair pathways involved into chemoresistance and molecules developed and tested in clinical trials for resistant GBM and their respective inhibition sites. Red, blue and green highlighted molecules correspond to MGMT, APE1 and PARP systems inhibitors respectively

1.5.1.1 MGMT inactivation

In consideration of the well-known role of MGMT contribution to TMZ resistance, direct or so-called suicide MGMT inhibitors have been developed in the last 30 years based on the O^6MeG structure. Here, also helped by *in silico* methods, QSAR analysis has been performed to understand and determine which are the most important modifications that can be done in order to increase MGMT inactivation (**Chart 2A** and **Figure 7**).[33]

A)

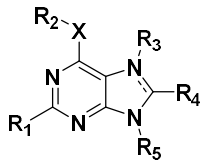

R_1 = OH, F, NHAc, $NHCH_3$, $NHCOCOH_3$, $N(CH_3)_2$, H

X = O, S

With X = O, R_2 = allyl, Bn, 4-Halo-Bn, 3-CH_2NH_2Bn, 2-CH_2NH_2Bn, -(CH_2)-4-Br-2-thiophene, -(CH_2)-3-F-4-pyridine, Ph, void

R_3 = CH_3, $CH_2COCH_2CH_3$, $CHCO_2Na$, CH_2CN, $CH_2CH(OH)CH_2CH_3$, Bn

R_4 = NH_2, CH_3, OH, CF_3, Br

R_5 = 2-deoxyribose, ribose, $(\beta$-D-glucose$)_8$, $CH_2CH(OH)CH_2CH_3$, CH_2CO_2Na

B)

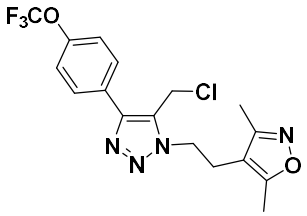

AA-CW236

C)

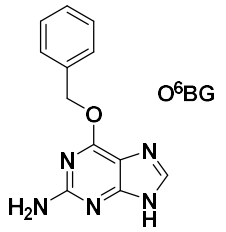

O^6BG

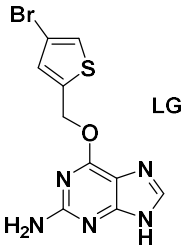

LG

D)

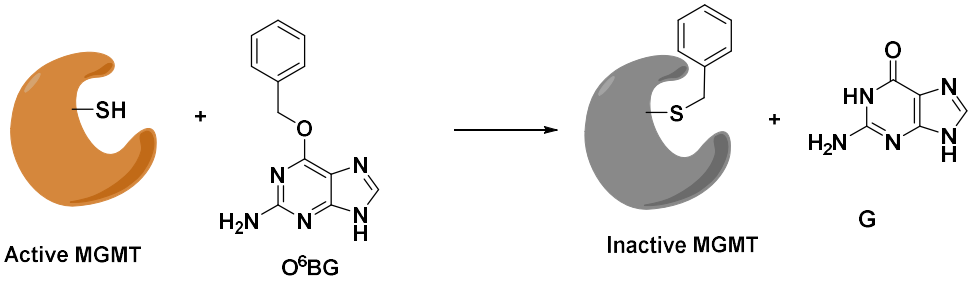

Chart 2A) Generic structure for MGMT suicide inhibitors. Colors in red and green depict changes where activity against MGMT can be abolished or maintained respectively in comparison with O^6MeG as substrate. **B)** Structure of a non-canonical MGMT inactivators **C)** Structure of MGMT inactivators that reached clinical trials **D)** Representation of inactivation of MGMT by O^6BG.

There are five modifications in the O^6MeG core that alter the MGMT inactivation capacity (**Chart 2A**). First of all, the elimination of the 2-exocyclic aminogroup (R_1 = H, F, OH) or its substitution (R_1 = NHAc, $NHCH_3$, $N(CH_3)_2$) diminish the activity or renders compounds inactive since the hydrogen bonds between this group and Cys145 and Val148 are lost.[34,35] Secondly, the change of the O by a S substituent in the position 6 also eliminates the activity since a hydrogen bond with the Ser135 of the

active site needs to be formed.[35] Thirdly, due to a steric hindrance to the Cys residue, all the substituents in the position N^7 (R_3) except for a methyl group abolish the MGMT activity.[35]
In the case of modifications that maintain or increase the MGMT activity, researchers found that for the C_8 (R_4) position small substituents like Br, CH_3, CF_3, OH and NH_2 can still fit in the active site and interact with and inactivate the enzyme.[33,34] Nevertheless, the most studied and extended analogues were achieved by modifying the groups in the position O^6 of the ring (R_2) and on the N^9 of the guanine (R_5).[29,35–40] In the case of the R_2 substituent, methyl and allyl groups have been tested but due to the kind of reaction, methylenaromatic groups like benzyl, 2-methylenpyridine or 2-methylenthiophene have been shown to be the better inactivators since these types of moieties are better substrates for a S_N2 reaction. For R_5 modification, substituents are also able to inactivate the enzyme although less efficiently when R_5 = H. There is no clear tendency regarding size and it seems that negatively charged substituents completely eliminate the capacity of inactivation. Finally but less interesting in the context of the Thesis, elimination of the 1,3-imidazole ring abolish the compounds activity as shown for bypyrimidine and triazine rings, however the exchange of 1,3-imidazole by triazoles, oxadiazoles, thiadiazoles, 1,2-imidazole or 1,4-bypyridine ring maintains their activity.[34,41,42]

There are not many non-O^6MeG analogues that inhibit MGMT described in the literature. To our knowledge, compound AA-CW236 (**Chart 2B**) is the only non-pseudosubstrate molecule described. It consist on a triazole moiety that bears a chloromethyl group that reacts with the Cys of MGMT by inactivating it. By profiling on a large panel of proteins, researchers demonstrate the selectivity of AA-CW236 towards MGMT *in vitro* and *in cellulo*.[43]

Two O^6MeG analogues called O^6Benzylguanine (O^6BG) and Lomeguatrib (LG) were shown to be excellent MGMT inhibitors *in vitro*, in cellular extracts, *in celullo* and in xenografts (**Chart 2C**). They also proved to enhance the alkylating effect of TMZ for several types of cancers like colon, melanoma, brain, breast or ovarian (**Figure 7**).[29,34–36,38–40,44] Due to these reasons, these two drugs reached clinical trials and were tested in combination with TMZ. For O^6BG and TMZ, a 28-days cycle Phase II clinical trial in glioma patients was carried. Here, O^6BG was administered as an infusion for 1 h at 120 mg/m^2, followed by a continuous infusion for 48 h at 30 mg/m^2 per day dose. The TMZ was orally administered right after the first hour of O^6BG infusion at a 472 mg/m^2 dose, a regime that permitted to deplete MGMT for 48 h. However, since the combination of the MGMT inhibitor plus TMZ showed high levels of myelosupression in bone marrow cells, the amounts of TMZ needed to be reduced up to 50% rendering to no restoration in the TMZ sensitivity for GBM patients without improving the actual treatment in comparison with TMZ alone.[45] [45]

In the case of LG, a Phase I study of patients with several solid tumors including glioma was performed. For this clinical trial LG was dosed at 20 to 120 mg/m^2 orally 12 h prior tumor resection and researchers observed that even if the MGMT depletion was achieved in 12 h, the very same expression was restored after 24 h.[40] The combination therapy was tested in a Phase II clinical trial dosing orally 40 mg of LG plus TMZ up to 200 mg/m^2 orally for 5 consecutive days every 4 weeks in melanoma cancers.[46] In addition a Phase I clinical trial with a similar regime was carried on melanoma patients where they used a TMZ surrogate called Dacarbazine.[39] Unfortunately, none of these clinical trials showed a better improvement on the current state of the treatment, where it was also highlighted the toxicity in bone marrow cells generated by the combination of the alkylating agent and TMZ and LG.

1.5.1.2 Chemotherapy strategies that exploit other DNA repair systems

Since TMZ damage involves other repair system like BER (**Figure 4,** page 9), inhibition of the enzymes that form this defence mechanism can be considered as an attractive target.

One of the validated targets of the BER pathway has been the APE1 enzyme inhibited by the use of methoxyamine (TRC-102, **Figure 7,** page 17). In this case, the type of inhibition is an indirect one since the methoxyamine reacts with the open form of the AP site forming a Schiff base that cannot be recognized by the APE1 enzyme. Due to this unrecognition of the AP site by APE1 and accumulation of toxic intermediates in the pathway that cannot be resolved by the enzymatic cascade, the deletereous effects mentioned above take place (**Figure 4**). Regarding this small molecule, a Phase I clinical trial using TMZ plus TRC-102 was carried out on a cohort of several solid tumours like: breast, lung, ovarian, melanoma or colorectal. In this trial, they determine the recommend the use of 150 mg/m^2 of methoxyamine intravenously on day one of treatment, followed by orally TMZ 200 mg/m^2 daily in five days on a total of 28-day treatment with no toxicity for the patients. Even if there were no brain tumours patients in this assay,[49,50] the results may be auspicious thinking on the current Phase II clinical trial that is being carried on GBM patients (NCT02395692). A second example of exploiting the BER system is via the direct inhibition of APE1 by APX3330. [51] The tolerability of this molecule is being currently tested in Phase I (NCT03375086) clinical trial for solid tumours. Even if no combination with TMZ is being carried so far, a positive result could make consider this drug use in combination for GBM treatment.

A second alternative to take advantage of the toxic intermediates created by this system is the inhibition of PARP-1 enzyme, the most studied of the 18 PARP enzyme family.[52,53] This enzyme senses

the SSB in DNA caused by TMZ or radiation among other events. Once its activated, the catalytic domain starts the poly(ADP) ribose transfer to its automodification domain, releasing the repairment cascade.[54] Inhibition of the PARP-1 enzyme, can force the DSB formation causing the effects previously mentioned (**Figure 4** and **Figure 5,** pages 9 and 11). Due to a higher overexpression in tumors, several PARP-1 inhibitors like Veliparib, or Olaparib (**Figure 7**) have been synthesized and assayed to restore TMZ sensisitvity in several cancer lines such as: ovarian, prostate, breast or brain cancer with the goal of exploiting the toxic intermediates of the BER system, although some investigation have cast on doubt regarding the real role in the BER system for PARP-1.[52,53,55] In a Phase I/II study in patients with pediatric glioma Veliparib has been used in combination with TMZ on a 28-days regime. The PARP-1 inhibitor has been orally dosed on the first day at 25 mg/m^2 before radiation together with TMZ 135 mg/m^2 for five days in a row until the cycle was repeated. In this study they observed no toxicity of the combination at these doses but they stated there is no improvement on the survival with TMZ alone since the one year OS of patients receiving combined therapy was 37% compared to 46% of the monotherapy alone.[56] Unfortunately a similar result was observed for a Phase II recurrent GBM adult patients,[56] where they used 2 randomized schedules (5 *vs.* 21 days). Veliparib was used on a 40 mg dose, twice a day plus TMZ (150 to 200 mg/m^2) daily on a total of 28 days of trial where the OS was only 4.7 months in both groups. Despite of these disapointing results and due to the evidence that Veliparib can enhance TMZ action when populations are stratified according to MGMT promoter methylation,[57] a Phase II/III clinical trial in newly diagnosed GBM is currently being carried (NCT02152982).

For recurrent GBM patients, a Phase I clinical trial was carried, were they used the combination of Olaparib plus TMZ on an intermitent regime since the neutropenia and thrombocytopenia side effects were observed. Hither a 150 mg daily dose of Olaparib for three days per week was administrated with 75 mg/m^2 per day of TMZ during 42 days after radiation where they observed, even if it was not the goal of the study a 6 months PFS of 39% was noted for the patients where the values range between 18 and 38% for the standar procedure.[58] Based on these results, two other clinical trials are currently being performed. The first one is a Phase I study that studies the combination of TMZ plus Olaparib in newly diagnosed GBM patients, but in this case stratifying the patients according their MGMT promoter methylation (CRUKD/16/010). As second trial is the Phase I/IIa study of Olaparib plus TMZ in adults for unresectable or partially unresectable tumors (NCT03212742).

1.5.2 Chemotherapy in combination using other alyklating agents

As it was introduced before, TMZ is not the only alkylating agent that has been used in cancer treatment (**Chart 2**). Other alternatives using the chloroethylating agents previously mentioned were carried. Unfortunately, the use of systemic BCNU and LG either in adults or childrens in either Phase II or Phase III for melanoma or brain tumor cancers was considered a failure due to the same problems as observed for TMZ plus O^6BG treatment,[48,50,59] namely: myelosupression and the need to reduce the alkylating agent dose that rendered no improvement for the treatment.

As noted, most of recurrent GBM cancers occur two centimeters away from the original resection site, and the myelosupression originated by the systematic combination of the alkylating agents plus the MGMT pseudosubtrate have led to investigate the use of other alternatives to surpass these inconvenients. In that sense, biodegradable BCNU polymer wafer patches (also called Gliadel) have been designed in order to deliver BCNU for two weeks in the tumor area. In this Phase II clinical trial, O^6BG was administered at 120 mg/m^2 over 1 h on day 1 and repeated every 48 h on days 3 and 5. Then a continuous infusion of O^6BG at 30 mg/m^2 per was administered immediately the first O^6BG while BCNU wafers were administrated up to 61.6 mg per patient. Here, they increased the OS from 28 weeks to 50.3 weeks when comparing the wafer alone against the combined therapy. Also, they reduced the toxicity created by the systemic dosage but they noted the increase of hydrocephalus, cerebrofluidospinal fluid (CSF) leak and or CSF/brain infection in comparison with the wafer alone.[60] Last but not least, a Phase III trial was carried out using orally dosed CCNU (100 mg/m^2) on the first day after RT plus TMZ (100 to 200 mg/m^2) per day on days 2 and 6 of the six-week course using a stratified classification of patients according to MGMT promoter methylation status. Surprisingly, the results demonstrated that OS increased from 31.4 months to 48.1 months comparing TMZ alone with the combined therapy.[61]

1.6 Goals of the Thesis

In light of the aforementioned paragraphs and despite the enormous efforts conducted by the international scientific community, no novel approach has been considered successful so far. The multiple resistance factors, the progressive decline in neurologic functions due to the aggressiveness of the treatment, the tumor microenvironment among other aspects render the treatment of GBM rather difficult. Therefore, novel either chemo or immunotherapies, stratification of patients according to the biological markers such as promoter methylation status for a targeted and personalized therapy could be used to render a better prognosis of the disease that can improve life span and quality of patients.

In this Thesis, we explore the design of three novel strategies to inhibit MGMT activity in combination with TMZ for glioma treatment according to the next steps. The first is based on the indirect inhibition strategy that consist on the design of molecules able to interact with the MGMT substrate masking it from the MGMT action. The second one is the MGMT inhibition by the use of hybrid molecules targeting both MGMT active site and DNA. Finally, the photocaged strategy relies on the principle of designing a caged and unactive molecule that upon light irradiation releases an MGMT inhibitor for deactivating the enzyme in a controlled fashion.

In order to carry on these strategies, the following experimental approaches will be performed. These approaches, will be presented in more detail in the following chapters:

A) Synthesis of MGMT inhibitors
B) *In vitro* characterization of the Ligand DNA interaction
C) Studies of their photophysical properties
D) MGMT inhibition assays
E) *In cellulo* evaluation as single agents agains T98G cells
F) *In cellulo* evaluation in combination with TMZ

Chapter 2

Indirect strategy to inhibit MGMT

2 Indirect strategy to inhibit MGMT

2.1 Principle and State of the Art

The "classical" inhibition strategy of an enzyme (E) correspond to the use of a ligand or inhibitor (L) that inhibits the enzyme reducing its activity either for compiting by the access to the active site with the natural substrate (S), or by interacting with the enzyme-substrate (ES) transition state.[62,63] In the indirect inhibition strategy (IIS), also called "substrate targeting" or "substrate masking", the access of E to S is limited by the interaction of the ligand L with the substrate S that "masks" the transformation of S to the product (P). Worth mentioning is that this concept is from the reaction kinetics point of view, indistinguable from the competitive inhibition described by the Michaelis-Menten equation. The idea was firstly described by the Kodadek group where they designed molecules to target peptides that were involved in post translation modification (PTM) and followed by the Kukar group were the target corresponded to interact with γ-secretase modulators that were involved in the anti-inflammatory process in Alzheimer's disease (**Figure 8**).[62,64]

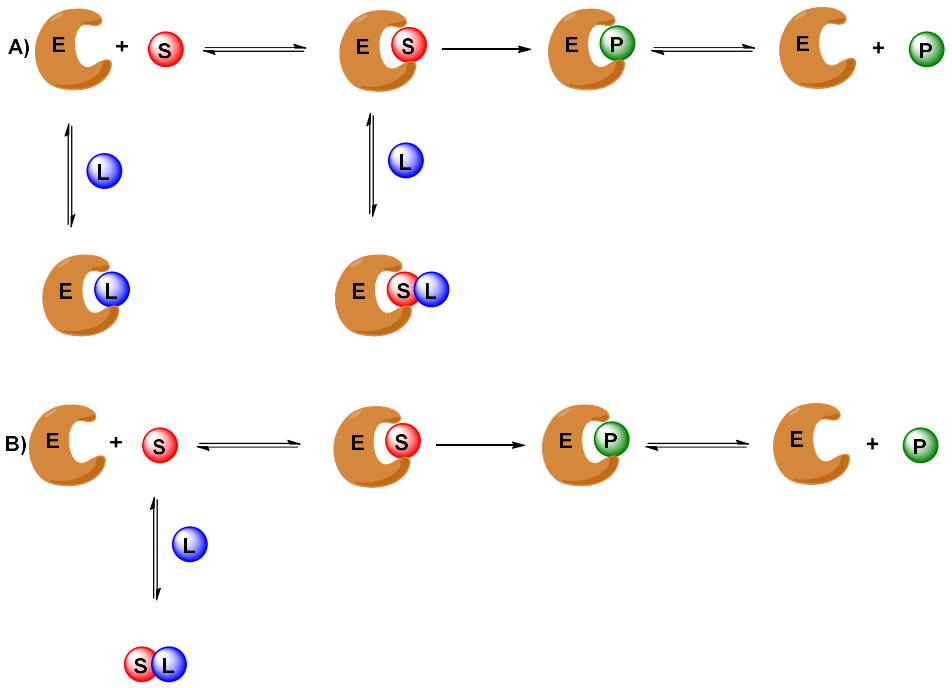

Figure 8 Representative scheme of **A)** classical "competitive" *vs*. **B)** indirect inhibition strategies
E = Enzyme, S = Substrate, L = Ligand, P = Product.

2.1.1 APE1 inhibitors and AP sites-interacting molecules

As it has been mentioned, AP sites can be formed by the action of TMZ over the DNA. One strategy for IIS is to develop compounds able to react with this type of scaffold with the purpose of alter the cascade of BER system. This could lead to the accumulation of the toxic intermediates that forms the system causing the negative consequences already described for the cell. Notably, the best example of the IIS can be found in the BER inhibitor methoxyamine (**Chapter 1**), a molecule that has reached clinical trials for cancer treatment including GBM.[65] This small molecule is able to chemically react with the open form of the AP site forming a covalent bond and then cleaving the DNA (**Figure 7**). A second group of molecules have been explored to non-covalently interact with the AP sites (**Chart 3A**).[66–70] The ligands synthesized consist of hybrid molecules containing a nucleobase (either adenine or 2,6-diaminopurine) that acts as an abasic site recognition scaffold, a positively charged linker that interacts with the negatively charged groups of the phosphate backbone and finally, a 6-chloro-2-methoxyacridine ring that plays the role of a DNA intercalator. The molecules (**69.1**, **69.2** and **69.4**) were tested in L1210 (mouse lymphoma lymphocyte) cell line and in A549 cell line (lung human carcinoma) and they displayed a GI_{50} values after 24 h of incubation of 1.6, > 10 µM and 33 µM for L1210 respectively and 0.1, 0.05 and 10 µM for A549 respectively.[69] For compound **69.4**, the potentiation of the cytotoxicity of the BCNU agent *in cellulo* led researchers to test the validity of the model in mice with P388 leukemia where they observed that the combination of 60 days with 2 mg/kg plus 6 mg/kg of BCNU allowed the mice to survive on a 100% rate in comparison with the non-treated control (or double the survival population compared to BCNU treatment alone). A third family of indirect inhibitors was developed by the Teulade-Fichou team (**Chart 3B**).[71,72] Here, a group of napthalenophanes that work similarly to the molecules mentioned above was developed to target the abasic site, inhibiting APE1 enzyme *in vitro* and having also interesting properties *in cellulo* to inhibit T98G cell line growth.[73] In this case, compounds 2,7-BisNP-O4Me and 2,7-BisNP-S demonstrate a GI_{50} against this cell line of 3.2 and 1.2 µM and both demonstrate to act synergically when combined with TMZ after 96 h of incubation as determined using CompuSyn Software. Finally, an interesting concept for targeting AP sites has been developed by the Teramae group. Even if the molecules have not been used in combination therapy but for detecting single-nucleotide polymorphisms (SNP detection), researchers have explored the possibility to selectively detect the canonical nucleobases facing an AP site. By changing the hydrogen bond acceptor/donor pattern, π-stacking surface and methylation pattern, researchers managed to synthesize molecules that selectively differentiate adenine (Lumazine, diMe Lumazine and Alloxazine),[74–76] cytosine (AND, ATMD, 3-MIX)[77], guanine (Pterin, diMe Pterin)[74,78] and thymine (8-MIX and Lumichrome) residues opposite to AP sites in ds DNA context (**Chart 3C**).[74,77]

A)

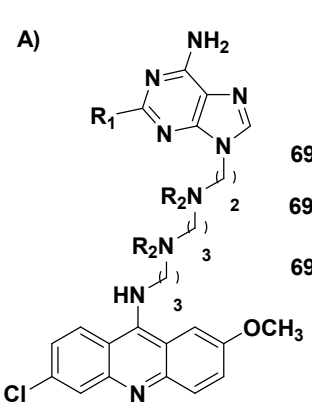

69.1 (R_1 = H, R_2 = H)

69.2 (R_1 = NH_2, R_2 = H)

69.4 (R_1 = H, R_2 = )

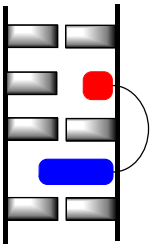

B)

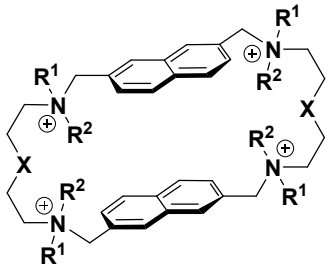

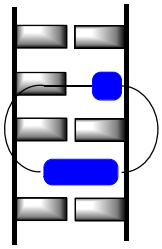

2,7-BisNP-S (R_1 = R_2 = H, X = S)

2,7-BisNP-O4Me (R_1 = R_2 = Me, X = O)

C)

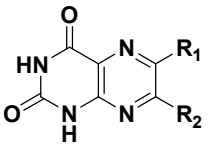

Lumazine (R_1 = R_2 = H)

diMe Lumazine (R_1 = R_2 = CH_3)

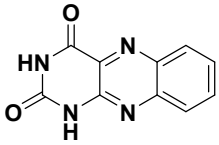

Alloxazine

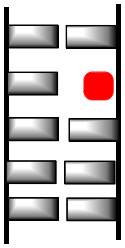

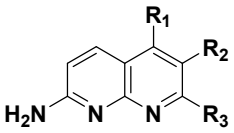

AND (R_1 = R_2 = R_3 = H)

ATMD (R_1 = R_2 = R_3 = CH_3)

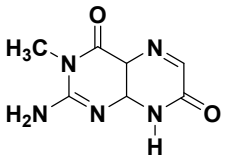

3-MIX

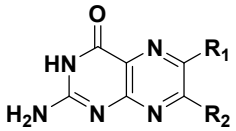

Pterin (R_1 = R_2 = H)

diMe Pterin (R_1 = R_2 = CH_3)

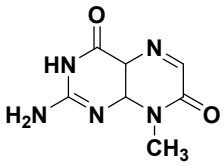

8-MIX

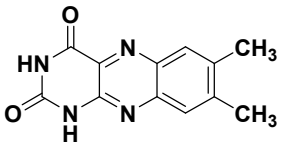

Lumichrome

Chart 3 Small molecules targeting abasic sites designed by the **A)** Lhomme and **B)** Teulade-Fichou group and **C)** by the Teremae group with their corresponding mode of interaction in an AP site

2.1.2 Indirect MGMT inhibition

In the case of MGMT IIS, the concept is quite similar, the goal is to develop a ligand that interacts with a dsDNA bearing O^6MeG selectively in comparison with another type of dsDNA to mask MGMT interaction (**Figure 9**).

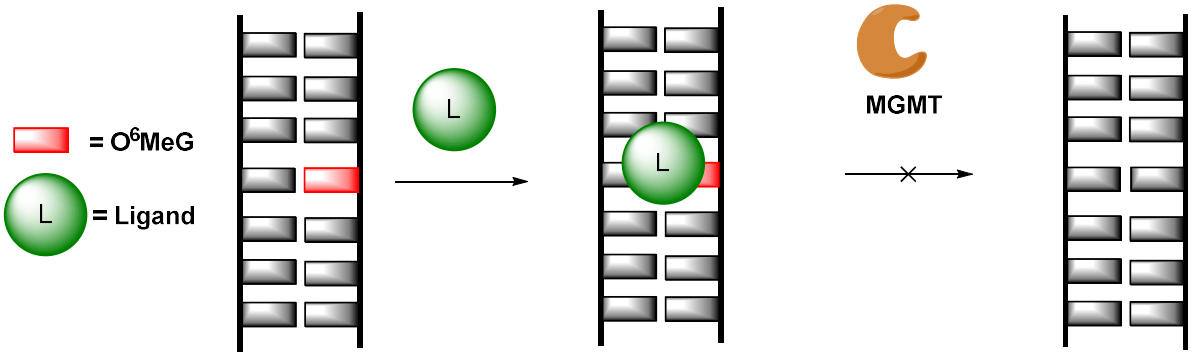

Figure 9 Representative scheme for IIS of MGMT

So far no compound has reached clinical trials however several strategies of indirect MGMT inhibition can be found in the literature. The first one was described by the Luedtke group[79] and relied on two cationic porphyrins called DIGPo**r** and Zn-DIGPor (**Chart 4**). The development of the metalloporphyrin was based on the idea that the metal containing molecule (Zn-DIGPor) could interact with dsDNA bearing an O^6MeG:C pair, extruding mismatched bases from the helix upon interaction, as it was observed for some Ru complexes, impeding the access of it to the active site of the MGMT enzyme.[80] In this article, the researchers demonstrated that both compounds can interact with dsDNA containing either a G or an O^6MeG in its sequence by the use of thiazole orange (TO) displacement assays. They showed that both DIGPor and Zn-DIGPor had a slight preference for the O^6MeG dsDNA instead of the G counterpart (comparing K_i G ds DNA/K_i O^6MeG dsDNA) in a 1.3 and 1.6 ratio for DIGPor and Zn-DIGPor respectively. In agreement with their hypothesis and following what they observed in the TO displacement assays, both compounds managed to inhibit MGMT activity in an enzymatic coupled assay. In this case, compound DIGPor showed EC_{50} = 30 µM whereas for Zn-DIGPor the EC_{50} was decreased 12 times to yield a value of 2.5 µM. Finally, the compounds were tested in a SF188 cell line (MGMT overexpressing GBM cell line) were they noted that at 1 µM none of the compounds was toxic after 96 h and when they were used in combination with TMZ (GI_{50} = 2.2 mM, the necessary concentration to diminish 50% of the cells viability) they managed to potentiate its GI_{50} in 1.8-fold for DIGPor and 3.1-fold for Zn-DIGPor rendering GI_{50} values of 1.1 and 0.7 mM respectively.[79]

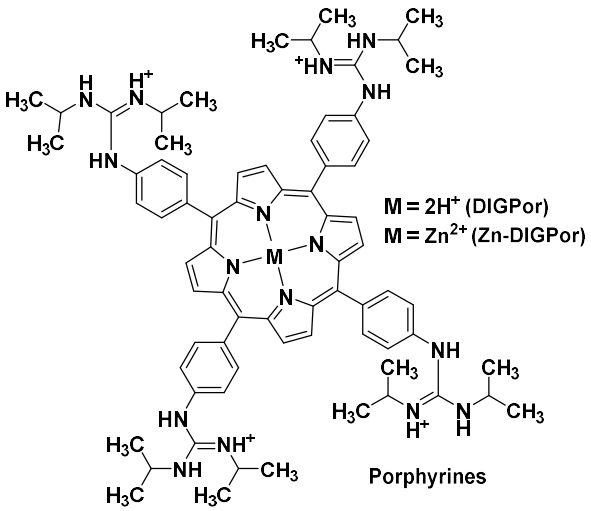

Chart 4 Porphyrin and metaloporphyrin used for selective bind O^6MeG:C pairs in dsDNA[79]

The second example of small molecules that can interact with O^6MeG were developed by the Sturla group. Inspired by Benner's previous work[81] who managed to develop a non-canonical hydrogen bond targeting by modified and artificial nucleobases, the Sturla group started a strategy to develop small molecules that could possibly interact with O^6MeG once incorporated into the opposite DNA strand. The modified nucleobases called dZ, 3-deaza-C, 4-thio-U, BIM, Benzi, Peri, Per, EXBIM and ExBenzi were incorporate into a single stranded DNA (ssDNA, **Chart 5A**). Afterwards, each ssDNA was annealed with another ssDNA that faced in front of the modified nucleobases the four canonical nucleobases (A, C, T and G) or three other modified nucleobases (O^6MeG, O^6BG or the abasic site Φ). The rationale behind the selection of these nucleobases was to study their capacity of stabilization of a dsDNA by changing the hydrogen bond pattern, hydrophobicity and the π stacking properties of the molecules. In a first article, they studied the capacity of stabilization of these dsDNA by UV melting experiments. In this article, researcher proved that by changing the parameters mentioned above plus the pH, O^6MeG can be discriminated in a dsDNA. Being dZ the ligand that stabilize it the most ($\Delta G°$ = -17.0 compared to -16.1 and -15.7 kcal/mol of -3-deaza-C and 4-thio-U, respectively) although less than the O^6MeG:C base pair ($\Delta G°$ = -18.3 kcal/mol).[82] In a second article it was found that Benzi was the molecule that stabilizes in a higher quantity the dsDNA when it faced O^6MeG (+ 0.6 °C in comparison to the O^6MeG:C base pair).[83] Important to note that this pseudo-base pair could decrease MGMT activity by 20% when compared with the O^6MeG:C base pair.[84] Along with other remarks they conclude that for small probes (i.e.: BIM and Benzi) the DNA stabilization is led by enthalpy reasons (hydrogen bond interaction) while stabilization for larger probes (Per and Peri) is driven by entropy (π stacking interactions).[83] In sequential articles, researchers extended the π surface of BIM and Benzi by adding a benzene ring to the novel molecules creating ExBenzi and ExBIM and they repeated the

thermal stabilization assays in the same conditions. Even if BIM and Benzi were not included in this article, by comparing the $\Delta G°$ values, the slight increase of the stability of the duplex by 0.5 kcal/mol due to their higher surface area that allows them to interact with the neighbor bases. As well, the addition of a benzene ring increases the conjugation of the π system and permits them to have fluorescent probes that are sensitive to their environment, having a redshift on the λ_{em} when the nucleobase is facing O^6MeG.[85] Finally and understanding the value of the modified nucleobases the ExBIM and EXBenzi probes were used to detect and quantify the presence of O^6MeG in DNA in the KRAS gene.[86]

A third and last example of a selective recognition of O^6MeG can be found in the use of a modified oligonucleotide called FT-ODN containing a 6-thioguanosine bearing a 2-methyliden-1,3-diketone group in a ssDNA (**Chart 5B**). The use of the probe is based on the higher reactivity of the 2-amino group of the O^6MeG in comparison with the G nucleobase at neutral pH. Indoubtly, due the electron donor effect of the methoxy group. The transfer of the methylidine group containing an alkyl residue was used as a substrate for a click chemistry reaction with a fluorescent probe like FAM. Even if there are no MGMT studies in this article, its value that the difference of reactivity of the O^6MeG base can be used to detect site-specific modifications and its quantification by HPLC in dsDNA.[87]

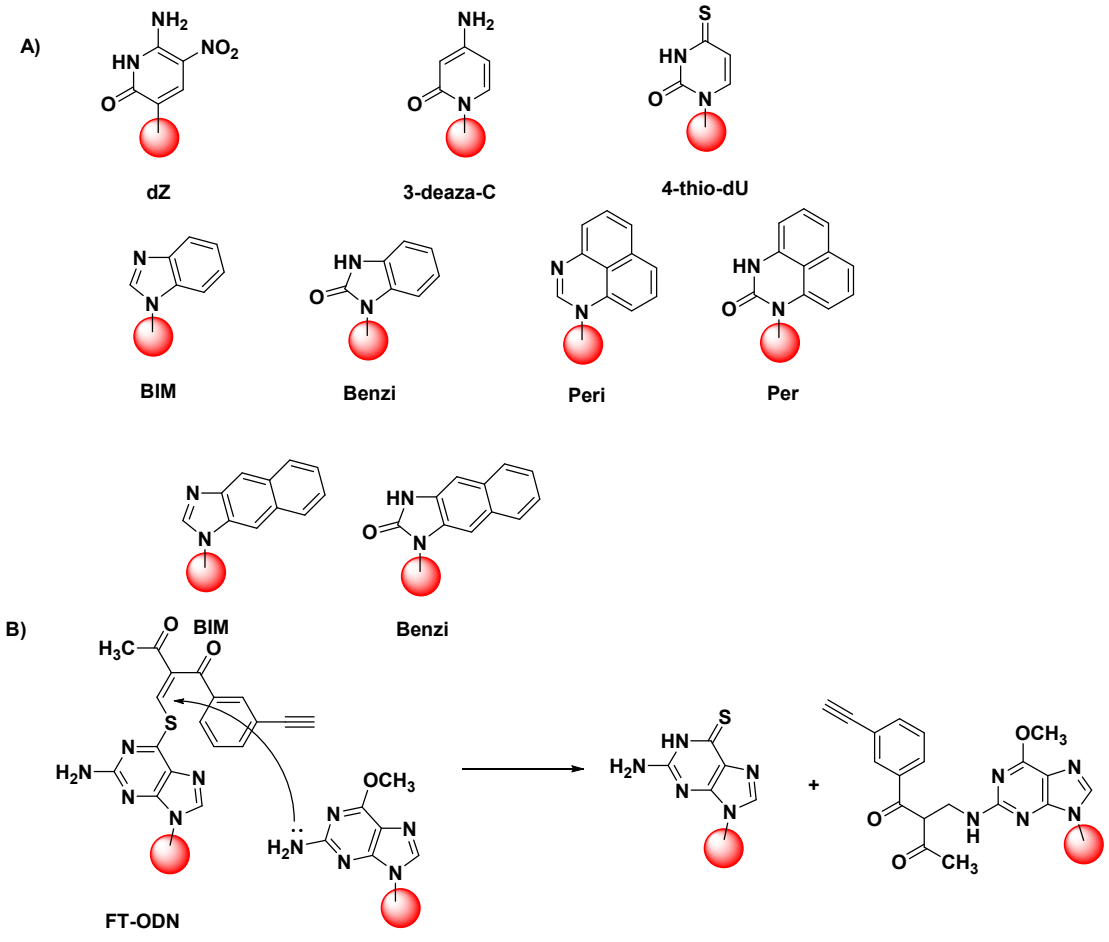

Chart 5 Small nucleobases incorporated to DNA able to recognize O^6MeG

2.2 Aims of the work

Based on the IIS we suggested the synthesis of small molecules with a hydrogen bond pattern that could be complementary to the ones present in the O^6MeG base. Considering that O^6MeG can, in principle, form three hydrogen bond in an Aceptor Aceptor Donor (AAD) fashion we propose that our molecules can have the possibility of forming at least two hydrogen bonds in a Donor Donor Aceptor (DDA) manner (**Figure 10**). We hypothesized that binding of such molecules to O^6MeG residues in dsDNA would stabilize the intrahelical conformation of the latter, masking it from MGMT resulting in an indirect inhibition effect.

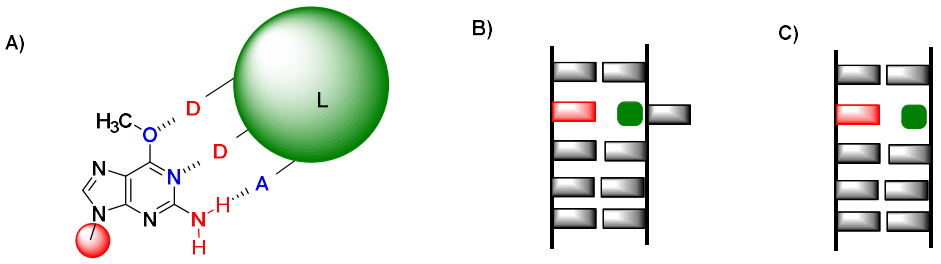

Figure 10A) Schematic representation of O^6MeG:Ligand interaction proposed for the IIS. Proposed binding modes to the **B)** O^6MeG:C and C) O^6MeG:Φ base pairs being Φ an abasic site analogue

2.3 Results and discussion

2.3.1 Synthesis

The aim for this section of the Thesis is to design three types of scaffolds: i) 8-azaquinolones derivatives ii) G derivatives and iii) 6-aminouracil derivatives (**Chart 6**).

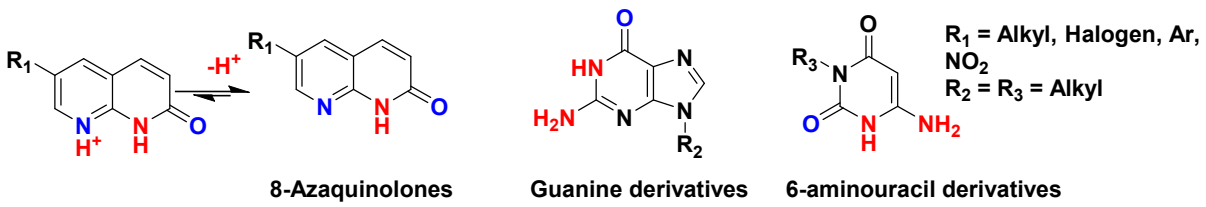

Chart 6 Molecules synthesized as a first attempt to target O^6MeG

Synthesis of 8-azaquinolines

With the purpose of obtaining different 8-azaquinolones with substituents on the position 6 of the bicyclic compound, several strategies were carried (**Scheme 1**). The first one exploited a previously described methodology,[88] that started with the *N*-pivaloylation of 2-aminopyridine in basic conditions, that yielded the *N*-protected pyridines **1** and **2** in very good yields. After they were obtained, an anion was generated with *n*-BuLi at -78 °C that reacted with DMF to give two formylated products **3** and **4** in fair to moderate yields. These molecules bearing an aldehyde group, reacted with the enolate of *t*-butylacetate on an aldol condensation to obtain in moderate yields the β-hydroxy esters **5** and **6**. Finally, in the presence of HCl 5N on a refluxing system, the β-hydroxyesters were cyclized to yield the 8-azaquinolones **7** and **8**, once again in fair to moderate yields.

The second strategy was based on the achievement of a molecule containing the lipophilic nitro group. To obtain it, a Heck coupling was performed on the 2-aminopyridine bearing a bromine group on the position 3 that yielded **9** in moderate yields. Once achieved this conjugated compound, a cyclization in acidic conditions allowed us to obtain the product **10** in good yields.[88]

The last strategy assayed consisted in the condensation in acidic conditions of 2-bromomalonaldehyde and 2,6 diaminopyridine to obtain the 2-amino 1,8-naphthyridine **11** in fair yields. This compound, was transformed upon diazotization into **12** in good yield (**Scheme 1B**).[89]

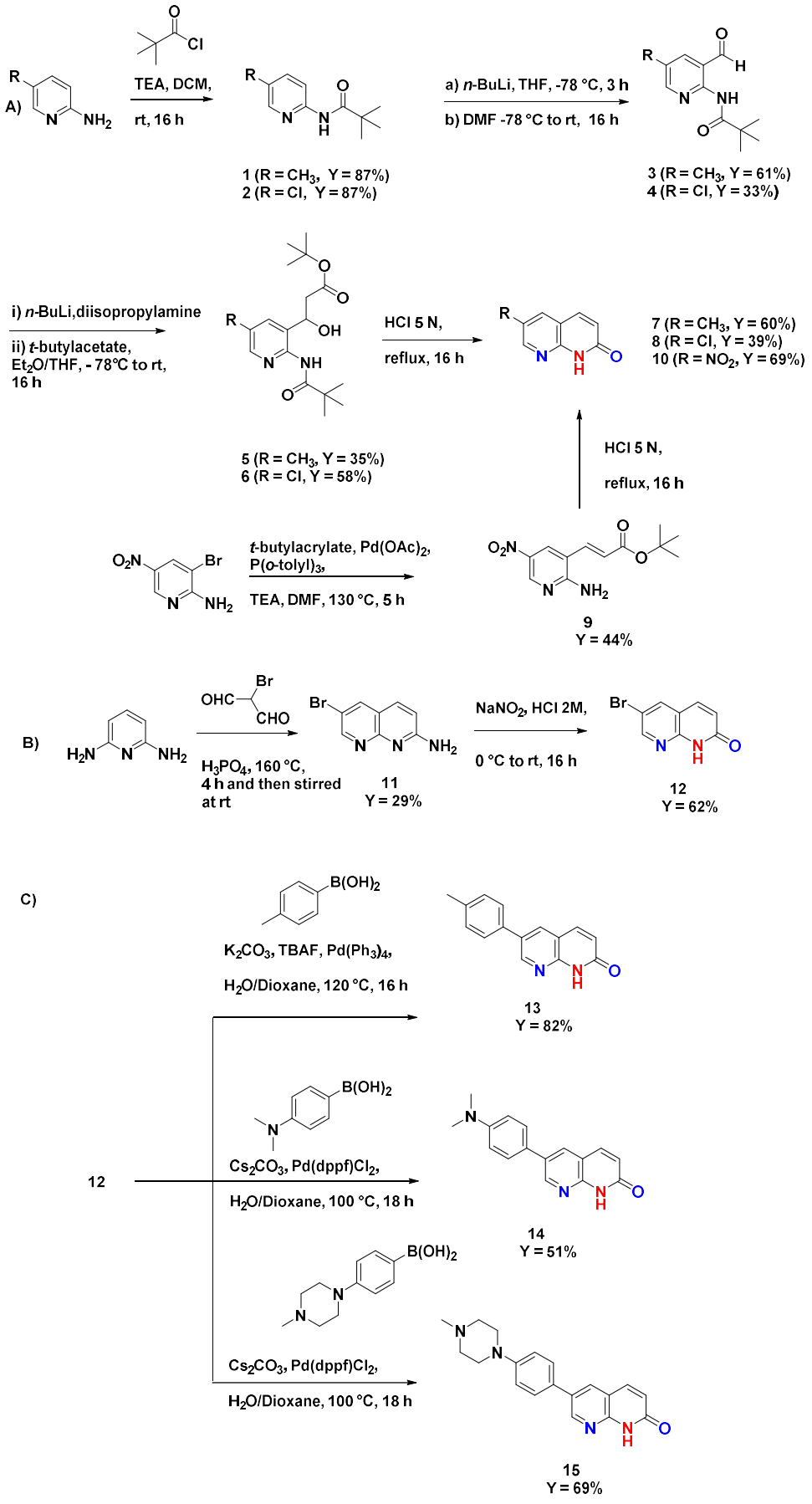

Scheme 1 Synthesis of 8-azaquinolones

Since **12** contains an aromatic bromine, a Suzuki Cross-Coupling was performed by the use of *p*-tolylboronic acid and $Pd(PPh_3)_4$ as catalyst, employing a modified procedure described in the literature,[90] to obtain **13** in very good yields. However, when the electron rich *p*-dimethylaminophenylboronic acid was used in the same conditions no reaction was observed. The second attempt used the same conditions as for **13** but with the employment of $Pd(Dppf)Cl_2$ instead of $Pd(Ph_3P)_4$[91,92] were the yield was only 2%. Because base nucleophilicity plays an important role for the nucleophile exchange step after the oxidative addition of the **12** in the catalytic cycle,[93] a base exchange from K_2CO_3 to AcOK was performed rendering the same negative results. Finally, we decided to use Cs_2CO_3 instead of K_2CO_3 and the yield was increased to obtain to **14** in good yields (59%, **Table 1**). A possible explanation could be that since Cs^{2+} cation can be better solvated in aqueous solution than K^+, CO_3^{2-} counterion will be more "released" and more available for the reaction. As a final remark, using the conditions optimized before a (4-(4-methylpiperazin-1-yl)phenyl)boronic acid was used to obtain **15** in good yields (**Scheme 1C**).

Table 1 Optimization of Suzuki Cross-Coupling for the obtention of **14**

Base	Additive	Catalyst	Solvent	Temperature (°C)	Time (h)	Yield (%)
K_2CO_3	TBAF	$Pd(Ph_3P)_4$	Dioxane/H_2O	120	96	0
K_2CO_3	TBAF	$Pd(Dppf)Cl_2$	Dioxane/H_2O	120	18	2
AcOK	-	$Pd(Dppf)Cl_2$	Dioxane	90	18	0
Cs_2CO_3	-	$Pd(Dppf)Cl_2$	Dioxane/H_2O	100	18	59

Synthesis of Guanine derivatives

The goal of these synthesis reposed on the addition in the position N^9 of the guanine an alkyl chain bearing a nitrogen atom with the aim to establish electrostatic interactions between the guanine derivative and the phosphate backbone of the DNA. Therefore, attempts to alkylate 2-amino-6-chloropurine using the *N*-dimethylaminopropyl chloride were performed (**Table 2**).

In this case, several conditions including: modifications on the base, temperature, reaction time and the presence of catalyst such as I_2 were assayed. For this reaction, the K_2CO_3 base in the presence or absence of I_2, showed little conversion to the products even at 7 days of reaction time. The increase of the temperature did increase the conversion with a concomitant raise in the isomer N^7 formation or other degradation products (as judged by LCMS and TLC). For these reasons, Cs_2CO_3 replaced K_2CO_3 since it is a stronger base, and this showed a slight exchange on the conversion to the product although in some cases the formation of the N^7 isomer increased the complexity of the purification process.

Therefore, another strategy was adopted (taking into account the previous conditions evaluated before) that involved the alkylation of alkyl chains bearing a bromine as leaving group (**Scheme 2**).

Table 2 Optimization for conditions for N^9 -2-amino-6-chloropurine alkylation in DMF as solvent

Base	Temperature (°C)	Catalyst	Time (d)	Ratio (P/SM)
K_2CO_3	RT	-	1	0.15
K_2CO_3	RT	I_2	1	NR
K_2CO_3	80	-	1	Degradation
K_2CO_3	60	-	1	2.27 (Degradation)
K_2CO_3	60	I_2	1	1.23 (Degradation)
K_2CO_3	RT	I_2	7	0.3
Cs_2CO_3	RT	-	7	1.7 (33% Yield, 6:1 ratio of N^9/N^7)
Cs_2CO_3	RT	-	1	0.5
Cs_2CO_3	60	-	1	1.58 (<20% Yield)

For this objective, 2-amino-6-chloropurine was placed in DMF with Cs_2CO_3 in the presence of *n*-bromobutane or **16** to yield compounds **17** and **18** in good to fair yields respectively. Once obtained these alkylated products, a basic hydrolysis and replacement of the chlorine group, yielding **19** and **20** in good yields was carried.[94] For the compound containing a NH-Boc group, a deprotection in dry dioxane with hydrogen chloride, permitted to obtain **21** in excellent yield.

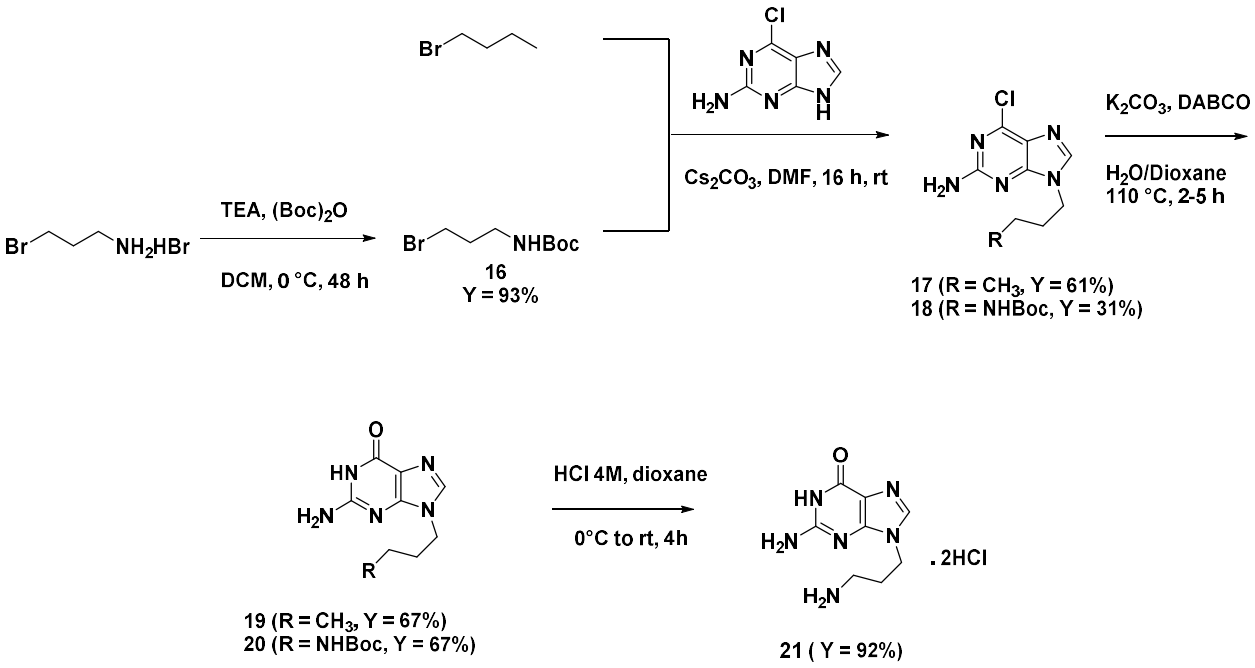

Scheme 2 Synthesis of N^9 guanine derivatives

Synthesis of 6-aminouracil derivatives

Another scaffold was made in order to obtain molecules derived of 6-aminouracil. Since this molecule possess two faces that can interact through hydrogen bonds with O^6MeG, Muller's procedure was performed in order to block the N^3 for obtaining a molecule with the pattern complementary to O^6MeG on it.[95] The starting material was heated in neat HDMS in the presence of $(NH_4)_2SO_4$ as catalyst, then *n*-bromobutane and a saturated solution of $NaHCO_3$ were added in order to obtain a precipitate that was purified for achieving **22** in low yields. In other attempts of N^3 alkylation when using either *N*-dimethylaminopropyl chloride or **16**, no product was obtained probably due to the unstability of the *N*-Boc group at high temperatures (**Scheme 3**).

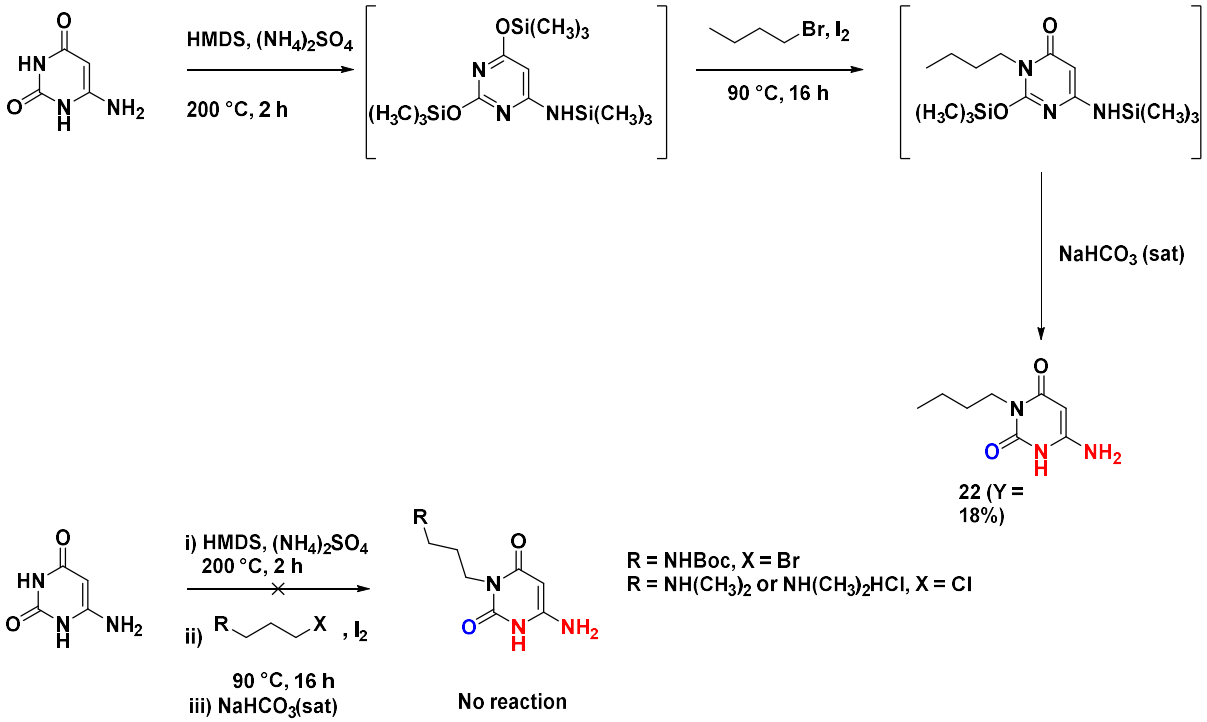

Scheme 3 Synthesis of 6-aminouracil derivatives

2.3.2 Thermal stabilization of dsDNA

Once obtained the molecules, their capacity to stabilize a dsDNA containing an O^6MeG residue was studied by melting temperature measurements (T_m, which is considered as the temperature where half of dsDNA is dissociated into a ssDNA). The first experiment consisted in the use of the Forster Resonance Energy Transfer (FRET) principle. The method relies on the use of a fluorescent emitting probe (F, FAM) on the 5' end of a DNA strand whose fluorescence emission is quenched by quencher (Q, TAMRA) that is found on the 3' end of the complementary strand (**Figure 11A**). An increase of temperature in solution will denaturate the dsDNA and the FAM:TAMRA pair will not be found in proximity, therefore the quenching is eliminated and an increase in fluorescence is observed due to the emission of the FAM probe. [72,96,97] By plotting the fluorescence signal as a function of temperature a sigmoid curve can be obtained and the melting temperature T_m can be retrieved. In the case a ligand (L) can stabilize the dsDNA through specific or non-specific binding, an increase in the T_m is observed leading to a shift on the plot towards higher temperature value (**Figure 11B**). In the case of UV melting experiments, the principle is the same but there is no F/Q probe and the property measured is the absorbance at λ =260 or 270 nm, and the denaturation of the dsDNA leads to an increase of the absorbance due to disrupted base stacking.[98]

The ligands were tested against different types of 17-base pair double strand DNA (17 bp dsDNA) containing the O^6MeG:C pair or O^6MeG:Φ (being a synthetically Φ incorporated abasic site, represented by a THF residue). The oligonucleotide bearing an abasic site opposite to O^6MeG represents a "pseudo-substrate" designed to select heterocyclic motifs recognizing the O^6MeG residue, as it was already exploited in related studies (**Figure 11D**).[99] Without competing for binding with the cytosine residue in the O^6MeG:C pairs: it was expected that this way could allow the identification of even low-affinity, but selective O^6MeG ligands.

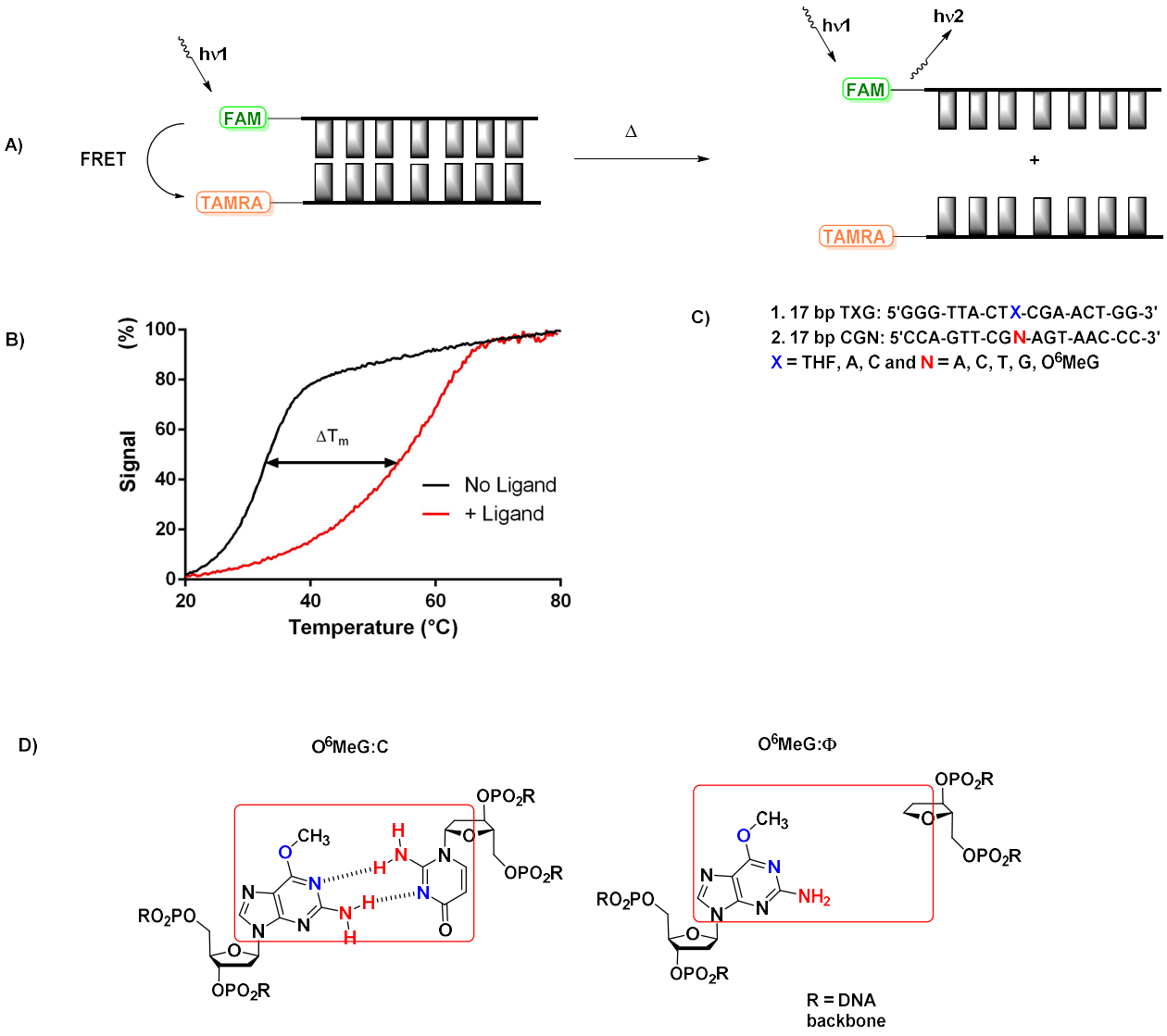

Figure 11A) Principle of the FRET melting experiment **B)** Typical T_m experiment obtained either by FRET or UV methods **C)** 17-bp sequences used for the experiments **D)** dsDNA will contain either a O^6MeG:C base pair or a O^6MeG:Φ as a AP site surrogate

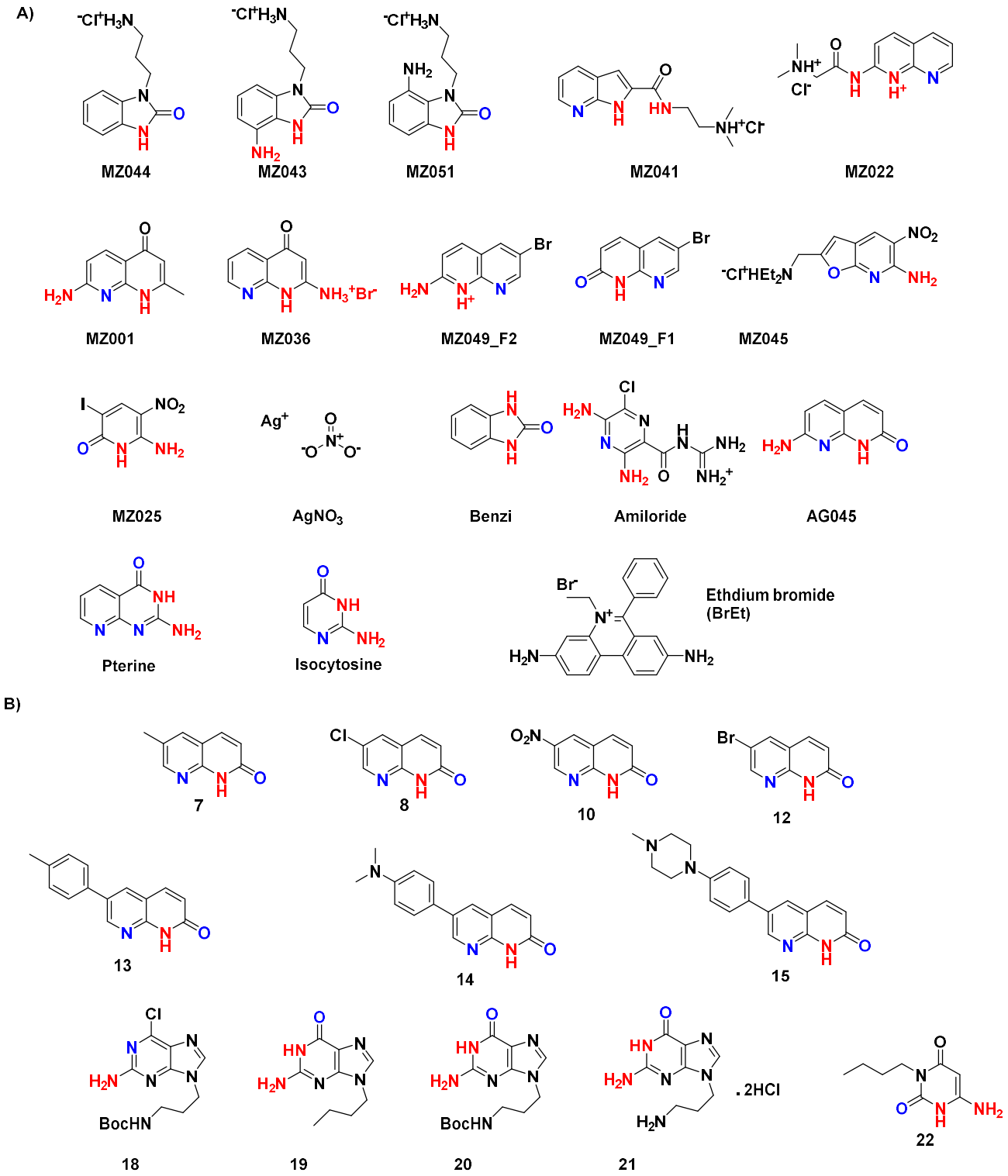

Chart 7A) Molecules synthesized or purchased used before the beginning of the Thesis **B)** molecules synthesized during this Thesis

Before the beginning of the Thesis, a previous work was started by Dr. Michela Zuffo and it consisted in the synthesis of several ligands with a variety on the characteristics mentioned above (**Chart 7A**). From this panel, 17 ligands were synthesized or purchased where for example: Benzi was reported as

a O^6MeG stabilizing molecule as well as three other molecules (**MZ022**, **MZ036** and **MZ049_F2**) that contained the scaffold for the recognition of a G:Φ site.[74,78] In addition, $AgNO_3$ was added to the assays because it has been reported that silver ions can bind C:C mismatches,[100] other guanine-like analogues [101], and because it could potentially bind the O^6Me:C base pair in a similar way, and also because another metal like Ni^{2+} was reported to inhibit MGMT activity in cellular extracts.[102] Finally ethidium bromide (**BrEt**) was used as a non-specific DNA ligand.[103]

The first assay was carried using a FRET melting set up, and it was observed that except for $AgNO_3$ that stabilized (unselectively) both DNA containing O^6MeG. For the fully matched ds DNA (O^6MeG:C) none of the other compounds was able to stabilize the duplex. In case of the O^6MeG:Φ surrogate, compounds **MZ022**, **MZ031**, **MZ043**, **MZ054** or **Benzi** were able to increase the T_m in an average of + 3 °C when they were used at 5-times more than the dsDNA concentration (2.5 *vs.* 0.5 μM). However, this stabilization was not concentration-dependent since the increase of ligand concentration did not show an increase in T_m, which made us to suppose that the first results were artifacts and non specific interactions. Finally, another remark of this experiment was the results of the lack of stabilization of the **Benzi** molecule as it was previously reported (**Figure 12A-B**).

The second experiment carried was the stabilization of the ds DNA by UV with the purpose of increasing both the DNA (10 μM) and ligand concentration (300 μM) to find low affinity ligands. In these circumstances **MZ022**, **MZ049_F2** and **Pterin** stabilized the G:Φ dsDNA by + 7.9, + 2.7 and + 2.1 °C respectively, as it was expected according to the literature. **Ag^+** and **BrEt** stabilized as well the DNA but the T_m could not to be calculated due to its high value, for the rest of the compounds none of them was able to stabilize dsDNA. Regarding O^6MeG:C DNA, **BrEt** and **Ag^+** stabilize it in a non-selective fashion, whereas **Benzi** repeated the same results as the FRET melting experiment failing increase the T_m. In the case of **Isocytosine**, it increased the T_m by + 1.9°C but considered it was used in a 30-fold higher concentration than the DNA the stabilization property was considered extremely weak and no further experiments were done with it (**Figure 12C-D**).

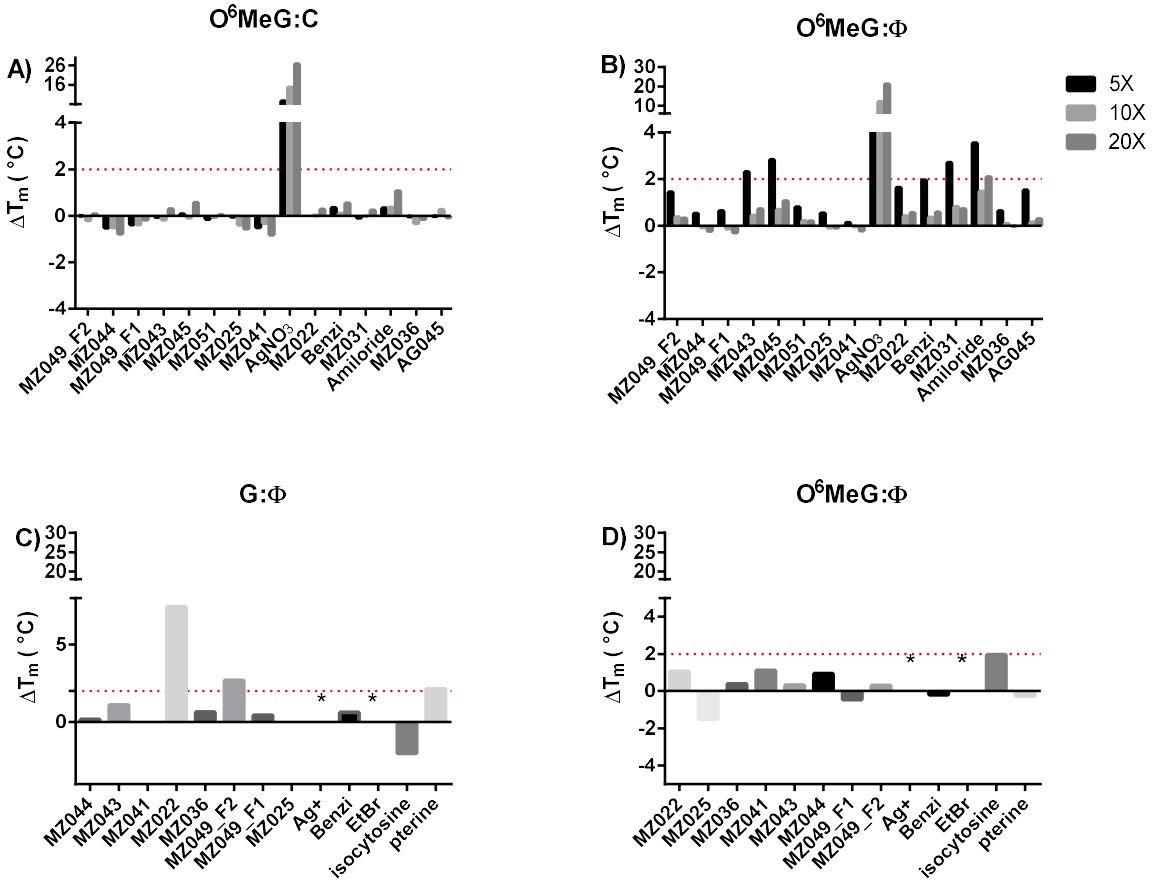

Figure 12 DNA stabilization experiment of the previously synthesized ligands studied by **A-B)** FRET, here the experiments were carried in Lithium Cacodylate buffer 10 mM, pH = 7.5 and 10 mM KNO_3 with 17-bp dsDNA containing 5' FAM on C or Φ strand, 3' TAMRA on O^6MeG strand. [DNA] = 0.5 µM, [Ligand] = 2.5, 5 and 10 µM (Represented as 5X, 10X and 20X). The samples were heated from 25 to 95°C with a 0.5 °C/min rate and the fluorescence was recorded at λ_{em} = 518 nm. **C-D)** UV melting experiments of 17 bp dsDNA containing G or O^6MeG facing a synthetic abasic site (G:Φ) and O^6MeG:Φ respectively). The experiments were carried as above [Ligand] = 300 µM, [DNA] = 10 µM. Samples were heated from 17-80 °C with a 0.2 °C/min rate and the absorbance was recorded for the heating and cooling process at λ_{abs} = 260/270 nm. For all the experiments, melting temperatures (T_m) were obtained by the first derivative method and the result are expressed as $\Delta T_m = (T_{m,ligand} - T_{M,vehicle})$.* denotes that no value could be obtained due to a large stabilization of the duplex by the evaluated molecule (*n* = 1)

In pursue of obtaining a small molecule that could bind O^6MeG the interaction of 11 novel compounds synthesized and with two types of 17-bp dsDNA, one containing O^6MeG:C and the other one O^6MeG:Φ, were tested by UV-melting in identical conditions. The 8-azaquinolones were tested at 300 μM, for the guanine and 6-aminouracil derivates the chosen concentration was 100 μM because the absorbance at 260 nm was too high at 300 μM whereas for **BrEt** the work concentration was 60 μM, corresponding to 30X, 10X and 6X-fold concentration respectively comparing with the DNA (**Figure 13A-B**). For the O^6MeG:C dsDNA, none of the compounds induced a positive stabilization larger than + 2 °C . In fact, the only particularities were observed for **13** who exerted a chaotropic effect generating a reduction of stability by -4.3 °C in the DNA.[104] On the contrary, **BrEt** caused an increase on the T_m of + 27 °C even when used in a much more reduced concentration of 60 μM. With O^6MeG:Φ, the scene was repeated and the sole compound that stabilized the DNA with a higher value than + 2°C was compound **18** (+ 2.3 °C) whereas **10** destabilized the DNA by reducing the T_m by -4.7 °C. Again, **BrEt** showed to interact with DNA on a non-specific manner increasing the T_m in 27 °C.

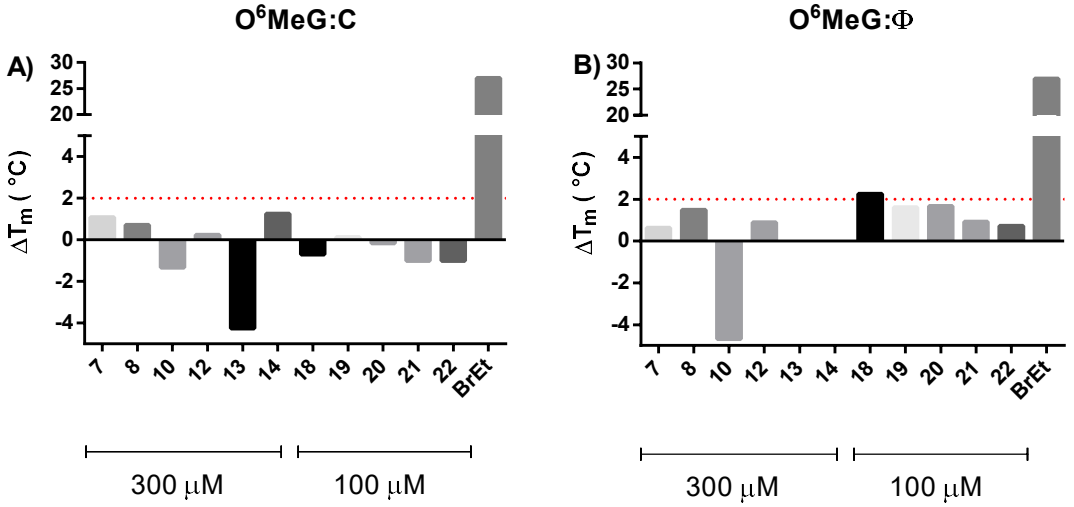

Figure 13 UV melting experiments of 17-bp dsDNA containing **A)** O^6MeG facing C (O^6MeG:C) or **B)** a synthetic abasic site (O^6MeG:Φ). The experiments were carried as described in **Figure 12**. [8-azaquinolines] = 300 μM, [Guanine and 6-aminouracil derivatives] = 100 μM. [DNA] = 10 μM, [BrEt] = 60 μM was included as a prototypical DNA intercalating compound (*n* = 1)

Bearing in mind these results described above, and even if the conditions of the assays were explored to find low-binding affinity ligands to discriminate O^6MeG dsDNA, no compound was able to interact and stabilize this DNA surrogate.

2.3.3 Photophysical properties of 8-azaquionolones and potential as fluorescent probes

We note that compound **14** is an electron push-pull system, composed by the dimethylamino group (Electron Donor Group, EDG) and the azaquinolone (Electron Withdrawing Group, EWG). Another way of seeing it is by a composition of three major blocks: the 8-azaquinoline ring, the phenyl ring and the *p*-dimethylamino group. The deconstruction of it, towards **13** and **7**, simplifies the structure yielding a less conjugated aromatic system that renders to a blue-shifted emission in fluorescence compared to **14** in the organic aprotic dioxane (λ_{em} = 485, 402 and 377 nm respectively,**Figure 14A**). Their fluorescence was also studied in different solvents (**Figure 14B-D**). Surprisingly, compounds **7** and **13** also appeared to be fluorescent (although on a minor extent and at shorter wavelengths compared to **14** in dioxane) in more polar and protic solvents such as acetone or an aqueous buffer at pH 7.24 where **14** was not (**Figure 14B-D**). This remaining fluorescence of **13** or **7**, can be ascribed to the intrinsic fluorescence of the 8-azaquinolone core (**7**) plus the addition of the tolyl group (**13**). Also interesting to point out is that **14** showed a clear solvatochromic effect regarding its fluorescence (**Figure 14D**). Increasing the polarity of the solvent leads to a red-shift in the fluorescent emission spectra from 488 nm in dioxane to 570 nm in acetone. This could be explained if **14** is seen as a push-pull system. In the ground state, the molecule is planar achieving its maximal conjugation. Once it is excited, there is a charge separation in what is called the Locally Excited state (LE), which is still planar, but with a different dipolar moment than in the ground state. Once this happens the solvent needs also to rearranges in the surrounding area of the LE to decrease the energy of the system. When the solvent rearrange, the LE also does rotating the *p*-dimethyl amino bond into a Twisted Intramolecular Charge Transfer (TICT) state, where the molecule has lost its conjugation and has a lower energy than the LE. The emission of energy from this excited state, is done from a lower energy state, explaining why there is a red shift on the emission, as it was reported for other biaryl compounds bearing a *p*-dimethylamino group (**Figure 14G**).[91,92] As well, we can observe a quantitative loss in the fluorescence emission of **14** when the polarity is augmented as it can be pointed out from the quantum yield values in dioxane, toluene or THF (φ = 0.21, 0.19, 0.14 respectively). In case of acetone or aqueous buffer and due to the low fluorescence, no values were determined. A hypothesis to explain and complement the idea mentioned above could be that once the polarity of the solvent increases, the capability of these to have establish hydrogen bond increases. After excitation of the molecule, a proton transfer to or from the 8-azaquinolone moiety and the solvent may occur to quench the fluorescence. Furthermore, a charge recombination, or to the relaxation through the solvent by simple vibration of the excited state can occur that can also deplete the fluorescence.[93]

Since proton transfer can be an explanation for fluorescence quenching of **14** in aqueous media, the effect on this property by the addition of NaOH or TFA to buffer or to dioxane was studied (**Figure 14E-F**). When adding either NaOH or TFA to the buffer we observe a change in the absorbance spectra compared to the spectra of **14** in the buffer at neutral pH, which could be considered as the average of both spectra recorded in acidic and basic conditions. What is surprising of this experiment is the increase of fluorescence in acidic conditions, resembling the fluorescence of **13** in buffer at pH 7.24 (λ_{em} = 386 nm). Here the protonation of the *p*-dimethylamino group or the N^8 in **14**, blocks the electron transfer through the core and results in fluorescence similar to **13**. In the case of the emission spectra in basic conditions, the excitation neither at 297 nm nor at 360 nm showed any significant increase in fluorescence. In the case of the same experiment in dioxane, the absorption spectra remained almost identically. However, fluorescence emission in the presence of NaOH slightly decreased about 20% in a similar trend than observed (**Figure 14E-F**).

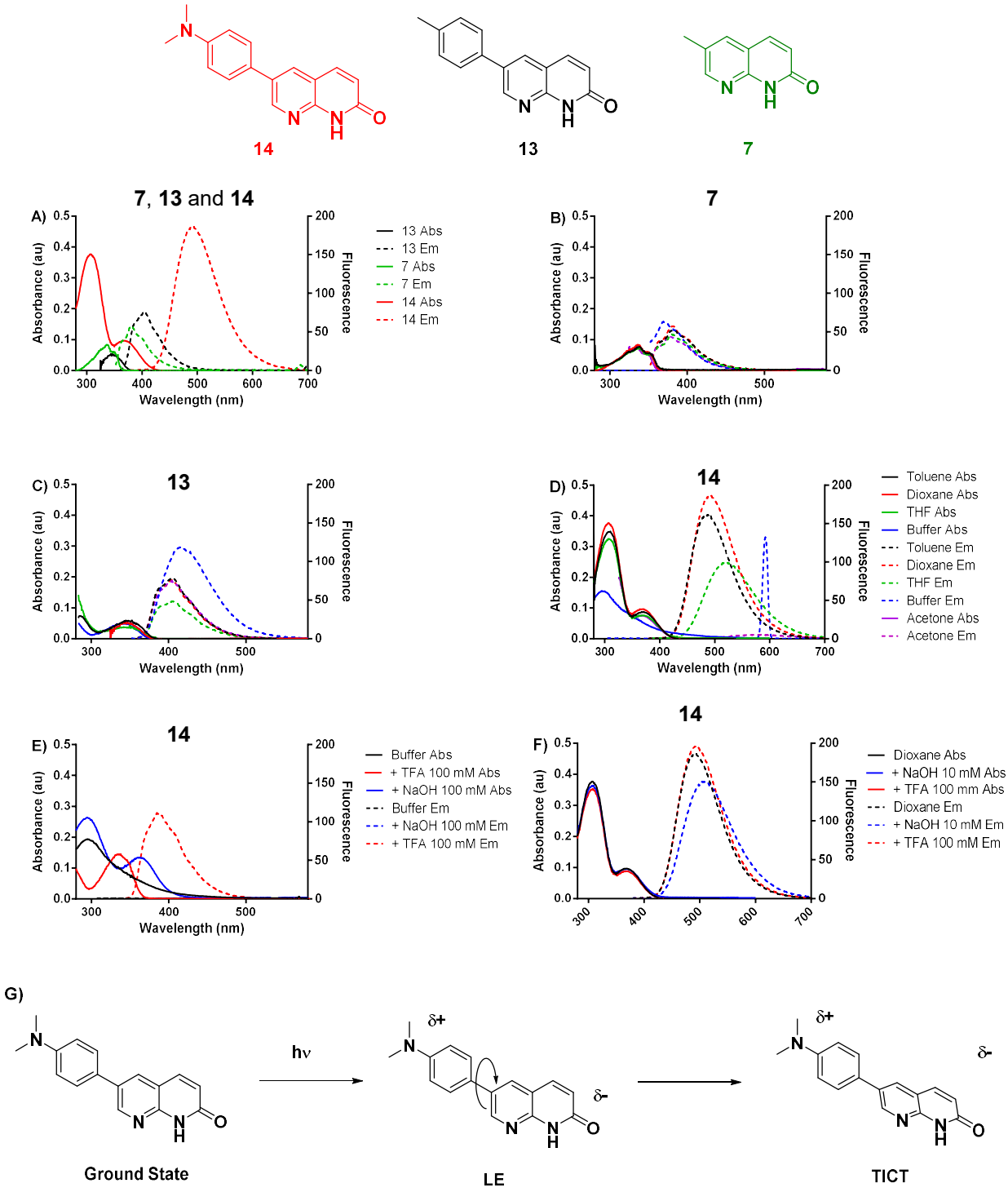

Figure 14A-G) Photophysical properties of different 8-azaquinolones. Figures show absorbance spectra an fluorescence emission spectra at [8-azaquinolone] = 10 μM in **A)** dioxane for compounds **7**, **13** and **14** **B)** compound **7** **C)** compound **13** and **D)** compound **14** in different solvents, then compound **14** in **E)** buffer and **F)** dioxane with different concentrations of acid or base G) Scheme of Twisted Intramolecular Charge Transfer formation (TICT) of **14** after excitation through a Locally Excited (LE) state. In the case where the absorbance spectra showed to peaks, excitation was performed at its right shifted maxima. λ_{exc} =300-360 nm, PMT = 550 V, Slith $_{exc/em}$ = 5 nm.

Due to these fluorescent properties in acidic conditions and the capacity of having hydrogen acceptors, **14** absorbance and fluorescence was studied in the Britton-Robinson Buffer (BRB), a buffer that allows a working range of pH from 2 to 12 (**Figure 15A-F**). [105] In this case, at pH near neutrality (6.86) we observe an absorbance maxima at 298 nm. Once acidity increases, this peak decreases and its maxima is red-shifted achieving the highest value at 334 nm. (**Figure 15A**). When studied at basic pH's, the absorbance maxima of 298 nm suffers an hyperchromic effect which is slightly blue shifted to 295 nm. In addition, it is worth noting the appearance of a small peak at 265 nm and another red-shifted peak at 365 nm at pH 12.02.

A second experiment was performed by exciting at different wavelengths according to the pH. At neutral and acidic pH, fluorescence was recorded by exciting at two different wavelengths (300 and 334 nm). As shown (**Figure 15C-D**), compound **14** showed a higher fluorescent emission at 386 nm after exciting at 334 nm comparing the excitation at 300 nm. In agreement with data observed (**Figure 14E**), fluorescence increased inversely proportional to pH reaching its maximal emission at pH 2.82. In the case of neutral or basic pH, compound **14** showed no fluorescence upon exciting at 334 nm or at 360 nm for basic conditions (data not shown).

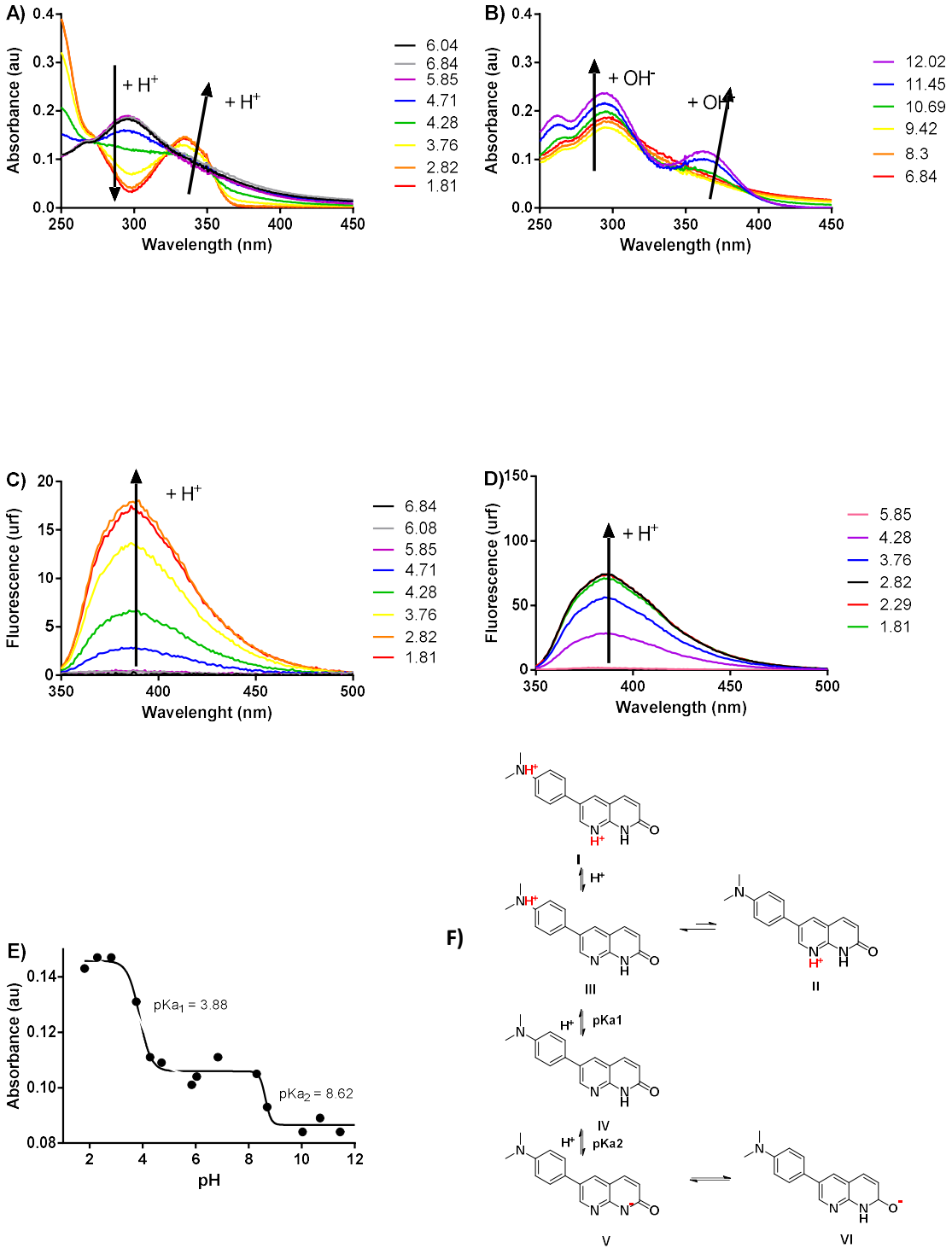

Figure 15A-B) Absorbance spectra of **14** in different pH conditions in the Britton-Robinson Buffer, **C)** and **D)** Emission spectra when λ_{exc} = 300 nm and 334 nm respectively [**14**] = 10 µM, PMT = 550 V, Slith $_{exc/em}$ = 5 nm. **E)** pK_a determination of **14** by plotting its absorbance at λ = 334 nm and determined by a biphasic non-linear fitting curve. **F)** Proton exchange equilibrium of **14**

These absorbance and fluorescence changes upon pH variation are strictly correlated with how the molecules accepts proton on the *N* atoms. Taking into account the spectroscopic changes in different pH's, the absorbance at 334 nm was plotted as function of the former. Using a biphasic non-linear regression, pKa's were determined as 3.88 and 8.62. Based on Marvin Sketch software,[106] the value of 8.62 corresponds to the pKa of the conversion from **IV** to **V** whereas in 3.88 is the exchange of proton from **III** (and **II**) to the medium to yield to **IV**. (**Figure 15E-F**). By using the Forster cycle equation,[107] the acidity of the excited state of compounds **II** and **III** was calculated. A value of pK_{a1}* of -4.5 was determined, meaning that the compound behaves as a superphotoacid.

As observed by the fluorescence and absorbance spectra and based on the results obtained, we can conclude that the neutral **IV** and anionic **V** forms do not emit light upon excitation at 300-360 nm and once **14** is protonated to yield **II** and **III**, fluorescence increases. From here two hypotheses can be drawn: one is that the emitting molecule is the protonated form of the molecule. However compounds **7** and **13** are fluorescent at pH 7 while being neutral therefore this idea was ruled out. The second alternative relies on the idea that neutral **14** represents a push-pull system. As stated the excitation of the neutral form creates a charge separation that can be rapidly quenched on the excited state eliminating the fluorescence. If **14** is protonated, it can be thought that since there are no available electrons from the nitrogen of the *p*-dimethylamino group, there is no push-pull system. If this system is deleted, the core resembles the core of **13** which is fluorescent, explaining the increase of this phenomena in **14** when pH is decreased**.**

2.3.3.1 Interaction of 8-azaquinolones with DNA

According to Nakatani's publications, where they use a two-head compounds where the napthrydine part recognizes guanine and the 8-azaquinolone moiety recognizes adenine. These molecules were used to detect adenine nucleobases in G:A mismatches and $(CAG)_n$ trinucleotides repeats (**Figure 16A**).[108,109] They proposed a hydrogen bond formation between the N^1 and the exocyclic amino group of the adenine with NH and N^8 of the 8-azaquinolone respectively plus an hydrogen bond formation between the NH, the O^6 and the exocyclic amino group of the guanine with the N^1, N^8 and the exocylcic aminogroup of the naphtopyridine.[108,109] Also, and in the presence of DNA, derivatives of the Alloxazine and Lumazine family, showed a "light-off" effect in their respective fluorescence emission. This effect was enhanced especially in the presence of DNA containing A:Φ sites therefore suggesting the 8-azaquinolones as selective A:Φ detectors.[74–76,78] Considering these data, and bearing in mind the different properties of fluorescence of **14** in organic aprotic solvents and how a proton acceptance increases the fluorescence, we decided to study if this small molecule could be used to sense hydrophobic pockets in DNA, more precisely abasic sites in DNA (**Figure 16B**).

On a contrary trend to what is observed in the Lumazine and Alloxazine family, we noticed a "light-up" effect with a red shifted emission of the compound **14** (black line, λ_{em} = 386 nm) in the presence of DNA (λ_{em} = 390 – 400 nm). In the case of a fully matched DNA (AT, red line) a 2-fold increase is observed (**Figure 16C**). Whereas for the entire DNA containing abasic sites set, the increase was about 2.2 to 3-fold compared to **14** alone but without any selectivity with respect to the orphan base. These results demonstrate that the molecules is able to interact non-specifically with DNA increasing their fluorescence. Nevertheless, neither compound **14** nor the rest of the 8-azaquinolone series was able to stabilize a DNA containing abasic sites or a fully matched DNA on UV melting experiments. Being **12** the most interesting of this set since it has an opposite behaviour in the presence of A:Φ 9 (- 4.1 °C) and T:Φ (+ 2.7 C). For the A:Φ experiment, **13** destabilize the DNA by – 3.4 °C and the rest of the compounds (**7**, **8** and **10**) did not change the T_m in an absolute value > 1 °C. Respecting T:Φ, **7**, **8** and **10** augmented the T_m in 2.5,1.5 and 2.4 °C and compounds **13** and **14** did not change the stability of it. Finally, for the A:T, all the compounds destabilize the melting temperature by - 1 °C average, a value that can be considered within the experimental error. In all the experiments, **BrEt** enhanced the T_m in values higher than 25 °C as it was observed in pervious experiments denoting once again the unespecifity of this ligand towards DNA (**Figure 16D-F**).

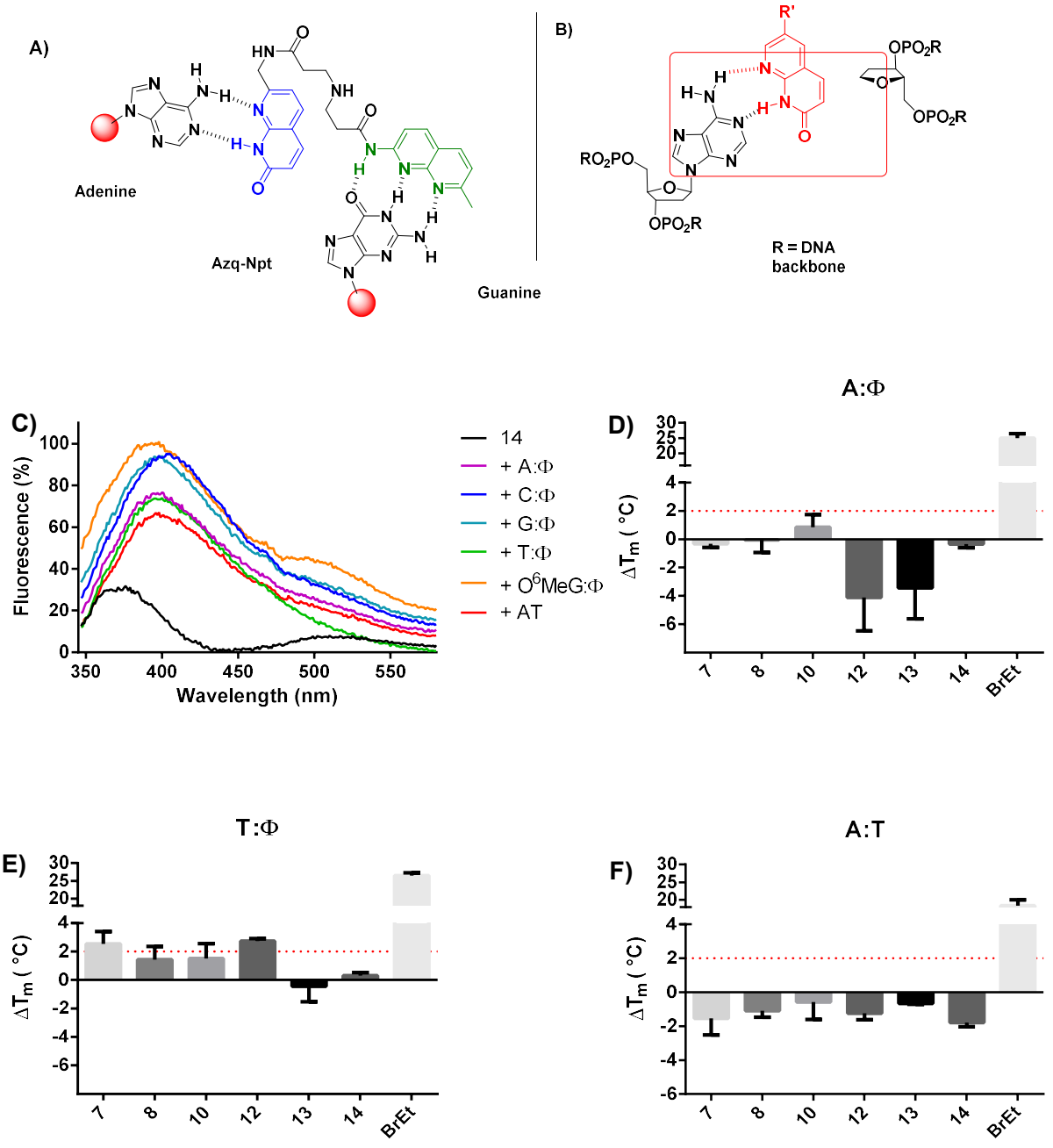

Figure 16A) Molecule designed by Nakatani that detects A:G mismatches and CAG repeats and **B)** our strategy to detect AP sites **C)** Fluorescence emission spectra of **14** in the absence or presence of 17-bp dsDNA upon excitation at 300 nm**.** [**14**] = [DNA] = 10 µM, 10 mM Potassium Cacodylate Buffer, KNO_3, 10 mM, pH 7.24, $slith_{Exc/Em}$ = 5 nm. **D-F)** UV melting experiment for dsDNA in the prescence of 8-azaquinolones. Values represent the mean ± S.D (*n* = 3) Experiments were carried in the same conditions, [8-azaquinolones] = 300 µM, [BrEt] = 60 µM, [DNA] = 10 µM.

*2.3.3.2 Synthesis of compound **15**, photophysical and DNA interaction properties*

Finally, with the purpose of having a compound that could either: i) maintain or increase its fluorescent "light-up" selectivity towards a specific DNA modification and ii) see whether this interaction could be reflected on a UV melting experiment to search for DNA stabilizing ligands. We proposed a new molecule that contained a *N*-methyl piperazine ring assuring its protonation at neutral pH therefore to be able to establish electrostatic interaction with the phosphate backbone of the DNA. Its synthesis was performed using Pd(dppf)Cl_2 as a catalyst and allowed to obtain **15** in good yields (**Scheme 1,** page 35).

Similar experiments were carried as before such as UV absorbance and fluorescence emission spectra in order to compare **14** and **15** (**Figure 17A-G**). In this case, although the UV absorbance spectra in organic solvents remained similar with two peaks at 285-300 nm and 340-360 nm, the fluorescence emission spectra was diminished for **15** on a 6-fold value in dioxane or THF and 12-fold in toluene compared to **14** (**Figure 17A-C**). Bearing in mind the aforementioned fluorescent characteristics of **14** in acidic conditions, analysis of absorbance/fluorescence spectras were performed in the BR buffer. In an opposite trend as observed for **14**, UV absorbance of **15** remained similar on the 2.8-12 pH range, having two absorbance maxima in the 300 nm and 350 nm region. In these conditions, a hyperchromic effect was seen when pH is decreased. When pH increased, the hyperchromic effect was observed, a shoulder in the 260 nm range appeared, and also a red-shift was observed for the long wavelength maxima is observed from 348 to 360 nm (**Figure 17D-E**).

In addition, compound **15** showed very weak fluorescence emission was noted at 386 nm after exciting at 300 nm or 340 nm at neutral pH being this one around 5-fold weaker when excited at 340 nm in comparison with 300 nm. Finally, emission spectra were recorded but no changes upon pH modification, contrary to what was observed for **14** (data not shown).

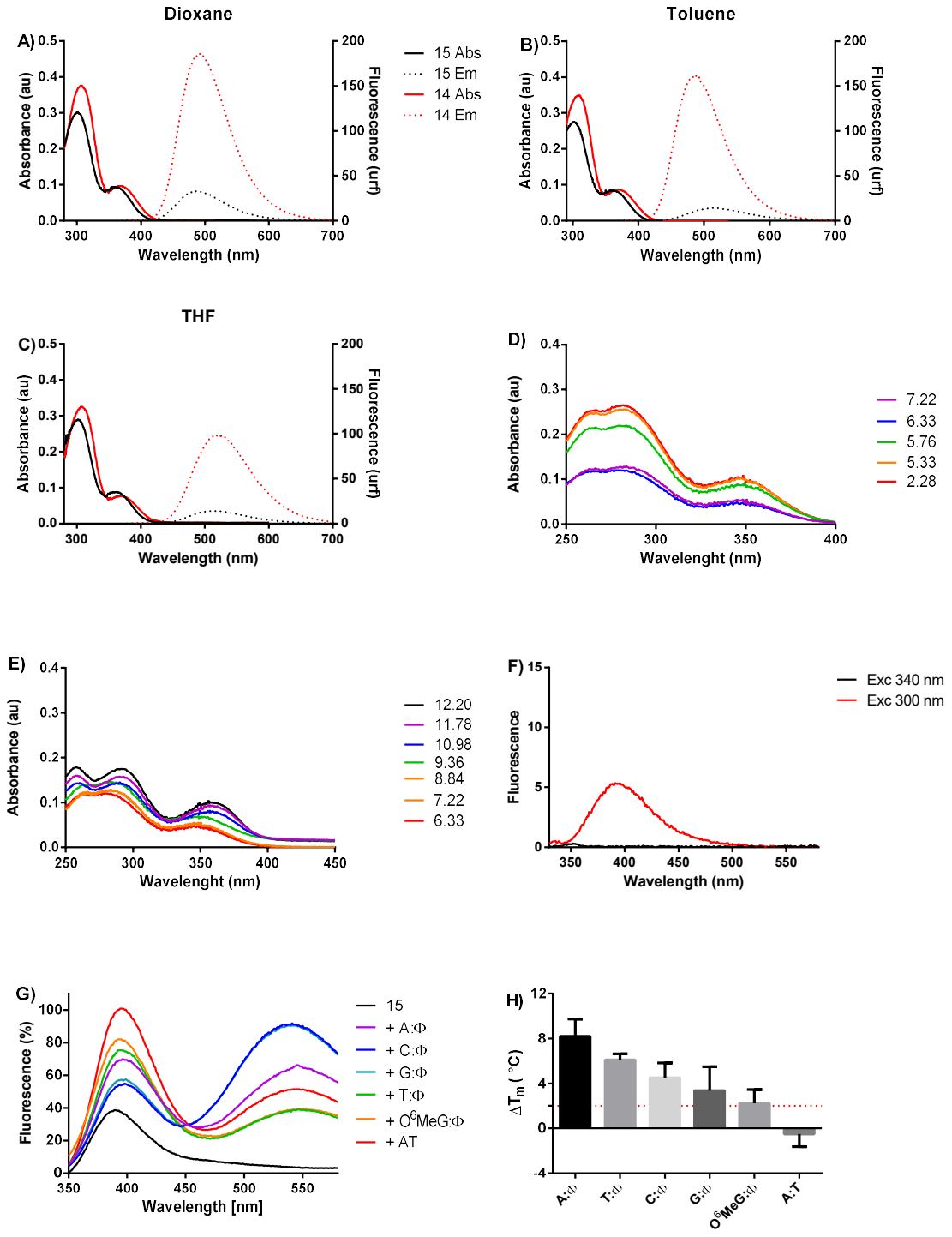

Figure 17A-C) UV absorbance and fluorescence spectra in different solvents for **14** and **15,** λ_{exc}= 340-360 nm [8-azaquinolone] = 10 µM. **D-E)** UV absorbance spectra of **15** in the Britton-Robinson Buffer **F)** Fluorescence emission spectra of **15** at pH 7.2 in buffer alone at 300 nm or 340 nm **G)** and in the absence or presence of 17-bp dsDNA upon excitation at 300 nm [DNA] = 10 µM**. H)** UV melting experiments were carried in the same conditions described before.

The lack of fluorescence in neutral pH is in agreement with data observed for **14** because neutral or anionic forms of **14** were not fluorescent due to the reasons mentioned above. Surprisingly, in acidic conditions (pH 2.28) the molecule showed no fluorescence neither. This result was striking since we were expecting the same results as with **14**. According to the Marvin Sketch software,[106] five species could be formed on a pH range of 0 to 14 (**Figure 18A-B**).

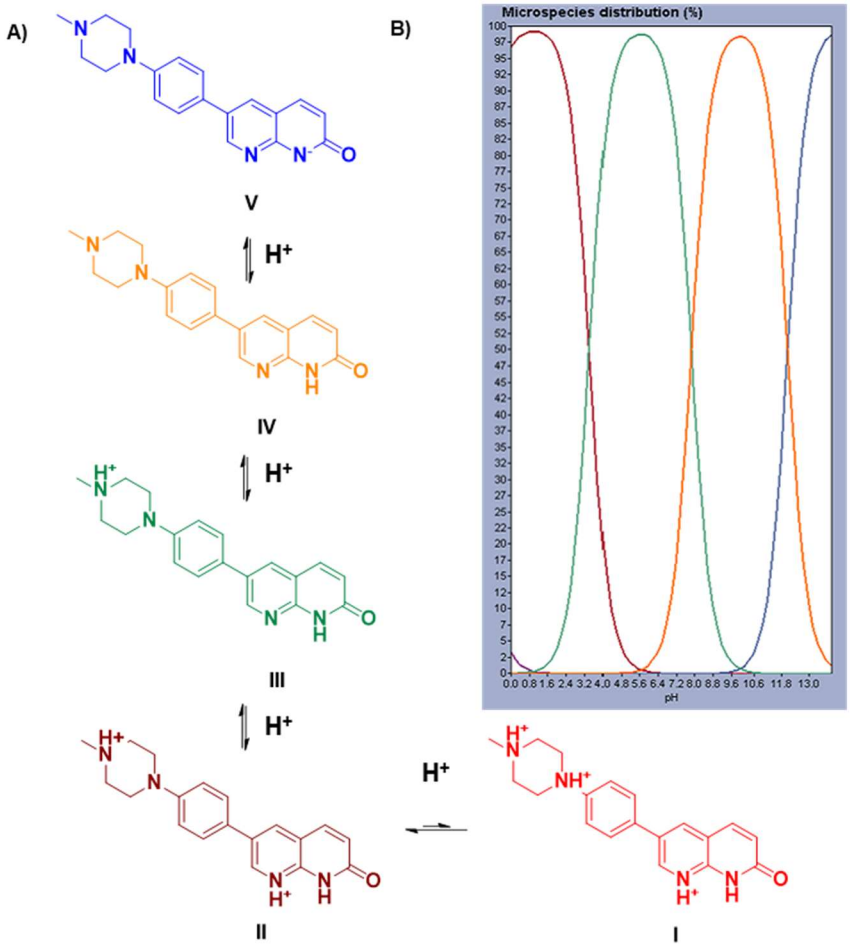

Figure 18A-B) Acid-Basic equilibria of **15** microspecies

From pH 10 to 12, the anionic and neutral species of **15** are the most predominant ones (**IV** and **V**) that we assumed they were not fluorescent. Once the pH is reduced, the first nitrogen atom to be protonated is the atom that bears the *N*-methyl group in the piperazine ring **III** and not the *N* atom in *p*-position. This compound is formed almost in a 100% at pH 5.8, a pH where analogue **14** started to be fluorescent (**Figure 15D**, page 49). As it was observed for compound **14**, in order to achieve fluorescence, the elimination of the push-pull system needs to be gained. We could imagine that if the acidification process continues, the next atom to be protonated is the *N* in the *p*-position of the phenyl group. Surprisingly and according to **Figure 18B**, molecule **II** is the most predominant specie

(98%) even at pH 0, with a small contribution of **I**, formed on a 2%. With the protonation of the N^8 in the azaquinolone, the fluorescent core is eliminated explaining why fluorescence increase cannot be achieved.

A similar experiment that evaluated the fluorescence of **15** in the absence or in the presence of dsDNA was performed (**Figure 17E**). As it was observed for **14**, once **15** is challenged with DNA, the molecule elicits a "light-up" effect for all the types of dsDNA with some interesting differences compared to **14** (**Figure 17G**). First, the light emission of **15** and dsDNA in the 386-392 nm range reaches the highest value for a fully matched dsDNA (AT, 2-fold increase). This is opposite to the data observed for **14** in which this value was the lowest (2.5-fold increase compared with compound alone), whereas for the dsDNA containing abasic sites, the fluorescence increment was lower ranging from 1.4 to 2-fold. Surprisingly, a second emission peak appears in the 534-540 nm range for all the experiments when DNA was present. This longer emission wavelength was observed when the compound was studied in organic solvents (λ_{em} = 485-508 nm). In this case, the fluorescence increment was even higher compared to **15** alone in buffer, ranging from a 10-fold for T: Φ and O^6MeG: Φ dsDNA to 24-fold for C:Φ and G:Φ dsDNA.

Finally, a UV melting experiment was carried out in the same conditions as described before. Here, compound **15** was able to stabilize dsDNA's containing abasic sites but not fully matched double strands. (**Figure 17G**). This stabilization, shows a preference for A:Φ abasic sites on a + 8.2 °C ΔT_m, followed by a + 6.1 °C for T:Φ, +4.5 °C for C:Φ and + 3.4 °C for G:Φ , + 2.2 °C O^6MeG:Φ and -0.49 °C for A:T, an indicative of the absence of non-specific binding to fully matched DNA. Bearing in mind this results that they stabilize DNA, the second emission peak around 550 nm could be the emission peak of the DNA.**15** complex, different to the emission peak of **15** alone.

As it has been described in the previous pages, among the 28 synthesized molecules, none showed preferential stabilization of dsDNA containing O^6MeG in the UV-melting experiments. Among the molecules synthesized, compounds **14** and **15** showed interesting fluorescence changes upon varying pH and solvent properties. Although **14** and **15** proved to have an increment on the fluorescent emission upon challenging with several types of dsDNA, these "light-up" properties are unspecific and could not be used to selectively detect DNA abasic sites. However, **15** did selectively stabilize an abasic site in dsDNA in the UV melting experiments, with a slight preference but low selectivity for the AP site facing an orphan A residue (A: Φ > T: Φ > C: Φ > G: Φ > O^6MeG:Φ >>AT).

2.3.4 *In cellulo* experiments

2.3.4.1 Principle of the cytotoxicity experiments

Cytotoxicity of compounds was determined on human derived glioblastoma cell line called T98G. This cell line is a pluriploid cell line widely used as a model for drug development for GBM treatment.[30,110,111] It is an MGMT overexpressing cell line[29,111,112] that confers resistance to alkylating agents such as TMZ or streptozotocin.[111–114] As well it has other features like overexpression of multidrug resistance associated proteins[29,30] (MRP) or the mutation of the pro apoptotic p53 protein[113] that provides them resistance to other drugs like ACNU, BCNU, cisplatin, vincristine or doxorubicin.[30,113]

The chosen method to measure cell viability was by the employement of the commercially available kit CellTiter-Glo® developed by Promega.[115] This kit bases its activity to measure the viability of the cells as a function of the ATP production in the cell (**Figure 19A**). CellTiter-Glo® contains within its reaction mixture the luciferase enzyme that transforms the substrate luciferine into oxyluficerin and light in a reaction that is ATP-dependent. Therefore, light emission is considered as an indirect indicator of viability. The employment of this reagent is compatible with a 96-well plate format that allows the study of several conditions in a high throughput manner for drug screening.[116,117]

This assay consisted on seeding the T98G cells in a 96-well plate where after 4 h of attachment compounds were added and incubated for 96 hours, a value that corresponds approximately to four replication cell cycles for this cell line.[110] The chosen amount of time was based on the premise that TMZ needs at least two replication cell cycles to cause its cytotoxic effects(**Figure 19B**).[5,17,114] Once finished this time, the readout was performed as explained above and viability was normalized against the vehicle control (DMSO, 0.5% v/v).

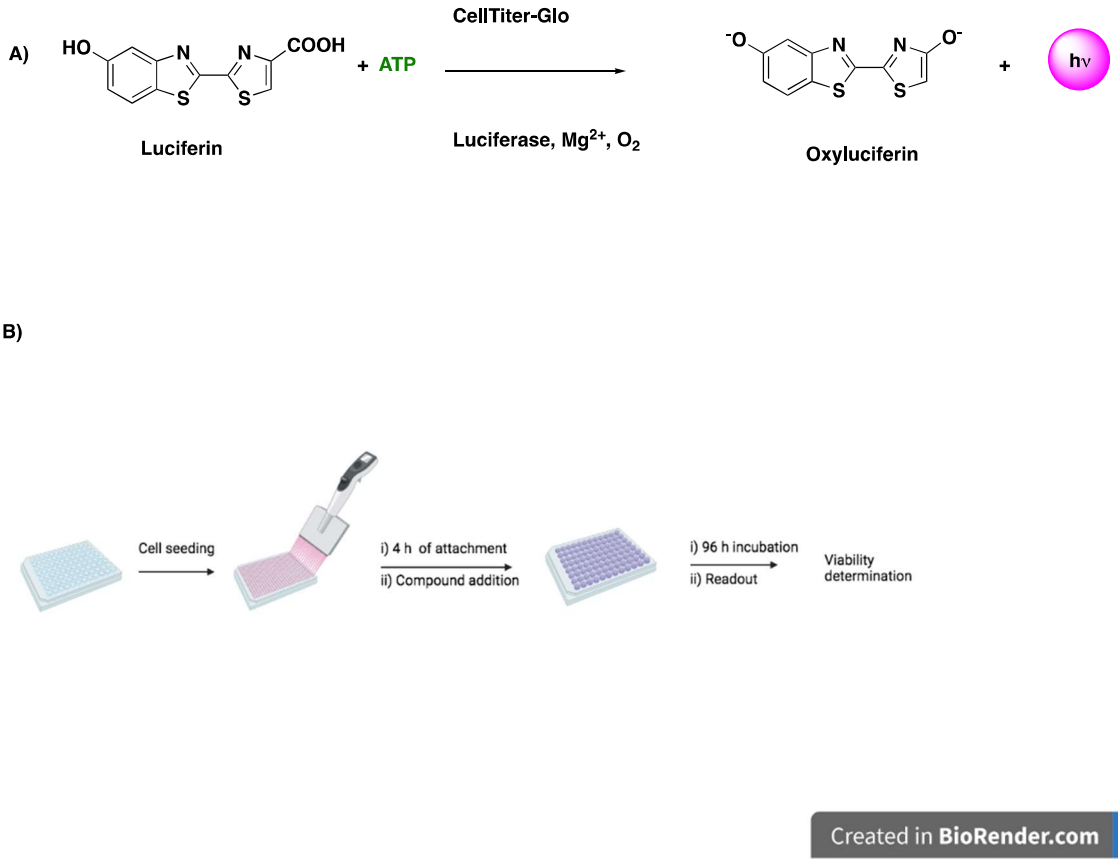

Figure 19A) Reaction for ATP detection by the CellTiter-Glo® kit and **B**) Design of for the determination of viability of T98G cells after exposure to the synthesized compounds

After determining the cytotoxicity of the compounds as single agents, the combination with TMZ was carried to search for a synergistic effect. According to the literature, the result of the combinations of two or more agents can be classified in three categories. A synergic effect is observed when the effect of the combination of two (or more) agents is higher than the sum of the individual effects of each compound. An additive effect is found when the result of the combination matches the individual sum of each individual compound effect and finally, an antagonist effect when the effect of the combination is lower.[118–120]

In spite of this simple definition, the difficulty to determine this categories with a valid methodology has been a subject of debate for almost one century. Here, we based our analysis in two different methods to study and to determine these effects.

The first method is the Bliss analysis and is what is called an effect-based strategy. It assumes that drugs do not interact within each other and they both exert the same effect (cell death or reduction of viability) by a probabilistic process. It considers the theoretical effect of the combination of two (or more) compounds (A and B) as the product of the effect caused at each individual dose. In terms of

viability, the theoretical viability of the combination of compound A at a dose a plus compound B at a dose b is given by equation (**1**).

$$V_{Theo,[A(a)+B(b)]} = V_{Exp,A(a)} \times V_{Exp,B(b)} \quad (\mathbf{1})$$

If $V_{Theo,[A(a)+B(b)]} > V_{Exp,[A(a)+B(b)]}$: Synergy

If $V_{Theo,[A(a)+B(b)]} = V_{Exp,[A(a)+B(b)]}$: Additive

If $V_{Theo,[A(a)+B(b)]} < V_{Exp,[A(a)+B(b)]}$: Antagonism

The model states that if the theoretical values of the effect of the combination of A and B is higher than the experimental value a synergy is taking place, if the values are equal we have an additive effect and if the theoretical values are lower than the expected there is an antagonist effect. This method is very useful since it can be used in any range of concentration of the dose response curve (DRC) for each compound and a statistical significance can be obtained from these results. However it assumes that drugs do not interact with each other, and even if a statistical value can be obtained from the comparison of the theoretical and experimental values, no quantitative value of synergy can be obtained.[118–120]

The second approach is the Loewe additivity and is a dose-effect based strategy and it relies on the concept of additivity that defines the Combination Index (CI) as the equation (**2**):

$$CI = A(a)/VA(a) + B(b)/VB(b) \quad (\mathbf{2})$$

CI = 1, additive effect

CI < 1, synergy effect

CI > 1, antagonist effect

Being A(a) the dose a of compound A, $V_{A(a)}$ the viability of cells when compound A is used at dose a; B(b) the dose of compound B at dose b and $V_{B(b)}$ the viability of cells when B is used at b. The sum of these ratios defines the theoretical CI as one. The principle of this approach states that if the experimental value is lower, equal or higher than one a synergic, additive or antagonist effect is observed. (Equation **2**). Based on the Loewe additivity principle, the CompuSyn software developed by Chou bases its functioning. Three positive aspects can be mentioned from this software, first it is a user-friendly software that only needs a simple desk computer. Second that allows to determine the CI values (and therefore synergy, antagonism or additivity) in a quantitative way and finally it allows

the obtention of other data such as the isobologram graphs or the polygonogram graphs, which are graphs that help to visualize synergy, antagonism or additive effects when the number of drugs used is higher than two.[121,122] Yet if a great ammount of information can be generated from this software and it can give a tangible value of the synergy, there are some backdraws or pitfalls to take into account. First, a DRC needs to be obtained, therefore, it can not be used for compounds where this experiment can not be performed because the compound is not active or insoluble at high concentrations. Since the values for determining the CI are obtained from the average of the individual replicates from each result, no statistical analysis can be carried for the analysis of synergy.

2.3.4.2 Cytotoxicity of compounds in T98G cells

Study of cytotoxicity as single agents

Compounds were first screened in the T98G cell line at a fixed concentration of 10 µM (**Figure 20A**) using TMZ as a positive control (GI_{50} = 375 µM, **Figure 20B**). As observed for the first set of hybrids synthesized by Dr. Zuffo, none of the compounds was able to diminish the viability in a value lower than 50%, with compound **MZ049_F2** being able to diminish the viability by 12% compared to the untreated control of DMSO. Surprisingly, compounds **MZ001**, **MZ022**, **MZ043**, **MZ044** and **MZ051** showed a viability higher than 130% (143, 165, 172, 208 and 242% respectively). One explanation could be given is that the products could stimulate cell growth explaining the higher value of viability. To explore the possibility, viability was checked by manual cell counting at the same conditions. Values of viability for compounds **MZ001**, **MZ022**, **MZ043**, **MZ044** and **MZ051** were 94, 87, 82, 93 and 140% respectively. With these results, the hypothesis of a growth-stimulating compound was discarded. Because CellTiter Glo®measures viability as a function of ATP, an alternative explanation contemplated is that compounds elicit ATP production as it has been observed for small aromatic and pseudoaromatic molecules in primary corticoid neurons in mice[123] , HepG2 hepatocytes, Sol8 myoblast or 3T3 fibroblasts,[124] although this possibility was not confirmed. A third possible explanation are for ligands that resemble the luciferin substrate, that can stabilize the enzyme and increasing its concentration inside the cell giving a higher signal than the control,[125] giving the false impression of a higher viability for this conditions. Besides, the Ag^+ ion was tested at the same concentration displaying a viability of 5%. This toxicity has been observed for Ag-bearing compounds in other types of pancreatic cells like PANC-1 and 1.2B4,[126] and with **$AgNO_3$** in H-ras 5RP7 cell line[126] since they increase apoptosis levels in the mentioned cells. Furthermore, silver nanoparticles have been used in U251 glioma cells as TMZ sensitizer,[127] arresting the cell cycle in phase G_2/M increasing the apoptotic levels in the cell.

For the 8-azaquinolone family the sole compound active was compound **15** with a result in the viability of 56%. Compounds **7**, **8**, **10** and **13** showed a viability > than 75%, In the case of **14**, a similar situation was constated like described before. By using CellTiter Glo® the apparent viability was 163 % whereas by cell counting its value corresponded to 97% concluding it is not active. For the N^9 guanine derivatives and compound **22**, only **18** was able to diminish the viability in a significant proportion (57%) whereas the rest of the molecules showed a viability more than 75%.

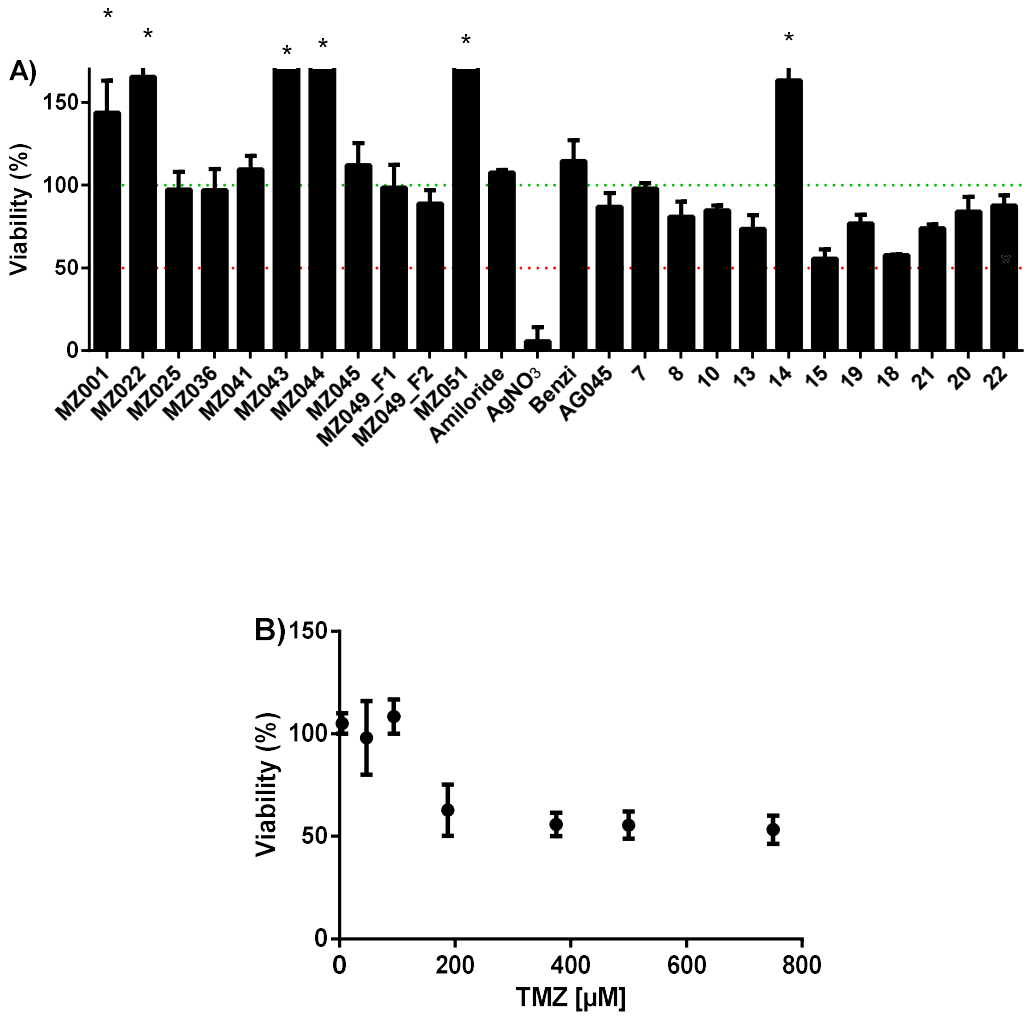

Figure 20A) Screening of indirect inhibitors at 10 µM against T98G after 96 h of incubation. **B)** Dose response curve of TMZ against the same cell line. Experiments show the mean ± S.D (*n* = 3-8).* Denotes compounds with abnormal viability value by CellTiter Glo® kit determination, that were lately corroborated by cell counting experiments

Study of cytotoxicity in combination with TMZ

A second experiment was performed by the combination of the ligands at a fixed concentration plus TMZ (**Figure 21**). TMZ concentration used was 94 µM where it did not show any toxicity at this concentration (viability 108%, **Figure 20B**). Compounds were added and incubated for 96 h after CellTiter Glo® read out and the experimental viability of this combination ($V_{A+B,}$ Exp) was compared with the expected theoretical viability (V_{A+B},Theo, calculated according to **Eq 1**). In this case, a potentiation of TMZ activity was desired by the combination. **MZ025**, **Benzi** and **MZ036** were able to decrease the theoretical viability on a 10% which was not considered statistically significant after a ONE WAY ANOVA test. Compounds **MZ022**, **MZ044**, **MZ051, AG045** and **7**, which again showed interference in the combination assay, were not re tested by cell counting. As we can observe from this graph, none of the compounds was able to potentiate TMZ's activity, indicating that they do not inhibit any of the multiple pathways linked to TMZ resistance.

As mentioned previously, TMZ's major products are the N^7MeG and N^3MeA formation which then are depurinated forming AP sites (C:AP and T:AP respectively). As observed from fluorescent and UV melting experiments, **15** was able to interact and stabilize abasic sites. Considering these two observations, we were expecting that **15** could increase the cytotoxicity of TMZ in the cell by stabilizing the AP sites *in cellulo*. However, it was not the case presumabiliy due to the fact that the concentration of **15** in *in vitro* experiments (300 µM) was much higher than the used for the cytotoxic screening (10 µM). A target prediction using the SwissADME platform[128] revealed that this molecule had a 53% of probability of being a kinase target, especially the Ser/Thr protein kinases PIM 1 and PIM 3 responsible for cell survival and proliferation and no enzyme related with the BER system.[93] This data that could explain why **15** is toxic by itself and why no synergy is observed.

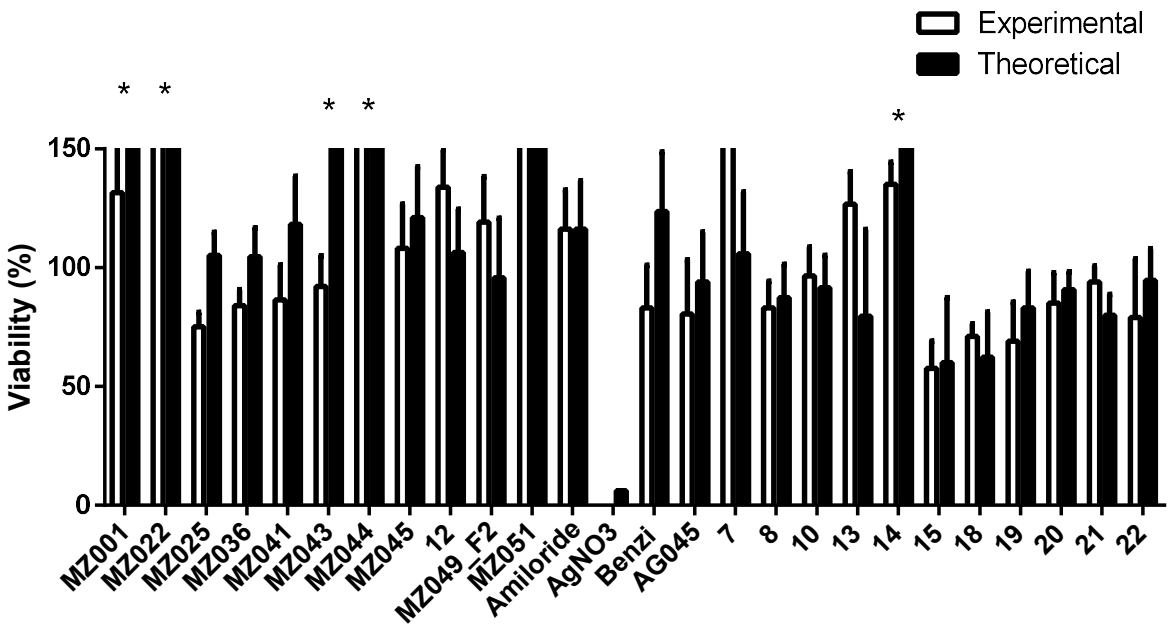

Figure 21 Bliss comparative analysis of combination of indirect inhibitor (10 µM) with TMZ at 94 µM. Black bars represent V_{A+B}, Theo and its theoretical S.D. (see Experimental Section); white bars represent the mean of the experimental viability $V_{A+B,}$ Exp ± S.D (n =3). * Denotes compounds with a viability higher than 150%

2.4 Conclusions

In this part of the Thesis we have systematically explored the indirect inhibition strategy targeting MGMT. Here, eleven heterocyclic compounds were synthesized by varying its hydrogen bond donor/acceptor pattern, together with their size, hydrophobicity and π surface, as potential ligands that could bind to O^6MeG residues in DNA. The capacity of these molecules to stabilize a dsDNA bearing a O^6MeG:C or a O^6MeG:Φ site surrogate of an AP site was studied by UV melting experiments trying to obtain compounds that bind and stabilize O^6MeG-containing dsDNA structures. Unfortunately, none of the compounds was able to stabilize the surrogates to a significant extent, similarly to what was observed for the previously synthesized molecules in our laboratory.

It is interesting to highlight that the compound Benzi, previously described as a selective O^6MeG partner (when incorporated into the opposing DNA strand) did not stabilize the DNA surrogates used in our hands. Factors like DNA sequence, length, concentration of DNA and ligand, type of buffer or ionic concentration may be responsible for these differences. However, the biggest difference between the methodologies is how the ligand is found in solution. In Sturla's articles, Benzi is incorporated as a nucleobase in front of the O^6MeG base and not freely in solution as in our models. This way, the entropic factor is dramatically reduced as well. Because it was also proved that Benzi conformation of the glycosidic bond between N^9 of the nucleobase and C'1 of the sugar are *anti*, the probabilities to create the necessary bonds with O^6MeG to stabilize the DNA are increased. In our case, the ligand is free in solution, where the probabilities for the interactions are reduced even if the concentrations of ligands are 10 to 30 times higher than the DNA. For the binding opposite to O^6MeG residue, the ligand should flip out the opposite C (or accommodate himself in the AP site facing O^6MeG), position itself in front of the base and stablish the proper hydrogen bonds. In other words the stability of the ligand:modified nucleobase interaction should be high enough to be the driving force that surpasses and compensates all the events mentioned above.

Comparing this strategy with the natural process of detection of O^6MeG by MGMT the process seems quite unlikely to be achieved by small molecules. Worth reminding, is the fact that the cell has develop a unique suicide enzyme along the thread of evolution to selectively detect only one type of DNA modification. MGMT cooperatively scans the DNA and has multiple interaction points with DNA, something that does not occurs in our model. Most importantly, MGMT also binds to G residues as well (meaning it does not have a binding selectivity) but it does not reacts with them since the recognition is based mainly on the specific reactivity of the Cys towards the methyl group in O^6MeG. Therefore and considering our results, the recognition of this DNA lesion by small ligands seems quite unlikely at least *in vitro*.

Because some 8-azaquinolones were described as AP site ligands, the ability of these derivatives to stabilize selectively this type of lesion was evaluated. In here, we found that compound **15** slectively stabilizes A:Φ site in UV melting experiments and also had a "light–up" effect upon binding to DNA, albeit without selectivity towards A:Φ containing duplexes.

These results encouraged us to test **15** together with all the previously synthesized compounds in T98G cell line to study the possibility for binding AP sites created by TMZ in the cell. Unfortunately, none of the compounds showed a great cytotoxicity against this cell line either alone or in combination with TMZ, indicating that they do not interefere with the patwhays linked to TMZ resistance. Because neither the *in vitro* nor *in cellulo* strategy for developing drugs to use in combination with TMZ worked for the IIS, this apprach was abandoned and two new strategies were explored.

Chapter 3
MGMT inhibition with hybrid drugs

3 MGMT inhibition strategy with hybrid drugs

3.1 Principle and State of the Art

As explained in the Introduction, MGMT overexpression is the main cause of TMZ resistance in GBM but not the sole one. In fact, diseases (cancer included) are generally a combination of dysfunctions in the cellular machinery that makes difficult their treatment by a single drug. In this part of this Thesis, we propose the inhibition of MGMT by hybrid drugs as an approach to overcome the multiple resistance mechanisms that the GBM cell contains that confers resistance to current treatment.

The concept of hybrid molecule can be defined as the combination of two chemical entities to enhance or amplify each other's activity, modulate one activity or the other or to exert dual activity inside a cell.[129] There are at least three methods for combining each individual molecule. The chosen method depends on the chemistry of the corresponding scaffolds and on the ability for this new hybrid to remain (or not) biologically unaltered. The first method consists in the use of an in-cell hydrolysable functional group such as an ester, an amide or a carbamate. The second option, is the union through a non-cleavable linker such as an alkyl chain, a polyamino group, a polyethyleneglycol linker or finally, through a triazole linker. The third option, may be the most difficult one, consists in overlapping the chemical entities or pharmacophores in one single fused molecule. These strategies are reviewed in Decker *et al.*[129] The hybrid strategy has several advantages such as tackling two targets with only one molecule, or having a new chemical entity with only one pharmacokinetics and pharmacodynamics (PK/PD) profile. For the hybrid no drug-to-drug interaction should be observed, an easier formulation can be obtained or a lower toxicity can be achieved. However, this very same advantage could turn into a disadvantage since a balance in the design should be taken into account for compounds that individually have a very uneven concentration range of activity. In spite of these challenges, this strategy has been applied for designing receptor ligands/enzyme inhibitors, to fight tropical parasitic diseases, Alzheimer's disease, cancer or in the design of molecules to control oxidative stress.[129]

3.1.1 Hybrid drugs for cancer treatment

In the case of cancer research, molecules in different stages of the clinical studies can be found (**Chart 8**). For example: Estramustine is a drug currently used in Phase II for breast cancer treatment (NCT02866955). This molecule uses estradiol, that targets the estrogen receptor (ER) in metastatic breast cancer downregulating its cascade that involves cell proliferation[130] combined with the alkylating agent normustine that targets DNA.[131] Another example could be Lucitanib (E-3810), which is a hybrid containing a quinoline moiety that inhibits tyrosin kinases[132] and the naphthalene core, proved to inhibit the vascular endothelial growth factor receptor 2 (VEGFR2).[133] This compound was used in Phases I/IIa for solid tumours were a defect on VEGFR2 was observed (NCT02747797) but surprisingly the clinical trial was called off due to the lack of supply of the drug by the manufacturer. A third example is CUDC-907, a compound tested in Phase I for several solid tumours like colorectal, sarcoma, breast or ovarian.[132] CUDC-907 bears an hydroxamic acid moiety responsable for the histone deacetylase (HDAC) inhibition plus a thienopyrimidine scaffold implied in the phosphoinositide 3 kinase (PI3K) and the mammalian target of Rapamycin (mTOR) inhibition.[134] Another example is the molecule Pexidartinib (PLX3397) holding a sulfonamide group responsable for BRAF Ser/Thr kinase cascade inhibition[134] connected to the trifluoromethyl pyridine that inhibits inflammatory processes necessary to tumor growth.[135] This molecule was tested in Phase II of clincal trials for GBM patients since it was observed that the molecule targeted the colony stimulating factor 1 receptor (CSF1R), responsable for cancer infiltration and migration.[134] Even if the compound was not toxic in the regime used, no improvement was observed comparing with the already used strategies. Currently, a Phase I/II trial is being conducted with the compound in combination with RT and TMZ in newly diagnosed GBM patients (NCT01790503). Finally, Curaxin CBL013 was tested in clinical trials for advanced solid neoplasms (NCT01905228), contains a carbazole and the amino chain from the quinacrine that activates p53 protein that facilitates NF-κB inhibition. Not less interesting; this chimera was demonstrated in preclinical models the ability to delete GSC cells.[136]

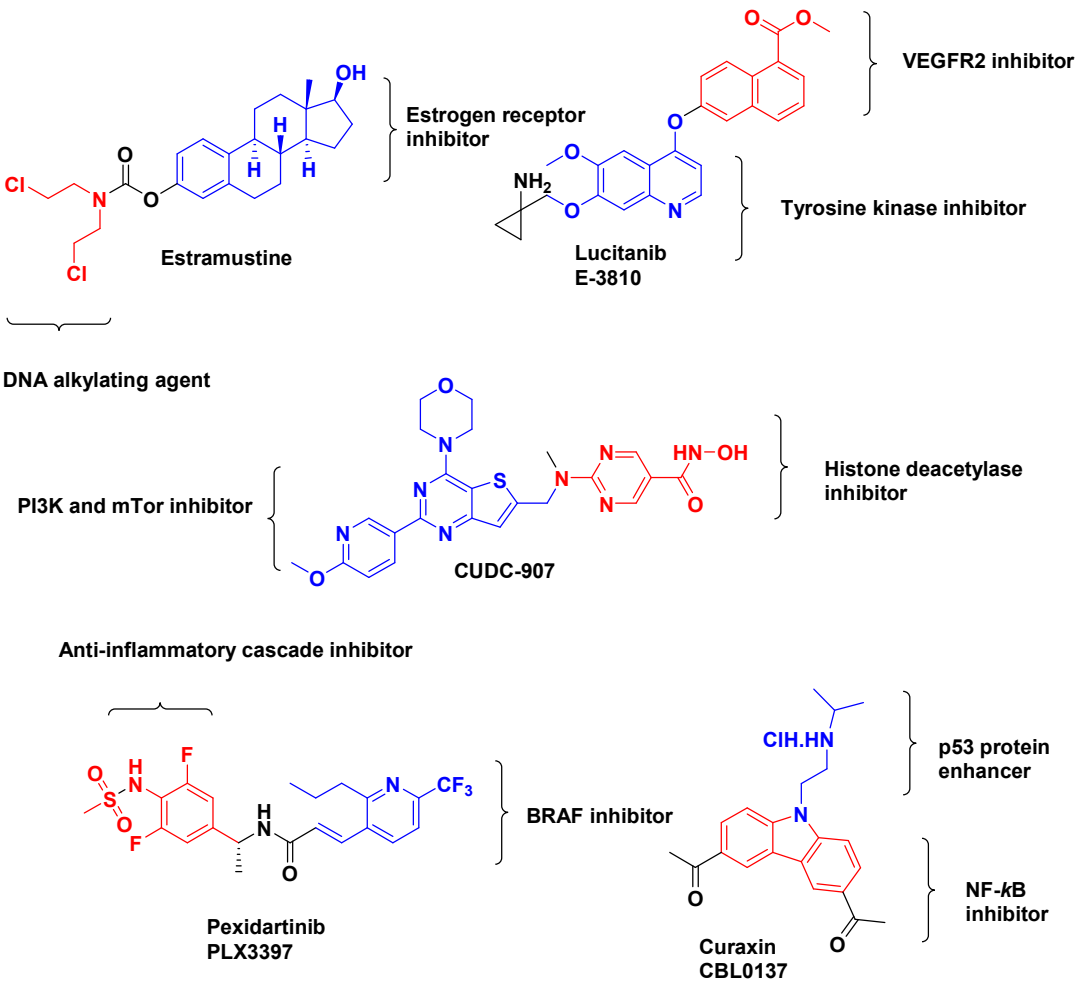

Chart 8 Hybrid molecules used in clinical trials for cancer treatment

3.1.2 Hybrid drugs targeting MGMT

There are other, less advanced examples of hybrid molecules, for example the ones that contain MGMT inhibitor scaffolds (**Chart 9**). One example is MR-30, a hybrid that contains a quinazoline moiety that targets the EFGR which is highly implied in the activation of the DNA repair systems *via* XRCCC1. With this hybrid, researchers performed *in cellulo* experiments in a lung carcinoma (A549) and a melanoma cell line (A375) where they demonstrate the capacity of inhibiting both targets. More interesting to highlight is that the combination of MR-30 (10 µM) and TMZ in a pulse-sequence strategy was able to reduce the GI_{50} of the latter from 283 µM and 222 µM in 2 and 1.5-fold in A549 and A375 cell lines, respectively, after 8 days.[137] A second example are the molecules designed by the Zhao group that consisted in O^6BG molecules attached by the Bn ring (**138.6**) or by the N^9 (BGCNU) to a chloronitrosourea agent that acts as an alkylating and ICL agent. The molecules were evaluated against three types of glioma cell lines with different levels of MGMT expression (SF126, SF767 and

SF763). For the first molecule (**138.6**) GI_{50} after 24 h was 50, 25 and 35 µM which corresponded to 6.4, 20 and 28-fold lower than the combination of O^6BG (20 µM) and ACNU in SF126, SF767 and SF763 cell lines respectively.[138] The second molecule, BGCNU, had higher GI_{50} values of 52, 58 and 60 µM, corresponding to values 6.9, 6.9 and 17-fold lower than the combination of O^6BG and ACNU in SF126, SF767 and SF763 cell lines respectively.[139] With both compounds, researchers demonstrate that the effect of the cell viability is more affected regarding the amount of intrinsic MGMT expressed. In other words, the higher the level of expression of the target enzyme, the more affected will the viability be when MGMT is inhibited in combination with an alkylating agent. A final example is the O^6BG-triazene hybrids (**140.20-33**) that were conceived to achieve simultaneous MGMT inhibition and a release of the diazomethane alkylating agent *in situ*. These molecules were tested in a large panel including breast, ovarian, prostate, lung, non small lung cancer, colon, renal, leukaemia and CNS cell lines. Respecting CNS cancer, it was found that **140.26** showed GI_{50} after 48 h in the range of 8-11 µM versus SF-268, SF-295, SF-539, SNB19 and U251 cell lines.[140]

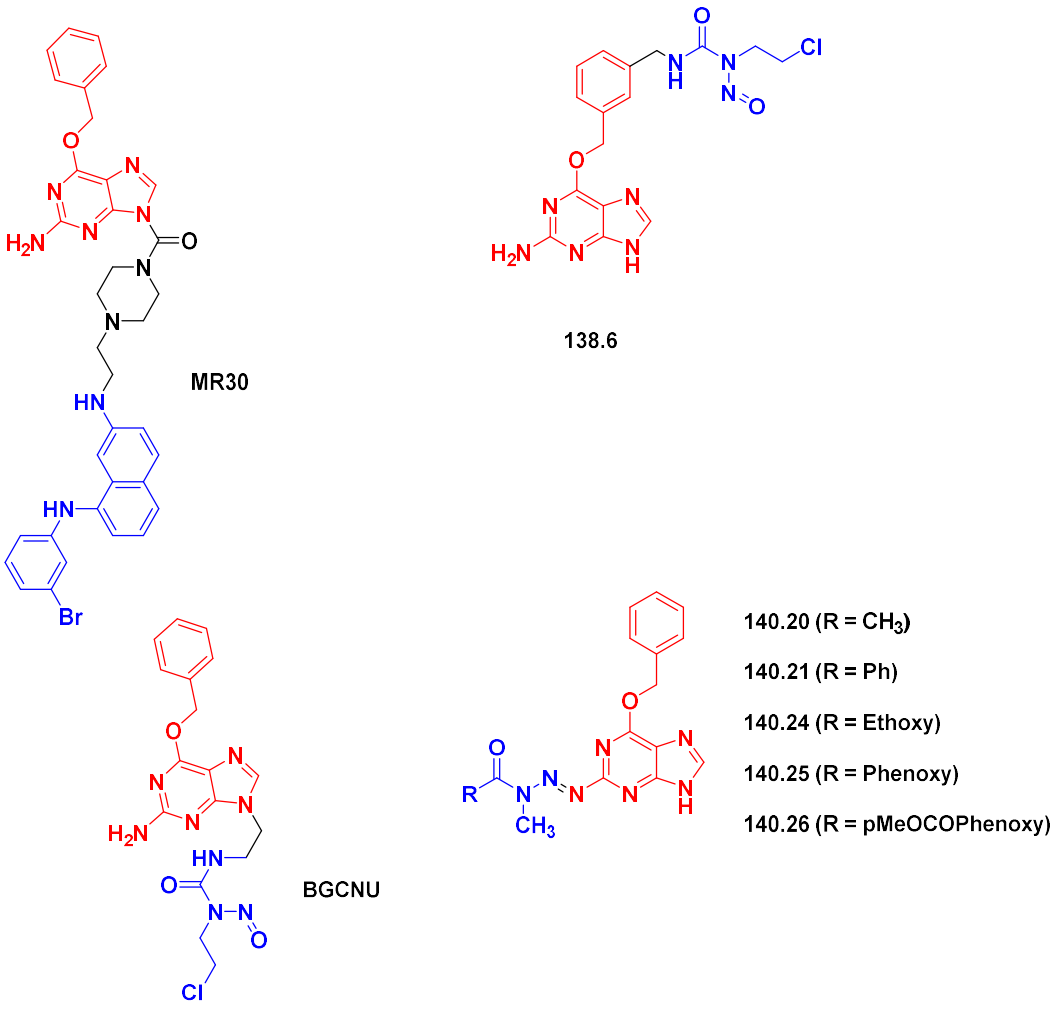

Chart 9 Hybrid molecules containing O^6BG

3.1.3 Hybrid drugs containing an acridine core

An interesting scaffold used in the medicinal chemistry area are the well-known DNA intercalators that can inhibit enzymatic process like DNA/RNA polymerases agents.[141–143] Within this particular group we find the 9-aminoacridine (9-AA) scaffold and its analogue, 9-amino-6-chloro-2-methoxyacridine (Acr) contained in quinacrine (QC**, Chart 10**). QC is a drug that has been used for more than one century to treat infectious diseases like malaria, Giardia or amebiasis or due to its anti-inflammatory activity for treating bronchial asthma or rheumatoid artrithis.[143] Despite being considered a mere DNA intercalator, QC has been shown to be non-mutagenic, non-cancerogenic and non DNA-damaging agent, which is the reason why it has been used in several drug-repurposing programs for cancer treatment. In cancer cell lines, the molecule has been first postulated as Topoisomerase II inhibitor although researchers have cast doubt on this mechanism of action as the reason for the cytotoxicity in cancer cells since its IC_{50} (concentration that inhibits 50% of the enzyme activity) values *in vitro* are dissimilarly higher than the *in cellulo* GI_{50} values.[144–147] There are other mechanisms proposed such as the inhibition of the phospholipase 2 (PLA2) whose cascade produces pro-inflammatory processes needed for angiogenesis and tumor development. Another observed effect in cancerous cell lines is the activation of the p53 tumor suppressor protein by QC, which is mutated and dysfunctional in more than 50% of cancers. According to the literature, QC binds DNA and inhibits the binding of one of the proteins member of the heterodimer that facilitates transcription (FACT) complex.[136,148–154] This union impedes the binding of a high mobility group protein (HMG) called structure specific recognition protein 1 (SSRP1), an effect that activates p53 expression. As well, it enhances the binding of another transcription factor called HMGA1, which inhibits NFκB transcription, eliminating the capacity of the last one to sequester p53 protein. But since QC has been shown to be active in p53 gene-deleted cells other mechanisms have been proposed for its action in cells like the inhibition of the heat shock factor 1 (HSF-1) and the HIF-1α which are necessary for tumor growth under the stress conditions were they develop.[143,147] Due to the multi-target effects and the interesting *in celullo* properties as a multi-targeting compound, QC is currently being tested in Phase I/II in combination with the anti-metabolite Capecitabine in metastatic colorectal cancer [155] or in Phase I with the EGFR inhibitor Erlotinib in non small lung cancer cells where it was shown to be well tolerated, but with limited efficacy.[156]

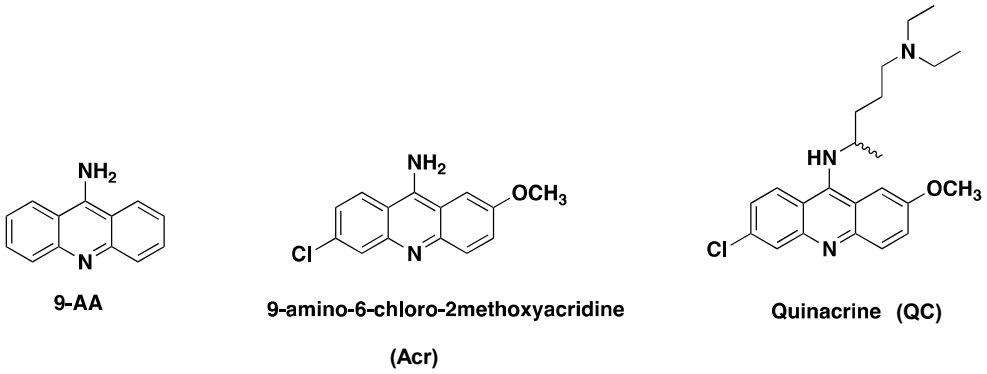

Chart 10 Acridine scaffolds

As mentioned before, molecules designed to target AP sites have been linked to an **Acr** ring since the latter can intercalate with DNA increasing the hybrid affinity (**Chart 3**).[69,157,158] Moreover, the **Acr** fragment has been extensively exploited in the design of hybrid drugs targeting malaria with a napthalenediimide core (**159.2a-b**) that provides a redox capacity of killing the intracellular stage of the parasite, or with the artemisinin drug (**160.6**).[159,160] Molecules designed by the Zimmerman group (**161.1** and **163.9**) target trinucleotide $(CUG)_n$ or tetranucleotide $(CCUG)_n$ RNA repeats that sequester the MBNL1 protein causing Myotonic Dystrophy Type 1 (DM1) or Type 2 (DM2), respectively.[161–163] A final example are the molecules designed by the Bierbach group were a 9-AA core is linked to a Pt containing-molecule plus the drug tamoxifen to treat breast cancer. Here reserarchers observed that molecule **164.10** in MCF-7 cells and MDA-MB-231 they GI_{50} after 72 reached a 3.5 and 21.4 μM value.[164]As well, in a lung cancer cell line called NCI-H460, 60 hybrids were tested showing for example that compound P2-A1 had a 2.5 nM GI_{50} value after 72 h (**Chart 11**).[165]

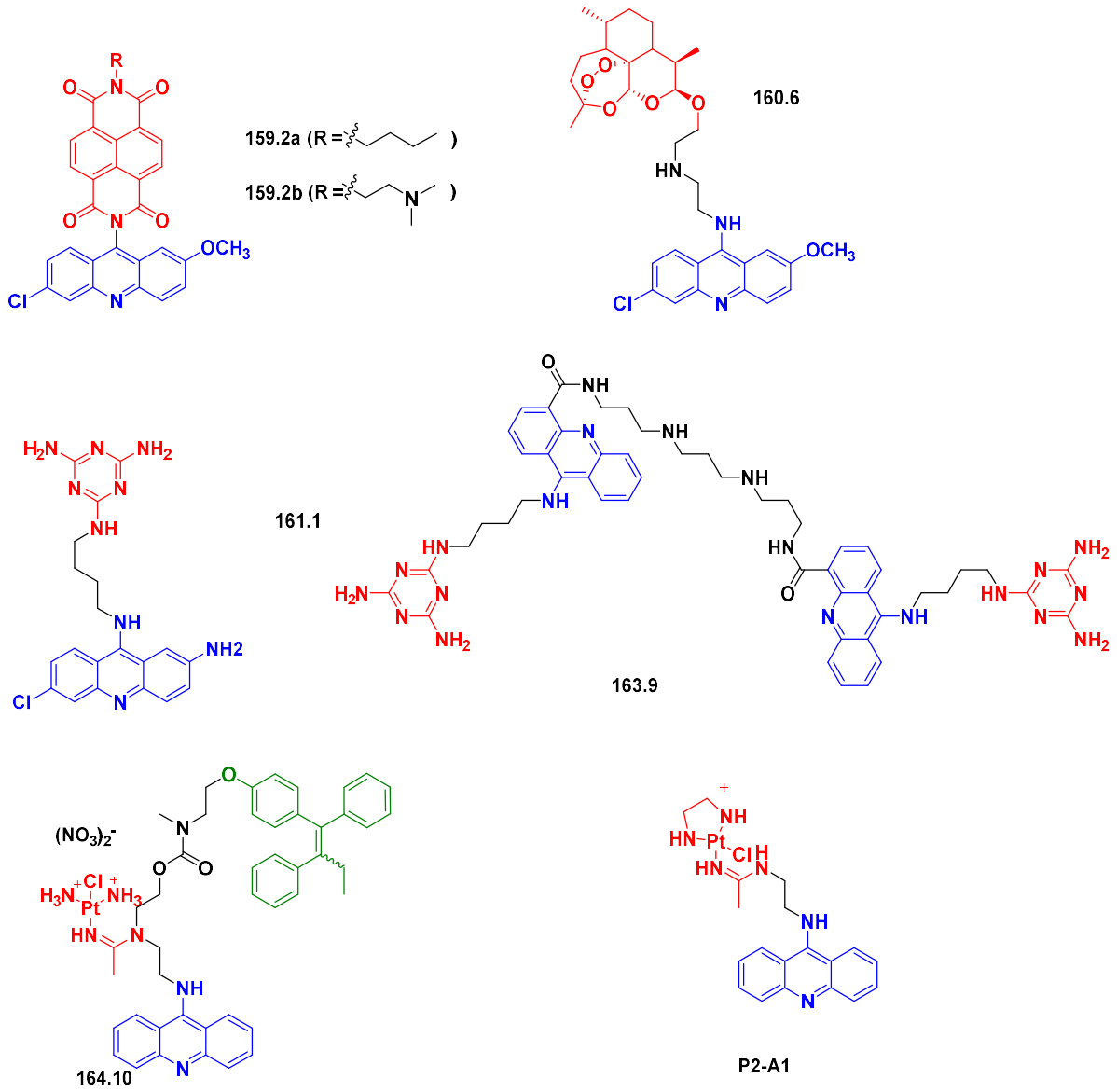

Chart 11 Hybrid drugs containing an acridine core

3.2 Aims of the work

Based on the hybrid strategy, we propose to synthesize molecules containing the O^6BG core combined with the **Acr** scaffold with the goal of obtaining a molecule capable of inhibiting MGMT that could confer the biological properties of the **Acr** core. Since it was discussed that O^6BG modifications in the Bn group and the N^9 atom maintained the ability to inactivate MGMT in comparison with O^6BG, two types of hybrids (Bn hybrids and N^9 hybrids) were designed (**Chart 12A**). The idea of this strategy consists in the use of the core (**Acr**) that will be bound to the O^6BG in a stacked or inactive conformation. After unstacking, the open or active conformation could interact with DNA through **Acr** exposing the O^6BG to inactivate MGMT. Due to MGMT mechanisms, according to the type of hybrid used; two different inactivation MGMT products could be obtained (**Chart 12B**).

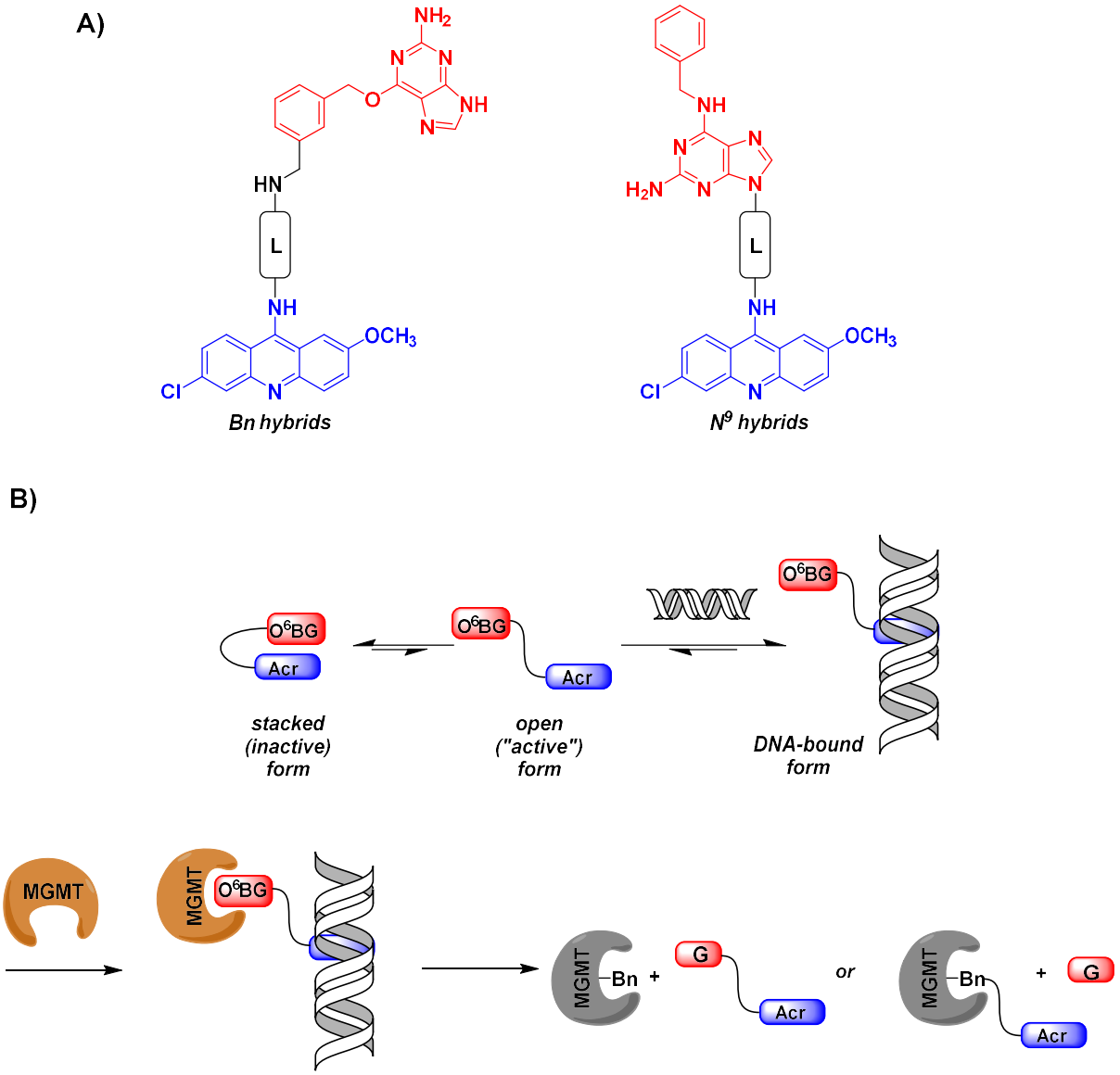

Chart 12A) General structure for hybrids **B)** Mechanisms of MGMT inactivation with the O^6BG-Acr hybrids.

3.3 Results and discussion

3.3.1 Synthesis

3.3.1.1 Bn hybrids

In this approach, we carried out two different paths to achieve our hybrid molecules of type (**A** in **Figure 22**). The **Path A** consisted on the introduction of the acridine ring by a S_NAr as a final step as it was already reported in the literature for similar substrates.[161,163,166] In this case, the commercially available acridine **B** reacts with the guanine derivative **C**. This scaffold can be constructed by the nucleophilic substitution of the 6-chloroguanine **D** with the protected alcohol **E**, which can be previously obtained from the aminoalcohol **F**. **Path B**, can be achieved by introducing an amide bond in between the acridine **G** and the guanine derivative **H**, each of them can be obtained from the commercially available starting materials **B** and **D** respectively.

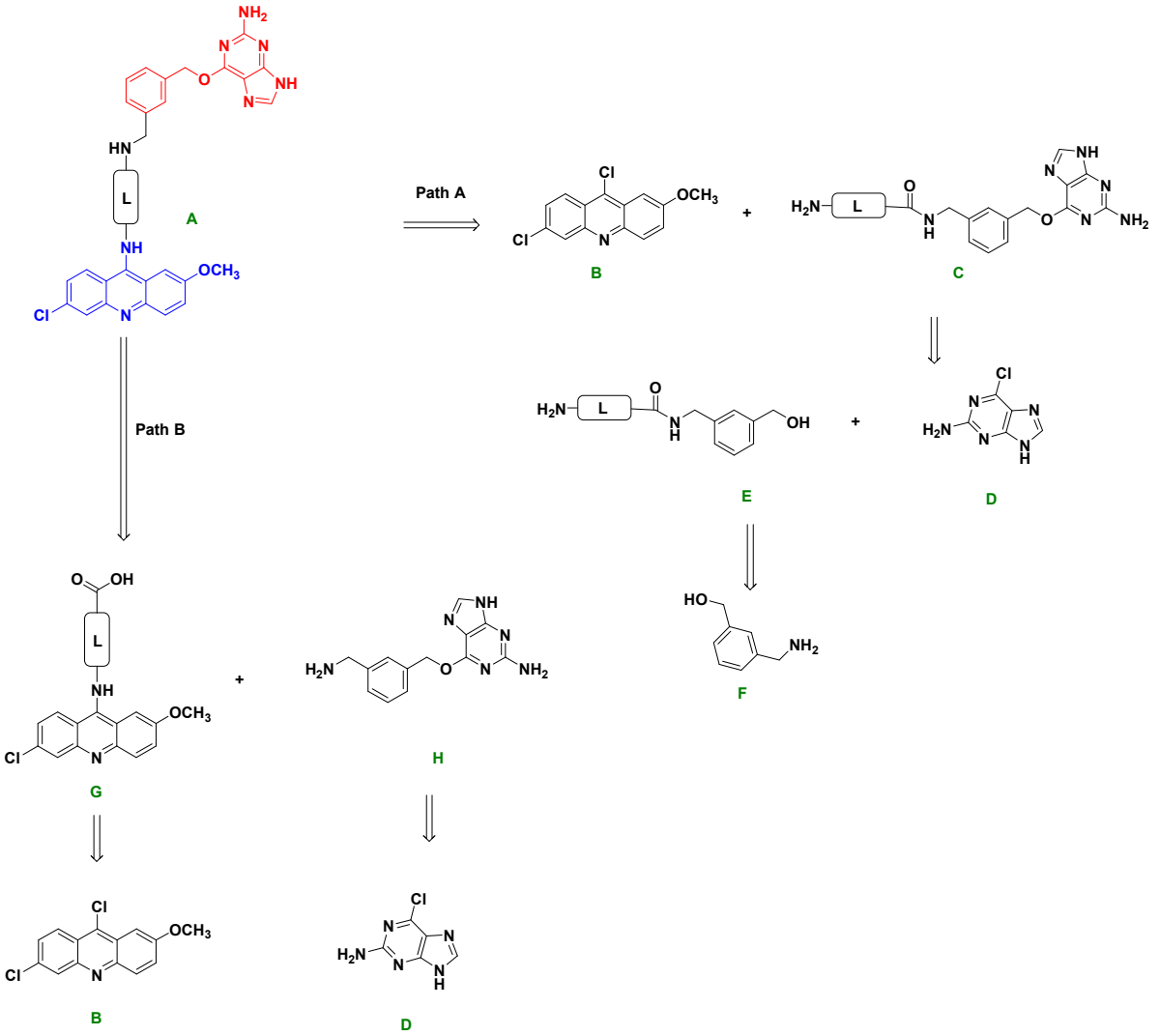

Figure 22 Retrosynthetic analysis for Bn hybrids

Path A: introduction of the acridine ring as the final step

For the obtention of the nucleophilic compound **C**, a synthetic route based on an already described methodology was performed and is based in the classic SNAP-TAG route developed by Johnsson's group.[37] For that, the building block **23** (**F** in **Figure 22**) was synthesized in a large scale using two types of reductive methods previously reported in the literature.[37,167] The reduction on a 10 g scale of 3-cyanobenzoic acid using $THF.BH_3$ complex or methyl 3-cyanobenzoate with $LiAlH_4$ as reducing agents yielded the obtention of the desired product in 98% and 44% respectively. Despite being more expensive, but because of a better yield, the $THF.BH_3$ complex proved to be more beneficial from an economical point of view as reducing agent. The product **23**, was coupled with the *N*-Boc protected β-alanine **24**[168] using EDCI and HOBt in a classical amide bond formation reaction to yield **25** in good yields (**Scheme 4**).

Once this benzyl alcohol was obtained, the next step consisted in attaching it to the guanine moiety. In order to perform this step, an activation of the 2-amino-6-chloropurine **D** was carried out through the formation of the quaternary salt **26** which was obtained in good yield.[169] Once this compound was isolated, a nucleophilic substitution was carried out in the presence of **25** and *t*-BuOK to obtain **27** in low yield[169]. The *N*-Boc protected group of **27** was removed with HCl in dioxane and then this crude was treated with an Amberlite IRA 402-OH ion exchange resin, and without isolation, the intermediate free amine (**C** in **Figure 22**), reacted with the activated phenoxyacridine **28** in basic conditions.[166,170,171] In this reaction, the formation of the Bn hybrid (**A** in **Figure 22**) was observed by LCMS in trace amounts, with the concomitant transformation of **28** into acridone. Although this strategy of S_NAr on 9-phenoxyacridines is widely reported in the literature and described as efficient, two points must be highlighted in order to attempt to explain the lack of formation of the hybrid **A**. The first one that could be considered is the lower temperature compared to previously described reactions (80 °C instead of 110-120 °C), and the second, is the use of the HCl in dioxane as deprotecting agent for the Boc-protected amino group in **27**. This could not only lead to the *N*-Boc deprotection but also to the debenzylation in the guanine.

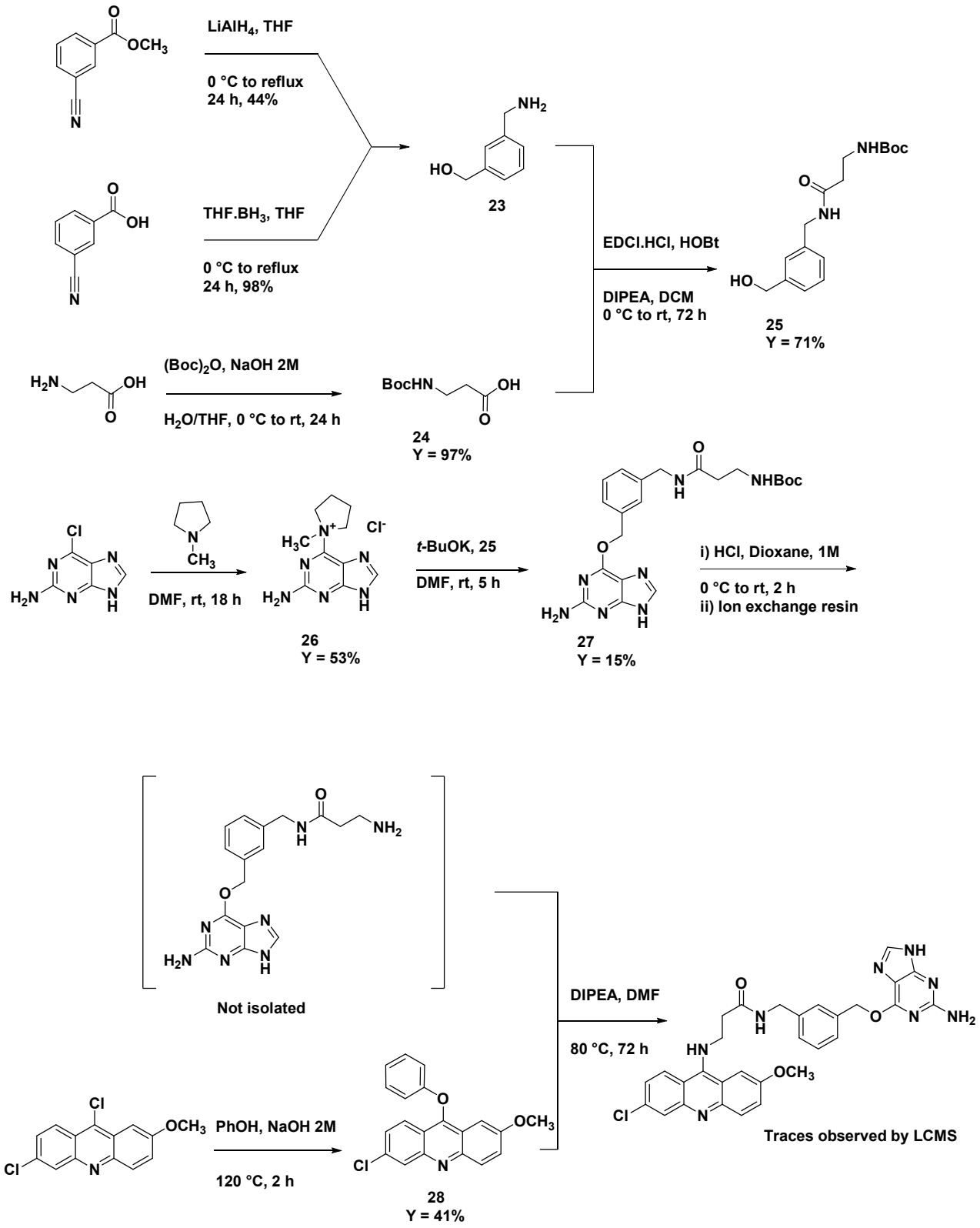

Scheme 4 Synthesis of Bn hybrid molecules by Path A

Path B: linker formation through an amide bond as the final step

Taking into account these two obstacles (the low yield to obtain **27** and the lack of formation of a feasible Bn hybrid), another strategy (**Path B** in **Figure 22**, page 77) was successfully exploited. This path was a useful strategy because it allowed us to prepare several types of carboxyacridines **G** and to obtain the modified benzylguanine **H**. It is worth mentioning that **H** with its aminomethyl group in *meta* position demonstrated to be a better inhibitor of MGMT in comparison with O^6BG, and it was also shown to increase the toxicity of the alkylating agent BCNU in HT29 cells.[37]

Synthesis of the ω -aminoacid linkers

Before constructing the carboxyacridines, and due to the commercial unavailability of some linkers, the precursors of these compounds where synthesized as described below (**Scheme 5**).

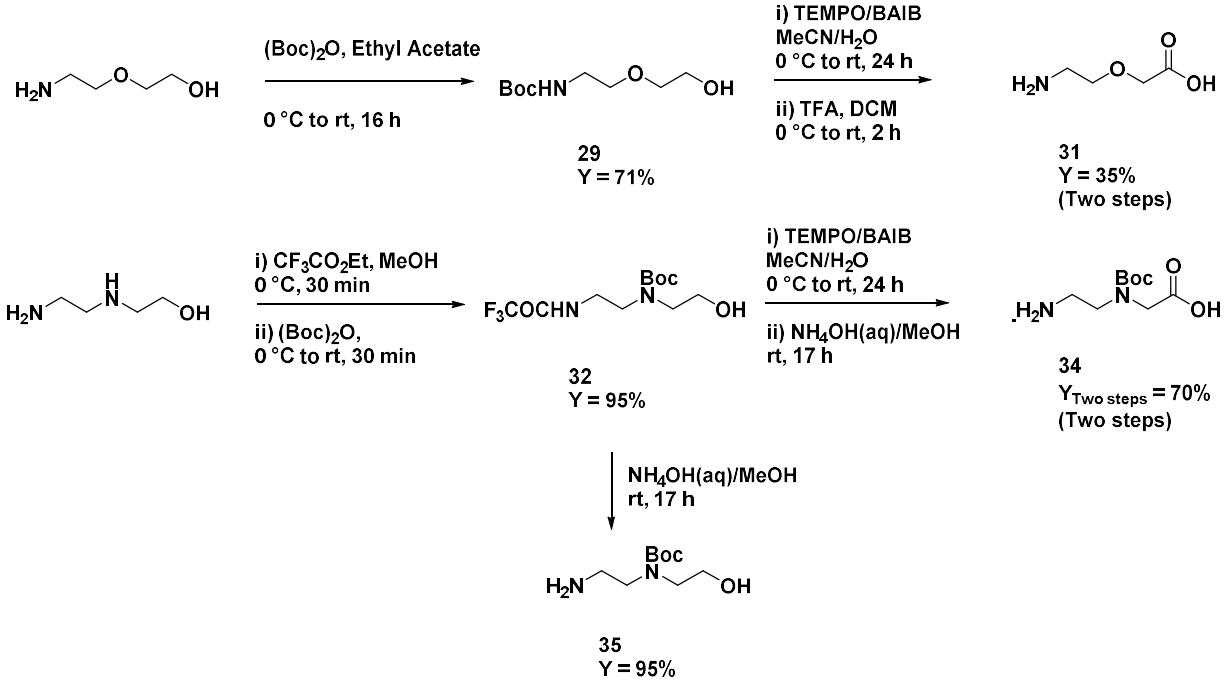

Scheme 5 Synthesis of the ω -aminoacidic linkers

When an oxygen atom was inserted in the linker, the aminogroup of aminoalcohol was protected as a carbamate to yield the compound **29** in very good yield.[172] The alcohol group was submitted to oxidation to a carboxylic acid, first by using $NaIO_4/RuCl_3$ as oxidant and catalyst[173]. Since in the assayed conditions the starting material did not react, a second system was performed by using bis(acetoxy) iodo benzene (BAIB) as an oxidant and TEMPO as a catalyst. This led to the obtention of the carboxylic acid **30** which then was converted into the aminoacid **31** in a moderate yield considering the two steps of reaction.[172]

A similar strategy was conducted to obtain a ω-aminoacid containing a nitrogen atom in its chain. To obtain this molecule, an orthogonal protection was carried to form the di-protected alcohol **32** in excellent yields.[174] The diprotected alcohol was oxidized by the TEMPO/BAIB system to yield **33**, and its primary aminogroup was deprotected in an aqueous basic media to yield **34** in very good yields. In addition, the primary aminogroup of **32** was deprotected in the same conditions to render the monoprotected amino alcohol **35** an excellent yields.

Synthesis of carboxyacridines, **G**

Once the nucleophilic aminoacids were obtained, a general strategy for preparing carboxyacridines was performed. It consisted on heating the 9,6-dichloro-2-methoxyacridine **B** in phenol to obtain an activated intermediate **28** *in situ* or previously synthesized and add the nucleophilic aminoacid afterwards for achieving the desired product (**Scheme 6**).

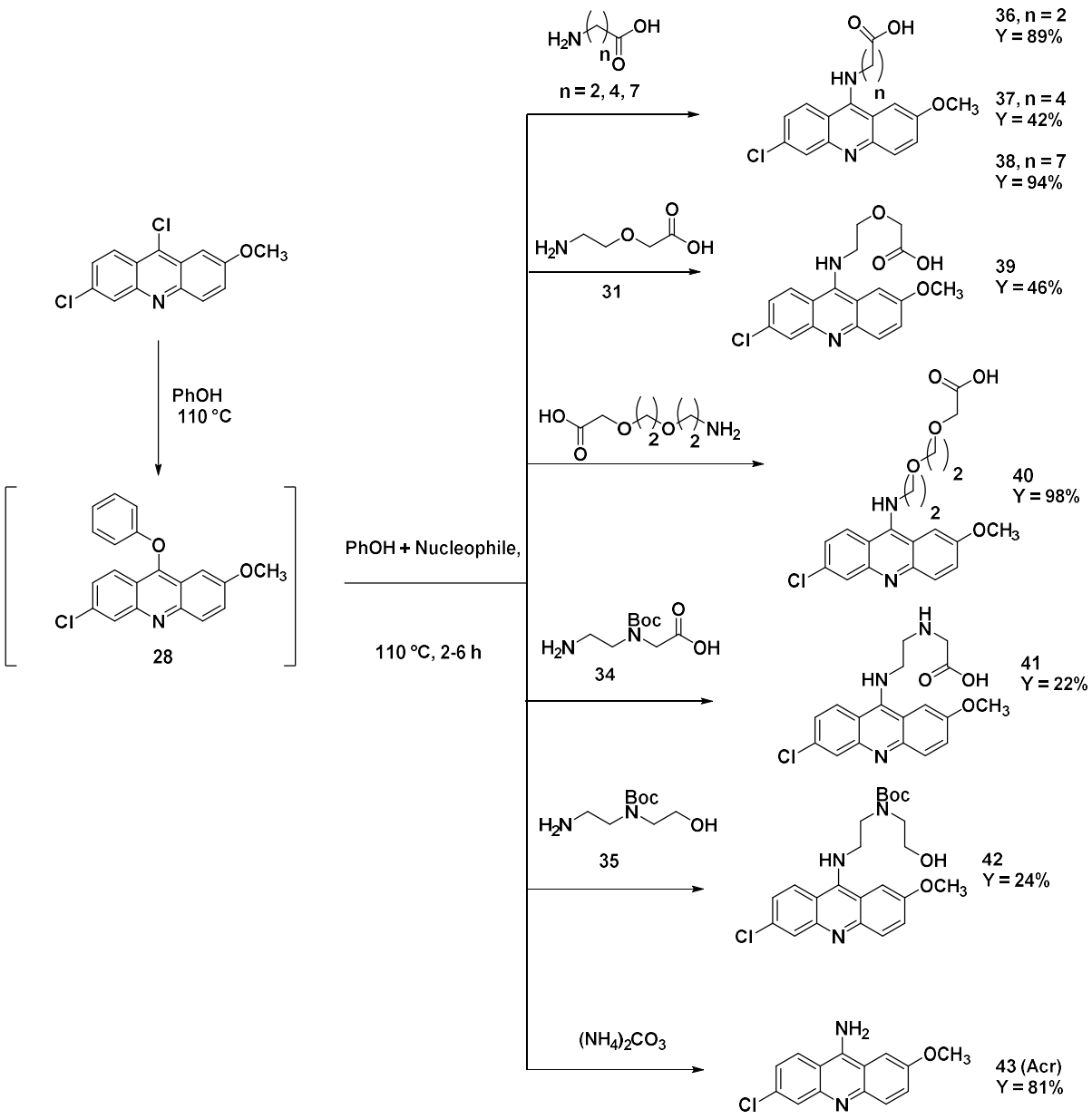

Scheme 6 Synthesis of carboxyacridines plus alcohol **42** and 9-aminoacridine **43**

In this case, three groups of nucleophiles were used, where the first one were the commercially available ω-amino acids that yielded the products (**36**, **37** and **38**) in good to excellent yields. The second class of nucleophiles corresponded to oxygen-bearing chains, and the use of this aminoacids was carried as described above to yield the carboxyacridines in good (**39**) to excellent yields (**40**). The third class corresponded to the aminoacids with a secondary *N*-protected amino group in the linker. When **34** was used, the product was observed by NMR and LCMS, corresponding to a *N*-Boc deprotected compound (**Figure 23A**). After its obtention, two questions arose regarding this reaction. First, since there is no more *N*-Boc group, we asked ourselves by which amino group the

linker was attached. This question was answered by the use of a HMBC experiment (**Figure 23B**), which shows that signal A, corresponding to the CH_2 in the α position to the exocyclic 9-aminoacridine atom, has a long-distance correlation with the aromatic carbon in the position 9 of the ring. Since we do not know which event occurs first (the nucleophilic substitution or the *N*-Boc deprotection) we asked ourselves if similar reactions were reported in the literature for similar systems. And, we could confirm that in similar acridine systems, when nucleophiles containing polyamine groups are used, the major product corresponds to the attachment through the primary and not through the secondary amine.[164,165,175] Since these reactions showed that the primary amine reacted on a preferably fashion than on a secondary one, we cannot rule out the possibility that due to the harsh reaction conditions (110 °C with a weak acid donor such as PhOH) compound **34** is first deprotected and then reacts to form **41**.

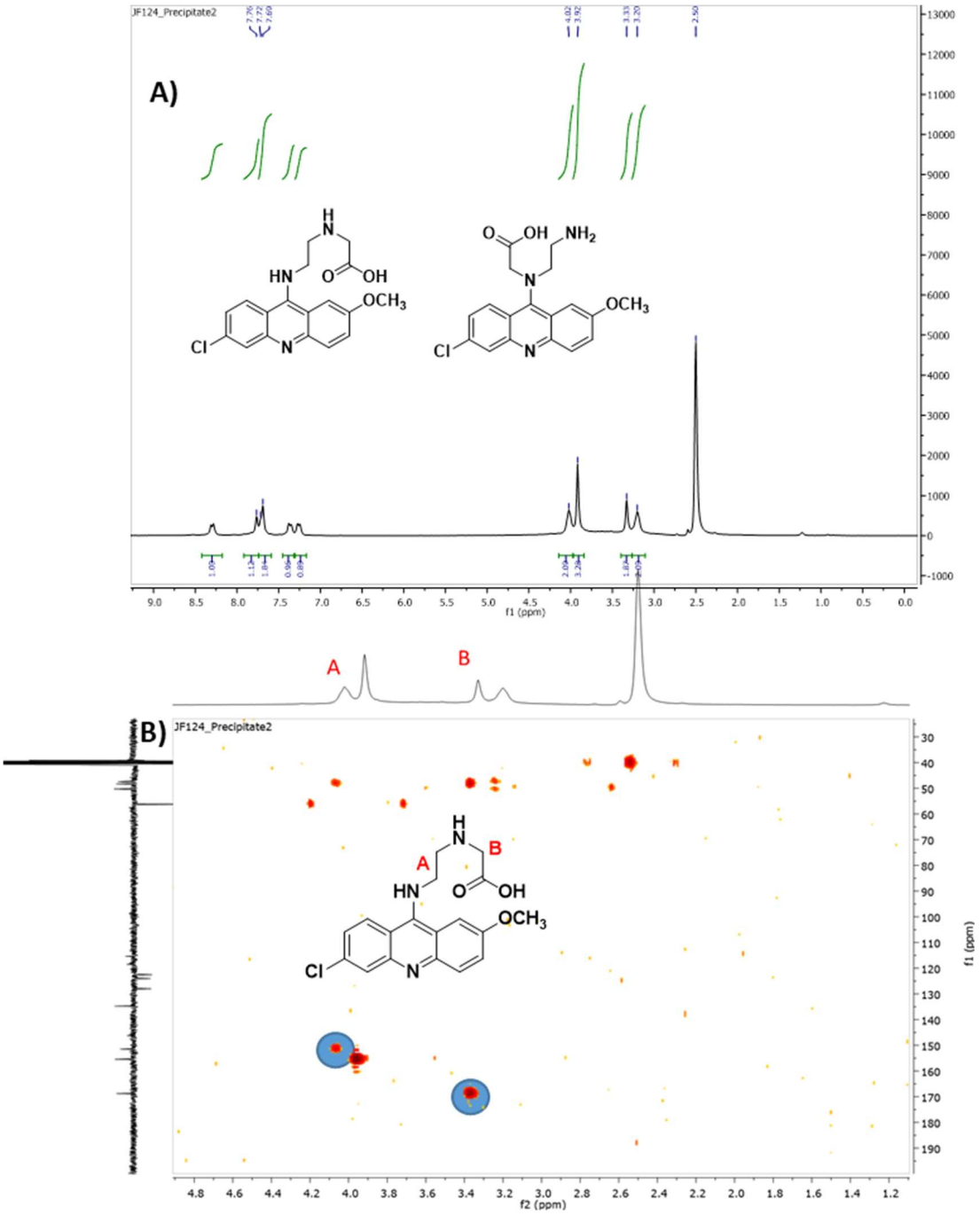

Figure 23A) ^{1}H NMR and **B)** HMBC experiments for **41** configuration's determination

In addition, we wanted to determine if in the harsh reaction conditions the *N*-Boc group is always cleaved. To address this point, we treated aminoalcohol **35** in the same conditions, which was converted in low yield into the *N*-Boc protected **42**. From these data, we can partially conclude that the *N*-Boc deprotection in the PhOH/heat system is substrate dependent. The last compound of this series was the 9-aminoacridine **43** (**Acr**), which was designed as a control molecule, was obtained in excellent yield. [159,176]

By looking at the yields, we observe a big differences if we compare in between the carboxyacridines synthesis. The first explanation that could be given it is the fact that they do not follow exact the same protocol because for the obtention of **36**, **37**, **39** and **41** the nucleophile and the phenol were mixed together with the starting acridine, in contrast to the synthesis of **38**, **40** and **43** were phenol and the acridine were mixed prior nucleophile addition. However, the main reason may be found in the purification method used to obtain the compounds. Compounds **36**, **37**, **39** and **41** were precipitated at pH 7, the difficulty to filter them and their partial solubility (for **37**, **39** and **41**) in aqueous solution made them difficult to obtain, while **38** and **40** were purified by chromatography. The possibility of having these seven carboxyacridines could help us to obtain a small variety of hybrids where the length and the nature of the linker was modified for having an idea of how this modifications alter the biological and biophysical properties of the molecules.

Optimization of the synthesis of 6-((3-(aminomethyl)benzyl)oxy)-9H-purin-2-amine, **H**

This path includes the protection of the amino group of **23** into a trifluoroacetamide **44** in a good yield.[37,169] Then, a nucleophilic substitution was performed to attach the benzylic moiety to **26**, obtaining **45** in good yield. Finally, this trifluoroacetamide compound was deprotected in an aqueous basic medium to yield the amine **46** (**H** in **Figure 22**) in a moderate yield (**Scheme 7**).

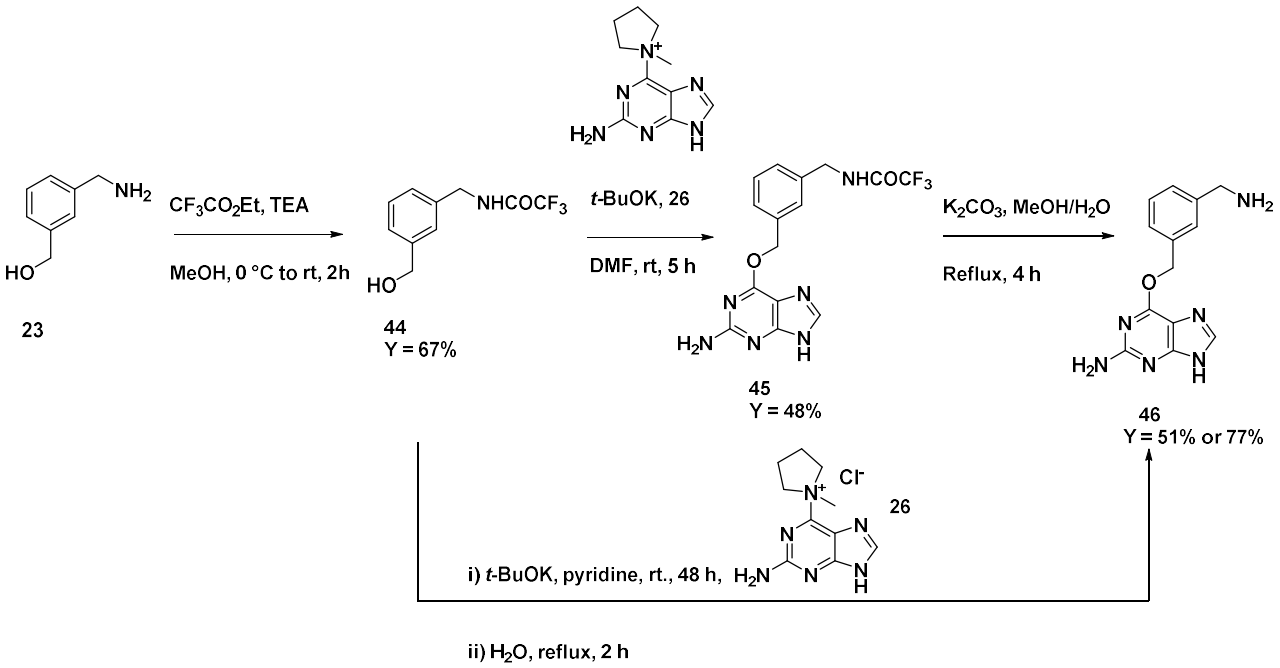

Scheme 7 Construction of the nucleophilic amine **H**

Since the compound **46** was needed on a gram scale, several attempts were performed to reproduce and to increase the yield of **45**. These included the increase on the reaction time, the amount of base

and of nucleophilic agent; unfortunately this strategy was unsuccessful when using DMF as a solvent. Considering the literature, there are only two published papers where the obtention of **46** is described, with yields between 35 and 51% after 3-5 h.[37,138] With an aminomethyl group located in *para* position to the benzylic alcohol, the yields reported for this nucleophilic substitution step were above 80%.[169] Therefore, an attempt to study more thoroughly this reaction was performed, but this time with a modification of the solvent from DMF to pyridine. While studying the reaction by TLC and LCMS, we could observe that after 6 h, besides the formation of our desired product **45**, other by-products were formed, namely through the deprotection **44** into **23**, the formation of **46** from **45** and also probably the oxidation of **46** in its benzylic position leading to the corresponding benzaldehyde. Therefore, we forced the reaction to completition by subsequent addition of the base and the alcohol (up to 8 and 3 equivalents, respectively). After detecting no more changes by TLC and LCMS, water was added and the reaction was brought to reflux. In this way, **46** was obtained in 77% yield (**Scheme 7**).

Amide bond formation for Hybrid synthesis, **A**

The carboxyacridine derived from the β-alanine aminoacid **36** was made to react in the presence of the EDCI/HOBt coupling agents with the amine **46** in DCM. The reaction was stirred for 72 h at room temperature to yield the hybrid **47** in a low yield of 19 %. After this reaction, we decided to replace the carbodiimide EDCI with the hexafluorophosphate derivative HBTU, which allowed us to obtain the same compound in a shorter reaction time, although, with a better (but, still low) yield of 34% (**Scheme 8**). The same methodology was employed for carboxyacridines **38** and **40** to yield hybrids **48** and **49** in very good yields.

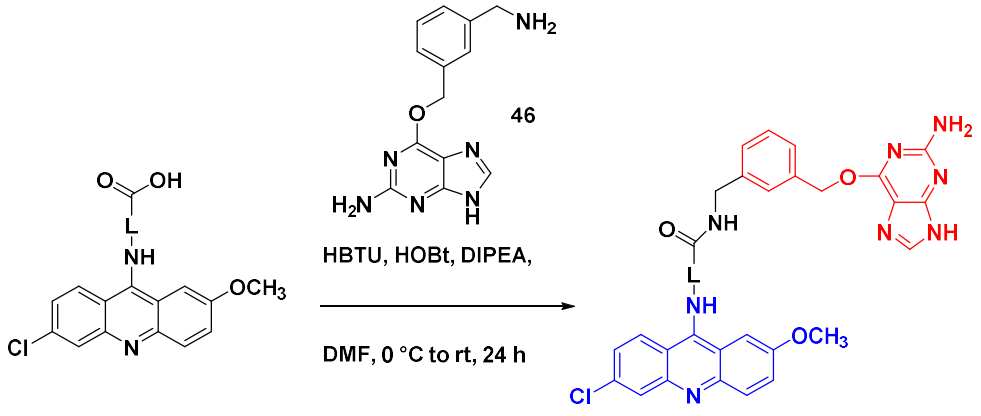

Scheme 8 Amide bond formation for Bn Hybrids synthesis

In the case of carboxyacridines with an intermediate linker length (5 atoms), the use of the HBTU/HOBt system was also applied for the coupling of **46** and the carboxyacridine derived from the γ-aminovaleric acid **37** (**Scheme 9**). The obtention of the pure hybrid (Y = 29%, but less than 90% pure as judged by NMR) remained elusive. Unfortunately, the deguanylated product was difficult to separate from the desired product by silica gel chromatography. Other purification methods were attempted such as Al_2O_3 chromatography, reverse phase purification, recrystallization or washing with an aqueous solution of K_2CO_3. Since, as judged by LCMS, a small portion of this deguanylated by-product was formed in the reaction, it was still a question if this by-product was formed due to the HBTU/HOBt coupling agents, the purification method or during the reaction itself. That is why we decided to re assay the reaction with EDCI.HCl/HOBt but the impurity was still formed in the reaction. Here, the product was formed in a lower yield (19%, less than 90% pure as judged by NMR) with the same impurity. Finally, a third attempt was made to obtain the NHS activated ester, but due to the length of the linker, an intramolecular reaction occured forming a γ-lactam (#) as product as indicated by LCMS analysis of the reaction mixture. Envisioning that the nature of the linker may play a role in this deprotection/impurity formation, the acid containing an oxygen atom **38** was used with the HBTU/HOBt system, but unfortunately a deguanylated product was observed with similar results as for **37** (Y = 45%, purity by ^{1}H-NMR < 90%). Due to these difficulties, the hybrids with carboxyacridine containing a 5 atom linker were discarded.

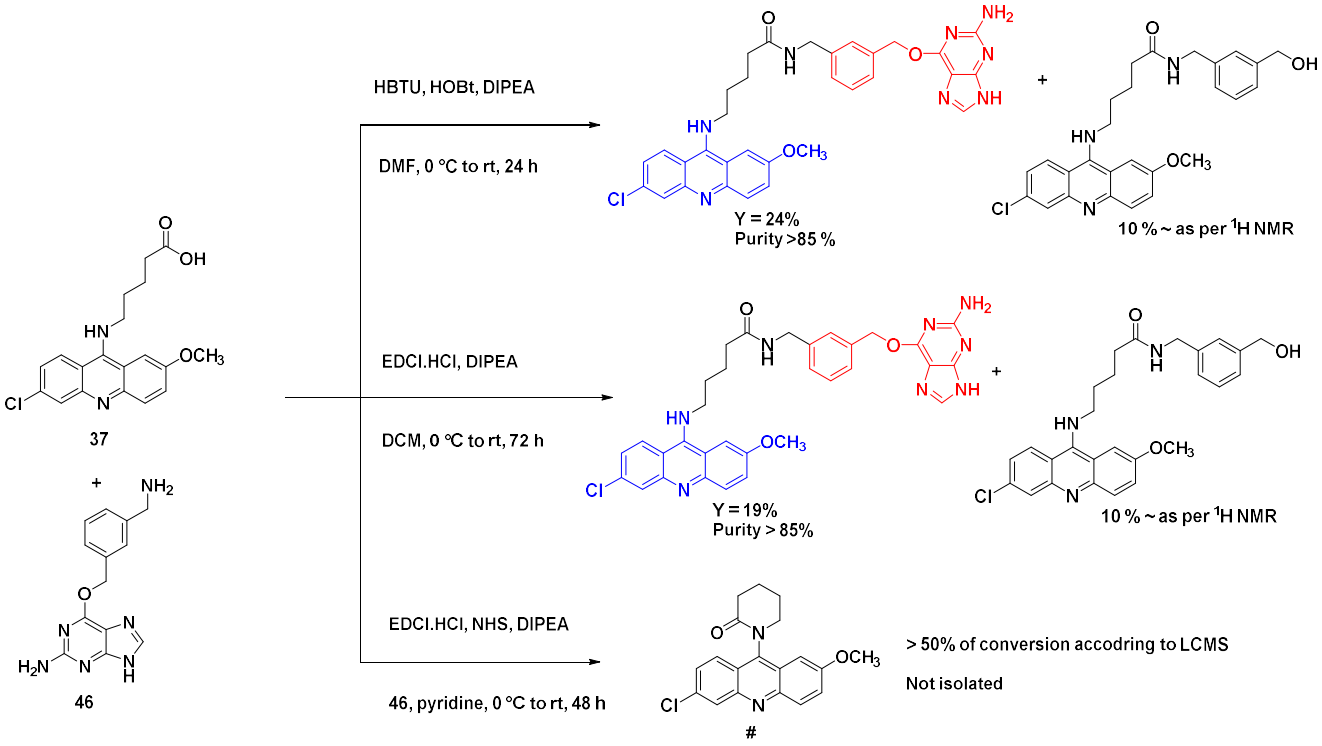

Scheme 9 Attempted synthesis of Bn hybrid with carboxyacridine **37**

3.3.1.2 N^9 hybrids

This approach dwelt in developing the expertise of the attachment of the acridine and benzylguanine through N^9 of the latter. We assayed two routes according to our retrosynthetic analysis (**Figure 24**). In **Path A**, we propose to insert the benzyl moiety in the final step using a nucleophilic substitution in the position 6 of the guanine of the intermediate **K**. This intermediate can be obtained from the nucleophilic substitution of the commercially available **B** with the N^9-alkylated guanine **L**, prepared from 6-chloroguanine **D**. **Path B** consists in joining the acridine **B** and the O^6BG derivative **M** on the last step, with **M** being easily available by N^9 alkylation of O^6BG. Although the nature and the length of the spacer are not exactly the same as for the first type of approach (namely the union through the benzyl ring), it has served as a good training method for learning the techniques to use and because some unexpected but valuable compounds have been obtained.

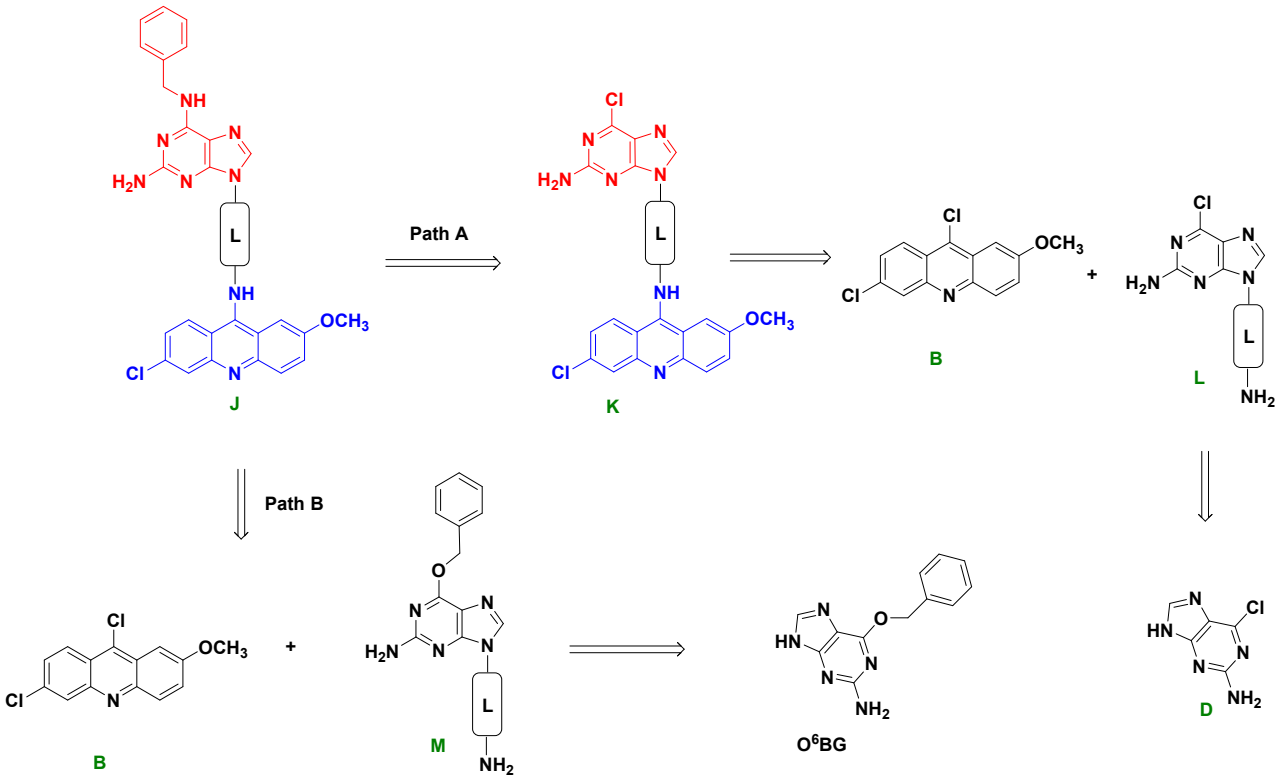

Figure 24 Retrosynthetic analysis of the N^9 hybrids

Path A: insertion of the benzyl ring through nucleophilic substitution at the position 6 of the guanine ring as the final step

In this strategy, 4-bromobutyl amine was protected as a carbamate in excellent yield (**50**) and with this bromoalkyl reagent, an alkylation on the N^9 position for the chloroguanine **D** was performed using the conditions established in the first part of the Thesis to give **51** in moderate yield. Following the carbamate deprotection in acidic conditions to obtain intermediate **L** (which was not isolated), the compound was made to react with the activated acridine **28**. Unfortunately, chloroguanine derivative **K** could not be obtained but, instead, the products of phenoxy substitution (**52**) and the chlorine hydrolysis (**53**) at the position 6 of guanine were isolated in low yields (**Scheme 10**).

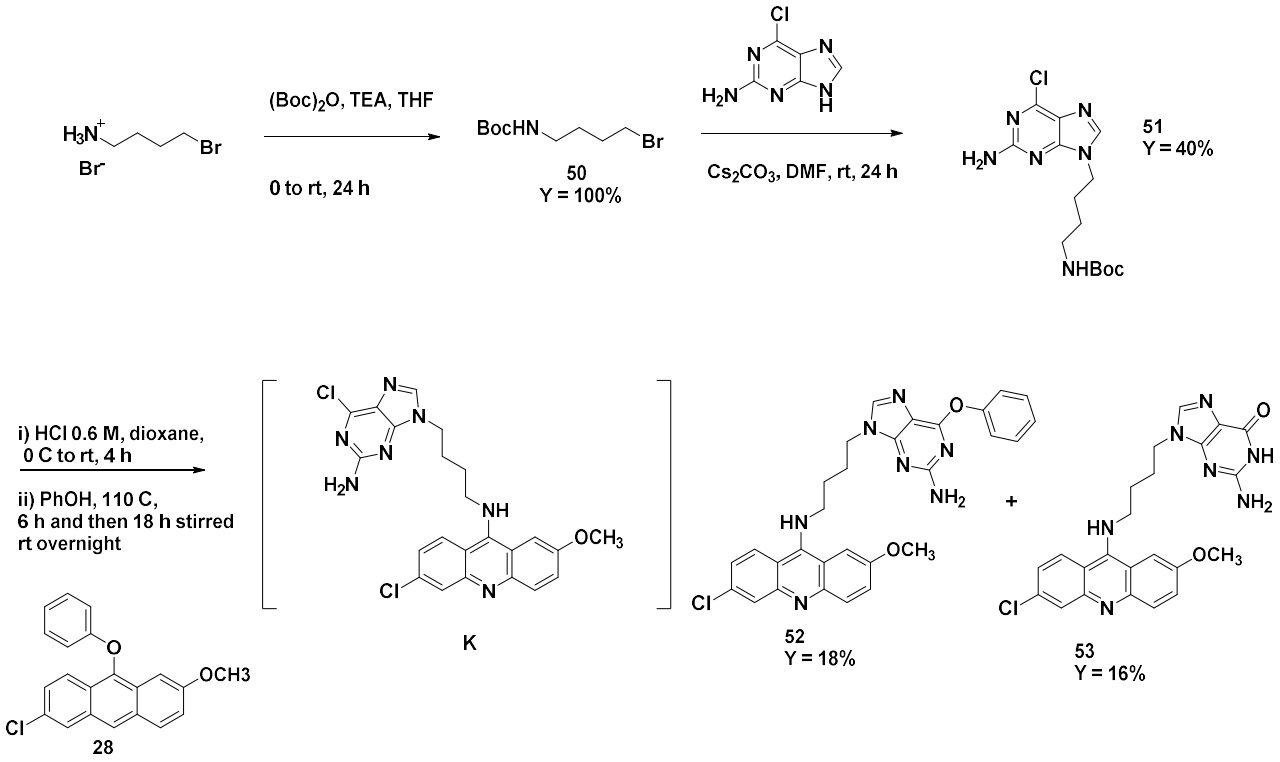

Scheme 10 Synthesis of N^9 hybrids via Path A

Path B: Nucleophilic substitution in the acridine B as final step

Since chloroguanine **51** turned out to be incompatible with the harsh reaction conditions (PhOH and heat) the benzyl group was introduced before the acridine attachment (**Scheme 11**). Starting from O^6BG, an alkylation with **50** was performed to render **54** in a moderate yield. Once achieved, a similar two-step deprotection/substitution procedure was performed as in the **Path A**. The *N*-Boc deprotection with HCl/dioxane followed by a nucleophilic substitution of the amino deprotected **54**

with the activated acridine **28** was carried. Unfortunately, this strategy did not lead to the desired product hybrid (**J** in the **Figure 24**). Once again, the use of acidic conditions for the deprotection of *N*-Boc protected group in **54** together with the severe nucleophilic subsitution conditions led to the debenzylation of the position 6 of the guanine to give **53**.

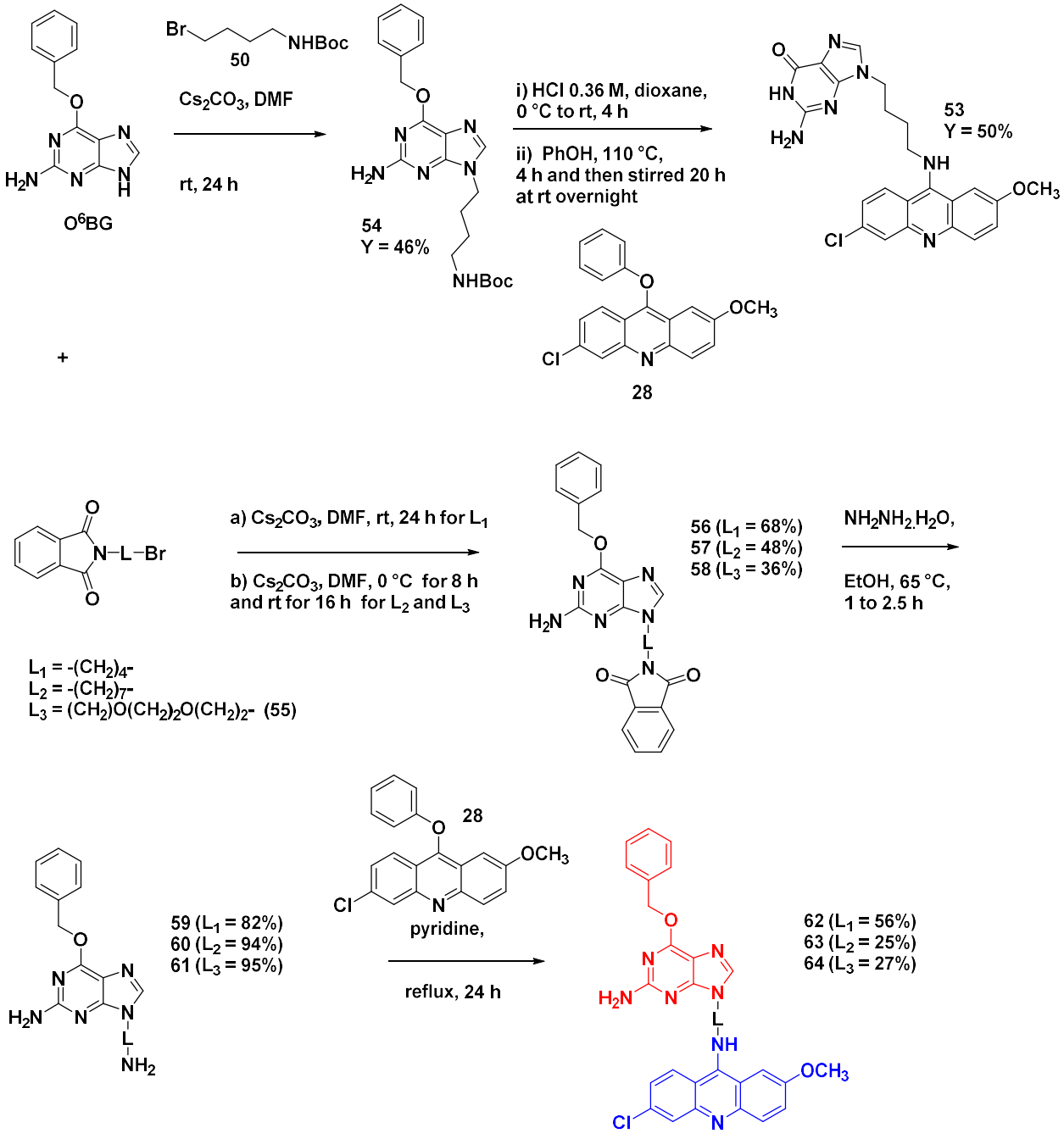

Scheme 11 N^9 hybrid synthesis by path B

Although it is not the same molecule, a similar issue was already observed in the Path A with compound **51** (**Scheme 10**). Typically, deprotection of benzyl groups is achieved by hydrogenolysis or

heating at low pH.[177] But taking into account the protonation N^3 of the guanine ring, the deprotection in acidic conditions can be achieved in milder conditions,[178] through a similar process to the removal of the methyl group from O^6MeG by MGMT, a result that has been observed for debenzylation of O^6BG in acidic conditions (**Scheme 10**).[179]

Keeping in mind that *N*-Boc group (requiring acidic deprotection) and the PhOH/heat conditions had to be avoided, a third attempt was performed, in this case using a commercially available (4-bromobutyl)phthalimide (**Scheme 11**). The O^6BG was alkylated to obtain **56** in good yield and the procedure was repeated with the commercially available (8-bromobutyl)phtalimide and with compound **55** that was obtained according to previously described methods.[180] When the length of the linker was extended and the reaction was repeated as for the obtention of **56**, the N^7 alkylation product was also formed (**Table 3**). Once the *N*-phthalimide molecules were obtained, this protective group was removed with the help of hydrazine in EtOH, to give **59**-**61** (**M** in **Figure 24**) in excellent yields.[139] For the coupling with the acridine core, the use of **28** in pyridine lead to the obtention of hybrids **62**-**64** in fair to good yields.

Table 3 N^9 alkylation optimization with long chain bromophtalimides

Alkylating agent	Conditions	Yield N^9 (%)	Yield N^7 (%)
8-(bromooctyl)phtalimide	24 h, rt	28	14
	-10 °C for 4 h and then 20 h at rt	33	32
	0 °C for 8 h and then 16 h at rt	48	29
55	24 h, rt	17	30
	-10 °C for 4 h and then 20 h at rt	33	31
	0 °C for 8 h and then 16 h at rt	36	37

Altogether, we have synthesized a panel of compounds varying in the attachment site and the linker's nature (**Chart 13**). Among these compounds we can find the "controls" such as: O^6BG, LG and **46** as the compound already described as a more potent inactivator of MGMT compared to O^6BG.[37] Two N^9 substituted benzylguanines containing a terminal phthalimide (**56**) and an amino group (**59**) whose 2-carbon analogue was shown to interact in *in silico* models with the active site of the MGMT when its amino group is protonated[139] and the acridine control **43** (**Acr**). Three Bn hybrids (**47**-**49**) and three N^9 hybrds (**62**-**64**) with different linker's length and nature. Finally, two miscellaneous compounds **52** and **53** were included to determine the influence of the Bn group in position 6. These compounds were used in the following *in vitro* and *in cellulo* assays.

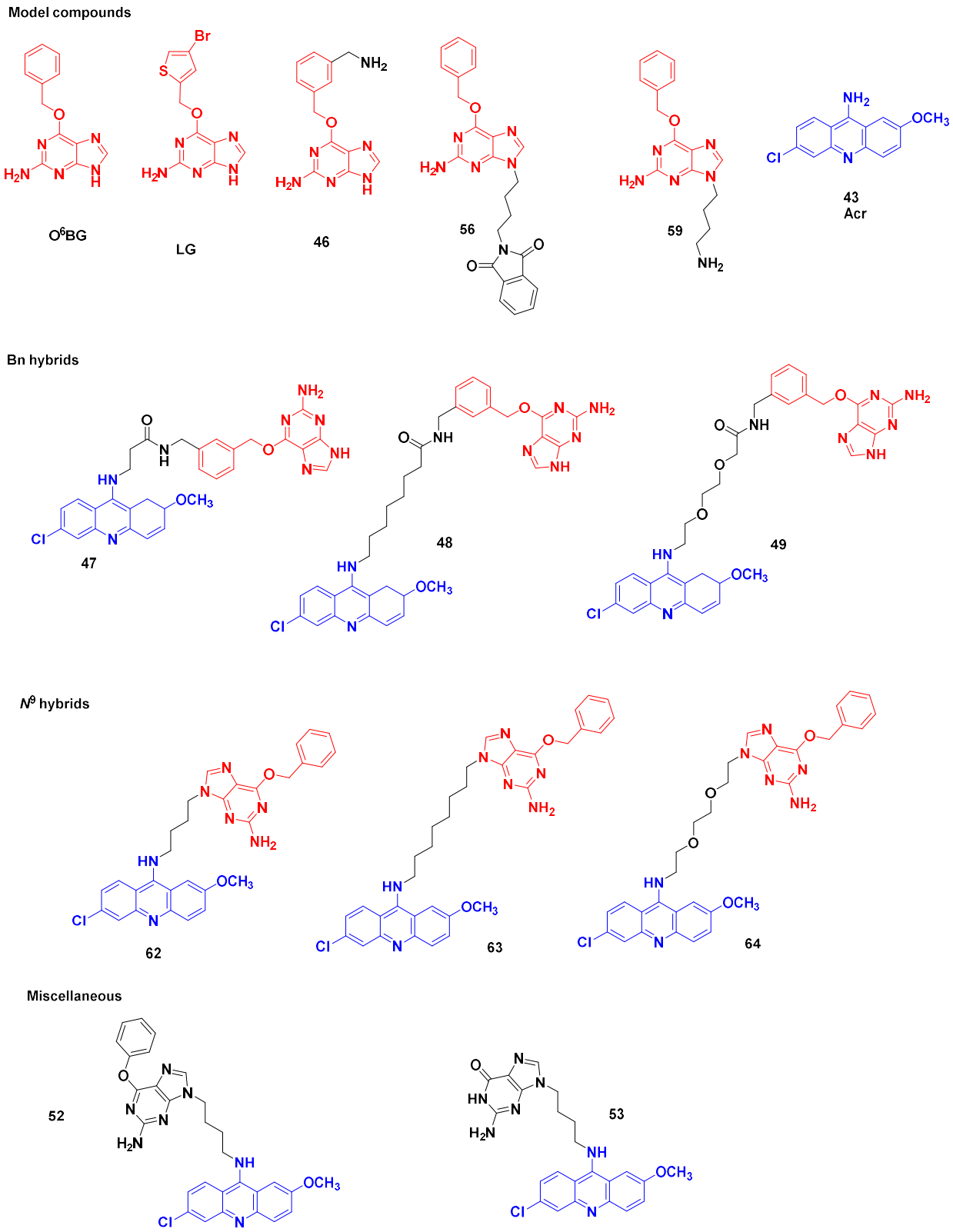

Chart 13 Structure of compounds used for *in vitro* and *in cellulo* assays

3.3.2 *In vitro* properties

3.3.2.1 Self-stacking of BG-acridine hybrids and interaction with ds DNA

Photophysical properties of the hybrids

As shown in **Chart 12B** (page 76), one of the first hypothesis to study regarding the hybrids is their ability to change from an intra-stacked and inactive conformation into an open non-stacked one. As reported in the literature, hybrids containing 9-aminoacridine with nucleic acid bases are known to adopt predominantly an intramolecularly-stacked (folded) conformation in aqueous solutions at low concentrations, which is characterized by hypochromism of the acridine chromophore in the absorbance spectra.[181,182] To evaluate the intrinsic conformation of the hybrids, we analyzed their photophysical properties in several solvents in comparison with reference compounds **Acr** and O^6BG (**Figure 25A-H**).

Firstly, for the control intercalator **Acr** an hyperchromic effect in the short-wavelength (250-300 nm) is observed when polarity of the solvent is decreased, an effect that is also observed for all hybrids but in a more enhanced manner because the fold in absorbance for this area is 1.5 to 2-fold higher. Secondly, an effect worth being highlighted is the red shift of the long wavelength absorbance peak (350–475 nm) by 3-20 nm. Additionally, if we compare the short-wavelength absorbance bands, we observe that the absorbance for the hybrids is much less than the **Acr**, a result that gives an indication of intramolecular stacking.

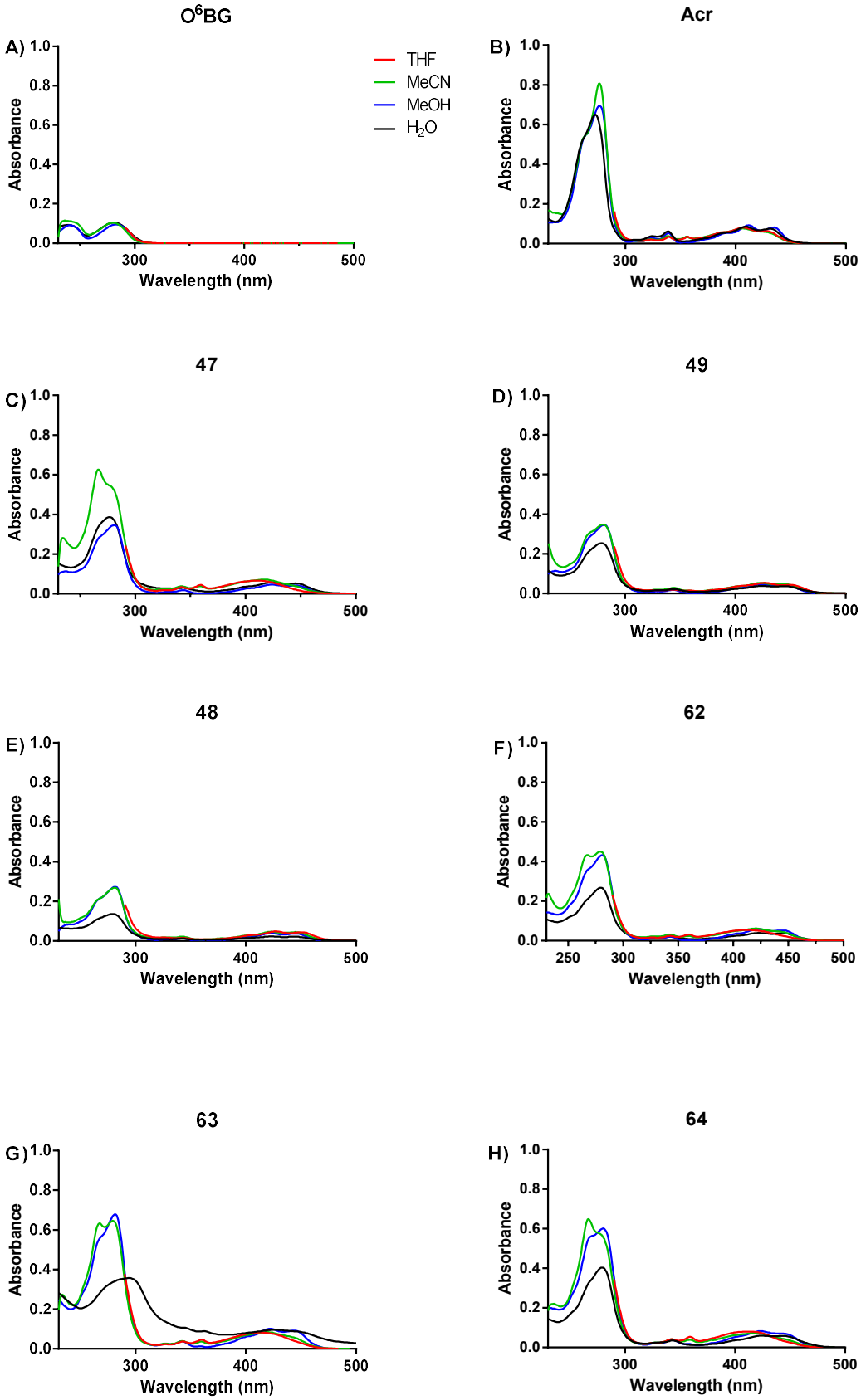

Figure 25 UV absorbance spectra of hybrids in different solvents, [Ligand] = 10 µM

As observed, the stacking effect is more pronounced in aqueous solutions (**Figure 26A-B**). The values of hypochromism (*H*, %), i.e., the ratio of the oscillator strength (the absorbance) of the hybrids to the sum of those of reference compounds **Acr** and O^{6}BG (**Table 4**), provide a semi-quantitative value of this effect.[181,182]

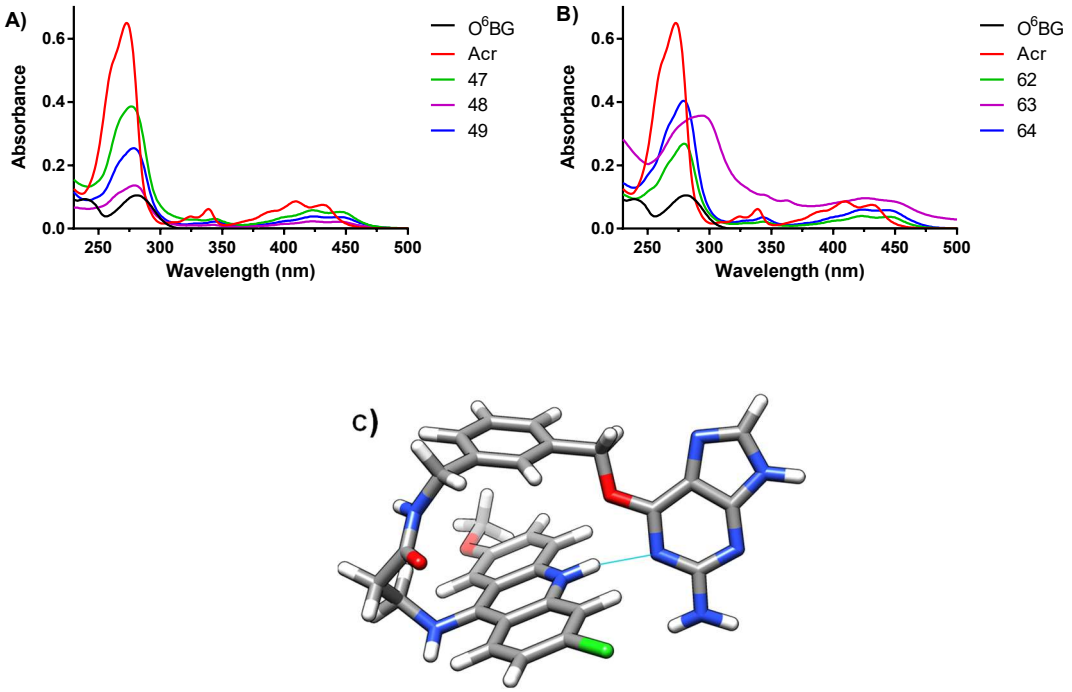

Figure 26 UV absorbance of **A)** Bn hybrids and **B)** N^9 Hybrids in H_2O at 10 µM. Compound **63** was not completely soluble in this condition **C)** Molecular model of compound **47**. The model was built in Maestro Version 12.5.139 (www.schrodinger.com) and optimized using LigPrep and MacroModel modules with OPLS3 force field in water solvent

In the case of Bn hybrids **48** and **49** in aqueous solution; this molecules were most prone to self-stacking (*H* = 77 and 60%, respectively), opposite to their short-linker analogue **47** (*H* = 27%). The result is opposite to what was reported for a series of acridine–nucleobase conjugates, where short linkers (e.g., C_3) were shown to have the highest degree of intramolecular stacking. [181] This can be explained by a model where the attachment of the linker through the benzyl residue leads to the stacking of the latter with the acridine ring instead of the guanine moiety, as suggested by molecular modelling (**Figure 26C**). As can be seen, this conformation is stabilized through an intramolecular hydrogen bond (cyan, *d* = 1.99 Å) between the protonated N^9 atom of the acridine residue and the N^1 atom of the O^{6}BG moiety. For N^9 hybrids, the short-linker derivative **62** expectedly showed the highest degree of self-stacking (*H* = 48%); of note, the analysis of compound **63** was approximate due to its poor aqueous solubility whereas for **64** the value was 36%. To evaluate the efficiency of the intramolecular stacking,

we recorded absorption spectra of the hybrids in aqueous solutions at different temperatures (20 to 75 °C). No significant changes were observed in this temperature range (**Figure 27**), indicating the high stability of the folded conformation in aqueous solution as it also was observed in the literature for a series of Adenine-C_x-Acr (where X = 3,5 or 6) where changes in the *H* values was less than 5% indicating that the intramolecular stacking between chromophores is quite stable and difficult to disrupt.[181]

For organic solvents like MeOH, THF or MeCN, the self-stacking was significantly less efficient except for compound **48** that showed high hypochromism even in these conditions probably due to hydrophobic interactions of its long CH_2 chain (**Table 4**). As a trend, all Bn hybrids showed higher *H* values than N^9 hybrids in organic solvents, confirming that the way of how the scaffold are attached impacts on their conformational structure.

Table 4. Photophysical properties of compounds.

Compound	Hypochromism (*H*, %)[a]				Fluorescence quantum yield (*Φ*)[b]			
	THF	**MeCN**	**MeOH**	**H_2O**	**THF**	**MeCN**	**MeOH**	**H_2O**
Acr					0.22	0.22	0.42	0.36
47	31	15	8	27	0.12 *(0.55)*	0.06 *(0.27)*	0.07 *(0.17)*	0.08 *(0.22)*
48	67	63	61	77	0.06 *(0.27)*	0.04 *(0.18)*	0.06 *(0.14)*	0.01 *(0.03)*
49	38	50	49	60	0.06 *(0.27)*	0.05 *(0.23)*	0.06 *(0.14)*	0.01 *(0.03)*
62	44	34	36	48	0.09 *(0.41)*	0.07 *(0.32)*	0.06 *(0.14)*	0.01 *(0.03)*
63	5	6	0	13	0.08 *(0.36)*	0.09 *(0.41)*	0.05 *(0.12)*	0.05 *(0.14)*
64c	0	12	6	36	0.09 *(0.41)*	0.09 *(0.41)*	0.06 *(0.14)*	< 0.01 *(< 0.03)*

[a] Calculated from absorption spectra, [Ligand] = 10 µM (**Figure 24** and **Figure 25**). [b] From fluorescence spectra, [Ligand] = 1 µM; quantum yield reference: Coumarin 153 (*Φ* = 0.38, **Figure 27**).[183] The values in parentheses are the ratios of the quantum yield of the compound to that of acridine **Acr** in the same solvent.

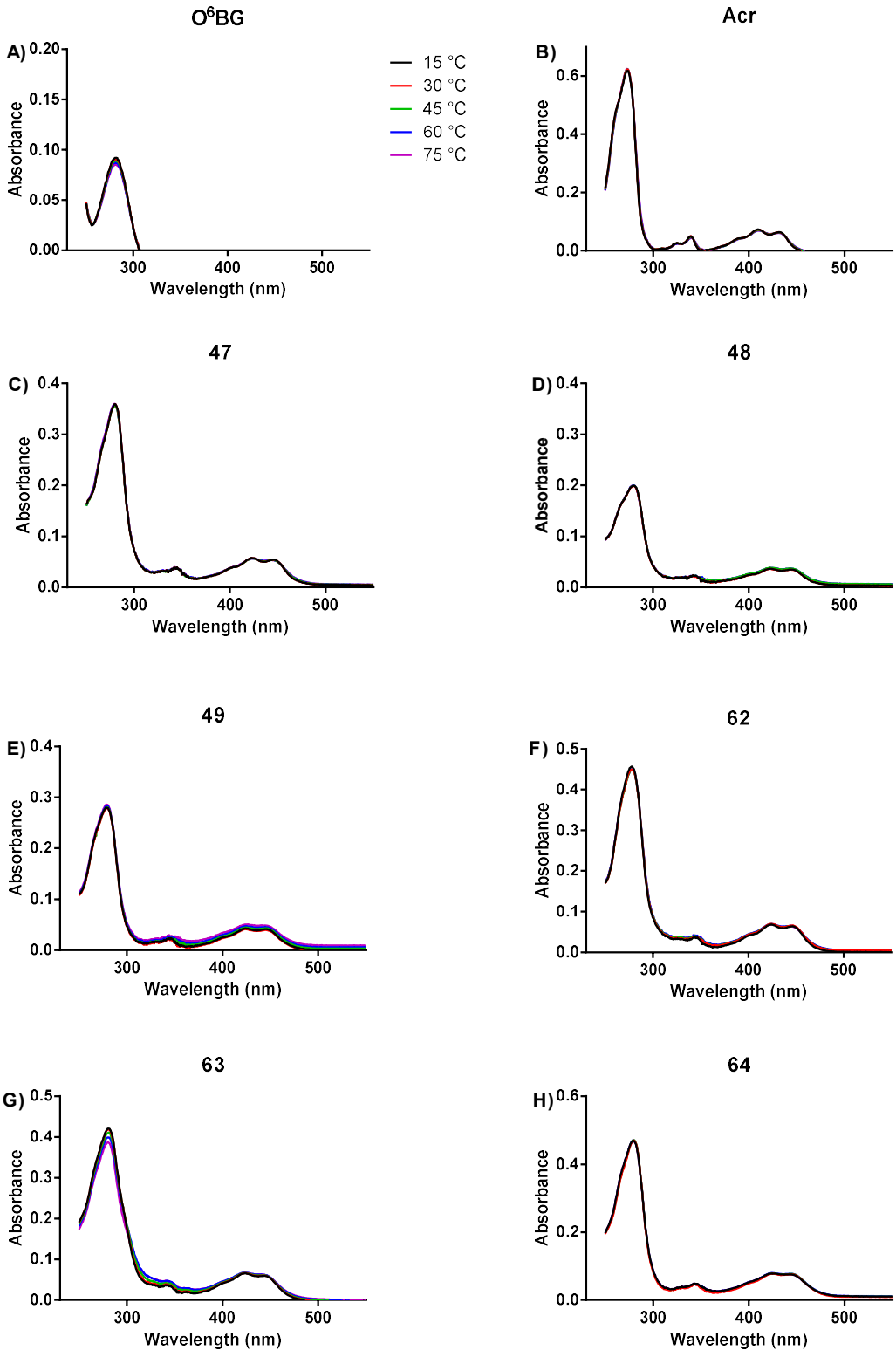

Figure 27 UV absorption spectra of compounds in H_2O on a 15 to 75°C range, [Ligand] = 10 µM

Due to the fluorescence of the acridine core,[161,184] we decided to study the stacking effect by measuring this property. As we can observe from **Figure 28**, the fluorescence data confirmed the

results already observed in UV absorbance. A strong intramolecular stacking can be suggested since the quenching in aqueous solutions goes from 4.6-fold for **47**; (similarly to what is observed in the literature for Guanine-C_6-Acr hybrids) up to 700 fold in the case of **64**, comparing with **Acr** (**Table 4**). In organic solvents, the quenching effect of the O^6BG moiety was much less pronounced confirming that in these solvents the stacking effect is decreased. Altogether, these results confirm that self-stacking properties of acridine–O^6BG hybrids can be modulated by the attachment mode of the two moieties (Bn *vs.* N^9 attachment) and the length of the linker, with Bn hybrids **48** and **49** showing the most stable folded conformation.

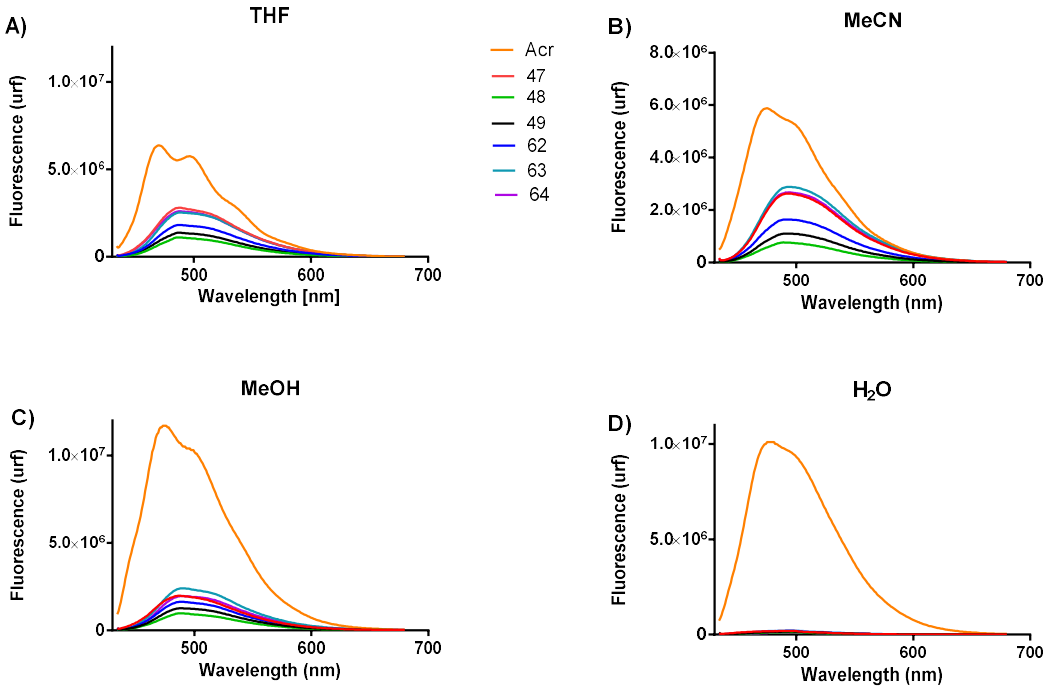

Figure 28 Fluorescence emission spectra of hybrids in different solvents. [Ligand] = 1 µM, λ_{exc} = 424 nm, excitation and emission slits: 5 nm.

Interaction with DNA

The second point of our strategy was to analyze how the folded conformation could influence the DNA-binding properties of the hybrids, since the binding to a non-damaged, fully matched DNA duplex would require the opening of the folded form, to allow the intercalation of the acridine ring. The DNA-binding properties of the compounds were initially studied by spectrophotometric titrations with calf thymus DNA (CT DNA, **Figure 29**).[185] In the case of all hybrids, addition of CT DNA led to a further decrease of the intensity of the long-wavelength absorption bands but without concomitant red shift; the latter was observed only in the case of acridine **Acr** behaving as a typical intercalator (**Figure 29D**). These results provide evidence that all hybrids interactwith DNA. The values of dissociation constants (K_d, **Table 5** and **Figure 29G**), determined by non-linear fitting of binding isotherms, indicate that the DNA affinity of the hybrids (K_d = 13 to 23 μM) was not dramatically different with respect to acridine **8** (K_d = 16.1 μM). These results indicate that, independently on the attachment mode and the length of the linker connecting the two moieties, all hybrids interacted with dsDNA.

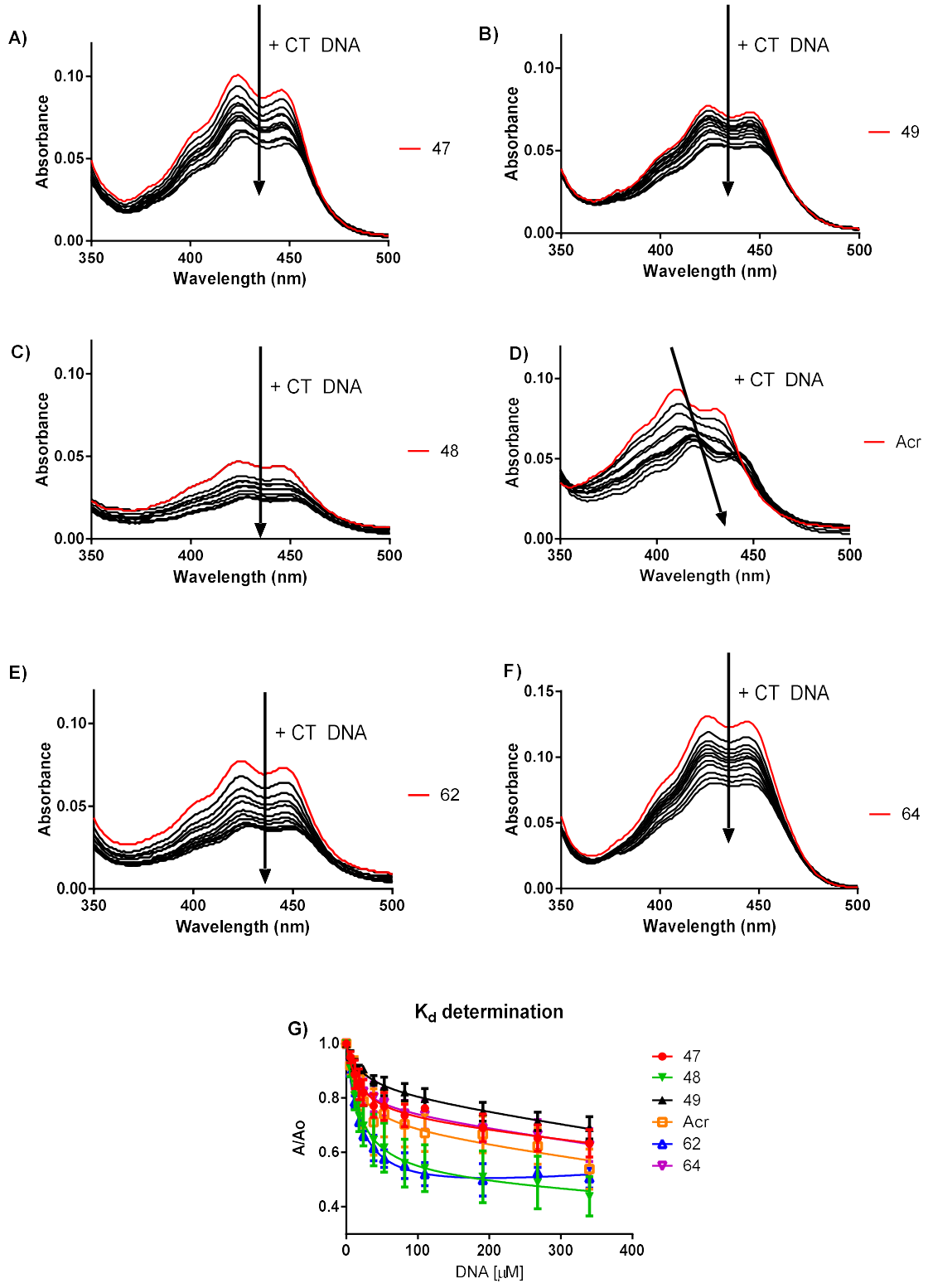

Figure 29A-F) Titration isotherms titrations of CT DNA to solutions of ligands ([Ligand] = 20 µM in 10 mM $LiAsO_2Me_2$, 100 mM KCl buffer, pH 7.2. The arrow indicates the changes in the absorption spectra **G)** Data are means ± SD from at least three independent experiments. Lines represent the fitting of experimental data to the One Site Binding model, with K_d values given in **Table 5**.

Table 5. DNA-binding properties of compounds, obtained from spectrophotometric titrations and thermal denaturation experiments with calf thymus (CT) DNA.

Compound	K_d / μM [a]	ΔT_m / °C [b]
Acr	16.1 ± 8.7	8.5 ± 0.6
47	16.2 ± 6.3	1.5 ± 1.1
48	14.3 ± 6.1	0.2 ± 0.5
49	23.4 ± 8.8	–0.7 ± 0.7
62	19.1 ± 2.9	0.6 ± 1.0
63	ND	0.7 ± 0.6
64	13.4 ± 5.4	–1.4 ± 1.2

[a] Binding constants, obtained from spectrophotometric titrations presented in **Figure 29**. Data are means ± S.D. (n = 3). [b] Ligand-induced shift of melting temperature of CT DNA from **Figure 30A**; conditions: [CT DNA bp] = 12.5 μM, [Ligand] = 6.25 μM in 10 mM $KAsO_2Me_2$, pH 7.2.

The interaction of the drugs with CT DNA was also studied through thermal denaturation experiments, which provide a measure of the ligand-induced stabilization of the DNA duplex through a shift of melting temperature (ΔT_m). The results (**Figure 30A** and **Table 5**) indicate that acridine **Acr** strongly stabilized CT DNA (ΔT_m = + 8.5 °C); in contrast, none of hybrids induced significant effect on the thermal stability of CT DNA. These results induced us to think that even as interaction with the DNA was taking place, the intercalation was not happening as expected. Therefore, a displacement assay of BrEt was performed in similar conditions as described in the literature (**Figure 30B**).[103] In this case, BrEt's fluorescence is enhanced when it intercalates with DNA and its displacement by another molecule (i.e; intercalator) leads to a drop of this property. As observed for **Acr** molecule, there is a decay on the fluorescence that indicates the intercalation of the control that shows a DC_{50} (concentration necessary to displace 50% of BrEt bound to CT DNA) of about 8 μM. Contrary to what is observed for the hybrids where almost no displacement was observed indicating that the way for these molecules interact with DNA differs from the control **Acr**. A final experiment was carried based on the induced circular dichroism (ICD) observed upon the binding of the molecules with DNA. As noted, molecules do not possess a chiral center therefore no circular dichroism (CD) footprint should be observed when the molecules are analyzed by this technique. Once a solution of **Acr** and CT DNA is studied, a positive increase on the signal that resembles the original absorption spectra in aqueous solution is observed

in the CD spectra (**Figure 30C**); in a similar way as observed for BrEt or the minor groove binder berenil[186,187]. Even if compound **62** showed a positive ICD signal at λ = 340 nm,, the spectra does not ressembles the control **Acr**, in particular due to the lack of a band at 360-450 nm, therefore we can conclude that **62** (and by extension the other hybrids) do not bind DNA in the same way as **Acr**

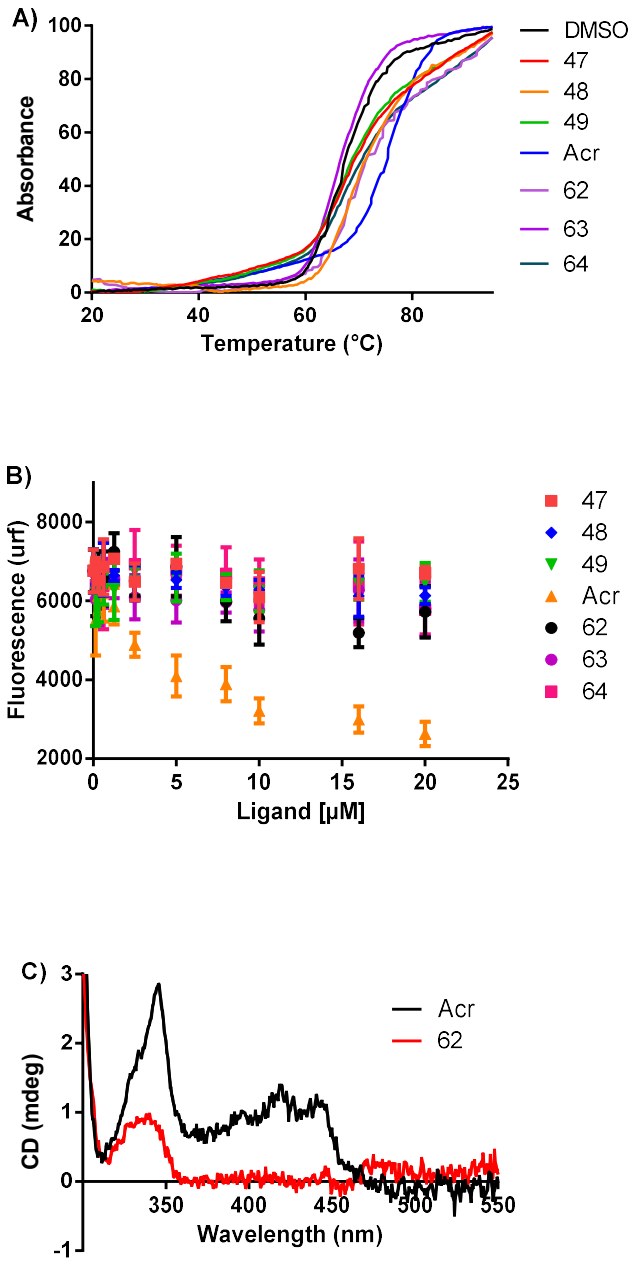

Figure 30A) Thermal denaturation experiment of CT ; conditions: [CT DNA] = 12.5 µM, [Ligand] = 6.25 µM in 10 mM $KAsO_2Me_2$, pH 7.2. **B)** Changes of fluorescence intensity upon displacement of ethidium bromide (BrEt) from CT DNA by acridine–BG hybrids and compound Acr. Conditions: [CT DNA bp] = 2 µM, [BrEt] = 1 µM, [Ligand] = 0–20 µM in 10 mM $LiAsO_2Me_2$, 100 mM KCl buffer, pH 7.2; λ_{ex} = 545 nm, λ_{ex} = 595 nm. Data are means ± S.D. (*n* = 3-5) **C)** Induced circular dichroism spectra of complexes of compounds **Acr** and **62** [50 µM] in the presence of excess CT DNA [500 µM bp] in 10 mM $LiAsO_2Me_2$, 100 mM KCl buffer, pH 7.2.

In summary, the photophysical properties of the hybrids gave evidence that they adopt an intramolecular stacked conformation in aqueous solutions, characterized by hypochromic and bathochromic effects on the acridine chromophore and a strong reduction of the fluorescence quantum yield, comparing with the reference acridine **Acr**. This conformation, stabilized by π-stacking interactions between the acridine and guanine units, is stable in a wide temperature range in aqueous solutions, but is disrupted in organic solvents. In this regard, the behavior of our acridine–O^6BG hybrids is analogous to that of the conjugates of acridine with native nucleobases,[184,188] with O^6BG residue behaving as an efficient fluorescence quencher similar to guanine. While in the series of N^9-hybrids (**62**-**64**) shorter linker resulted in more efficiently stacked hybrids (as estimated by the value of hypochromism *H*), in the series of Bn hybrids **47**–**49** the derivative with the shortest linker (**47**) displayed the lowest hypochromism, meaning the least intrastacked. This can be explained by a molecula r model in which the benzyl group serving as the attachment point for the two moieties stacks with the acridine ring, interfering – at least partially – with the stacking of the guanine residue.

Regardless the efficiency of intramolecular stacking, all hybrids were found to bind to double-stranded DNA with similar affinity, as indicated by photometric titrations, but without intercalation of the acridine moiety and thermal stabilization of the DNA duplex. This behavior is similar to that of structurally related intercalator–nucleobase conjugates that, despite their binding to double-stranded DNA evidenced by isothermal photometric titrations, do not lead to thermal stabilization of the undamaged duplex [66,67,189], and can be rationalized by a model where acridine–BG hybrids interact with DNA through external binding mode (**Scheme 12**). This is presumably due to the fact that energetic gain resulting from DNA intercalation by acridine is insufficient to compensate for the penalty necessary to unfold the intramolecularly stacked ligand. Although the details of this DNA binding are unknown, we still can hypothesize that after binding, O^6BG scaffold can still be achieved.

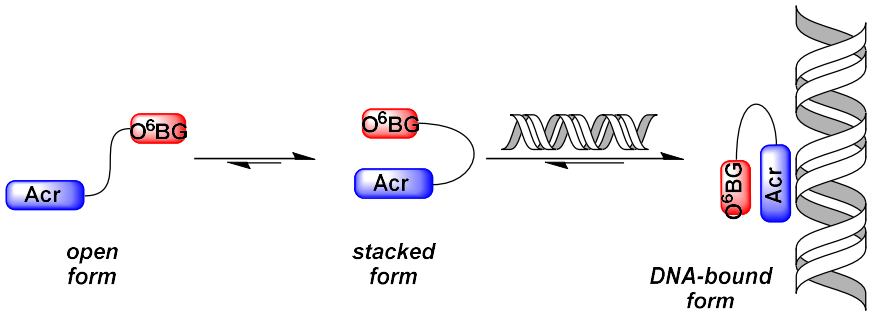

Scheme 12. Actual properties of O^6BG–acridine hybrids according to our experiments. In the absence of DNA, the hybrids exist mainly in the intramolecular stacked form. Addition of dsDNA leads to external binding characterized by increased hypochromism of the acridine moiety.

3.3.2.2 *In vitro MGMT inhibition*

In order to study the efficiency of the synthesized compounds to inhibit MGMT activity, an *in vitro* coupled enzymatic assay was performed.[79,190,191] In this gel electrophoresis-based assay, the activity of MGMT is monitored through the cleavage of a fluorescently labeled 26-bp DNA oligonucleotide by restriction endonuclease (Bsp119I), that can occur only after demethylation of an O^6MeG residue within the restriction site (5'-TT^C(O^6MeG)AA-3' / 5'-TT^CGAA-3') by MGMT (**Figure 31A-D**). A first comparative analysis was performed using the drug concentration of 12.5 µM and a reaction time of 5 min. A control assay was performed to verify the effect of the compounds on the activity of the Bsp119I endonuclease in the conditions of the coupled assay (**Figure 31C**); none of the compounds was found to inhibit this enzyme to a significant extent (> 4%), confirming that, in the conditions of the coupled assay, the observed effect was exclusively due to MGMT inhibition.

In the coupled assay, reference inhibitors O^6BG and LG inhibited MGMT activity by 25% and 94%, respectively (black bars in **Figure 31D**). In the series of Bn hybrids, the activity of compounds **47** and **49** was comparable to that of O^6BG (around 21% of inhibition), whereas compound **48** proved to be significantly more potent (47% inhibition). In the series of N^9 hybrids, compounds **62** and **63** showed an efficiency similar to that of O^6BG (18% and 23% inhibition, respectively), while compound **64** proved to be the least efficient with only 5% inhibition. Among other compounds, 3-aminomethyl-BG **46** inhibits the enzyme by 43%, in agreement with its previously documented higher activity than O^6BG,[37] whereas N^9 substituted O^6BG derivatives **56** and **59** inhibited the enzyme by 22% and 37%, respectively. Unexpectedly, acridine **Acr** revealed to be a strong MGMT inhibitor, inhibiting 48% of enzymatic activity. Likewise, acridine hybrids **52** and **53**, lacking the benzyl moiety and thus unable to react with MGMT *via* a benzyl transfer inhibited the enzymatic activity by 15% and 16%, respectively. Consequently, for the hybrid derivatives it is difficult to determine which part of the molecules (O^6BG, acridine, and/or both) contribute to their MGMT inhibitory effect.

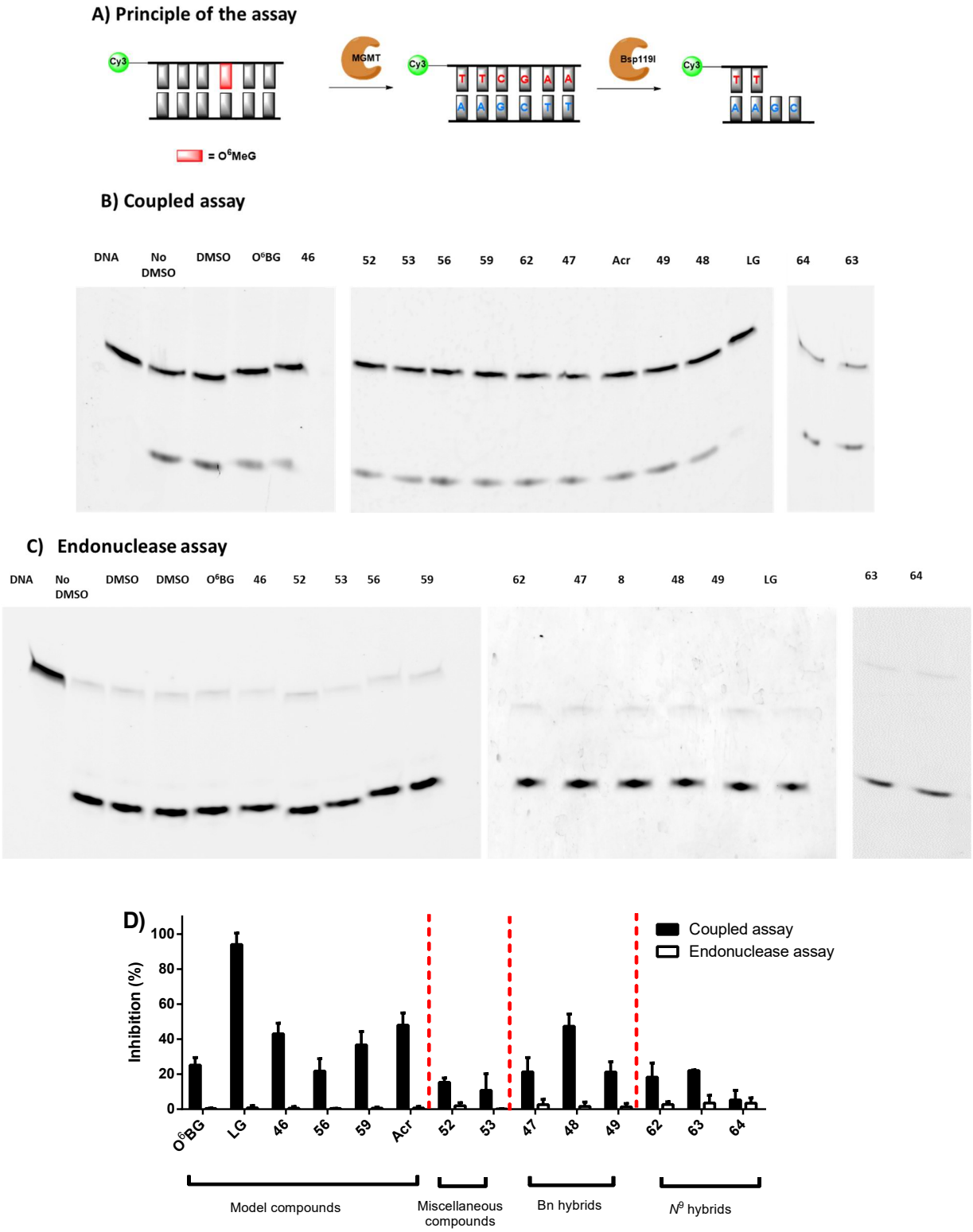

Figure 31. *In vitro* inhibition of MGMT activity. **A)** Principle of the coupled enzymatic assay. Representative gel denaturating assays of **B)** coupled and **C)** Endonuclease assays. D) Results for coupled and endonuclease assays In all cases, [inhibitor] = 12.5 µM, [substrate] = 200 nM, [MGMT] = 800 nM, [Bsp119I] = 0.2 U mL^{-1}. Data are means ± S.D. (*n* = 3-5)

In order to study the irreversible inhibition (inactivation) of MGMT by the hybrids, another assay was performed by preincubating the enzyme and the drugs for 30 min prior to addition of the substrate (blue bars in **Figure 32**). As expected, pre-incubation increased the inhibitory efficiency of O^6BG from 25 to 88%, giving evidence of irreversible inhibition. However, in the case of acridine **Acr** pre-incubation also increased the effect (from 48 to 85%), also suggesting an irreversible inhibition; this may be due to a reaction of acridine with the enzyme, or a non-specific inhibition mechanism.[192] The same effect, i.e., an increase of inhibition up to ~80%, was observed for all hybrids except **47** and **49**, whose activity reached only ~50% inhibition in this setting. The lower activity of **49** in fact agrees with their stronger intrinsic self-stacking properties (as evidenced by higher hypochromism values, cf. **Table 4**) that render both parts of the molecule less available for interaction with the enzyme. Conversely, in the case of **48** and **62–63**, it is difficult to attribute the increase of inhibition activity observed upon pre-incubation with the enzyme to irreversible inhibition by O^6BG or acridine moieties of the hybrid.

Finally, to evaluate the effect of DNA binding on the inhibitory activity of the hybrids, we assayed the activities in the presence of 40 µM (base pairs) CT DNA, i.e., non-substrate DNA (green bars in **Figure 32**). In the case of O^6BG, the inhibitory activity was slightly increased in the presence of CT DNA (from 25 to 31%), in agreement with previous reports,[193] whereas for acridine **Acr** it was reduced from 47% to 20%, a fact that can be explained by partial sequestration of the compound by DNA. In the case of the hybrid drugs, the inhibitory activity of compound **64** was increased from 5 to 21%, following the trend of O^6BG. For the other drugs, the level of inhibitory activity was either maintained (**47**, **53** and **63**) or reduced (**48**, **49**, **52** and **62**) in the presence of CT DNA; again, the reduction of inhibitory activity can be interpreted as partial sequestration of the inhibitor by non-substrate DNA or the poor availability of the DNA-bound molecule for a reaction with the enzyme (**Scheme 12**). These results indicate that these compounds may be potent in '*in cellulo*" conditions since CT DNA affects little their activities.

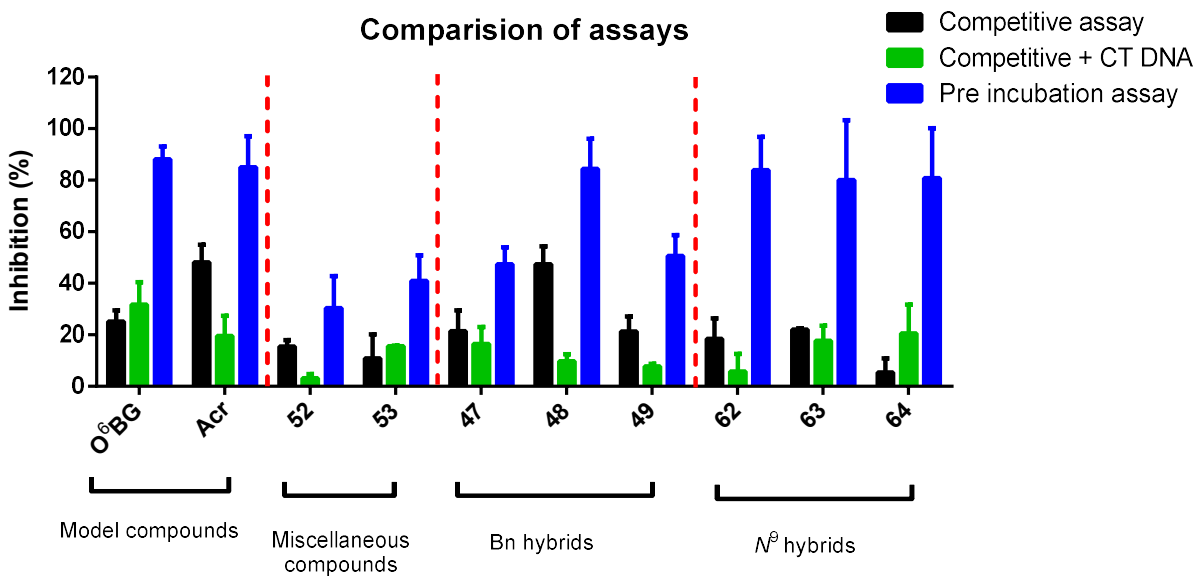

Figure 32 Comparison of *in vitro* inhibition of MGMT activity. Comparison of MGMT observed in coupled assay performed in standard conditions (black bars), in the presence of calf thymus DNA (40 µM base pairs, green bars), and upon 30-min preincubation of compounds with the enzyme (blue bars). In all cases, [inhibitor] = 12.5 µM, [substrate] = 200 nM, [MGMT] = 800 nM, [Bsp119I] = 0.2 U mL^{-1}. Data are means ± S.D. (*n* = 3-5).

Altogether, the *in vitro* MGMT inhibition data revealed several complex patterns. In the standard conditions of this assay, the drug and the methylated DNA substrate compete for irreversible reaction with the enzyme (**Scheme 13**); as a result, the observed inhibitory effect stems from a combination of thermodynamic (i.e., the affinity of the drug to the active site of the enzyme) and kinetic (i.e., the velocity of reaction of the enzyme with the drug, relative to that of O^6MeG DNA substrate) effects. In addition, for DNA-binding inhibitors such as our hybrids, the presence of substrate or non-substrate DNA in the assay may play an additional role by sequestering the inhibitor, as evidenced by decreased inhibitory activity in the presence of CT DNA for most hybrids except for compound **64**.

An interesting finding of our experiments was the fact that model **Acr**, devoid of O^6BG group, efficiently inhibited MGMT activity, with an inhibitory effect superior to that of O^6BG in the conditions of the standard assay (**Figure 31D**). One possible explanation of this finding would be a non-specific inhibitory effect due to sequestration of the DNA substrate in the intercalative complex. However, two facts speak against this hypothesis: (i) several well-known, strong DNA intercalators (ethidium bromide, daunomycin, doxycycline, and coralyne) did not inhibit MGMT in identical conditions (data not shown); (ii) the efficiency of MGMT inhibition by **Acr** dramatically increased when this compound was pre-incubated with the enzyme, similarly to what was observed with O^6BG (cf. **Figure 32**), whereas a mechanism based on a substrate-targeted inhibition (i.e., assuming that **Acr** interacts with the DNA,

but not with the enzyme) would suggest identical activity in both setups. Altogether, these data indicate that **Acr** inhibits the activity of MGMT, either through tight or irreversible binding or, eventually, due to aggregation effects leading to adsorption and loss of the enzyme. However, an experiment using Triton X-100 at 0.01% was carried in order to disrupt possible aggregation process where we observed that **Acr** was still able to inhibit MGMT in an average of 15%, which may be an indicative proof to discard the adsorption problem.[192] Worth noting is that, in our hands, the 9-AA molecule was also able to inhibit the enzyme by 17% which suggest that also this kind of core can be an MGMT inhibitor scaffold. Interestingly, during the preparation of this manuscript, MGMT binding of structurally related acridone derivatives was suggested on the basis of molecular docking experiments;[194] moreover, inhibition of MGMT activity by other polyaromatic compounds was also documented.[195] Inactivation of MGMT by the acridine residue can also explain the inhibitory effect of the hybrids **52** and **53** that do not contain a O^6BG moiety, as well as an increase of the inhibitory activity of all hybrids observed upon pre-incubations of compounds with the enzyme prior to addition of the target. It is clear that the properties of O^6BG–acridine hybrids are strongly influenced by the acridine moiety that, on one hand, modulates the properties of the O^6BG counterpart by stacking interactions and by interaction with DNA, (**Scheme 13**) and, on the other hand, interacts with the enzyme itself, at least in the case of compound **Acr**.

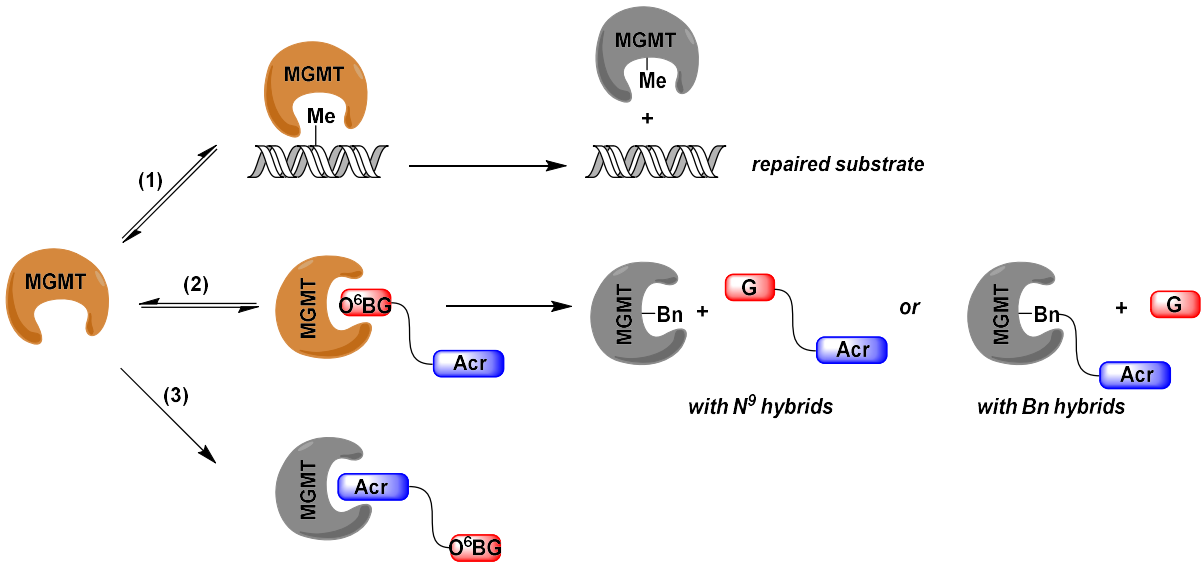

Scheme 13 Inhibition of MGMT by O^6BG–acridine hybrids. (1) Repair of the DNA substrate by MGMT; (2) inhibition of MGMT by O^6BG–acridine hybrids through irreversible reaction of the O^6BG moiety; (3) irreversible inactivation due to the acridine moiety. The inactivated MGMT is shown in gray.

3.3.3 *In cellulo* experiments

3.3.3.1 Cytotoxicity of compounds in T98G cells

Cytotoxicity of compounds as single agents

The viability of T98G cells once exposed to the panel of molecules described in **Chart 13** was studied as described in **Chapter 2**. The results are presented in **Chart 14** following a colour code where compounds with no cytotoxic effect (GI_{50} > 25 µM), with moderate cytotoxicity (10 µM < GI_{50} < 25 µM) and cytotoxic (GI_{50} ≤ 2 µM) are displayed in green blue and red respectively.

As a first assay to evaluate their cytotoxicity, the compounds were tested as monotherapy in a 0.03-750 µM concentration range (**Figure 33A-B**). As a summary of these GI_{50}, we can analyse their activities regarding how the scaffolds are attached compared to the parent compounds. First of all, O^6BG turned out to be non-toxic in our conditions (viability at 25 µM = 85%, GI_{50} = 92 µM), results which were in concordance with already described data for different cancerous cell lines (e.g., GI_{50} > 100 µM at 24 h in HT-29 cells) [36,38,138,139] In the case of the intercalator **Acr**, it showed the highest toxicity of all the evaluated compounds with a GI_{50} = 0.64 µM, an already described property for this kind of molecules.[196]

For O^6BG derivatives named "model compounds" the addition of a substituent on the benzyl ring as in **46** showed no change on the toxicity (viability at 25 µM = 71%). Also, the N^9 modification through an aliphatic chain did not change their properties substantially (viability at 25 µM: 67% and 99%, for **56** and **59** respectively). In the case of the miscellaneous compounds: we can observe a very cytotoxic activity for **52** (GI_{50} = 0.77 µM) but a total loss of the activity for **53** (viability at 25 µM = 100%). This can indicate that the attachment of a heterocyclic ring to the guanine core can increase the activity of the compounds (O^6BG *vs.* **52**) but not every type of ring (**52** *vs.* **56**). In addition, it highlights the importance of the substituent on the position 6 of the guanine (**52** *vs*. **53**).

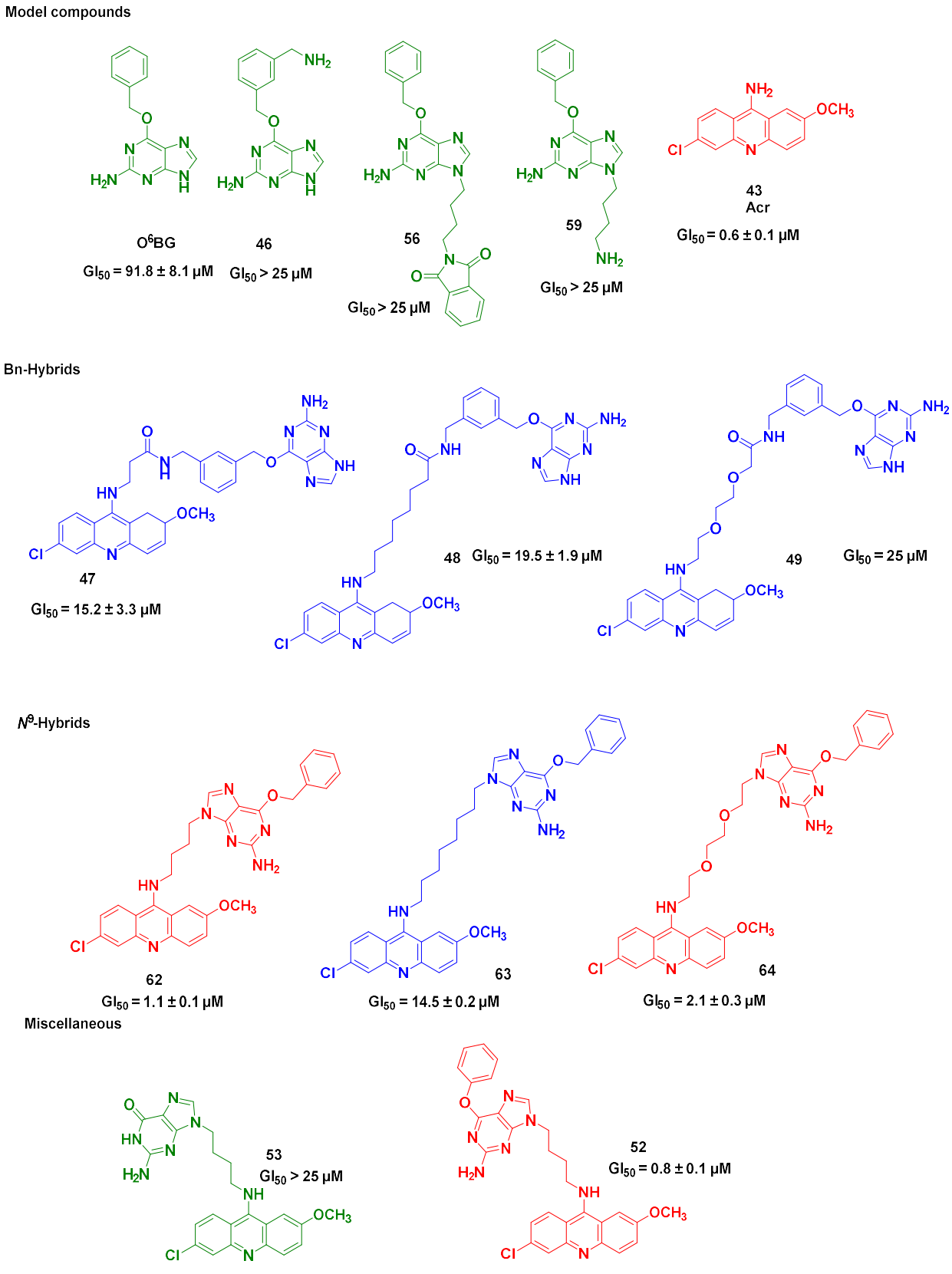

Chart 14 Summary of cytotoxicity of hybrid molecules screened after 96h in T98G cells

As to the hybrid compounds, **62** showed to have the higher potency (GI_{50} = 1.1 μM), slightly lower than the 9-aminoacridine **Acr** and the acridine derivative with a 6-phenoxy group **52**. An increase on the length of the linker from four to seven carbons lead to a drop of almost ten times in the cytotoxicity probably to the precipitation of the compound **63** (as observed by microscopy). Once two carbons are replaced by two oxygen, the solubility of the molecule (in this case **64**) is increased and therefore its cytotoxic effect is restored in the same range as **62**. Benzyl-attached hybrids (**47**, **48** and **49**) demonstrated to be more active than their model compounds but at least one order magnitude less active than the N^9 attached hybrid **62** and **64**. In the case of these three compounds, we can observe a slight decrease of the cytoxicity when the length (**47** *vs.***48**) and the polarity is increased (**48** *vs.* **49**), similarly to what is observed for N^9 hybrids.

From this first round of experiments we can conclude that: 1) the cytotoxicity of the compounds can be increased when an 9-aminoacridine ring is present in the molecule 2) the substituent on the O^6 position on the guanine plays an important role on the molecule's cytotoxicity and 3) N^9 hybrids molecules are more potent than Bn hybrids.

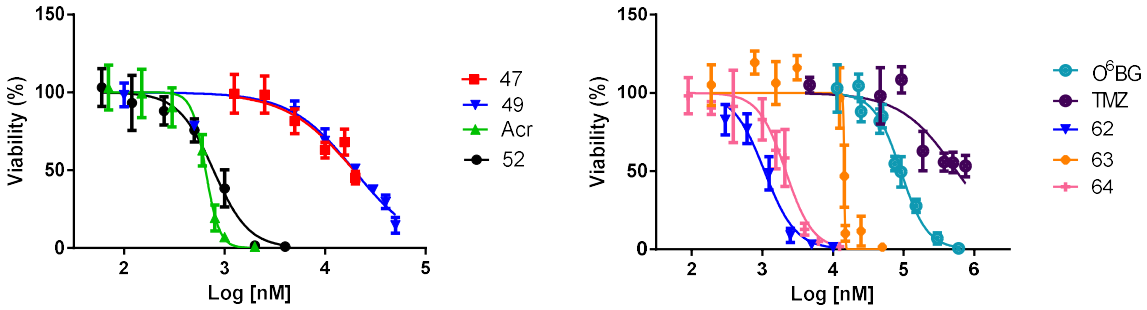

Figure 33 Dose–response curves for the viability of T98G cells in the presence of drugs. Experimental points are mean ± SD values ($n \geq 3$). GI_{50} values were determined using the GraphPad software by fitting normalized response vs. log [drug] with a variable-slope curve, Y=100/(1+10^((LogGI_{50}-X)*HillSlope))

Cytoxicity in combination with TMZ

As a second step, we performed combination treatments with the previously mentioned compounds and TMZ. In these experiments, compounds were pre-incubated for 2 h aiming to deplete MGMT in a typical procedure for the assessment of MGMT inhibitors.[29,36,37,79,137–139] Single concentration of compounds was used either at their GI_{50} values or at 25 μM when GI_{50} was higher than it. Two hours after, TMZ was added at at 94, 188 and 375 μM (108, 63 and 53% of viability respectively). Compounds were incubated completing making a total of 96 h of incubation.

The results of the combination are presented in **Figure 34** and were analysed using the Bliss Independence model described before. First of all, the control O^6BG was found to induce a clear synergic effect with TMZ used at a concentration of 94 μM, in agreement with what was observed in T98G and other MGMT-proficient cell lines.[29,111,137] In the case of O^6BG derivatives **46**, **56** and **59** also demonstrated synergy with TMZ in these conditions ($p < 0.0001$); these observations are in line with the previously documented ability of compound **46** to potentiate the activity of BCNU in the HT29 cell line [37]. Unexpectedly, **Acr** also demonstrated strong synergy ($p < 0.0001$) with sub-toxic concentrations of TMZ. In case of the hybrids, none of the Bn attached compounds were synergic, whereas among the N^9 hybrids, compounds **62** and **64** were synergic and compound **63** probably as antagonist (cf. **Figure 34** footnote).

Surprisingly once TMZ concentration was increased (188 or 375 μM), none of the O^6BG derivatives devoid of the acridine moiety proved to be synergic. At 188 μM TMZ, compounds **47** and **48** even showed an antagonist effect, while an additive effect was observed for all other compounds. Finally, at 375 μM TMZ, only compound **62** and **64** exhibited a synergic effect while **Acr**, **48**, **56**, **59** and **63** were antagonist (**Figure 34B-C**). In contrast to sub-toxic conditions of TMZ concentrations where the cell death is due to one predominant mechanism, i.e. O^6MeG-induced toxicity , the increase of TMZ concentration shown to decrease of the synergic effect. One explanation is related with what is called single agent dominance (SAD), a phenomena that occurs either when the concentration of both agents is dissimilar or when both have different time to exert their action. In this case, the action of a compound leads to a“cytotoxicity burst” effect, i.e., activation of multiple stress responses, in near-cytotoxic conditions, that leaves no place for the action of the other compound.[197,198]

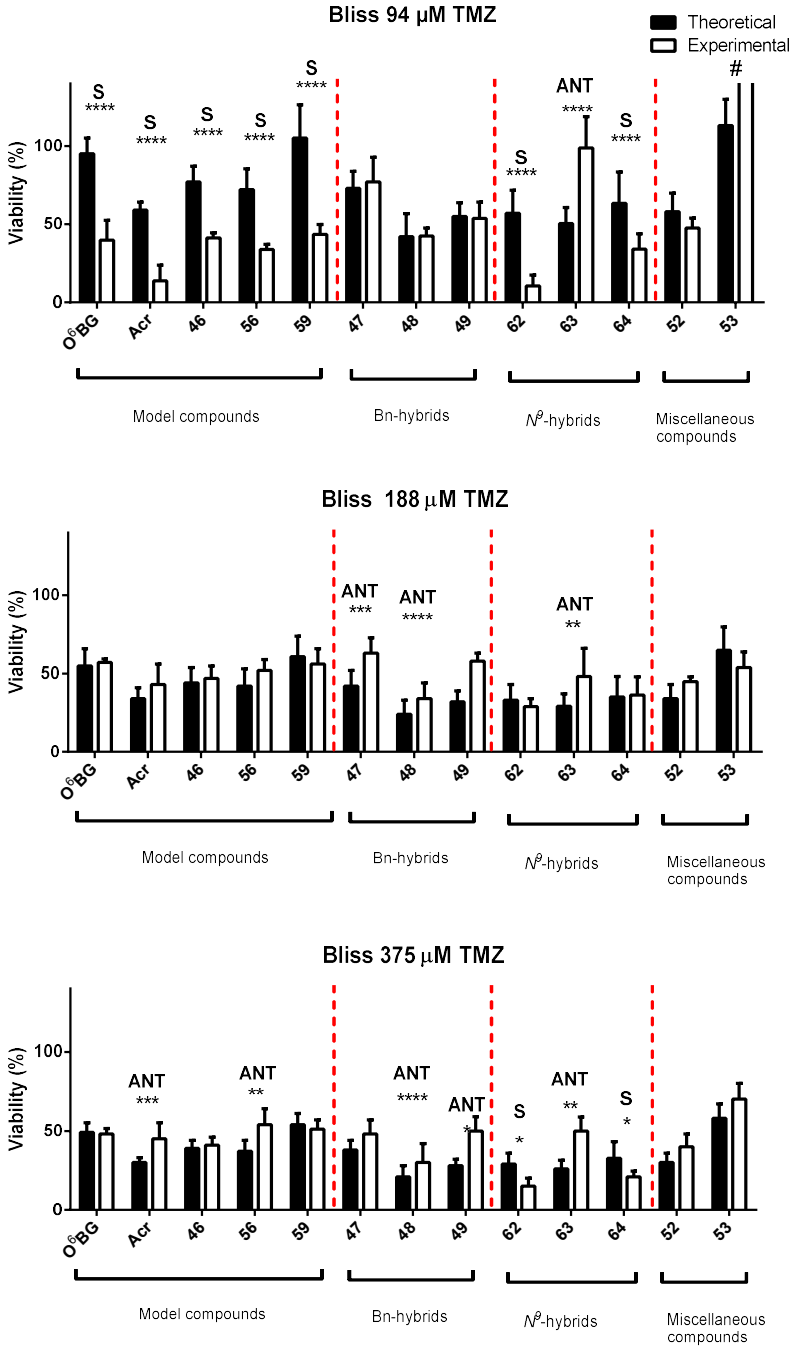

Figure 34 Bliss analysis of combinations of drugs (at their GI_{50} values, or 25 µM if GI_{50} ≥ 25 µM) with TMZ **A)** 94 **B)** 188 and **C)** 375 µM in T98G cells. Black bars represent $V_{Theo,A+B}$ and its theoretical S.D. (see SI); white bars represent the experimental viability $V_{Exp,A+B}$ ± S.D (n ≥ 3). S and ANT stands for synergy or antagonism, respectively. One-way ANOVA with Sidak post-test comparison statistical analysis was performed; **** denote p values below 0.0001. # V > 150% was determined using CellTiter-Glo® kit; however, a cell counting experiment for this condition revealed a viability of ≥ 85%, indicating an interference with the CellTiter-Glo® kit. Therefore, this result was not taken into account

Furthermore, the effect of the combination of TMZ plus **62** or **64** was studied and compared with the control O^6BG in a grid of concentrations (from ⅛ GI_{50} to GI_{50}, **Figure 35**). The viability data were analyzed by employing the Chou–Talalay method as implemented in the software CompuSyn (**Chapter 2**).[121,122] In this method, the effect of the drug combination is represented by the value of Combination Index (CI), with CI > 1 being indicative of antagonist effect, CI < 1 of a synergic effect, and CI ≈ 1 of an additive effect, respectively. The results are represented as CI values as a function of the drug concentration, grouped by the employed TMZ concentrations. As a general trend, it can be observed that, for each TMZ concentration, CI values decrease and the synergy increases at low concentration of both drugs, reaching CI values as low as 0.2–0.3 at 47 µM TMZ and subtoxic (⅛ GI_{50}) concentration of the drugs. The comparison of CI values in **Figure 35** shows that both hybrids are at least as efficient as O^6BG in exerting synergy with TMZ in T98G cells, albeit at 40- to 80-fold lower concentration (comparingGI_{50} values of O^6BG vs. **62** and **64**).

Similarly to the *in vitro* properties observed, the molecular design of hybrids has an influence on their cytotoxic effects, as illustrated by the fact that the activity of all hybrids fall in the range between the weakly cytotoxic O^6BG and the highly cytotoxic acridine **Acr**. However, while all hybrids inhibited – to a varied extent – MGMT activity *in vitro*, only N^9 hybrids **62** and **64** exerted drug synergy upon co-treatment with TMZ in MGMT-expressing T98G cells.

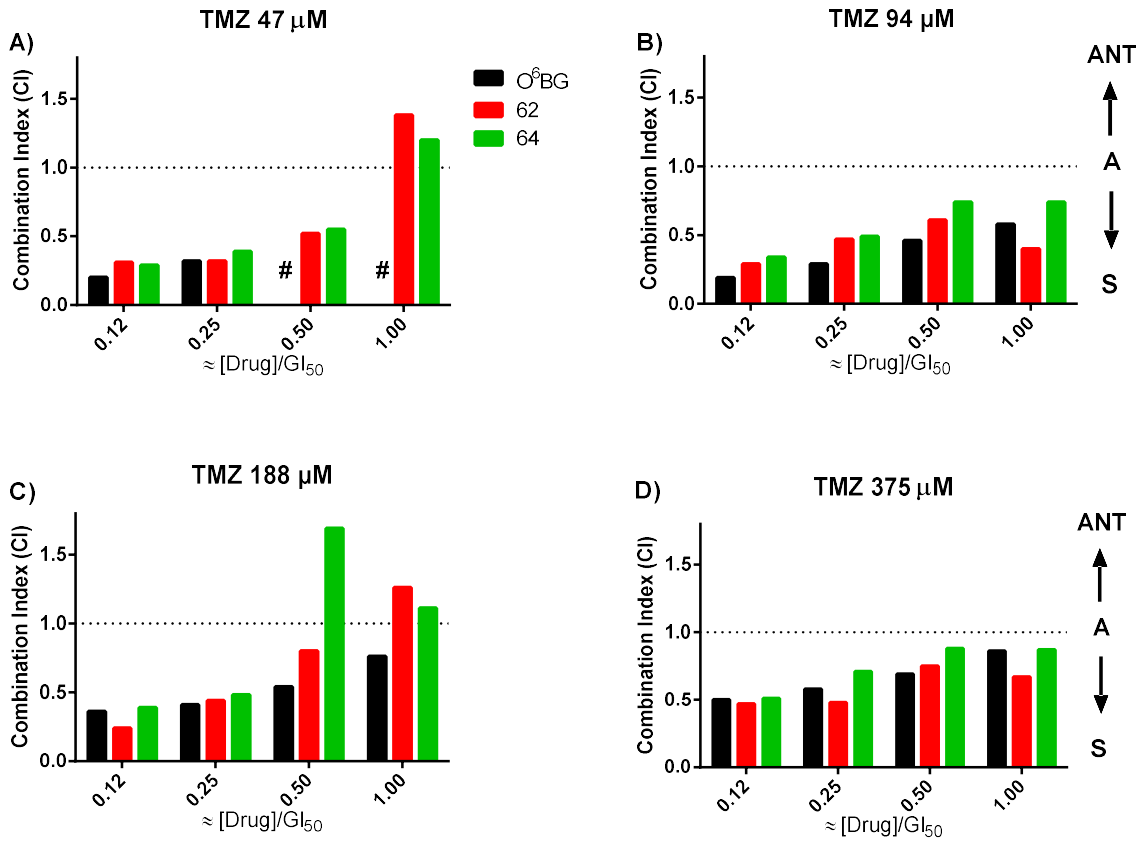

Figure 35 Combination Index (CI) values for combinations of drugs BG, **62** and **64** with TMZ in the range of concentrations from ⅛ GI_{50} to GI_{50} for each drug (GI_{50} = 92 µM for BG, 1.1 µM for **62** and 2.1 µM for **64**). #: these combinations were not analyzed due to an artifact similar to that observed in **Figure 21** (page 63), where the viability determined using CellTiter-Glo® kit was > 100% whereas viability by cell counting was ≈ 30%. Each CI value results from three biological replicates.

3.3.3.2 *Approaches to understand the mechanism of action of compound 62*

Even if the molecules were designed to inhibit MGMT, the synergic effect observed for compound **62** does not prove the *on target* effect of the molecule in cells, despite having the O^6BG scaffold. In order to better understand the mode of action of this hybrid, several experiments were carried to determine its actual target.

Microscopy studies

Thanks to fluorescent properties of the acridine moiety, the cellular localization of hybrids can be assessed by fluorescence microscopy. Towards this end, live-cell images of T98G cells were acquired after 96 h of incubation with compound **62**. The green fluorescence of **62** was observed in the cytosolic region but not in the nucleus, as can be seen by the use of the far-red emmiting nuclear stain DRAQ5 (**Figure 36**).

It is also worth noting that the distribution of **62** in the cytosol was not homogeneous; instead, the compound localized in the perinuclear region, as could be observed by the inspection of *Z*-stacked series of images. Despite the presence of DNA-interacting acridine moiety, compound **62** was found to localize in perinuclear region of the cytoplasm; indeed, its presence in the nucleus of live cells could not be detected by confocal microscopy even upon long incubation time (96 h). This finding is rather unexpected, as structurally similar acridine–melamine hybrids were shown to adopt strictly nuclear localization;[161] however, it can be rationalized taking into account the absence of intercalative DNA binding by the hybrids. Moreover, similar peri-nuclear localization was observed for acridine dimers.[199]

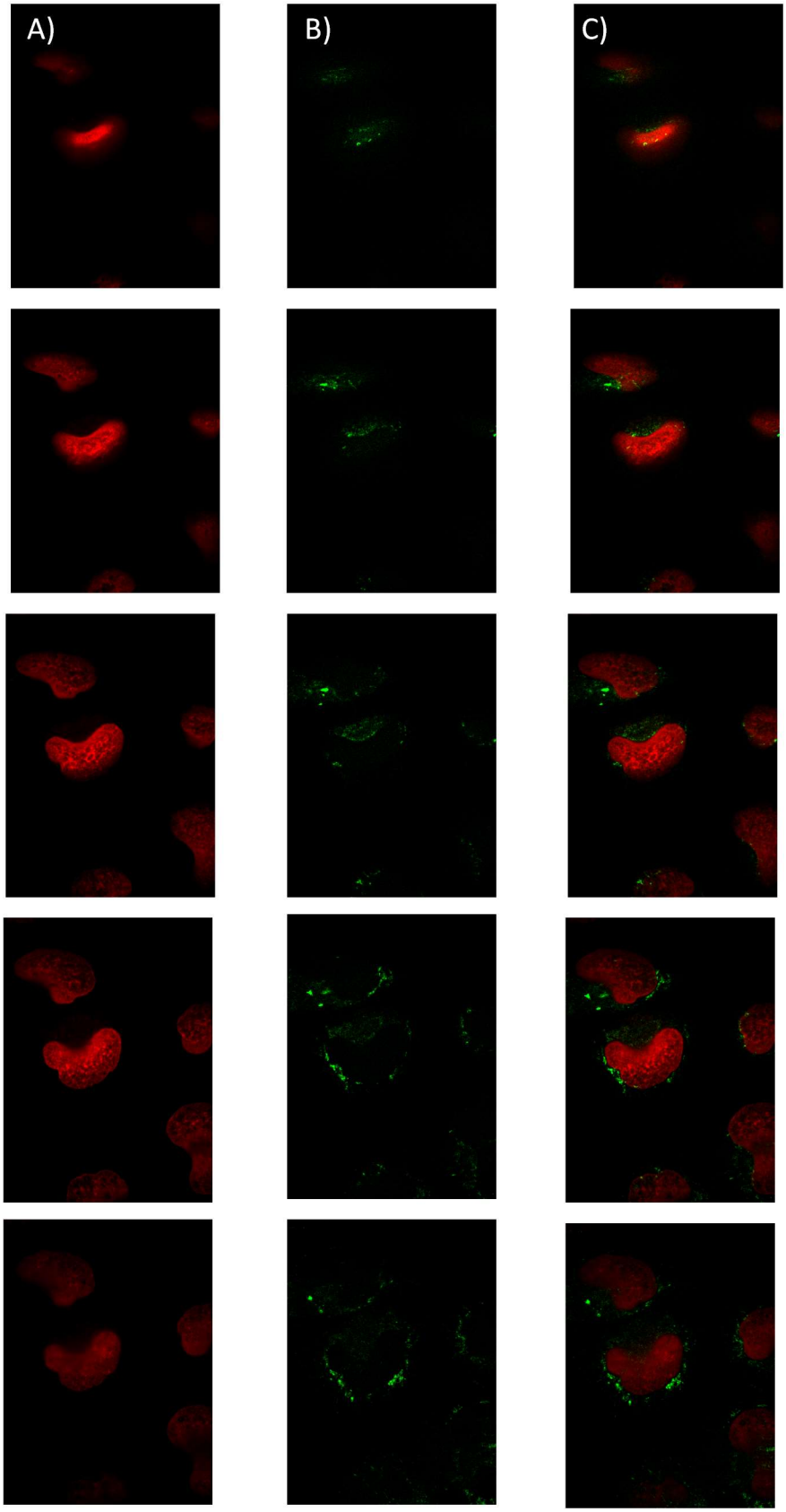

Figure 36 *Z*-stacked series of confocal images of live T98G cells after 96 h of incubation in the presence of compound **62** (1.1 µM). **A)** Fluorescence of DRAQ5 (642 / 700 nm channel); **B)** fluorescence of compound **62** (488 / 525 nm channel); **C)** merged image

Inactivation of cellular MGMT

In order to verify that treatment with the hybrid **62** inactivates MGMT in live cells, we analyzed the residual activity of MGMT from cell extracts of T98G cells, following the treatment with compound **62** or O^6BG as a positive control (2 µM, 2 h) using the same coupled enzymatic assay (**Figure 31**).[190,200] The results (**Figure 37**) indicate that **62** was indeed able to inactivate cellular MGMT in these conditions (by 50%), however less efficiently than O^6BG (95% inhibition) which was employed at the same concentration. These results demonstrate that, in agreement with its *in vitro* MGMT inhibition activity (cf. **Figure 31**), **62** is also able to target MGMT in cells leading to its inactivation.

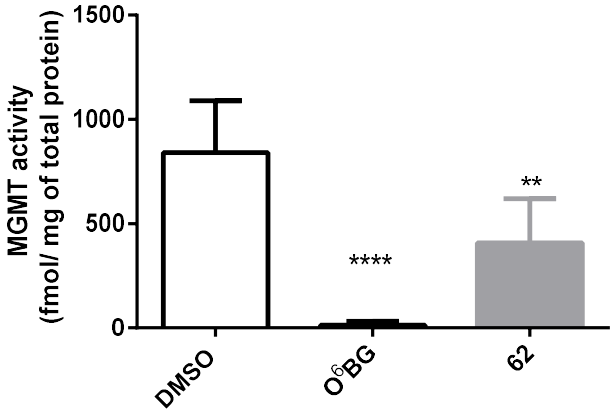

Figure 37. Inactivation of cellular MGMT activity in T98G cells treated for 2 h with compound **62** (2 µM), O^6BG (2 µM), or DMSO (0.5 %, v/v) as a vehicle. The MGMT activity determined by PAGE analysis was normalized to the total protein concentration in cellular extracts. Data are means ± S.D. (n = 3). One-way ANOVA; ****: $p \leq 0.0001$, **: $p \leq 0.01$

An interesting thing to highlight is that since MGMT is known to adopt both nuclear and cytosolic localization,[19,201] the absence of nuclear staining by **62** is consistent with partial inactivation of cellular MGMT; however, it may also point to a different mechanism. Of note, the observed fluorescence may arise from the product of enzymatic debenzylation of **62** (i.e., compound **53**) accumulating, e.g., in transport vesicles.

DNA damage induction

As it was pointed out, TMZ can induce DNA damage that leads to DSB (**Figure 3**, page 7) and cell death. To get insight into the mechanisms of cell death in the conditions of synergistic co-treatment with TMZ and **62** (or O^6BG as a control), we assessed the level of DSB in T98G cells through immunofluorescence assay using anti-γH2AX, a phosphorylated histone representing a well-established DSB marker (**Figure 38A-F**).[202]

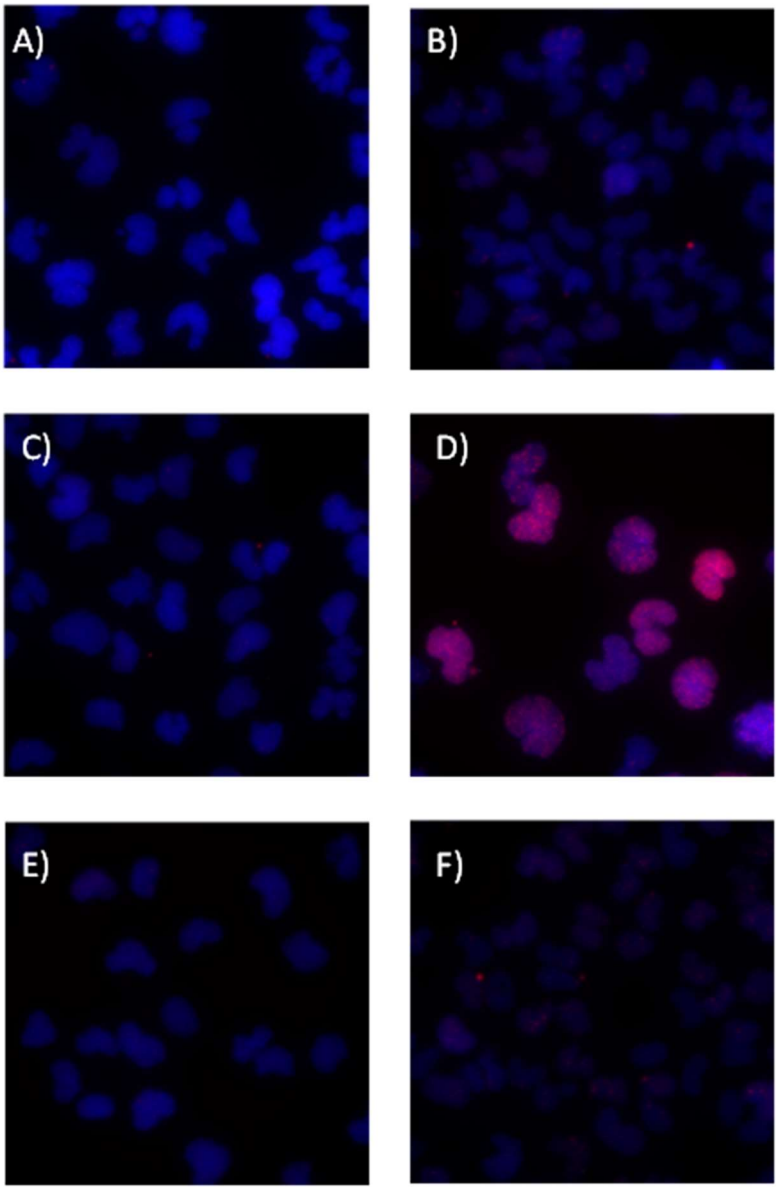

Figure 38 Impact of compounds on the number of nuclear γ-H2AX foci, as determined by immunostaining followed by fluorescence microscopy. Images represent Z-stacking of the fluorescence of the nucleus stained with DAPI (blue) and anti-γ-H2AX stained with AlexFluor™-555 (red). Cells were incubated for 96 h with compound vehicle **A)** (DMSO 0.5% v/v) **B)** TMZ (94 µM) **C)** O^6BG (92 µM) **D)** TMZ and O^6BG (94 and 92 µM, respectively) **E)** compound **62** (1.1 µM) and **F)** a combination of TMZ and **62** (94 and 1.1 µM, respectively).

As observed, TMZ (94 µM) treatment did not induce a significant change of the number or the size of γH2AX foci per nuclei; however, O^6BG (92 µM) and its combination with TMZ induced a strong and statistically significant increase of the number and size nuclear γH2AX foci (compared with DMSO). Suprisingly as well, O^6BG alone also showed an increase on this value, which is statistically significant than the combination of TMZ + O^6BG (**Figure 39A-B**). This results are in agreement with the proposed mechanism of action of TMZ leading to DNA adducts followed by the accumulation of DSB resulting from the futile repair of *O*^{6}MeG residues.[203–205] Remarkably, neither compound **62** (1.1 µM) nor its combination with TMZ induced an increase of the number or the size of γH2AX foci, despite a synergistic cytotoxic effect.

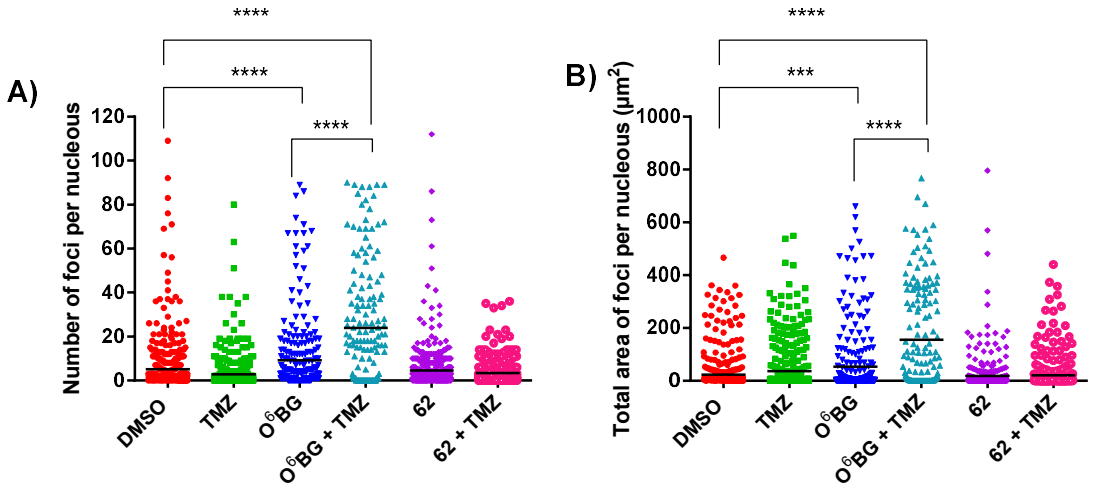

Figure 39A-B) Analysis of **Figure 38** was performed by FIJI software analysis. Black bars indicate the mean values of **G)** number of foci per nucleus or **H)** the total area of foci per nucleus. At least 150 cells were counted per condition; (*n* = 2). One-way ANOVA multi comparison with Tukey's post-test analysis; *** and ****: $p \leq 0.001$ and 0.0001 respectively.

<u>Cell death mechanisms</u>

Concerning the mechanisms of cell death underlying the cytotoxic effects of the hybrid **62**, we performed an Annexin V / propidium iodide (PI) cell death assay (**Figure 40A-C**). Neither TMZ[204] nor O^6BG treatments alone (despite O^6BG being a generator of DSB) significantly increased the proportion of cells undergoing apoptosis probably because the damage of the latter is repaired in time before entering apoptosis. However, their combination increased the fraction of apoptotic cells (from 2 to 8%) after 96 h, but not after 48 h (**Figure 40D**), in agreement with literature[29] and in line with the established DNA-damaging effects of this combination. Interestingly, compound **62** alone significantly increased the fraction of apoptotic cells (to 10%) after 96 h, but not after 48 h of treatment. The same

effect was observed for a combination of **62** with TMZ (11% after 96 h), indicating that the synergy of the cytotoxic effect of this combination does not stem form a synergistic apoptosis. In the fraction of necrotic or late apoptotic cells, no drug induced a significant change (**Figure 40B-C**). Finally, to confirm that the compound **62** triggers cell death by apoptosis, we assessed the activation of caspases using luminescent Caspase-Glo 3/7 assay.[206,207] The results (**Figure 40A**) clearly gave evidence of activation of caspases 3 and 7 in the cells treated with compound **62** (1.4-fold with respect to DMSO control), which was not further increased in a combination of **62** with TMZ.

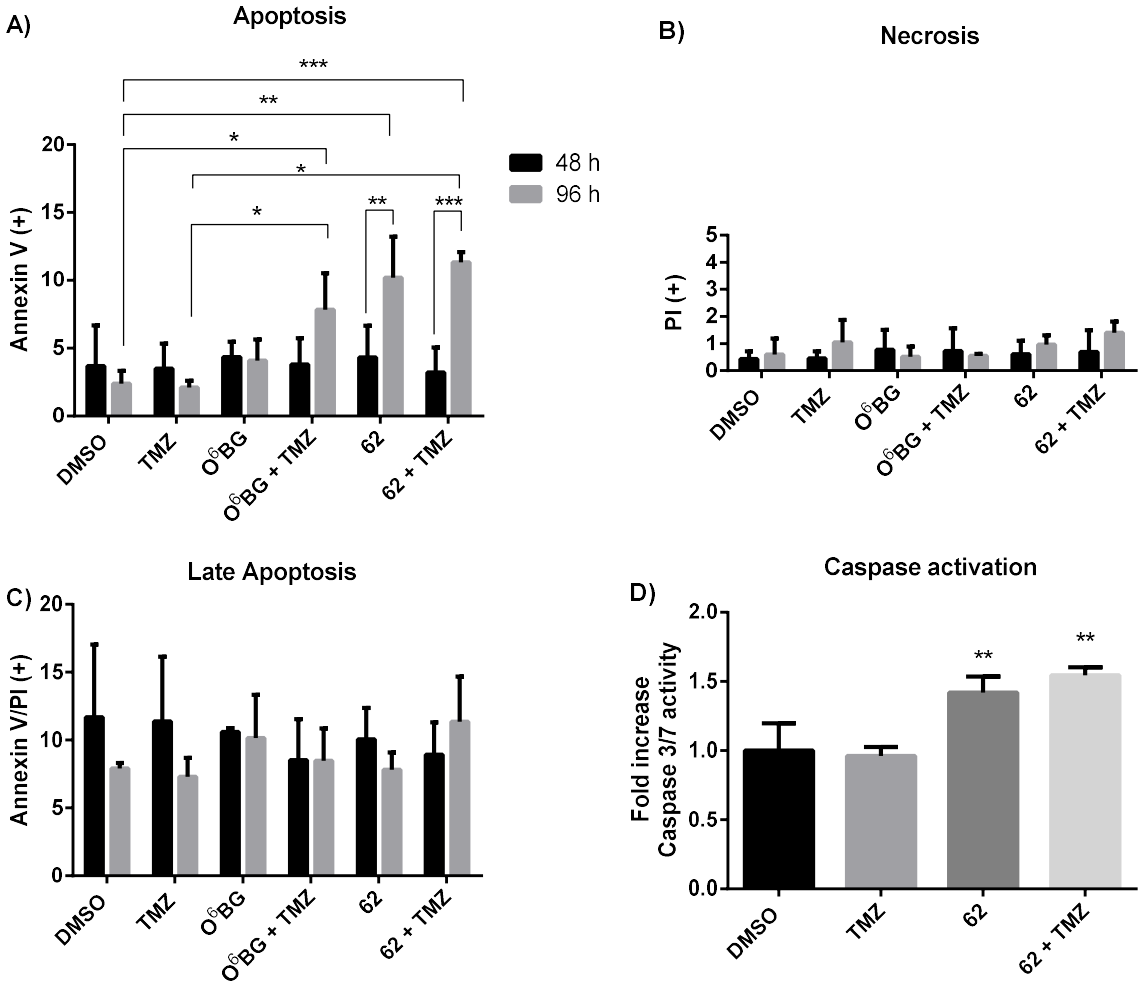

Figure 40A-D) Results of the Annexin V / PI assay: fractions of apoptosis in T98G cells after 48 h (black bars) and after 96 h (grey bars) of incubation with DMSO (0.5% v/v), TMZ (94 µM), O^6BG (92 µM), a combination of TMZ (94 µM) and O^6BG (92 µM), **62** (1.1 µM), and a combination of TMZ (94 µM) and **62** (1.1 µM), as determined by flow cytometry. Results represents mean ± S.D (*n* = 3-5) Two-way ANOVA with a Tukey's multi comparison post-test. **D)** Caspase 3/7 activity of T98G cells treated for 96 h in the same conditions as described above. One-Way ANOVA test with a Dunnet's multi-comparison post-test; * ** and *** denote values of $p \leq 0.05, 0.01, 0.001$ respectively.

While the synergy with TMZ and inactivation of cellular MGMT (**Figure 37,** page 120) may suggest that cellular effects of **62** are similar to O^6BG (**Figure 40A-C**), the mechanism underlying this synergy appears to be quite different. Indeed, while O^6BG and the combination of O^6BG with TMZ strongly increased the number of DSB, neither **62** alone nor in combination with TMZ did not show any DSB increase, giving evidence that cytotoxic mechanisms of this hybrid (and its combination with TMZ) are more complex. This is further supported by observation of a large fraction of cells undergoing apoptosis (as confirmed by the activation of caspases pathway, **Figure 40D**) upon treatment with **62** alone that is not further increased in combination with TMZ, whereas O^6BG treatment induced apoptosis only in the presence of TMZ (**Figure 40A**). In the case of combination of O^6BG with TMZ, the apoptosis clearly stems from the DNA damage, as evidenced by the strong increase of the number of γH2AX signals (**Figure 39**). In contrast, the combinations of **62** with TMZ leads to a synergic effect on the cytotoxicity level independently of DNA damage or increased apoptosis. This is plausible since TMZ may sensitize also glioblastoma cell lines via other pathways than DNA damage (such as autophagy)[208]. Indeed, the apoptotic effect of compound **62** may be attributed to the presence of acridine fragment that is able to activate many signaling cascades, as described for related 9-aminoacridine derivatives.[136,148–154]

***In silico* evaluation of drug-like properties**

From the practical point of view, the capacity of the O^6BG-Acr hybrid to inhibit the growth of a multidrug-resistant glioblastoma cell line alone or in combination with sub-toxic doses of TMZ represents a significant interest. To address the potential of therapeutic use for these compounds, we performed *in silico* evaluation of their physicochemical and ADME parameters and drug-likeness, including the potential to cross the BBB.[209] The results (**Table 6**) demonstrate that, in contrast to O^6BG and **Acr**, most hybrids can be seen as rather poor drug candidates according to the classical criteria of medicinal chemistry, with only **62** and **63** satisfying the Lipinski filter. However, the evaluation of BBB permeability using AlzPlatform database[210] indicates that most hybrids are potentially able to cross the BBB and reach brain tumors. It should be noted that brain tumors are known to compromise the BBB integrity, resulting in a vasculature known as the blood–tumor barrier (BTB), which is highly heterogeneous and characterized by non-uniform permeability, rendering its *in silico* prediction challenging [211,212].

Table 6. Selected physicochemical descriptors and *in silico* ADME parameters, pharmacokinetic properties, and drug-likeness of hybrids and reference compounds **Acr** and O^6BG.[a]

Cpd	MW	Fraction $C(sp^3)$	Rotatable bonds	HBA	HBD	TPSA ($Å^3$)	Lipophilicity						GI absorption	BBB permeability			Drug-likeness (no. of violations)		
							iLOGP	XLOGP3	WLOGP	MLOGP	Silicos-IT Log P	Consensus Log P		Swiss ADME	AdaBoost[b]	SVM[b]	Lipinski	Veber	Muegge
47	583.0	0.17	11	7	4	153.0	3.28	4.72	4.51	2.51	4.81	3.97	Low	No	Yes	Yes	No (2)	No (2)	No (1)
48	657.1	0.24	16	9	4	171.4	4.35	3.97	4.15	1.56	5.14	3.84	Low	No	Yes	Yes	No (2)	No (2)	No (3)
49	653.2	0.29	16	7	4	153.0	4.80	6.32	6.46	3.43	6.87	5.58	Low	No	Yes	Yes	No (2)	No (2)	No (4)
62	554.0	0.20	10	6	2	113.0	4.34	5.72	5.91	3.30	4.99	4.85	Low	No	Yes	Yes	Yes (1)	Yes (0)	No (1)
63	610.2	0.29	14	6	2	113.0	5.37	7.52	7.47	4.03	6.63	6.20	Low	No	Yes	Yes	Yes (1)	No (1)	No (2)
64	614.1	0.25	14	8	2	131.5	4.97	4.71	5.16	2.14	4.90	4.38	Low	No	Yes	No	No (2)	No (1)	No (1)
Acr	258.7	0.07	1	2	1	48.1	2.53	3.13	3.64	2.58	3.36	3.05	High	Yes	Yes	Yes	Yes (0)	Yes (0)	Yes (0)
O^6BG	241.3	0.08	3	4	2	89.7	1.49	1.55	1.37	0.65	1.60	1.33	High	No	Yes	Yes	Yes (0)	Yes (0)	Yes (0)

[a] Computed with SwissADME (http://www.swissadme.ch/); A. Daina, O. Michielin, V. Zoete, SwissADME: A free web tool to evaluate pharmacokinetics, drug-likeness and medicinal chemistry friendliness of small molecules, *Sci. Rep.* **2017**, *7*, 1–13.

[b] Computed with AlzPlatform BBB Predictor (https://www.cbligand.org/BBB/); H. Liu, L. Wang, M. Lv, R. Pei, P. Li, Z. Pei, Y. Wang, W. Su, X.-Q. Xie, ALzPlatform: An Alzheimer's Disease Domain-Specific Chemogenomics Knowledgebase for Polypharmacology and Target Identification Research. *J. Comput. Inf. Model.* **2014**, *54*, 1050–1060.

3.4 Conclusions

In this part of the Thesis the approach to target MGMT using hybrid molecules composed by two scaffolds such as **Acr** and O^6BG was explored. The purpose of attaching to the MGMT inhibitor O^6BG an **Acr** core was justified by the different effects that the latter can elicit in cancerous cells, with the objective of donating the hybrid a pharmacological added value capable to overcome the multiple t factors that generate resistance in GBM cells.

Altogether, six hybrids were synthesized differing on the linker length and nature and by modifying the way of attaching them, namely *via* the benzyl ring or the N^9 of the O^6BG scaffold. Upon the synthesis of this set of compounds, the goal was to have molecules in an intra-stacked (or inactive) conformation that upon changing of environment (by interaction of the **Acr** core to DNA), the O^6BG scaffold would be exposed to inactivate MGMT, increasing TMZ's cytotoxicity. The equilibria and the modulation of this property was successfully achieved with two opposite trends, being the N^9 hybrids more intra-stacked when the length of the linker was shorter and for the Bn hybrids less intra-stacked when the linker length was increased. Two other effects were demonstrated for this strategy. First, it was shown, contrary to our initial model, that the hybrids were able to interact but not to intercalate with DNA in comparison with the intercalator control **Acr**. And second, the hybrids were also able to inactivate MGMT in gel based assays, with different capacities of inhibition according to the assay employed. As a general rule, Bn hybrid are as good inhibitors *in vitro* as O^6BG whereas N^9 hybrids were less effective as the control. The *in cellulo* effects of the six hybrids, as well as other five compounds, were studied and we observed that the **Acr** cytotoxicity can be modulated depending on the attachment points. Bn hybrids showed to have a micromolar potency ($15 < GI_{50} < 25$ µM), whereas when the attachment was changed to the N^9, the cytotoxicity was increased to low-micromolar values for compounds **62** and **64** ($GI_{50} < 3$ µM). Interestingly, these two compounds showed synergy when combined with TMZ at sub-toxic concentrations of both hybrid and TMZ (1/8 GI_{50} values of each compound).

We could observe that compound **62** was able to inactivate cellular MGMT, validating our hypothesis and we also noticed that the molecule is able to generate apoptosis alone or in combination with TMZ in T98G cells. However, this apoptosis is not generated through the creation of DSB as seen for O^6BG with TMZ. The apoptotic process was explained by the activation of the pro-apoptotic cascade since it was observed by the activation of the Caspase 3/7 expression, which may be a consequence of the p53 protein activation. Of note and as it was observed for the synergic effect of **62** plus TMZ did not ascribed from a synergic increase in the apoptosis cascade.

Surprisingly as well, **Acr** was able to inhibit MGMT in our assays and also able to generate synergy in combination with TMZ, properties that are interesting for future drug discovery approaches to treat GBM.

According to *in silico* predictions both compound **62** and **Acr** could be able to cross the BBB and also fit the Lipinksi rules for orally available drugs that in conjunction with its biological properties makes them a good candidates to continue in the drug development process.

Chapter 4
Inhibition by photocaged molecules

4 Inhibition of MGMT by photocaged molecules

4.1 Principle and State of the Art

The problem of tumor selectivity is a recurrent issue in cancer treatment. One of the strategies employed by researchers to overcome this inconvenient is the use of an active molecule conjugated to a photolabile protective group (PPG). The idea of this approach consists that the addition of the PPG renders the compound inactive, that once is irradiated with a certain wavelength releases the active scaffold into the environment due to the removal of the PPG. Since the time and the amplitude of the excitation of the wavelength can be controlled by commercially available sources, the bioavailability and the pharmacodynamics of a certain molecule can be also spatio-temporally regulated (**Scheme 14**). Ideally, this strategy should fullfill certain criterias in order to be successfull. First of all, the addition of a PPG should lead to an inactive (or less active) caged molecule in comparission with the parental compound. Second, in order to avoid light cytotoxicity, PPG groups should be able to be removed fast and with low-energy wavelengths. Thirdly, the liberation of the PPG (or its by product) should not be toxic for the studied system.[213–217]

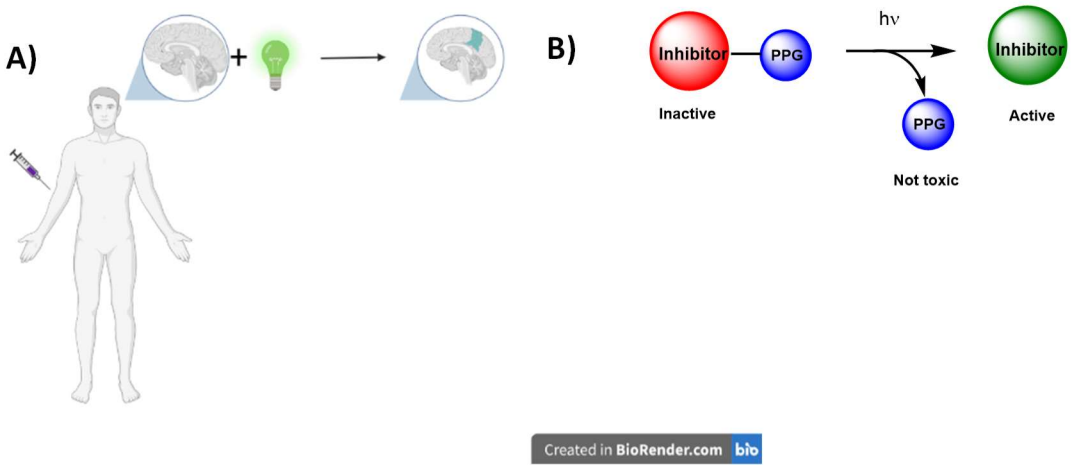

Scheme 14 Representation of **A)** uncaging of a photocaged drug in brain, the coloured area represent the activation of the drug in the tumour area **B)** design of a prototype caged molecule and its reaction upon light irradiation

The strategy of photocaging small molecules has been widely used in order to study cell physiological functions, such as gene regulation, cell cycle, migration, mobility, adhesion, nuclear and organelles transport, second messengers studies, protein engineering, cell trafficking, lineage.[213–217] According to the literature, several examples are found in pre clinical trials for cancer treatment, with PPGs varying in structure, reactivity and wavelength for PPG cleavage. In this part of the Thesis we will only be

focusing in nitrobenzyl derivatives as PPG (**Chart 15**).[213–217] One of the first examples is the use of Au nanoparticles (Au-NP) containing taxol by using photocaged folic acid (FA) on the surface to target the folate receptor (FR) which is overexpressed in cancer cells. The concept is based on the use of the *o*-nitrobenzyl group (ONB) to impede the recognition by the FR. Once irradiated with a Hg lamp, FA contained on the surface of the Au-NP was supposed be exposed and uptake by the FR, internalizing the nanoparticle and therefore the taxol drug. With this strategy, researchers managed to diminish the viability of HeLa cells upon irradiation but not in the absence of light, confirming the proof of concept of this strategy.[218] A second molecule is the caged vemurafenib, a drug that is used to inhibit Ser/Thr kinases in clinical trials for treatment of metastatic melanoma that are mutated in the $BRAF^{V600E}$ gene. Here, researchers sucessfully caged vemurafenib with an 4,5-dimethoxy-2-nitro-benzyl (DMNB) group, that upon irradiation at 365 nm, released the active scaffold in the melanoma cell line SKMel133.[219] The same PPG was used to cage the topoisomerase 1 inhibitor irinotecan. Upon irradiation at 405 nm, the release of the irinotecan was auspiciously and showed to reduce the viability of A549 cell lines both in *in vitro* and in mice xenografts.[220] Finally, by attachment of a DMNB PPG, the researchers were able to mask the activity of the tubulin inhibitor **220.2**, that upon irradiation at 365 nm, released the active scaffold and diminish the viability of two types of glioblioma cell lines like U251 and RN1.[221]

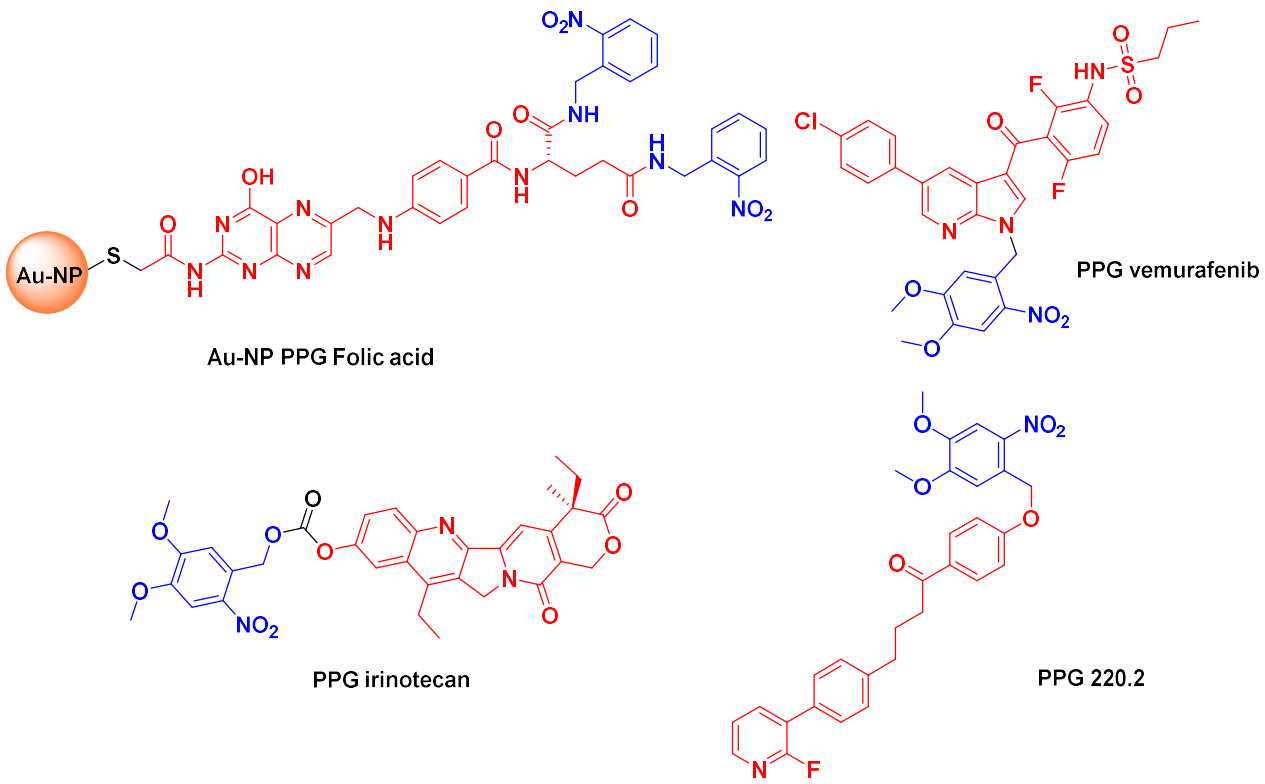

Chart 15 Photocaged molecules for drug treatment. Colours in red depict the active molecule and blue the photoprotective group (PPG).

Despite being great MGMT inhibitors, both O^6BG and Lomeguatrib failed in clinical trials when used in combination with TMZ. As stated before, the lack of selectivity for the MGMT inhibition in a cancerous cells *vs.* a normal cell, due to the sensitization of the healthy cells towards TMZ. One of the strategies for better achieving a release of the cytotoxic (alkylating) agent has been the use of the Gliadel wafers as seen in **Chapter 1**. Another possible strategy to improve the spatio-temporal action of MGMT inhibitors could be its activation using the photocaged precursors of the MGMT inhibitors. The strategy consists in attaching the active scaffold (namely the O^6BG) to a PPG group, impeding the off target effects, that in this case could be MGMT in non cancerous cells. In fact, photocaged O^6BG derivatives have been described in the SNAP/TAG strategy but their therapeutic utility as potential photocaged MGMT inhibitors has not been used. In this strategy, Johnsson *et al*. uses the O^6BG derivative to label a fused MGMT-hGST protein. Here, they use O^6BG conjugated to fluorescein or rhodamine derivatives, that once irradiated reacts with SNAP-tagged proteins and transfer the fluorophore to label the hGST.In this article O^6BG was protected with an ONB PPG group where both N^7/N^9 PPG isomers were isolated. By using the MGMT-hGST fused protein researchers demonstrated that group that the N^7 PPG isomer is the isomer which does not label the hGST before light exposure (due to the lack of reactivity, as explained in **Chapter 1**) whereas the N^9 PPG isomer shows some hGST labelling even before light irradiation (**Chart 16A**).[222]

Considering these data, the N^7 PPG isomer strategy attachment has been employed by the Staffort group for RNA editing *in vitro* and *in vivo*.[223,224] Hither, researchers use the 6-nitropyperonyloxymethoyl (NPOM) protecting group for O^6BG derivatives which are incorporated into a RNA sequence through its benzyl group. Upon irradiation at 365 nm, the guide RNA becomes a substrate of the MGMT protein fused to the human adenosine deaminase acting on RNA enzyme (ADAR). Once the PPG group is removed and the MGMT reaction takes place, the RNA becames closer to the ADAR active site that converts the adenine nucleotide into inosine (**Chart 16B**). As a final example of this strategy, during the preparation of this manuscript, a very interesting example of a caged MGMT inhibitor was disclosed as a preliminary report.[225] The probes developed by the Beharry group, used NPOM as a PPG group and were attached to the N^7 of O^6BG and LG. And its efficacy as photoactivatable probes targeting MGMT were shown *in vitro* and in MCF-7 cell lines (**Chart 16C**).

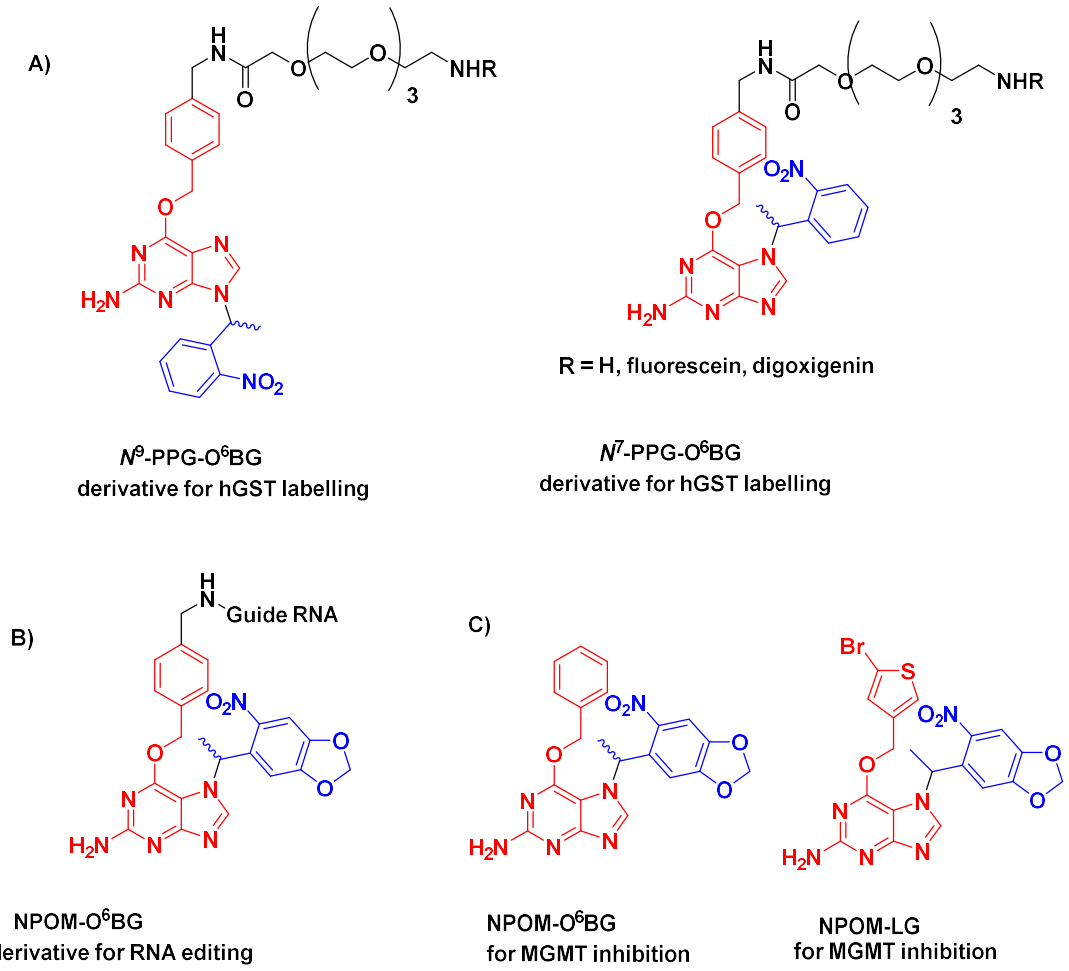

Chart 16 Photocaged O^6BG derivative molecules **A)** used for hGST labeling **B)** RNA editing and **C)** MGMT inhibition

4.2 Results and discussion: synthesis and *in cellulo* experiments

Considering the paragraphs mentioned above, we decided to "photocage" O^6BG with the goal of rendering it a less active MGMT inhibitor that upon irradiation with light should release the MGMT inhibitor. As a first approach to this strategy, we decided to use the *o*-ethylnitrobenzene moiety as a PPG since it seemed an easy and fast approach to study this strategy (**Scheme 15**).

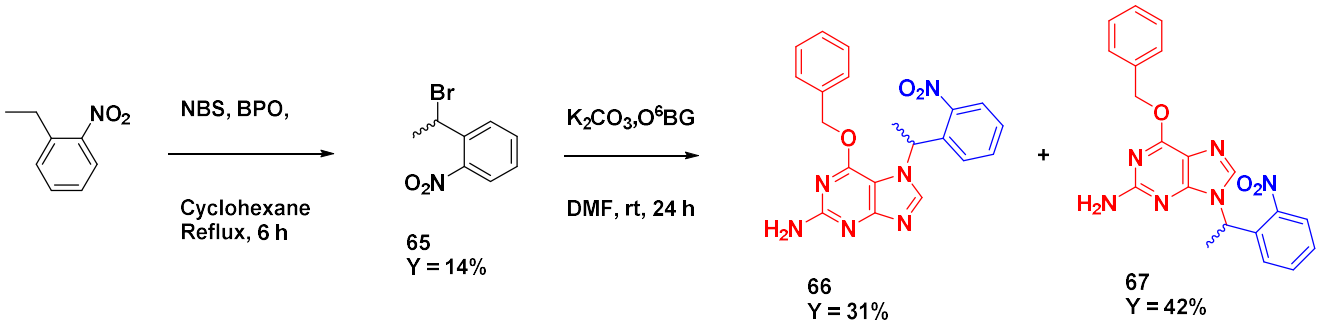

Scheme 15 Synthesis of photocaged O^6BG derivatives

This strategy relied in the monobromination of *o*-ethylnitrobenzene on its benzylic position by the use of *N*-bromosuccinimide (NBS) in the presence of the radical initiator benzoyl peroxide (BPO) which allowed us to obtain compound **65** in low yield. This brominated compound, was used for the alkylation of $O6^BG$ using K_2CO_3 as a base at room temperature. With this procedure, both isomers N^7 (**66**) and N^9 (**67**) were simoultaneously obtained in very good yields.

As stated before, one of the main premises for this strategy was to obtain compound not (or less) toxic than the parent (uncaged) compound, in this case O^6BG. Therefore, the cytotoxicity of these compounds was assayed as described in **Chapter 2**. After 96 h of incubation, the GI_{50} for **66** and **67** in T98G cell line were 0.5 and 40 µM for the N^7 and N^9 isomers respectively, indicating that these compounds are >180-fold and >2-fold times more toxic than O^6BG (GI_{50} = 92 µM, **Figure 41**). Especially in the case of the N^7protected derivative **66** that (on the basis of the literature data) was supposed to be an efficiently "caged" MGMT inhibitor, the high cytotoxicity was strongly discouraging. Even if the study for the MGMT *in vitro* inhibition was not carried, the *in cellulo* data was considered enough to stop this strategy, at least with this type of protecting group.

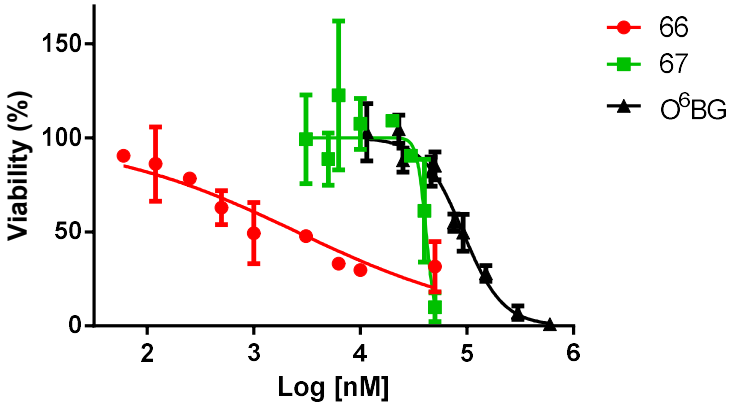

Figure 41 Dose–response curves for the viability of T98G cells in the presence of drugs. Experimental points are mean ± S.D values ($n \geq 3$). GI_{50} values were determined using the GraphPad software by fitting normalized response vs. log [drug] with a variable-slope curve, Y=100/(1+10^((LogGI_{50}-X)*HillSlope))

4.3 Conclusions

Photocaging molecules is an elegant strategy to mask an active drug in order to render it less active towards non-specific targets, that once irradiated in specific conditions it becomes active only in a desired locus. In this chapter we reherse as a proof of concept the caging of O^6BG using ONB as a PPG. The synthetic part consisted in the obtention of the two regioisomers **66** and **67** in two steps and its biological evaluation. Unfortunately, both compounds turned out to be more toxic than the parental compound. Considering that the isomer N^7 (**66**), which is supposed to be the caged and inactive molecule since MGMT should not be able to remove the benzyl group, is two order magnitude more cytotoxic than O^6BG, the use of the photocaged O^6BG was abandoned. Of note, and due to the last results observed in the literature, the choice of the PPG seems to be key for the success of the strategy; therefore, other PPG should be studied deeply.

Chapter 5
General conclusions

5 General conclusions

Cancer is a disease with a worldwide distribution that makes no distinction of age, gender or economical status. Among cancers, GBM is a particular type of brain cancer that is the most common one in adult population. Unfortunately, it is a fatal disease with no cure, that implies a very short life span for the patient. The palliative treatment consists in aggressive methods that strongly diminish the life quality of the patients. As stated in the introduction, this type of cancer has not only the biological hallmark of being a very aggressive, infiltrating and recurrent tumour with many exaxerbated biological characteristics such as the overexpression of MGMT, pump efflux for drug detoxification, GSC presence, etc. In addition, from a physical point of view, it has the particularity of being located in an area where more intrincated surgery procedures need to be carried in order to acces to this part of the human body. Of course, the modification by surgery of this very important organ can also lead to a loss of the cognitive and motility capacities of the patient. Likewise, another physical barrier like the BBB plays an undeniable and complicated hurdle necessary to overcome when we talk about drug dosing since not every molecule, used for non-brain chemo or immunotherapy treatment can be used. Considering the physical and biological factors, the scientific community has devoted enormous efforts to improve life quality, increase life expectancy or in the best case scenario to cure patients that suffer from GBM. The strategies often consist in multimodal approaches that try to overcome all these dificulties described above. In this Thesis, only pre or clinical trials covering chemotherapeutic approaches have been mentioned. Nevertheless, it is important to mention that other modalities have been used in order to ameliorate life quality by: developing better diagnostic tools such as magnetic resonance imaging (MRI) or fluorescent techniques to better localize the tumor niche. As well stratification of patients according to biomarkers expressions to improve the prognosis of the current therapy have been also carried. In addition, immunotherapy or acoustic methods based on the tumour treating fields (TTF) have reached clinical trials with this purpose. [2,3,226] Despite the enormous efforts, none of this method have been able to successfully improve GBM treatment.

In this Thesis, we have explored three new strategies that could be potentially applied from a therapeutical point of view. The first approach was based on the premise of designing small molecules varying their size, π-stacking capacities, charge, hydrophobicity and more important hydrogen bond formation capacity, towards a possible interaction with O^6MeG in order to mask the latter from MGMT action, therefore enhancing its biological relevance in glioblastoma cells. In this part, eleven molecules were synthesized and together with eighteen previously designed compounds, their capacity to stabilize dsDNA bearing O^6MeG nucleobases was studied by biophysical methods. In addition, their cytotoxic properties in the multi-drug resistant and MGMT overexpressing glioblastoma cell line T98G

were tested alone or in combination with TMZ. Unfortunately, none of the studied compounds were able to selectively stabilize dsDNA containing O^6MeG residues, neither in a O^6MeG:C base pair or in a simplified O^6MeG:Φ substrate.In addition, molecules did not show an interesting cytotoxicity versus T98G alone or when combined with TMZ. However, one 8-azaquinolone, molecule **15**, was able to selectively discriminate an AP surrogate that faced an adenine (A:Φ) in the opposite strand. This compound showed a selectivity in comparison with other type of base pair in DNA (A: Φ > T: Φ > C: Φ > G: Φ > O^6MeG:Φ >>AT) and also showed to be the most cytotoxic compound of this serie. Even if no increase in the cytotoxic properties of TMZ was observed in this cell line, a possible use of this compound in other type of cell lines should not be ruled out.

In the second strategy, the inhibition of MGMT by hybrid molecules was explored by the conjugation of the O^6BG warhead with the **Acr** moiety due to the demonstrated properties of the latter to activate cytotoxic pathways in cancerous cells. The intention was to award an added value to the O^6BG scaffold to exploit several cytotoxic pathways in the glioblastoma cells. Our concept, resided on the design of molecules that differed on their attachment points between O^6BG and **Acr** (N^9 and Bn ring) by varying also the linker's length and nature. This idea would allowed us to obtain compounds in two conformations (intramolecularly stacked or inactive, and open or active) to modulate their DNA interaction properties and MGMT inactivation *in cellulo*, increasing TMZ's action. By carrying this approach, we observed that for the hybrids the equilibria could be altered as well as their MGMT inhibition properties and their cytotoxic propeties. More interestingly, we found that hybrids **62** and **64** were able to generate a synergic effect when combined with TMZ when they were used in sub-toxic concentrations, in the same fashion but at much lower concentrations than O^6BG. The MGMT inhibition was successfully demonstrated for **62** in cellular experiments were we could validate our hypothesis. In addition, the benefit of the fusion of the **Acr** core into the hybrid was demonstrated by activation of the apoptosis process (as evidenced by the Annexin V assays) by the activation of the pro-apoptotic caspases 3 and 7 rendering a molecule with at least two biological effects in the T98G. The first one, MGMT inhibition, and the second, the activation of pro-apoptotic responses which are generally down-regulated in cancer. From a clinical point of view, the demonstration that these molecules are synergic with TMZ at sub-toxic concentrations, and tohave a multi-target effect could open the door to further studies in the drug development pipeline, since it could mean that a selectivity could be achieved for cells that overexpress MGMT and that are also TMZ-resistant by other means beside this protein overexpression.

Finally, based on the lack of spatio-selectivity of the O^6BG scaffold, the photocaged strategy was carried on the premise of obtaining an inactive molecule that upon light irradiation would release the O^6BG molecule. Unfortunately, the photocaged products turned out to be more toxic than the parental compound *in cellulo*, therefore no *in vitro* assays towards MGMT inhibition were carried. However and due to literature data, the key towards the success of the strategy may reside in the type of PPG group, therefore the use of different ones may be reconsidered.

As a summary of all three strategies carried on this Thesis, a rational design of molecules combined with their synthesis was done. In total, thirty three final molecules were synthesized by classical organic synthesis techniques. For these molecules, their *in vitro* properties such as DNA binding, fluorescence, intramolecular stacking or MGMT inhibition properties were studied. As well, their cytotoxic effect alone or in combination with TMZ was also analyzed in a glioblastoma cell line. In addition, other techniques such as fluorescence microscopy, flow cytometry or enzymatic assays were carried to better understand their mechanism of actions. Altogether, this represent, even in a very small scale, a manner that could help us to understand the causes and more important, the tools that could be employed in a future to treat this disease from a chemotherapeutic point of view.

Chapter 6
Perspectives

6 Perspectives

Further biological studies of compound 62

As noted in **Chapter 3**, hybrid **62** was observed to localize after 96 h in the perinuclear region of the T98G cells similarly to what was observed in the literature for acridine containing molecules.[199] One possibility is that the molecule enters the cell by the endocytic pathway and therefore is accumulated in an organelle that surrounds the nucleus such as the endoplasmic reticulum (ER). Another possibility is that the molecule enters by passive diffusion, exerts its action in the cell and then its accumulated in organelles for its degradation or expulsion from the cell. The co-localization of **62** and the tracking within time in live cells could be perfomed with specific dyes to target mitochondria, ER, Golgi apparatus or lysosome and this could help to anticipate and understand the fate of this hybrids in the cell.[199]

As well, from a mechanistic point of view, the construction of the hybrid molecule represents a challenging scaffold to study the importance of the pathways that lead to the cell death. As stated in the literature, the **Acr** core itself can increase the pro-apoptotic cascade.[147,152,225] Both for **62** and **Acr** the possible relationship between the activation of the caspase 3 and 7 together with an increase on the p53 expression may also be studied. In addition as explained in **Chapter 1**, stalling of the cell cycle by TMZ's action leads to an arrest in G_2/M. It could be interesting to study if this phenomenon is also a cause of death after the combination with **62**. Finally, as observed, the combination of **62** and TMZ did not increased DSB, but it does not mean neither that the DNA repair damage cascade has not been activated. These experiments could help us to understand which are the other targets of the hybrid in the cell and also to understand which are the causes that lead to synergy in the cell.[5,114]

To conclude an interesting issue to test is the selectivity of this strategy towards other overexpressing MGMT cell lines derived from liver, kidney, lung or colon as well towards non-cancerous cell lines.[15] These analysis could allow us to maximize the scope of these molecules.

Hybrid strategy targeting BER and MGMT

From a synthetic point, the hybrid strategy could be also exploited. In this case, instead of targeting the DNA by the **Acr** core, we could envisage the synthesis of a hybrid complex containing O^6MeG plus an abasic recognition site derived from methoxyamine.[227] Here, molecules could target both lessions produced by TMZ therefore enhancing its effect in cancerous cells (**Scheme 16**).

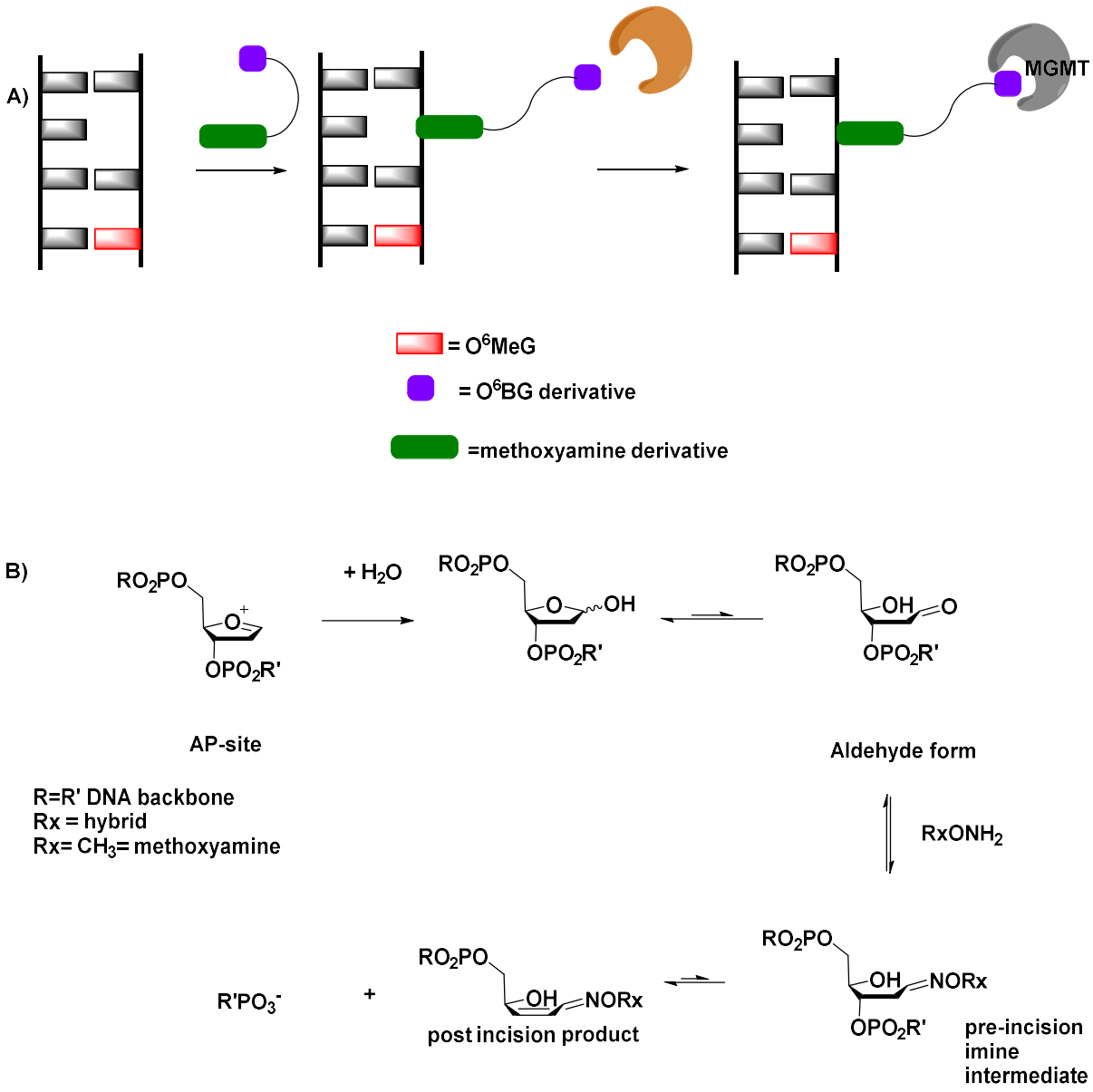

Scheme 16 Representative scheme for MGMT and abasic sites capturing

Once again, the molecules could be linked by the N^9 or the Bn ring of the O^6BG through a linker (**Figure 42**). For **Path A**, we proposed the synthesis of the final product **A**, obtained by the *N*-hydroxypthalimide removal. Here, the derivative **B** could be reached from the coupling of **46** and the carboxylic acid **C**, previously obtained from the diol **D**. In the case of N^9 attachment corresponding to the **Path B**, the N^9 substituted derivative **E** can be obtained through the alkylation by compound **F**.

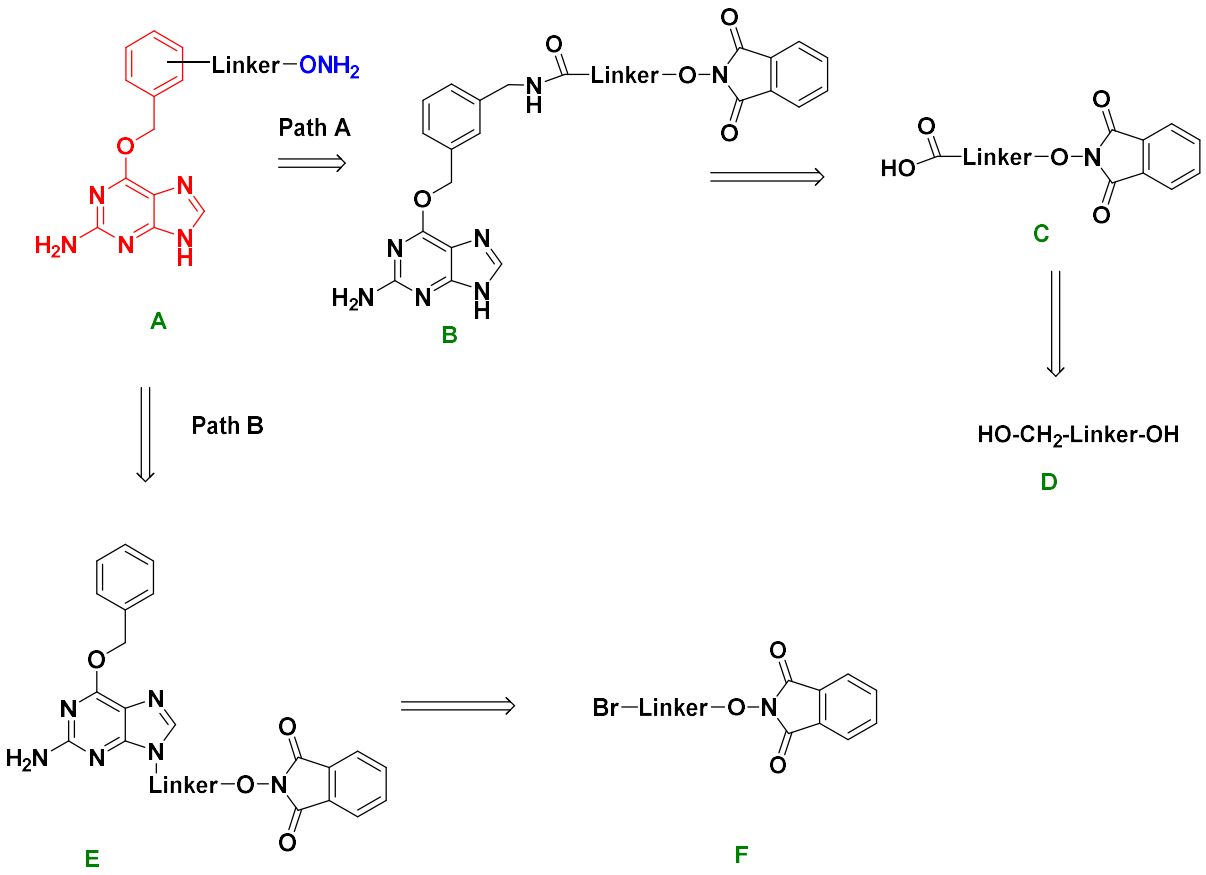

Figure 42 Retrosynthetic analysis for the obtention of hybrids to target MGMT and DNA abasic sites through the benzyl ring and N^9 of O^6BG Path A and B respectively.

So far and up to our knowledge, no mapping of the AP sites and the O^6MeG has been carried in DNA and is hard to predict which is the exact length of the linker to capture an MGMT near an AP site. In fact, we started this strategy and the preliminary results will be shown in the following lines.

In order to explore the Path A, we decided to start from 1,3-propanediol (**D** in **Figure 42**) as a starting linker. In our case, the decision of using a C_3 linker between the two scaffold resides on the observation that molecules containing an oxyamine derivative were the fastest in reacting with abasic sites.[227] This diol was converted into the *N*-hydroxyphtalimide **68** in fair yields by a Mitsunobu reaction. This monoprotected alcohol, was oxidized by two methods, the $NaIO_4/RuCl_3$ oxidation being the best oxidating couple.[228] Once the corresponding carboxylic acid **69** was obtained (Compound **C** in **Figure 42**) a first attempt of coupling with **46** and HBTU/HOBt was carried with a degradation of the acid and without observation of the product **B** as judged by LCMS. With the idea to obtain the activated NHS ester, **69** was placed with EDCI.HCl and the *N*-hydroxysuccinimde, but once again, the low yield of the obtention of the NHS intermediate made us abandon this strategy. A final attempt for the formation of the methyl ester was carried by refluxing **69** with MeOH and H_2SO_4 as a catalyst. Unfortunately, the reaction yielded to an ester in moderate yields (**70**) with the formation of the phtalimide ring opened

by-product (**Scheme 16**).

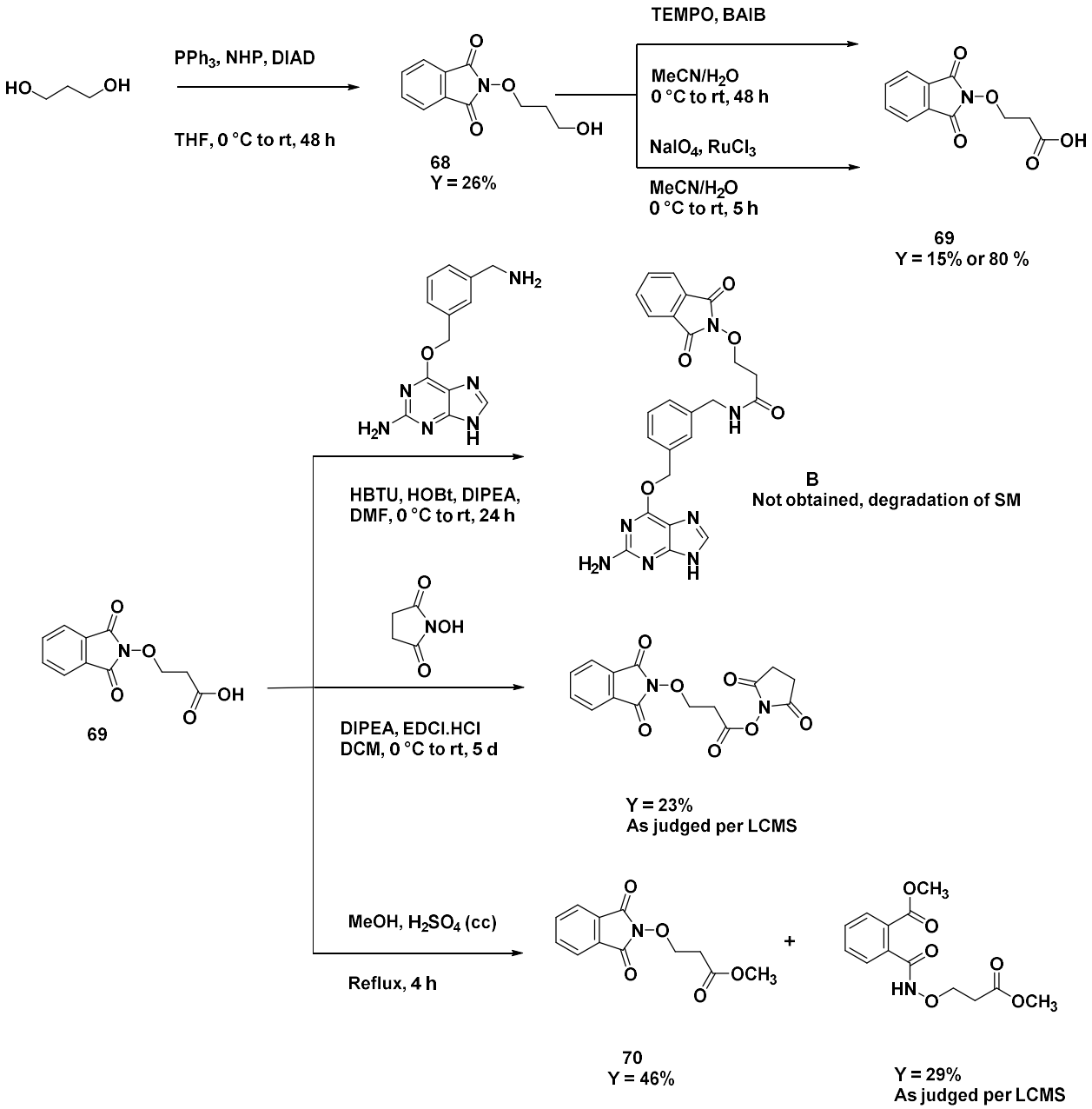

Scheme 17 Synthesis of the hybrids by the benzyl attachment using 1,3 propanodiol

Since hydroxypthalimides with a C_3 chain and a carboxylic group were reported as unstable[228] probably due to the elimination of hydroxyphtalimide as judging from the LCMS analysis, another attempt using a C_4 was assayed (**Scheme 18**). A Mitsunobu reaction over the 1,4 butanodiol was carried obtaining the alcohol **71** in low yield. After which it was oxidized to the carboxylic acid **72**, once again in low yields. Then a coupling with **46** lead to **73** in low yields which will be finally diprotected to yield compound **A**.

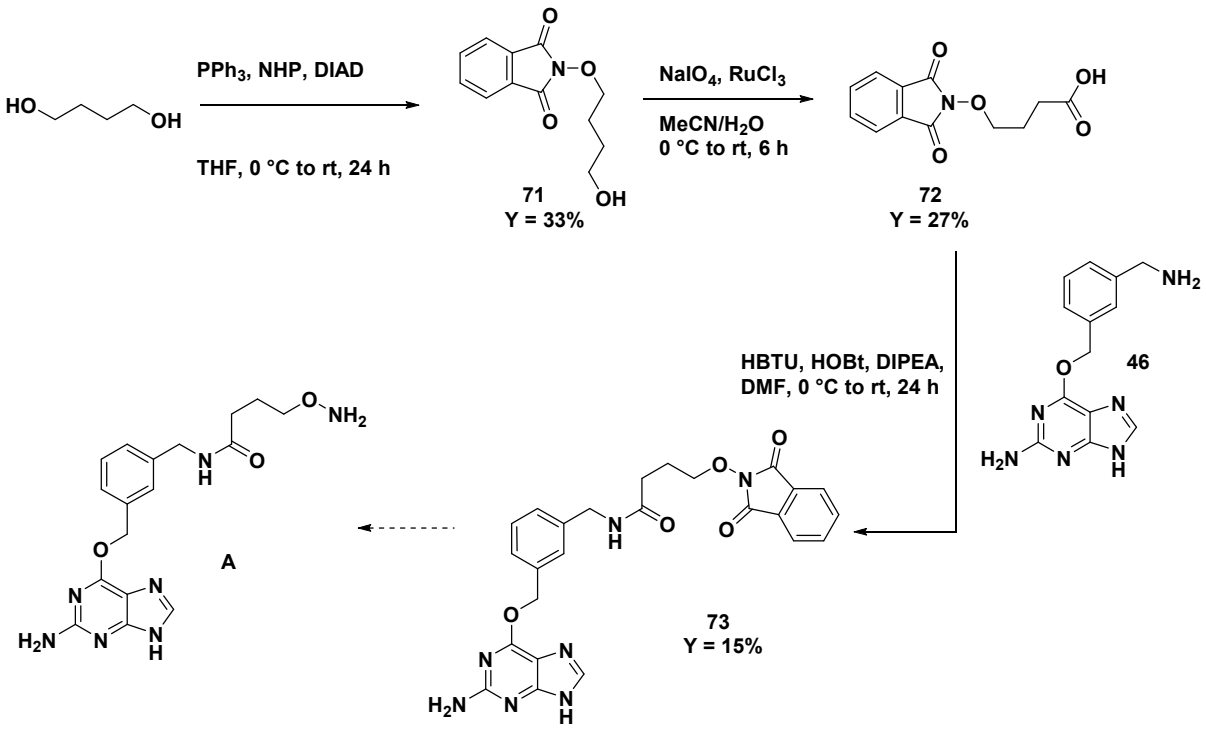

Scheme 18 Bn hybrid synthesis using a 1,4-butanediol as a linker

The other ongoing strategy is the N^9 alkylation of the O^6BG using the commercially available N-bromobutyl hydroxyphtalimide (**Scheme 19**). An alkylation using the conditions described in **Chapter 3**, allowed us to obtain the isomer N^9 (**74**, Y = 27%) in moderate yields. A final step of this strategy would be the deprotection of **73** into the hybrid **A**.

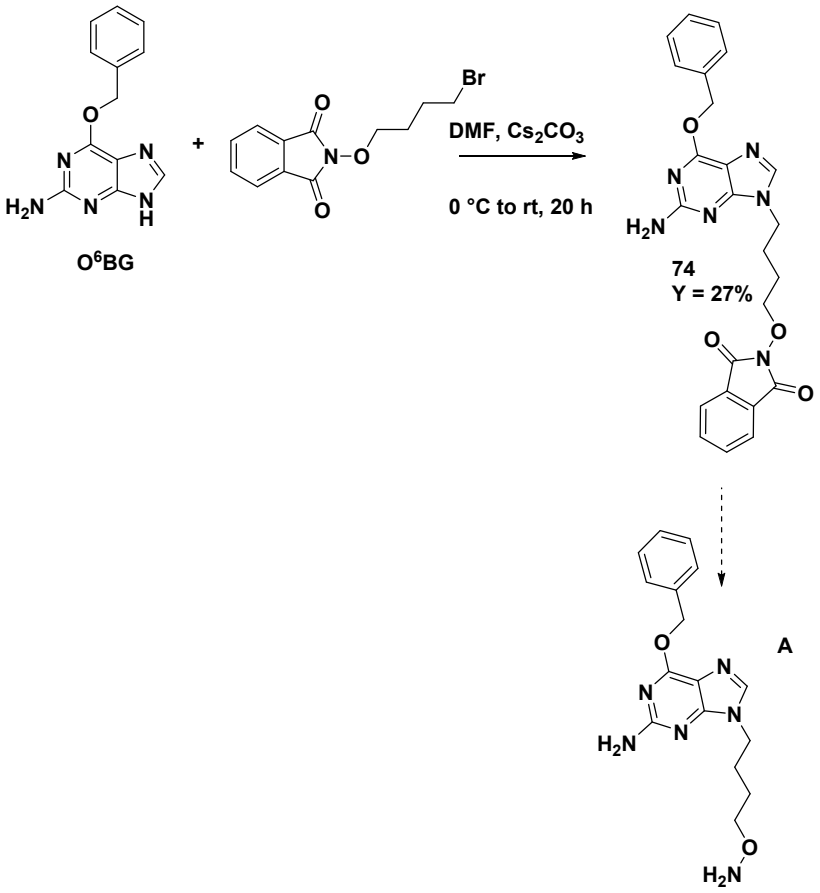

Scheme 19 $N^9$and N^7 hybrid of methoxyamine and O^6BG derivatives

Even if the synthesis and the biological evaluation of these hybrids has not been concluced, we believe that the obtention of these compounds could represent a unique scaffold that could target two type of damages created by TMZ. This targeting could also allow us to create compounds that may display synergy with TMZ to be used for GBM or other cancer treatment. Finally, since these molecules change on their attachment points, they could serve as tools to capture and pool down the complex formed with DNA and the enzymes that participate in its reparation.

Chapter 7
Experimental section

7 Experimental section

7.1 Chemistry

General remarks

All commercially available chemicals were reagent grade and used without further purification. NMR spectra were measured with a Bruker Avance 300 spectrometer at 25 °C; chemical shifts are given in ppm (δ) values. Multiplicities of ^{13}C NMR signals were determined from DEPT-135 or APT experiments. The purity of final compounds was assessed by LC/MS analysis (Waters Alliance 2525 equipped with a Phenomenex LunaOmega 3 µm Polar C_{18} 100A column and Waters 2996 photodiode array detector; eluent A: water with 0.1% HCOOH, eluent B: MeCN with 0.1 % HCOOH, gradient elution with 2 to 100% of eluent B). Mass spectra were obtained on a Waters ZQ spectrometer using electrospray ionization (ESI). Elemental microanalysis of all novel compounds was performed by the Service de Microanalyse, CNRS–ICSN, Gif-sur-Yvette, France. HRMS analysis were performed at the Small Molecule Mass Spectrometry platform of ICSN (Centre de Recherche de Gif Sur Yvette, France).

7.1.1 Indirect inhibitors

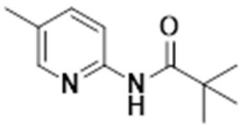

1

***N*-(5-Methylpyridin-2-yl)pivalamide (1):**[88,229] 2-amino-5-methylpiridine (1.0 g, 9.25 mmol) was dissolved in dry DCM (30.0 mL) under an Ar atmosphere, TEA (1.4 g, 13.87 mmol, 1.9 mL) was added and the reaction was cooled to 0 °C. Pivaloyl chloride (1.3 g, 11.10 mmol, 1.4 mL), was added dropwise and the reaction was stirred overnight. Solvent was removed by vacuum and the crude was purified by flash chromatography (SiO_2, eluent: Cyclohexane / AcOEt, 100:0 to 90:10, R_f = 0.24 in 90:10) to yield **1** (1.5 g, 8.04 mmol, 87%) of a white solid was obtained. ^{1}H NMR ($CDCl_3$, 300 MHz): δ 1.25 (s, 9H); 2.22 (s, 3H), 7.44 (dd, *J* = 8.6 Hz, 1.8 Hz, 1H), 7.88 (s, 1H), 8.00 (d, *J* = 1.8 Hz, 1H), 8.07 (d, *J* = 8.6 Hz). MS (ESI$^+$): *m/z* (%) 193.2 (100) [*M* + H]$^+$.

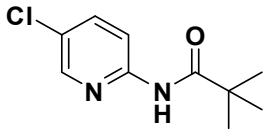

2

***N*-(5-Chloropyridin-2-yl)pivalamide (2)**:[88] 5-chloropyridin-2-amine (3.25 g, 25.3 mmol) was dissolved in dry DCM (100.0 mL) under an Ar atmosphere, TEA (3.84 g, 37.9 mmol, 5.3 mL) was added and the reaction was cooled to 0 °C. Pivaloyl chloride (3.66 g, 30.3 mmol, 3.7 mL), was added dropwise and the reaction was stirred overnight. Solvent was removed by vacuum and the crude was purified by flash chromatography (SiO_2, eluent: Cyclohexane: AcOEt, 100:0 to 90:10, R_f = 0.30 in 90 : 10) to yield **2** (4.46 g, 20.9 mmol, 87%) as a white solid. ^{1}H NMR ($CDCl_3$, 300 MHz): δ 1.28 (s, 9H), 7.59 (dd, *J* = 8.9 Hz, 2.8 Hz, 1H), 7.99 (s, 1H), 8.14 (d, *J* = 2.8 Hz, 1H), 8.16 (d, *J* = 8.9 Hz, 1H); MS (ESI$^+$): *m/z* (%) 213.2 (100) [*M* + H]$^+$.

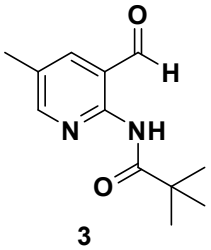

3

***N*-(3-Formyl-5-methylpyridin-2-yl)pivalamide (3)**:[88] Compound **1** (513 mg, 2.67 mmol) was dissolved in dry THF (6.00 mL) under an Ar atmosphere and cooled to – 78 °C. Then *n*-BuLi (512 mg, 8.00 mmol, 5.00 mL from a 1.6 M solution in hexanes) was added and the reaction was stirred for 3 h at 0 °C, then it was cooled again at – 78 °C and dry DMF (780 mg, 10.67 mmol, 0.84 mL) was added dropwise. The

reaction was quenched by adding an excess of aq. $NH_4Cl_{(sat)}$, and extracted exhaustively with AcOEt, organic layers were dried over Na_2SO_4, filtered, concentrated under vacuum and the crude was purified by flash chromatography (SiO_2, eluent: Cyclohexane / AcOEt, 100:0 to 50:50, R_f = 0.22 in 50:50) to obtain **3** (358 mg , 1.63 mmol, 61%) as a white solid. ^{1}H NMR ($CDCl_3$, 300 MHz): δ 1.42 (s, 9H), 2.39 (s, 3H), 7.85 (s, 1H), 8.50 (s, 1H), 9.91 (s, 1H), 10.68 (s, 1H); MS (ESI$^+$): *m/z* (%) 221.2 (100) [*M* + H]$^+$.

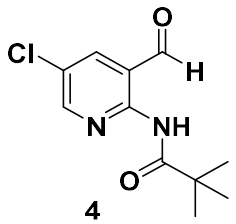

4

***N*-(5-Chloro-3-formylpyridin-2-yl)pivalamide (4):**[88] Compound **2** (582 mg, 2.73 mmol) was dissolved in dry THF (6.00 mL) under an Ar atmosphere and cooled to – 78 °C. Then *n*-BuLi (701 mg, 10.95 mmol, 6.84 mL from a 1.6 M solution in hexanes) was added and the reaction was stirred for 3 h at 0 °C then it was cooled again at – 78 °C and dry DMF (800 mg, 10.95 mmol, 0.84 mL) was added dropwise. The reaction was quenched by adding an excess of aq. $NH_4Cl_{(sat)}$ and extracted exhaustively with AcOEt, organic layers were dried over Na_2SO_4, filtered, concentrated under vacuum and the crude was purified by flash chromatography (SiO_2,eluent: Cyclohexane / AcOEt, 100:0 to 80:20, R_f = 0.30, in 80:20) to yield compound **4** (210 mg, 0.88 mmol, 33%) as a pale yellow solid. ^{1}H NMR ($CDCl_3$, 300 MHz) δ 1.37 (s, 9H), 8.02 (d, *J* = 2.6 Hz, 1H), 8.61 (d, *J* = 2.6 Hz, 1H), 9.89 (s, 1H), 10.63 (s, 1H); MS (ESI$^+$): *m/z* (%) 241.2 (100) [*M* + H]$^+$.

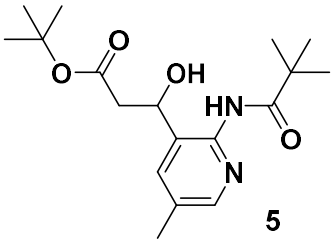

5

***tert*-Butyl 3-hydroxy-3-(5-methyl-2-pivalamidopyridin-3-yl)propanoate (5)**:[88] Diisopropylamine (797 mg, 7.88 mmol, 1.11 mL) was dissolved under an Ar atmosphere in dry Et_2O (3.00 mL) and the reaction mixture was cooled at – 78°C. *n*-BuLi (504 mg, 7.88 mmol, 4.92 mL from a 1.6 M solution in hexanes) was added and the reaction was stirred for 30 minutes then *t*-butylacetate (645 mg, 5.55 mmol, 0.74 mL) was added dropwise and the reaction mixture was stirred for another 30 minutes. Finally, compound **3** (434 mg, 1.97 mmol) was dissolved in dry THF (1.00 mL), added to the reaction mixture, and stirred for 1 h more until room temperature was reached. The mixture was stirred for 3 h extra to be quenched with an aq. solution of $NH_4Cl_{(sat)}$ (50 mL), extracted with AcOEt (4 x 80 mL), the organic layers were pooled and dried over $Na2_SO_4$, filtered and concentrated under vacuum. The crude was

purified by flash chromatography (Cyclohexane / AcOEt, 7:3 to 1:1, R_f = 0.27 in 1:1) to yield **5** (166 mg, 0.69 mmol, 35%) as a white solid. ^{1}H NMR (CD_3OD, 300 MHz): δ 1.34 (s, 9H), 2.38 (s, 3H), 2.65 (m, 1H), 5.17 (dd, *J* = 9.2 Hz, 4.2 Hz, 1H), 7.81 (d, *J* = 1.8 Hz, 1H), 8.19 (d, *J* = 1.8 Hz, 1H). MS (ESI$^+$): *m/z* (%) 337.3 (100) [*M* + H]$^+$.

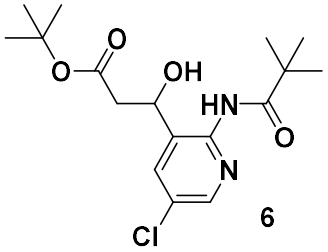

6

***tert*-Butyl 3-(5-chloro-2-pivalamidopyridin-3-yl)-3-hydroxypropanoate (6)**:[88] Diisopropylamine (521 mg, 5.15 mmol, 0.73 mL) was dissolved under an Ar atmosphere in dry Et_2O (4.00 mL) and the reaction mixture was cooled at – 78°C. *n*-BuLi (330 mg, 5.15 mmol, 3.22 mL from a 1.6 M solution in hexanes) was added and the reaction was stirred for 30 minutes then *t*-butylacetate (598 mg, 5.15 mmol, 0.69 mL) was added dropwise and the reaction stirred for another 30 minutes. Finally, compound **4** (310 mg, 1.29 mmol) was dissolved in dry THF (1.00 mL), added to the reaction mixture, and stirred for 1 h more until room temperature was reached. The mixture was stirred for 3 h extra to be quenched with an aq. solution of $NH_4Cl_{(sat)}$ (50 mL), extracted with AcOEt (2 x 80 mL), the organic layers were pooled and dried over Na_2SO_4, filtered and concentrated under vacuum. The crude was purified by flash chromatography (SiO_2, eluent: Cyclohexane / AcOEt, 90:10 to 70:30, R_f = 0.15 in 80:20) to yield compound **6** (268 mg, 0.75 mmol, 58%) as a a white solid. ^{1}H NMR ($CDCl_3$, 300 MHz): δ 1.34 (s, 9H), 2.71 (ddd, *J* = 16.5 Hz, 8.3 Hz, 8.3 Hz, 2H), 4.05 (d, *J* = 3.0 Hz, 1H), 5.03 (ddd, *J* = 8.3 Hz, 8.3 Hz, 3.0 Hz, 1H), 7.72 (d, *J* = 2.4 Hz, 1H), 8.34 (d, *J* = 2.4 Hz, 1H), 8.62 (s, 1H); MS (ESI$^+$): *m/z* (%) 301.2 (100) [*M* - C_4H_9]$^+$, 357.3 (80) [*M* + H]$^+$.

<u>General procedure for 8-azaquinolone formation</u>

The precursor was resuspended in HCl 5N (100-200 mg / mL) and the reaction was refluxed for 16 h. The reaction was cooled to room temperature and then K_2CO_3 was added to neutralize the solution, then the precipitated was filtered, washed with H_2O and dried over P_2O_5.

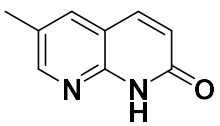

7

6-Methyl-1,8-naphthyridin-2(1H)-one (7):[88] Compound **5** (160 mg, 0.47 mmol) was treated by following the general procedure of 8-azaquinolone formation to yield **7** (46 mg, 0.28 mmol, 60%) as a

white solid. ^{1}H NMR (DMSO-d_6, 300 MHz): δ 2.33 (s, 3H), 6.53 (d, *J* = 9.7 Hz, 1H), 7.84 (d, *J* = 9.7 Hz, 1H), 7.90 (d, *J* = 1.9 Hz, 1H), 8.36 (d, *J* = 1.9 Hz, 1H), 12.04 (s, 1H); ^{13}C NMR (DMSO-d_6, 75 MHz): δ 17.2 (CH_3), 113.8 (C_q), 123.1 (CH), 127.2 (C_q), 136.0 (CH), 138.8 (CH), 147.9 (C_q), 150.8 (CH), 162.8 (C_q); MS (ESI$^+$): *m/z* (%) 161.2 (100) [*M* + H]$^+$; purity (HPLC): 100%.

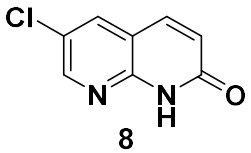

8

6-Chloro-1,8-naphthyridin-2(1H)-one (**8**)**:**[88] Compound **8**, was obtained from **6** (524 mg, 0.15 mmol) with a slight modification of general procedure for naphtyridine formation. Here, reaction was refluxed for 4 h and then stirred at room temperature for a total of 16 h to yield compound **8** (103 mg, 0.06 mmol, 39%) as a white solid. ^{1}H NMR (DMSO-d_6, 300 MHz): δ 6.63 (d, *J* = 9.5 Hz, 1H), 7.90 (d, *J* = 9.5 Hz, 1H), 8.30 (d, *J* = 2.4 Hz, 1H), 8.55 (d, *J* = 2.4 Hz), 12.33 (s, 1H);^{13}C NMR (DMSO-d_6, 75 MHz): δ 115.2 (C_q), 123.9 (CH), 124.4 (C_q), 135.7 (CH), 138.0 (CH), 148.3 (C_q), 148.5 (CH), 158.2 (C_q), 162.7 (C_q). MS (ESI$^+$): *m/z* (%) 181.2 (100) [*M* + H]$^+$; purity (HPLC): 95%.

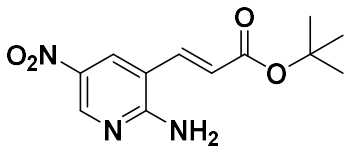

9

***Tert*-butyl (E)-3-(2-amino-5-nitropyridin-3-yl)acrylate (9)**:[230,231] 3-bromo-5-nitropyridin-2-amine (300 mg, 1.37 mmol) was dissolved in dry DMF (1.08 mL) under an Ar atmosphere together with *tert*-butyl acrylate (352 mg, 0.39 mL, 2.75 mmol), TEA (1.39 g, 1.91 mL, 13.76 mmol), $Pd(OAc)_2$ (30 mg, 0.14 mmol) and Tri(*o*-tolyl)phosphine (84 mg, 0.27 mmol) were added and the mixture was heated at 130 °C for 16 h. The reaction was filtered through a celite pack and concentrated under vacuum. The crude was resuspended in AcOEt (25 mL) and washed with H_2O (2 x 15 mL). The organic layers were pooled, dried over Na_2SO_4, filtered and concentrated under vacuum, and then purified by flash chromatography (SiO_2, eluent: Cyclohexane/ AcOEt, 4:1, R_f = 0.29) to yield compound **9** (161 mg, 0.60 mmol, 44%) as a yellow solid. ^{1}H NMR ($CDCl_3$, 300 MHz): δ 1.47 (s, 9H), 5.47 (s, 2H), 6.36 (d, *J* = 15.8 Hz, 1H), 8.32 (d, *J* = 2.5 Hz, 1H), 8.92 (d, *J* = 2.5 Hz, 1H); ^{13}C NMR ($CDCl_3$, 75 MHz): δ 27.1 (CH_3), 80.6 (C_q), 112.7 (C_q), 118.6 (C_q), 124.3 (CH), 129.9 (CH), 134.1 (CH), 145.8 (CH), 158.3 (C_q), 164.1 (C_q); MS (ESI$^+$): *m/z* (%) 210.2 (100) [*M* -C_4H_9]$^+$, (60) 266.2 [*M* + H]$^+$.

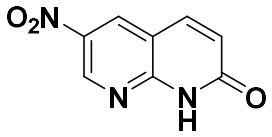

10

6-Nitro-1,8-naphthyridin-2(1H)-one (10):[230] Starting from **9** (510 mg, 1.92 mmol) and following the general procedure of naphtyridine formation, compound **10** (254 mg, 1.33 mmol, 69%) was obtained as a yellow solid. ^{1}H NMR (DMSO-d_6, 300 MHz): δ (ppm): 6.74 (d, J = 9.6 Hz, 1H), 8.13 (d, J = 9.6 Hz, 1H), 9.06 (d, J = 2.6 Hz, 1H), 9.30 (d, J = 2.6 Hz, 1H), 12.85 (s, 1H); ^{13}C NMR (DMSO-d_6, 75 MHz): δ 113.4 (C_q), 124.9 (CH), 132.0 (CH), 138.9 (C_q), 139.2 (CH), 146.0 (CH), 152.9 (C_q), 163.0 (C_q); MS (ESI$^+$): *m/z* (%) 192.1 (100) [*M* + H]$^+$; purity (HPLC): 96%; Elem analysis anal. calcd. for $C_8H_5N_3O_3$ (191.0): C, 50.27; H, 2.64; N, 21.98; found: C, 50.61; H, 2.71; N, 20.24.

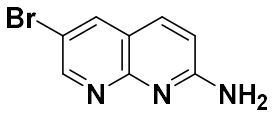

11

6-Bromo-1,8-naphthyridin-2-amine (11):[232] 2,6 diamino pyridine (2.0 g, 18 mmol) and 2-bromonalonaldehyde (2.7 g, 18 mmol) were dissolved H_3PO_4 (38 mL). The mixture was heated for 4 h at 160 °C, cooled to room temperature and stirred overnight. The reaction mixture was neutralized using NaOH pearls and extracted with AcOEt (5 x 100 mL). The organic layers were dried over Na_2SO_4, filtered and concentrated under vacuum. The crude was purified by flash chromatography (SiO_2, eluent: DCM / MeOH, 100:0 to 95:5, R_f = 0.3 in 95:5) to yield **11** (1.2, 5.2 mmol, 29%) as a pale yellow solid. ^{1}H NMR (DMSO-d_6, 300 MHz), δ (ppm): 6.84 (d, J = 8.8 Hz, 1H), 7.03 (s, 2H), 7.91 (d, J = 8.8 Hz, 1H), 8.88 (d, J = 2.6 Hz, 1H), 8.69 (d, J = 2.6 Hz, 1H); ^{13}C NMR (DMSO-d_6,75 MHz): δ 111.5 (C_q), 114.9 (C_2), 118.5 (C_q), 137.4 (CH), 138.1 (CH), 152.4 (CH), 155.7 (C_q), 161.9 (C_q); MS (ESI$^+$): *m/z* (%) 224.1 (100) [*M* + H]$^+$; purity (HPLC) : 95%.

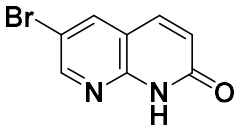

12

6-Bromo-1,8-naphthyridin-2(1H)-one, (12): Compound **11** (962 mg, 4.29 mmol) was dissolved in aq HCl (2M, 100 mL) and the reaction was cooled to 0 °C. Then, aq. $NaNO_2$ (2.9 g, 54 mL, 42.93 mmol,) was added dropwise and then the mixture was stirred overnight at room temperature. After 16 h, the aqueous solution was neutralized with aq. NaOH (1 M) and extracted with AcOEt (3 x 100 mL). The crude was purified by flash chromatography (SiO_2, eluent: DCM / MeOH, 99:1 DCM: EtOH, R_f = 0.1) to yield **12** (603 mg, 2.65 mmol, 62%) as a white solid. ^{1}H NMR (DMSO-d_6, 300 MHz): δ 6.62 (d, J = 9.5 Hz, 1H), 7.88 (d, J = 9.5 Hz, 1H), 8.40 (d, J = 2.1 Hz, 1H), 8.59 (d, J = 2.1 Hz, 1H), 12.34 (s, 1H); ^{13}C NMR

(DMSO-d_6, 300 MHz): δ 112.1 (C_q), 115.8 (CH), 124.3 (C_q), 138.1 (CH, 2C), 148.6 (CH), 150.6 (C_q), 162.7 (C_q); MS (ESI^+): *m/z* (%) 225.1 (100) $[M + H]^+$; purity (HPLC): 95%; HRMS (TOF ESI^+): calcd for $C_8H_6BrN_2O$ $[M + H]^+$: 224.9664, found: 224.9657.

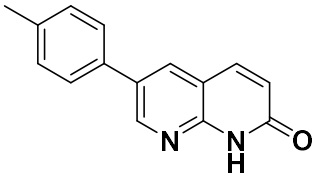

13

6-(*p*-Tolyl)-1,8-naphthyridin-2(1H)-one, (**13**): Compound **12** (310 mg, 1.39 mmol) was dissolved in H_2O (3.6 mL) and dioxane (0.74 mL) together with K_2CO_3 (2.28 g, 16.54 mmol), TBAF (576 mg, 2.20 mmol), 4-tolylboronic acid (375, 2.76 mmol) and $Pd(PPh_3)_4$ (279 mg, 0.13 mmol) . The mixture was heated for 16 h at 120 °C. The solvent was removed under reduced pressure and the crude was purified by flash chromatography (SiO_2, eluent: DCM / MeOH, 99:1 DCM/EtOH, R_f = 0.4) to yield **13** (267 mg, 1.14 mmol, 82%) as a pale yellow solid. ^1H NMR ($CDCl_3$, 300 MHz): δ 2.36 (s, 3H), 6.60 (d, *J* = 9.5 Hz, 1H), 7.31 (d, *J* = 8.1 Hz, 1H), 7.64 (d, *J* = 8.1 Hz, 1H), 7.97 (d, *J* = 2.3 Hz, 1H), 8.40 (d, *J* = 2.3, 1H), 8.81 (s, 1H), 12.27 (s,1H); ^{13}C NMR ($CDCl_3$, 75 MHz: δ 21.1 (CH_3), 114.1 (CH), 123.4 (C_q), 126.4 (C_q), 130.2 (C_q), 130.6 (CH), 133.6 (C_q), 133.7 (CH), 137.2 (CH), 139.1 (C_q), 148.5 (C_q), 148.7 (CH), 162.8 (C_q); MS (ESI^+): *m/z* (%) 237.3 (100) $[M + H]^+$; purity (HPLC): 100%; Elem analysis anal. calcd. (%) for $C_{15}H_{12}N_2O$ (236.2): C, 76.25; H, 5.12; N, 11.86; found: C, 75.88; H, 5.02; N, 11.15.

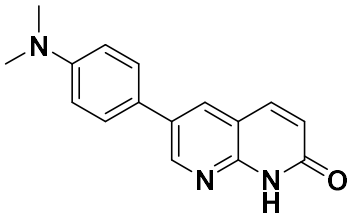

14

6-(4-(Dimethylamino)phenyl)-1,8-naphthyridin-2(1H)-one (14): Compound **12** (167 mg, 0.74 mmol) was dissolved in dioxane (5 mL), then $Pd(dppf)Cl_2$ (54 mg, 0.07 mmol) and aqueous solution of Cs_2CO_3 (1.86 mmol, 606 mg, 980 μL) together with 4-(dimethylamino)benzen-boronic acid (184 mg, 1.12 mmol) were added. The reaction was heated at 100 °C for 18 h. The solvent was removed and the crude was purified by flash chromatography (SiO_2, eluent: DCM / EtOH, 100:0 to 98:2, R_f = 0.13 in 98:2) to yield **14** (117 mg, 0.44 mmol, 59%) as a yellow solid. ^1H NMR (DMSO-d_6, 300 MHz): δ 2.95 (s, 6H), 6.58 (d, *J* = 9.5 Hz, 1H), 6.83 (d, *J* = 8.8 Hz, 2H), 7.60 (d, *J* = 8.8 Hz, 2H), 7.95 (d, *J* = 9.5 Hz, 1H), 8.30 (d, *J* = 2.4 Hz, 1H), 8.78 (d, *J* = 2.4 Hz, 1H), 12.13 (s, 1H;. ^{13}C NMR (DMSO-d_6,75 MHz): δ 40.3 (CH_3), 113.2 (CH), 114.6 (C_q), 123.7 (CH), 124.3 (C_q), 127.52 (CH), 131.1 (C_q), 132.79 (CH), 139.6 (CH), 148.37 (CH),

148.6 (C_q), 150.5 (C_q), 163.3 (C_q); MS (ESI^+): *m/z* (%) 266.2 (100), $[M + H]^+$; purity (HPLC): 95%; Elem. anal. calcd. for $C_{16}H_{15}N_3O$ (265.3): C, 72.43; H, 5.70; N, 15.84; found: C, 72.12; H, 5.61; N, 15.45.

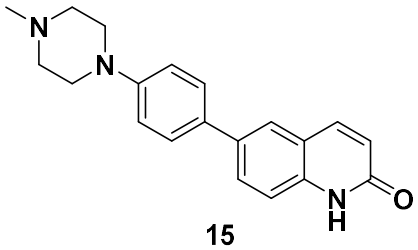

15

6-(4-(4-Methylpiperazin-1-yl)phenyl)quinolin-2(1H)-one (15): Compound **12** (150 mg, 0.67 mmol) was dissolved in dioxane (5 mL) together with of $Pd(dppf)Cl_2$ (24 mg, 0.03 mmol) , an aqueous solution of Cs_2CO_3 (543 mg, 1.66 mmol, 606 μL) and 4-(4-Methylpiperazin-1-yl)phenylboronic acid (147 mg, 0.67 mmol). The reaction was heated at 100 °C for 18 h. Then, poured in a mixture of DCM / MeOH (300 mL, 1:1) and filtered through a bed of celite. The solvent was removed by vacuum, re dissolved in DCM (250 mL), washed with NaOH aq (pH 9, 1 x 50 mL), the organic layer was dried over Na_2SO_4, filtered and concentrated under vacuum to finally be purified by flash cromatography (SiO_2, eluent: DCM / EtOH, 9:1, R_f = 0.15) to yield compound **15** (147 mg, 0.46 mmol, 69%) as a yellow solid. ^1H NMR (D_2O + DCl 0.01 M, 300 MHz): δ 2.89 (m, 5H), 3.10 (m, 2H), 3.59 (m, 4H), 6.37 (d, *J* = 9.4 Hz, 1H), 6.47 (d, *J* = 8.2 Hz, 2H), 6.75 (d, *J* = 8.2 Hz, 2H), 7.47 (d, *J* = 9.4 Hz, 1H), 7.60 (s, 1H), 7.98 (s, 1H); ^{13}C NMR (D_2O + DCl 0.01 M, 75 MHz): δ 42.7 (CH_3), 45.2 (CH_2), 52.7 (CH_2), 115.7 (CH), 121.8 (CH), 125.1 (C_q), 125.9 (CH), 129.8 (CH), 133.4 (CH), 135.2 (CH), 140.1 (C_q),143.7 (C_q), 143.9 (CH), 147.9 (C_q), 163.9 (C_q); MS (ESI^+): *m/z* (%) 321.4 (100) $[M + H]^+$; purity (HPLC): 97%; HRMS (TOF ES^+): calcd for $C_{19}H_{21}N_4O$ $[M + H]^+$: 321.1715, found: 321.1726.

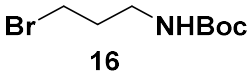

16

***tert*-Butyl (3-bromopropyl)carbamate (16):**[233] Under an Ar atmosphere, 3-bromopropylamine hydrobromide (5.1 g, 23.0 mmol) and $(Boc)_2O$ (5.1 g, 23 mmol) were dissolved in dry DCM (30.0 mL) and the reaction was cooled to 0 °C. Then TEA (2.8 g, 3.8 mL, 27.8 mmol) dissolved in dry DCM (30 mL) were added dropwise and the reaction mixture was stirred at room temperature for 48 h. The reaction was washed with aq. HCl 5% (1 x 20 mL), H_2O (1 x 30 mL), dried over Na_2SO_4, filtered and concentrated under vacuum. Compound **16** (5.2 g, 21.6 mmol, 93%) was obtained as a viscous liquid. ^1H NMR ($CDCl_3$, 300 MHz): δ 1.44 (s, 9H), 2.05 (m, 2H), 3.28 (q, *J* = 6.3 Hz, 2H), 3.44 (t, *J* = 6.50 Hz, 2H), 4.66 (s, 1H).

General procedure for N^9 alkylation of 6-chloro-9H-purin-2-amine

6-chloro-9H-purin-2-amine was dissolved in of dry DMF (250 mg /mL) with Cs_2CO_3 (1.5 to 2 eq.) and the bromoalkylating agent (1.2 eq.). The reaction was stirred for 16-24 h at room temperature. The solvent was removed under vacuum and purified by flash chromatography.

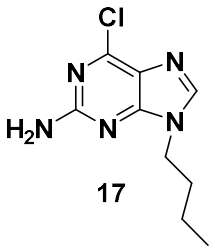

17

9-Butyl-6-chloro-9H-purin-2-amine (17):[234,235]Compound **17** was obtained by following the general procedure of N^9 alkylation starting 6-chloro-9H-purin-2-amine (500 mg, 2.95 mmol) and *n*-bromobutane (485 mg, 3.54 mmol). The crude was purified by flash chromatography (SiO_2, eluent: Cyclohexane : AcOEt, 60:40, R_f = 0.14) to yield compound **17** (407 mg, 1.79 mmol, 61%) as a white solid. ^{1}H NMR ($CDCl_3$, 300 MHz): δ 0.96 (t, *J* = 7.3 Hz, 3H), 1.33 (dq, *J* = 14.9 Hz, *J* = 7.3 Hz, 2H), 1.84 (dt, *J* = 14.9 Hz, *J* = 7.2 Hz, 2H), 4.08 (t, *J* = 7.2 Hz, 2H), 5.23 (s, 2H), 7.77 (s, 1H); ^{13}C NMR ($CDCl_3$, 75 MHz): δ 13.2 (CH_3), 19.9 (CH_2), 31.2 (CH_2), 43.7 (CH_2), 125.4 (C_q), 142.4 (CH), 151.3 (C_q), 153.9 (C_q), 159.1 (C_q); MS (ESI$^+$): *m/z* (%) 226.2 (100) [*M* + H]$^+$.

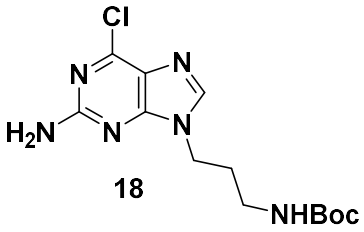

18

***tert*-Butyl (3-(2-amino-6-oxo-1,6-dihydro-9H-purin-9-yl)propyl)carbamate (18):** Starting from 6-chloro-9H-purin-2-amine (519 mg, 3.06 mmol) and **17** (874 mg, 3.67 mmol), compound **18** was obtained by following the N^9 alkylation protocol. The crude was purified by flash chromatography (SiO_2, eluent: DCM /EtOH, 98:2, R_f = 0.1) to yield the product **18** (307 mg, 1.14 mmol, 31%) as a white foamy solid. ^{1}H NMR ($CDCl_3$, 300 MHz): δ 1.5 (s, 9H), 2.03 (m, 2H), 3.14 (m, 2H), 4.16 (t, *J* = 6.57 Hz, 2H), 5.14 (bp, 3H), 7.83 (s, 1H); ^{13}C NMR ($CDCl_3$, 75 MHz): δ 28.4 (CH_3), 30.3 (CH_2), 37.3 (CH_2), 41.0 (CH_2), 80.2 (C_q), 125.3 (C_q), 142.4 (CH), 153.9 (C_q), 153.9 (C_q), 156.0 (C_q), 159.0 (C_q); MS (ESI$^+$): *m/z* (%) 327.3 (15) [*M* + H]$^+$, 271.2 (100) [*M* - C_4H_9]$^+$;Elem. anal. calcd. for $C_{13}H_{19}ClN_6O_2$ (326.1): C, 47.78; H, 5.86; N, 25.72; found: C, 47.3; H, 5.71, N, 25.01.

General procedure for chloroguanine hydrolysis[94]

200 mg of 2-amino 6-chloroguanine was resuspended in a H_2O / dioxane (1:1 mixture, 100 mg/mL) and then DABCO (1 eq.) and K_2CO_3 (1.2 eq) were added to the mixture. The reaction was refluxed for 2 – 5 h. The solvent mixture was removed under vacuum and the crude is purified by flash chromatography.

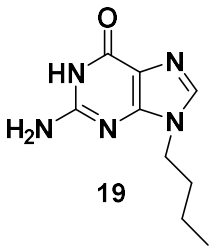

19

2-Amino-9-butyl-1,9-dihydro-6H-purin-6-one, (19):[234] Starting from compound **17** (179 mg, 0.79 mmol) and following the general procedure for 2-amino 6-chloroguanine hydrolysis, the crude was purified by flash chromatography (SiO_2, eluent: DCM / MeOH, 95:5 DCM:MeOH , R_f = 0.26) to yield compound **19** (110 mg, 0.53 mmol, 67%) as a white sticky solid. ^{1}H NMR (DMSO-d_6, 300 MHz): δ (ppm): 0.88 (t, *J* = 7.3 Hz, 3H), 1.23 (dt, *J* = 7.6 Hz, 7.3 Hz, 2H), 1.69 (m, 2H), 3.92 (t, *J* = 7.1 Hz, 2H), 6.42 (s, 1H), 7.67(s, 1H), 10.51 (s, 1H); ^{13}C NMR (DMSO-d_6, 75 MHz): δ 13.42 (CH_3), 19.2 (CH_2), 31.8 (CH_2), 42.3 (CH_2), 113.7 (C_q), 137.4 (CH), 151.1 (C_q); 153.4 (C_q), 156.8 (C_q), 158.6 (C_q); MS (ESI$^+$): *m/z* (%) 208.3 (100) [*M* + H]$^+$; purity (HPLC): 96%.

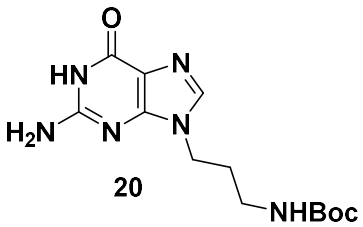

20

***tert*-Butyl (3-(2-amino-6-oxo-1,6-dihydro-9H-purin-9-yl)propyl)carbamate (20):** Starting from compound **18** (5.19 mg, 3.0 mmol) compound **19** was obtained following the general procedure for chloroguanine hydrolysis. The crude was purified by flash chromatography (SiO_2, eluent: DCM / MeOH, 100:0 to 93:7, R_f = 0.12 in 92:8) to yield compound **20** (139 mg, 2.0 mmol, 67%) as a white solid. ^{1}H NMR (DMSO-d_6, 300 MHz): δ 1.38 (s, 9H), 1.81 (m, 2H), 2.91 (m, 2H), 3.93 (t, *J* = 6.6 Hz, 2H), 6.44 (s, 2H), 6.91 (m, 1H), 7.69 (s, 1H), 10.54 (s, 1H); ^{13}C NMR (DMSO-d_6, 75 MHz): δ 28.7 (CH_3), 30.4 (CH_2), 37.6 (CH_2), 40.5 (CH_2), 78.1 (C_q), 117.1 (C_q), 137.9 (CH), 151.5 (C_q), 156.1 (C_q), 157.2 (C_q); MS (ESI$^+$): *m/z* (%) 309.3 [*M* + H]$^+$ (40), 253.2 (100) [*M* - C_4H_9]$^+$; purity (HPLC): 100%.

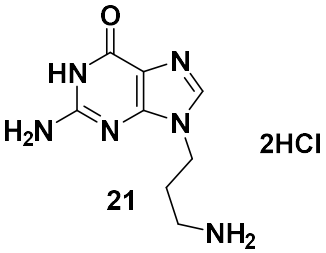

21

2-Amino-9-(3-(chloro-l5-azanyl)propyl)-1,9-dihydro-6H-purin-6-one, (21): Under an Ar atmosphere, compound **20** (64 mg, 0.2 mmol) was resuspended in dry dioxane (3 mL) at 0 °C and then HCl 4M in dioxane (2.0 mmol, 1 mL) was added. The reaction was stirred for 4 h at room temperature, then the solvent was removed and the white solid was washed with DCM (3 x 5 mL) to yield compound **21** (47 mg, 0.18 mmol, 92%) as a white solid ^{1}H NMR (D_2O, 300 MHz): δ 2.28 (t, J = 7.4 Hz, 2H), 3.08 (dt, *J* = 7.4 Hz, 6.8 Hz, 2H), 4.35 (t, *J* = 6.85 Hz, 2H), 8.85 (s, 1H). ^{13}C NMR (D_2O, 75 MHz): δ 26.6 (CH_2), 36.4 (CH_2), 42.1 (CH_2), 108.3 (C_q), 137.5 (CH), 150.2 (C_q), 155.3 (C_q), 155.4 (C_q). MS (ESI$^+$): *m/z* (%) 209.2 (100) [*M* - Cl]$^+$, purity (HPLC): 95% . Elem. anal. calcd. for $C_8H_{12}N_6O$ x 2.5 HCl (298.0): C, 32.10; H, 4.88; N, 28.07; found: C, 31.67; H, 4.87; N, 27.99.

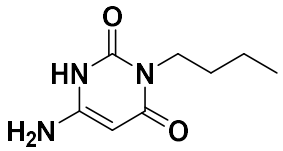

21

6-Amino-3-butylpyrimidine-2,4(1H,3H)-dione (21):[95,236] Under an Ar atmosphere, 6-aminouracil (482 mg, 3.79 mmol), was resuspended with HDMS (1.00 g, 6.44 mmol, 1.37 mL) and $(NH_4)_2SO_4$ (15.0 mg, 0.11 mmol). The reaction was heated at 200 °C until a clear solution was obtained, then cooled to 60 °C under an Ar stream where *n*-bromobutane (883.3 mg, 6.44 mmol, 0.69 mL) and I_2 (5.0 mg, 0.02 mmol) were additioned. The reaction was heated at 90 °C for 16 h and then cooled to room temperature. An excess of an aqueous solution of $NaHCO_{3(sat)}$ was added to the mixture. The solid was filtered and purified by flash chromatography (SiO_2, eluent: DCM / MeOH, 95:5, R_f = 0.20). Compound **21** (115 mg, 0.68 mmol, 18%) was obtained as a yellow solid. ^{1}H NMR (DMSO-d_6, 300 MHz): δ 0.84 (t, J = 7.30 Hz, 3H), 1.24 (ddd, *J* = 7.6 Hz, 7.4 Hz, 7.3 Hz, 2H), 1.42 (dt, *J* = 7.4 Hz, 7.3 Hz, 2H), 3.6 (t, *J* = 7.3 Hz, 2H), 4.53 (s, 1H), 6.15 (s, 2H), 10.29 (s, 1H); ^{13}C NMR (DMSO-d_6, 75 MHz) : δ 13.7 (CH_3), 19.6 (CH_2), 29.8 (CH_2), 38.9 (CH_2), 74.1 (CH), 150.9 (C_q), 153.5 (C_q), 162.9 (C_q);MS (ESI$^+$): *m/z* (%) 184.2 (100) [*M* + H]$^+$; purity (HPLC): 100%

7.1.2 O^6BG Acr hybrids

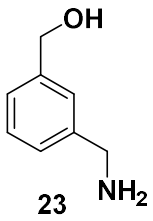

23

(3-(Aminomethyl)phenyl)methanol (23):[37] In a two-neck round flask under an Ar atmosphere, 3-cyanobenzoic acid (10.0 g, 67.9 mmol) was suspended in dry THF (50 mL) while cooling at 0 °C. THF•BH_3 complex (1 M in THF, 200.0 mmol, 200 mL) were added dropwise and the reaction was stirred for 24 h at room temperature. The mixture was neutralized with a mixture of concentrated HCl (37 %) and H_2O (1:1, 100 mL). The THF was removed under vacuum and then NaOH pellets were carefully added until pH 12 was reached.The aqueous phase was extracted with Et_2O (11 × 200 mL); the organic layers were dried over Na_2SO_4, filtered and concentrated under vacuum. The amino alcohol **24** (9.1 g, 66.3 mmol, 98%) was obtained as a white solid and immediately stored under Ar at –20 °C. ^{1}H NMR ($CDCl_3$, 300 MHz): δ 2.45 (s, 3H), 3.77 (s, 2H), 4.59 (s, 2H), 7.14–7.31 (m, 4H).

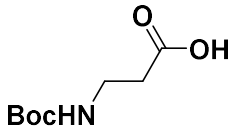

24

3-((*tert*-Butoxycarbonyl)amino)propanoic acid (24):[168] 2.00 g (22.45 mmol) of β-Alanine (2.0 g, 22.4 mmol) was dissolved in aq. NaOH (2M, 20 mL) and then cooled to 0 °C. Then, a $(Boc)_2O$ solution (2.38 g, 24.65 mmol) dissolved in THF (20 mL) was added dropwise and then the reaction was stirred at room temperature for 24 h. The THF was removed, the mixture was dissolved in DCM (50 mL) and then acidified with aq. HCl (5 %) up to pH 2. The aqueous phase was extracted with AcOEt (5 x 60 mL), the organic layer were pooled, dried over Na_2SO_4, filtered and concentrated under vacuum to yield compound **24** (4.10 g, 21.77 mmol, 97%) as a transparent sticky oil that solidifies to a white solid upon cooling were obtained. ^{1}H NMR ($CDCl_3$, 300 MHz): δ 1.43 (s, 9H), 2.55 (s, 2H), 3.37 (s, 2H), 5.13 (s, 0.65 H), 6.31 (s, 0.35), 10.67 (s, 1H); MS (ESI^+): m/z (%) 212 (5) [*M* + Na]$^+$ (5), 116 (100) [*M* - C_4H_9O]$^+$.

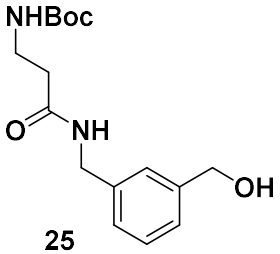

25

***tert*-Butyl (3-((3-(hydroxymethyl)benzyl)amino)-3-oxopropyl)carbamate, (25):** Under an Ar atmosphere, compound **23** (321 mg, 1.69 mmol) was dissolved in dry DCM (6 mL), together with DIPEA

(5.06 mmol, 621 mg, 837 μL), HOBt (229 mg , 1.69 mmol), EDCI.HCl (325 mg, 1.69 mmol) and 4-DMAP (10 mg, 0.09 mmol) at 0 °C and the reaction was stirred for 30 minutes. Then, compound **24** (233 mg, 1.69 mmol) dissolved in dry DCM (2 mL) and the mixture was stirred at room temperature for 72 h. The reaction was poured in DCM (30 mL) washed with aq. NaOH (1M, 1 x 15 mL), aq. HCl 5% (1 x 15 mL) and H_2O (1 x 15 mL). The organic layer was dried over Na_2SO_4, filtered and concentrated under vacuum. The crude was purified by flash chromatography (SiO_2, eluent: Cyclohexane / AcOEt, 50:50 to 20:80 gradient, R_f = 0.1 in 30:70) to yield compound **25** (370 mg, 1.19 mmol, 70%) as a sticky solid .^{1}H NMR ($CDCl_3$, 300 MHz): δ 1.41 (s, 9H), 2.41 (t, *J* = 5.9 Hz, 2H), 3.38 (dd, *J* = 6.4, 5.9 Hz, 2H), 4.40 (d, *J* = 5.7 Hz, 2H), 4.66 (s, 1H), 5.22 (s, 1H), 6.29 (s, 1H), 7.16-7.33 (m, 4H);^{13}C NMR ($CDCl_3$, 75 MHz): δ 28.3 (CH_3), 36.3 (CH_2), 36.7 (CH_2), 43.4 (CH_2), 64.9 (CH_2), 80.1 (C_q), 126.0 (CH, 2C), 126.1 (CH), 126.8 (CH), 138.4 (C_q), 141.0 (C_q), 152.2 (C_q), 171.4 (C_q); MS (ESI$^+$): *m/z* (%) 309 (50) $[M + H]^+$, 253 (100) $[M - C_4H_9]^+$.

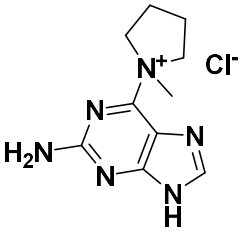

26

1-(2-Amino-9H-purin-6-yl)-1-methylpyrrolidin-1-ium chloride, 26:[37] Under an Ar atmosphere, 2-amino-6-chlorpurine (1.0 g, 5.89 mmol) of was re suspended in dry DMF (30 mL) and heated for 2 h at 50 °C to dissolve the reagent. Upon cooling to room temperature, 1-methylpyrrolidine (1.15 g, 13.47 mmol, 1.4 mL) was added and the mixture was stirred for 18 h. Then, cold acetone (2 mL) was added and the precipitate was filtered, washed with Et_2O (2 × 20 mL) and dried in vacuum to obtain **26** (791 mg, 3.10 mmol, 53%) as a white solid. ^{1}H NMR (DMSO-d_6, 300 MHz): δ 2.05 (m, 2H), 2.12 (m, 2H), 3.65 (s, 3H), 3.98 (m, 2H), 4.60 (m, 2H), 7.12 (s, 2H), 8.35 (s, 1H), 13.48 (br s, 1H); ^{13}C NMR (DMSO-d_6, 75 MHz): δ 21.4 (CH_2), 51.5 (CH_3), 64.0 (CH_2), 116.0 (C_q), 142.9 (CH),151.6 (C_q),158.6 (C_q), 159.0 (C_q); MS (ESI$^+$) *m/z* (%) 219.2 (100) $[M - Cl]^+$.

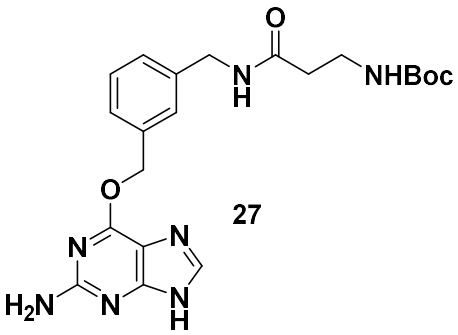

27

***tert*-Butyl (3-((3-(((2-amino-9H-purin-6-yl)oxy)methyl)benzyl)amino)-3-oxopropyl)carbamate (27):** compound **25** (420 mg, 1.36 mmol) and *t*-BuOK (302 mg, 2.70 mmol) were resuspended in dry DMF (20 mL) under an Ar atmosphere, and the mixture was stirred at room temperature for 30 minutes.

Compound **26** (230 mg, 0.90 mmol) was added and the mixture was stirred for 5 h at room temperature. One drop of aq.HCl 5% was added and then PBS (5 mL, pH 7.24) was added. The solvents were removed and the crude was purified by flash chromatography (SiO_2, eluent: DCM / MeOH, 93:7, R_f = 0.2) to yield compound **27** (66 mg, 0.20 mmol, 15%). ^{1}H NMR (CD_3OD, 300 MHz): δ 1.49 (s, 9H), 2.32 (m, 2H), 3.20 (m, 2H), 4.28 (m, 2H), 5.54 (s, 2H), 6.48 (m, 0.5 H), 7.14-7.35 (m, 4H), 7.74 (s, 1H), 8.34 (m, 0.5 H); MS (ESI$^+$): *m/z* (%) 442.1 (10) [*M* + H]$^+$, 342.2 (100) [*M* - $C_5H_9O_2$]$^+$.

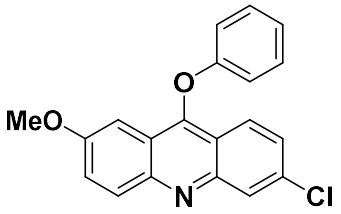

28

6-Chloro-2-methoxy-9-phenoxyacridine, **28**.[170]: PhOH (10 g, 106.3 mmol) was placed together NaOH (400 mg, 10.0 mmol) and 6,9-dichloro-2-methoxyacridine. (2 g, 7.2 mmol). The mixture was heated up to 120 °C for 2 h and then poured into an aq NaOH solution (2M, 50 mL). The aqueous phase was washed with DCM (3 x 40 mL), the organic layers were pooled and dried over Na_2SO_4, filtered and concentrated under vacuum. The crude was recrystallized from MeOH to yield **28** (960 mg, 2.9 mmol, 41%) as yellow needles ^{1}H NMR ($CDCl_3$, 300 MHz): δ 3.80 (s, 3H), 6.85 (d, *J* = 7.8, 2H), 7.06 (m, 1H), 7.15 (d, *J* = 2.7 Hz, 1H), 7.28 (m, 2H), 7.36 (dd, *J* = 9.2, 1.9 Hz, 1H), 7.47 (dd, *J* = 9.5, 2.7 Hz, 1H), 7.97 (d, *J* = 9.2, 1H), 8.11 (d, *J* = 9.5, 1H), 8.22 (d, *J* = 1.9 Hz, 1H). ^{13}C NMR ($CDCl_3$, 75 MHz): δ 55.5 (CH_3), 97.7 (CH_2), 115.6 (CH_2, 2C), 118.8 (C_q), 121.2 (CH), 122.8 (CH), 123.8 (C_q), 126.5 (CH), 127.3 (CH), 128.2 (CH), 130.0 (CH_2, 2C), 131.3 (CH), 135.4 (C_q), 148.5 (C_q), 148.6(C_q), 153.5 (C_q), 157.5 (C_q), 159.0 (C_q). MS (ESI$^+$): *m/z* (%): 336.2 (100) [*M* + H]$^+$.

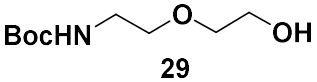

29

***tert*-Butyl (2-(2-hydroxyethoxy)ethyl)carbamate (29):**[172] 2-(2-aminoethoxy)ethan-1-ol (2.34 g, 22.26 mmol, 2.23 mL) was slowly dissolved AcOEt (10 mL) while keeping the reaction at 0 °C. In small portions, $(Boc)_2O$ (5.84 g, 26.76 mmol) was added and the reaction was stirred for 16 h at room temperature. The crude was diluted in AcOEt (50 mL), washed with aq. HCl 5% (1 x 30 mL) and H_2O (1 x 30 mL). The organic layer was dried over Na_2SO_4, filtered and concentrated. Compound **29** (3.91 g, 19.14 mmol, 86%) was obtained as a transparent oil were obtained. ^{1}H NMR ($CDCl_3$, 300 MHz): δ 1.45 (s, 9H), 2.34 (s, 1H), 3.32-3.36 (m, 2H), 3.54-3.59 (m, 4H), 3.73-3.76 (m, 2H), 4.99 (s, 1H); ^{13}C NMR ($CDCl_3$, 75 MHz): δ 28.4 (CH_3,), 40.3 (CH_2), 61.7 (CH_2), 70.3 (CH_2), 72.2 (CH_2), 79.4 (C_q), 156.1 (C_q); MS (ESI$^+$): *m/z* (%) 228.13 (50) [*M* + H]$^+$.

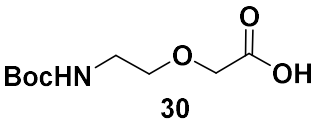

30

2-(2-(*tert*-Butoxycarbonyl)amino)ethoxy)acetic acid (30):[172] In a MeCN / H_2O mixture (5:1, 24 mL) compound **29** (1.05 g, 5.11 mmol) was dissolved and the reaction was cooled to 0 °C. In small portions, TEMPO (0.16 g, 1.02 mmol) and BAIB (3.58 g, 12.34 mmol) were added and the mixture was stirred then at room temperature for 24 h. After checking the disappearance of the starting material, $NH_4Cl_{(sat)}$ (20 mL) was added, and the mixture was extracted with AcOEt (4 x 80 mL). The organic layers were pooled, dried over Na_2SO_4, filtered and concentrated under vacuum. The crude was purified by silica flash chromatography (SiO_2, eluent: DCM /MeOH, 95:5 with 30 drops of HAc per liter of eluent, R_f = 0.2) to yield compound **36** (0.43 g 1.99 mmol, 39%) as a yellow oil. ^{1}H NMR ($CDCl_3$, 300 MHz): 1.45 (s, 9H), 3.35 (m, 2H), 3.63 (m, 2H), 4.14 (s, 2H), 5.12 (bp, 1H).

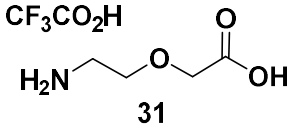

31

2-(2-((2,2,2-Trifluoroacetyl)-l4-azanyl)ethoxy)acetic acid (31): [172] In DCM (2 mL), compound **30** (294 mg, 1.34 mmol) were dissolved at 0 °C and TFA (1.5 g, 13.46 mmol, 439 μL) was added. The reaction was stirred at room temperature for 3 h. The solvent were removed under reduced pressure and the crude was washed with cold Et_2O (4 x 5 mL) to yield compound **31** (264 mg, 1.13 mmol, 84%) as a sticky oil was obtained.^{1}H NMR (CD_3OD, 300 MHz): δ: 3.16 (t, *J* = 5.0 Hz, 2H), 3.72 (t, *J* = 5.0 Hz, 2H), 4.14 (s, 2H); MS (ESI$^+$): *m/z* (%) 120.1 (100) [*M* - $C_2HO_2F_3$]$^+$.

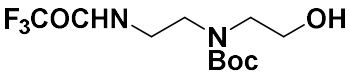

32

***tert*-Butyl (2-hydroxyethyl)(2-(2,2,2-trifluoroacetamido)ethyl)carbamate (32):** Under an Ar atmosphere, 2-((2-aminoethyl)amino)ethan-1-ol (566 mg, 5.43 mmol, 550 μL) was dissolved in dry MeOH (2 mL) and the mixture was cooled to 0 °C then, ethyl trifluoroacetate (772 mg, 5.44 mmol, 648 μL) was added dropwise. The mixture was stirred at 0 °C for 30 minutes until the disappearance of the starting material as judged by TLC using nynhidrine as staining agent. Finally, $(Boc)_2O$ (2.37 g, 6.50 mmol) dissolved in dry MeOH (1 mL) was added and the reaction was stirred for another 25 minutes at 0 °C. After the disappearance of the intermediate, the MeOH was removed and the crude was purified by flash chromatography (SiO_2, eluent: Cyclohexane / AcOEt, 7:3, R_f = 0.18) to yield compound **32** (1.55 g, 5.16 mmol, 95%) as a clear sticky oil. ^{1}H NMR ($CDCl_3$, 300 MHz): δ 1.46 (s, 1H), 3.16-3.70 (m, 8H), 7.86-8.10 (bp, 1H). Mixture of conformers ^{13}C NMR ($CDCl_3$, 75 MHz) δ: 28.0 (CH_3), 38.9 (CH_2), 40.7 (CH_2), 47.2 (CH_2), 51.2 (CH_2), 51.4 (CH_2), 61.0 (CH_2), 61.7 (CH_2), 80.0 (C_q), 81.2 (C_q), 106.8 (C_q),

114.0 (C_q), 117.8 (C_q), 119.7 (C_q), 148.1 (C_q), 148.2 (C_q), 151.4 (C_q); ^{1}H NMR (DMSO-d_6, 300 MHz): δ 1.38 (s, 9H), 3.18-3.19 (m, 2H), 3.32 (s, 4H), 3.45-3.47 (m, 2H), 4.73 (d, J = 3.6 Hz, 1H), 9.44 (m, 2H); ^{13}C NMR (DMSO-d_6, 75 MHz): δ 28.4 (CH_3), 38.2 (CH_2), 38.4 (CH_2), 46.5 (CH_2), 46.7 (CH), 49.7 (CH), 50.2 (CH), 79.15 (C_q), 118.3 (C_q, J = 154.3 Hz), 156.1 (C_q), 157.1 (C_q, J = 33.6 Hz); MS (ESI$^+$): *m/z* (%) 323.3 (10) [*M* + Na]$^+$, 201.1 (100) [*M* - $C_5H_9O_2$]$^+$.

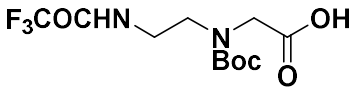

33

***N*-(*tert*-Butoxycarbonyl)-*N*-(2-(2,2,2-trifluoroacetamido)ethyl)gly, (33):** In a mixture of MeCN / H_2O (5:1, 18 mL), compound **32** (800 mg, 2.66 mmol) was dissolved and the reaction was cooled to 0 °C. Then, BAIB (2.32 g, 7.99 mmol) and TEMPO (83 mg, 0.53 mmol) were added portion wise and the reaction was stirred for 24 h at room temperature. Upon addition of $NH_4Cl_{(sat)}$ (20 mL), the reaction mixture was extracted with AcOEt (4 x 50 mL). The organic layers were pooled, dried over Na_2SO_4, filtered and concentrated under vacuum. The crude was purified by flash chromatography (SiO_2, eluent: DCM /MeOH, 95:5 with 30 drops of HAc per liter of eluent, R_f = 0.15) to yield compound **33** (595 mg, 1.89 mmol, 71%) as a sticky clear oil. ^{1}H NMR ($CDCl_3$, 300 MHz): δ 1.44 (m, 9H), 3.53 (m, 4H), 3.98 (m, 2H), 7.93 (s, 1H); ^{13}C NMR ($CDCl_3$,75 MHz): δ 28.1 (CH_3), 30.58 (CH_3), 38.4 (CH_2), 39.4 (CH_2), 47.3 (CH_2), 48.0 (CH_2), 49.9 (CH_2), 50.1 (CH_2), 81.8 (C_q), 155.8 (C_q), 156.5 (C_q); ^{1}H NMR (DMSO-d_6, 300 MHZ): δ 1.36 (m, 9H), 3.33 (m, 4H), 3.84 (m, 2H), 9.45 (m, 1H), 12.65 (bp, 1H); ^{13}C NMR (DMSO-d_6, 75 MHz): δ 28.2 (CH_3), 28.3 (CH_3), 37.9 (CH_2), 38.1 (CH_2), 46.4 (CH_2), 46.6 (CH_2), 78.9 (C_q), 132.9 (C_q), 155.2 (C_q), 155.4 (C_q), 172.3 (C_q), 172.1 (C_q); MS (ESI$^+$): *m/z* (%) 337.3 (5) [*M* + Na]$^+$, 215.2 (100) [*M* - $C_5H_{11}NO_2$].

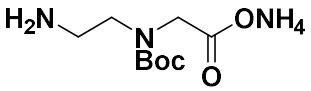

34

$^{\lambda}$5-Azanyl *N*-(2-aminoethyl)-N-(tert-butoxycarbonyl)glycinate (**34**): Compound **33** (559 mg, 1.78 mmol) was dissolved in MeOH (3 mL) and aq. NH_4OH (30%, 3 mL) were added and the reaction was stirred for 17 h at room temperature. The solvent was evaporated until dryness and the crude was washed with Et_2O (2 x 30 mL) to yield compound 34 (416 mg, 99%) as a white solid. ^{1}H NMR (D_2O, 300 MHz): δ 1.39-1.47 (s, 9H), 3.18 (m, 2H), 3.48 (m, 1H), 3.61 (m, 2H), 3.77 (m, 2H). ^{1}H NMR (DMSO-d_6, 300 MHz,): δ 1.33-1.40 (m, 9H), 2.93 (m, 2H), 3.17-.347 (m, 4H), 3.66-3.81 (3H);^{13}C NMR (DMSO-d_6, 75 MHz): δ 27.7 (CH_3), 27.8 (CH_3), 27.9 (CH_3), 37.2 (CH_2), 37.8 (CH_2), 46.0 (CH_2), 46.5 (CH_2), 50.9 (CH_2), 51.1 (CH_2), 79.3 (C_q), 79.5 (C_q), 155.5 (C_q), 171.5 (C_q), 171. 8(C_q), 172.4 (C_q); MS (ESI$^+$): *m/z* (%) 219.3 [*M* - NH_3]$^+$ (5), 163.2 [*M* - C_4H_9]$^+$ (60), 119.2 (100) [*M* - $C_5H_9O_2$]$^+$.

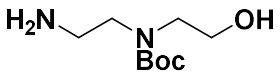

35

***tert*-Butyl (2-aminoethyl)(2-hydroxyethyl)carbamate, (35)**: Compound **32** (800 mg, 2.66 mmol) were dissolved in MeOH (3 mL) and aq. NH_4OH (30%, 3 mL) was added and stirred for 24 h at room temperature. The solvent was removed and the crude was purified by flash chromatography (SiO_2, eluent: DCM / MeOH / TEA, 90:10:1, R_f = 0.28) to yield compound **43** (541 mg, 2.63 mmol, 95%). ^{1}H NMR (DMSO-d_6, 300 MHz): δ 1.39 (s, 9H), 2.83 (t, *J* = 5.7 Hz, 2H), 3.22 (t, J = 5.4 Hz), 3.31 (m, 2H), 3.47 (t, *J* = 5.4 Hz, 2H), 5.54 (bp, 3H); ^{13}C NMR (DMSO-d_6, 75 MHz): δ 28.5 (CH_3), 38.9 (CH_2), 47.8 (CH_2), 48.2 (CH_2), 50.5 (CH_2), 50.8 (CH_2), 59.6 (CH_2), 59.9 (CH_2), 79.2 (C_q), 155.1 (C_q), 155.6 (C_q); MS (ESI$^+$): *m/z* (%) 105.2 (100)[*M* - $C_5H_{10}O_2$].

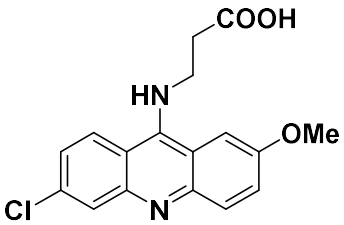

36

3-((6-Chloro-2-methoxyacridin-9-yl)amino)propanoic acid (36): In a two necked flask 6,9-dichloro-2-methoxyacridine (1.0 g, 3.59 mmol) was mixed with PhOH (4.0 g, 42.50 mmol) and β-alanine (247 mg, 3.89 mmol) and the reaction was heated for 3 h at 110 °C. The dark brown solution was cooled to room temperature an Et_2O (20 mL) was added. The yellow solid was filtered and dissolved in aq. NaOH (1 M, 100 mL) and re filtered again. The filtrate was acidified with HCl to pH 7. A yellow precipitated was formed, washed with H_2O (2 x 20 mL), MeOH (1 x 10 mL) and Et_2O (2 x 30 mL). The filtrate was dried under P_2O_5 to yield **36** (1.05 g, 3.17 mmol, 89%) as a yellow solid. ^{1}H NMR (DMSO-d_6, 300 MHz): δ 3.93-3.98 (m, 5H), 7.29 (dd, *J* = 9.2 Hz, 2.0 Hz, 1H), 7.40 (dd, *J* = 9.3, 2.4 Hz, 1H), 7.66 (d, *J* = 9.3 Hz, 1H), 7.81- 7.85 (m, 2 H), 8.36 (d, *J* = 9.2 Hz, 1H); ^{13}C NMR (DMSO-d_6, 75 MHz): δ 36.5 (CH_2), 46.5 (CH_2), 55.5 (CH_3), 100.9 (CH), 114.8 (C_q), 117.3 (C_q), 119.2 (C_q), 122.2 (CH), 124.1 (CH), 126.6 (CH), 130.1 (CH), 133.3 (CH), 145.6 (C_q), 147.9 (C_q),150.5 (Cq), 155.5 (C_q), 174.4 (C_q); MS (ESI$^+$): *m/z* (%) 331.2 (100) [*M* + H]$^+$.

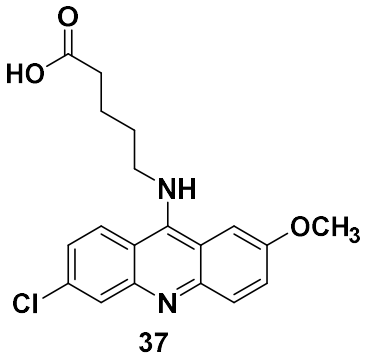

37

5-((6-Chloro-2-methoxyacridin-9-yl)amino)pentanoic acid (37): In PhOH (4.0 g, 42.50 mmol) , 6,9-dichloro-2-methoxyacridine (1.0 g, 3.59 mmol, and γ-aminovaleric acid (463 mg, 3.95 mmol) were mixed and the reaction was stirred for 2 h at 110 °C and then stirred overnight. The reaction was cooled down and Et_2O (30 mL) was added and the precipitated was filtered and redissolved in aq. NaOH (1M, 300 mL) and filtered again. The eluate was acidified with HCl to pH 7 and the precipitated filtered, washed with H_2O (1 x 30 mL), MeOH (1 x 30 mL) and Et_2O (2 x 30 mL) and dried over P_2O_5 to yield compound **37** (538 mg, 1.51 mmol, 42%) as a yellow solid. ^{1}H NMR (DMSO-d_6, 300 MHz): δ 1.56 (dt, *J* = 7.1, 6.9, 2H), 1.74 (dt, *J* = 7.1, 6.9 Hz, 2H), 2.22 (t, *J* = 7.1 Hz, 2H), 3.75 (t, *J* = 6.9 Hz, 2H), 3.93 (s, 3H), 7.30 (dd, *J* = 9.1, 1.8 Hz, 1H), 7.40 (dd, *J* = 9.3 Hz, 2.3 Hz, 1H), 7.62 (d, *J* = 2.3 Hz, 1H), 7.80 (d, *J* = 9.3 Hz, 1H), 7.86 (d, *J* = 1.8 Hz, 1H), 8.34 (d, *J* = 9.1 Hz, 1H); ^{13}C NMR (DMSO-d_6, 75 MHz): δ 22.4 (CH_2), 30.5 (CH_2), 33.8 (CH_2), 49.6 (CH_2), 56.1 (CH_3), 101.3 (CH), 115.0 (C_q), 117.5 (C_q), 123.0 (CH), 124.6 (CH), 127.1 (CH), 130.6 (CH), 133.9 (CH), 146.0 (CH), 148.4 (CH), 150.8 (CH), 155.5 (CH), 174.8 (CH); MS (ESI$^+$): *m/z* (%) 359.3 (100) $[M + H]^+$.

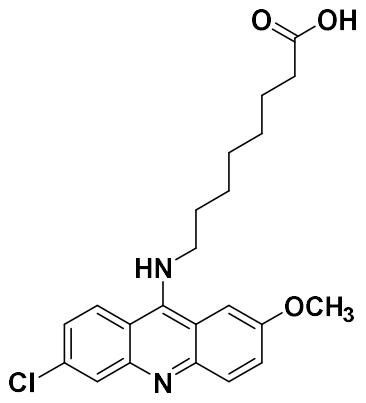

38

8-((6-Chloro-2-methoxyacridin-9-yl)amino)octanoic acid (38) : 6,9-dichloro-2-methoxyacridine (300 mg, 1.07 mmol) were mixed with PhOH (3 g, 31.80 mmol) under an Ar atmosphere and the reaction was heated at 70 °C for a period of 1 h. Then, 8-amino caprylic acid (189 mg, 1.18 mmol) was added and the temperature was increased to 110 °C for 3 h. The reaction was cooled to room temperature, the solid was filtrated, washed with Et_2O (2 x 30 mL) and purified by flash chromatography (SiO_2,

eluent: DCM / MeOH / TEA, 95:5:1, R_f = 0.20). Compound **38** (405 mg, 1.01 mmol, 94%) was obtained as a yellow solid. ^{1}H NMR (DMSO-d_6, 300 MHz): δ 1.42-1.49 (m, 6H), 1.51 (dt, *J* = 7.5, 6.9 Hz, 2H), 1.85 (dt, *J* = 8.1, 6.3 Hz, ,3H), 2.15 (t, *J* = 7.2 Hz, 2H), 3.96 (s, 3H), 4.03 (t, *J* = 6.9 Hz, 2H), 7.48 (dd, *J* = 9.2, 1.9 Hz, 1H), 7.65 (dd, *J* = 9.3, 2.3 Hz, 1H), 7.88 (d, *J* = 9.3 Hz, 1H), 7.95 (m, 2H), 8.5 (d, *J* = 9.2 Hz, 1H), 9.56 (s, 1H), 12.0 (s, 1H); ^{13}C NMR (DMSO-d_6, 75 MHz): δ 24.8 (CH_2), 26.5 (CH_2), 28.8 (CH_2, 2C), 29.5 (CH_2), 34.1 (CH_2), 49.2 (CH_2), 56.6 (CH_3), 104. 1 (CH), 110.9 (C_q), 114.9 (C_q), 118.6 (C_q), 121.8 (CH), 123.6 (CH), 127.2 (CH), 127.6 (CH), 129.1 (CH), 138.8 (C_q), 155.9 (C_q), 156.2 (C_q), 174.9 (C_q); MS (ESI$^+$): *m/z* (% : 401.3 (100) [*M* + H]$^+$.

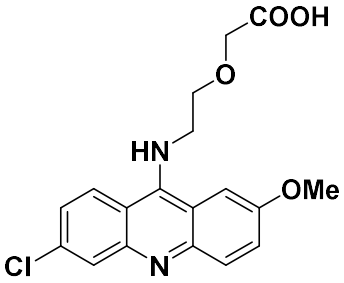

39

2-(2-((6-Chloro-2-methoxyacridin-9-yl)amino)ethoxy)acetic acid, (39): In PhOH (4.0 g, 42.50 mmol) 6,9-dichloro-2-methoxyacridine (857 mg, 3.08 mmol) were additioned together with **28** (800 mg, 3.43 mmol) DIPEA (1.0 g, 7.80 mmol, 1.29 mL). The sample was heated at 110 °C for 6 h until the disappearance of the starting material as judged by TLC. The reaction was cooled down and Et_2O (20 mL) was added, and the precipitated was filtered. Then, resuspended and gently stirred with aq. NaOH (1M, 300 mL). The solution was filtered and the filtrate was acidified with HCl until pH 7. The yellow precipitated is filtered again and washed with of H_2O (1 x 50 mL), MeOH (1 x 30 mL), Et_2O (2 x 30 mL) and then dried over P_2O_5 to yield compound **39** (506 mg, 1.41 mmol, 46%) as a yellow solid. ^{1}H NMR (DMSO-d_6, 300 MHz): δ 3.85 (m, 2H), 3.91 (s, 3H), 3.95 (m, 2H), 4.03 (m, 2H), 7.25 (d, *J* = 9.0 Hz, 1H), 7.40 (d, *J* = 8.9 Hz, 1H), 7.76 (d, *J* = 8.9 Hz, 1H), 7.83 (s, 1H), 7.93 (s, 1H), 8.50 (d, *J* = 9.0 Hz, 1H); ^{13}C NMR (DMSO-d_6, 75 MHz): δ 49.8 (CH_2), 55.8 (CH_3), 68.3 (CH_2), 68.9 (CH_2), 102.2 (CH), 113.1 (C_q), 116.1 (C_q), 122.4 (CH), 123.4 (CH), 124.9 (CH), 126.9 (CH), 127.8 (CH, 2C), 135.0 (C_q), 141.7 (C_q), 145.5 (C_q), 155.2 (C_q), 172.0 (C_q); MS (ESI$^+$): *m/z* (%) 361.2 (100) [*M* + H]$^+$.

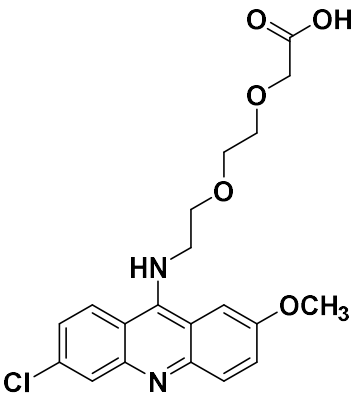

40

2-(2-(2-((6-Chloro-2-methoxyacridin-9-yl)amino)ethoxy)ethoxy)acetic acid (40): Under an Ar atmosphere, of 6,9-dichloro-2-methoxyacridine (300 mg, 1.07 mmol) were mixed with PhOH (3 g, 31.80 mmol) and the reaction was heated at 70 °C for a period of 1 h. Then, 2-[2-(2-aminoethoxy)ethoxy]acetic acid (194 mg, 1.18 mmol) was added and the temperature was increased to 110 °C for 3 h. The reaction was cooled to room temperature, and filtered. The solid was washed with Et_2O (2 x 30 mL) and purified by flash chromatography (SiO_2, eluent: DCM / MeOH / TEA, 95:5:1,R_f = 0.26) to yield **47** (426 mg, 1.05 mmol, 98%) as a yellow powder. ^{1}H NMR (DMSO-d_6, 300 MHz) : δ 3.55 (s, 4H), 3.71 (t, *J* = 5.2 Hz, 2H), 3.86 (*t*, J = 5.2 Hz, 2H), 3.93-3.95 (m, 5H), 7.34 (dd, *J* = 9.2, 2.1 Hz, 1H), 7.44 (dd, *J* = 9.4, 2.4 Hz, 1H), 7.64 (d, *J* =, 2.4 Hz, 1H), 7.83 (d, *J* = 9.4 Hz, 1H), 7.88 (d, *J* = 2.1 Hz, 1H), 8.38 (d, *J* = 9.2 Hz, 1H); ^{13}C NMR (DMSO-d_6, 75 MHz): δ at 40 °C 49.2 (CH_2), 55.5 (CH_3), 67.6 (CH_2), 69.6 (CH), 69.7 (CH), 69.9 (CH), 101.1 (CH), 115.1 (C_q), 117.6 (C_q), 122.8 (C_q), 124.1 (CH),126.1 (CH), 126.4 (CH), 129.6 (C_q), 133.6 (C_q), 145.1 (C_q), 147.1 (C_q), 147.3 (C_q), 150.6 (C_q), 155.1 (C_q), 171.4 (C_q); MS (ESI$^+$): *m/z* (%) 405.2 (100) $[M + H]^+$.

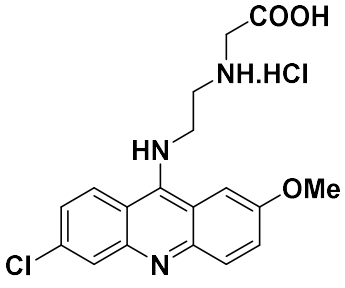

41

2-((6-Chloro-2-methoxyacridin-9-yl)amino)ethyl)glycine hydrochloride (41): In PhOH (4.0 g, 42.50 mmol) of 6,9-dichloro-2-methoxyacridine (400 mg, 1.43 mmol) and 415 mg (1.78 mmol) of **41** were mixed and heated at 110 °C for 2 h until the disappearance of the starting material as judged by TLC. After cooling, Et_2O (20 mL) was added, the precipitate was filtered and dissolved in aq NaOH (1M, 300 mL). The solution was filtered once again, and acidified with HCl to pH 7. A yellow precipitated was

formed, filtered, washed with H_2O (1 x 50 mL), MeOH (1 x 30 mL) and Et_2O (2 x 30 mL) and then dried over P_2O_5 to yield compound **42** (127 mg, 0.31 mmol, 22%) as a yellow solid. ^{1}H NMR (DMSO-d_6, 300 MHz): δ 3.20 (m, 2H), 3.33 (s, 3H), 3.92 (s, 3H), 4.02 (m, 2H), 7.25 (d, J = 7.3 Hz, 1H), 7.27 (d, J = 8.3 Hz, 1H), 7.69-7.72 (m, 2H), 7.76 (s, 1H), 8.30 (d, J = 8.3 Hz, 1H);^{13}C NMR (DMSO-d_6, 75 MHz): δ 47.4 (CH_2), 47.9 (CH_2), 50.2 (CH_2), 56.1 (CH_3), 103.6 (CH),115.4 (C_q), 118.(C_q), 122.6 (CH), 124.3 (CH, 2C), 128.4 (CH), 134.7 (C_q), 134.8 (C_q), 146.2 (C_q), 151.4 (C_q), 155.4 (C_q), 168.7 (C_q); MS (ESI$^+$): *m/z* (%) 360.3 (100) [M + H]$^+$.

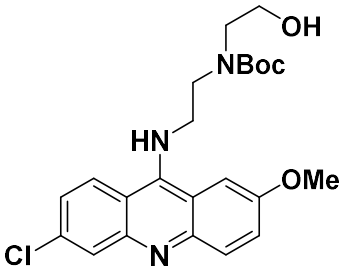

42

***Tert*-butyl (2-((6-chloro-2-methoxyacridin-9-yl)amino)ethyl)(2-hydroxyethyl)carbamate, (42):** In PhOH (4.0 g, 42.50 mmol), 6,9-dichloro-2-methoxyacridine (618 mg, 2.22 mmol) and **35** (500 mg, 2.44 mmol) were mixed and heated at 110 °C for 2.5 h until the disappearance of the starting material as judged by TLC. The reaction was cooled down and Et_2O (20 mL) was added. The orange solid was filtered and purified two times by flash chromatography (SiO_2, eluent: DCM /EtOH, 90:10, R_f = 0.18) to yield compound **42** (238 mg, 0.53 mmol, 24%) as an orange solid. ^{1}H-NMR DMSOd_6, 300 MHz, δ (ppm): 1.0 (s, 3H), 1.32 (s, 6H), 3.20 (m, 2H), 3.34 (s, 1H), 3.45 (m, 2 H), 1.09 (m, 1H), 3.96-4.02 (m, 5H), 4.83 (s, 1H), 7.32 (d, J = 8.6 Hz, 1H), 7.46 (d, J = 9.1 Hz, 1H), 7.65 (s, 1H), 7.82 (d, J = 9.1 Hz, 1H), 7.86 (s, 1H), 8.4 (m, 1H); ^{13}C NMR (DMSO-d_6, 75 MHz): δ 27.5 (CH_3), 27.9 (CH_3), 48.4 (CH_2), 49.8 (CH_2), 50.3 (CH_2), 55.6 (CH_3), 59.0 (CH_2), 59.4 (CH_2), 78.5 (C_q), 79.0 (C_q), 101.5 (CH), 112.9 (CH), 122.6 (CH), 124.8 (CH), 127.2 (CH), 134.7 (C_q), 140.5 (CH), 151.6 (C_q, 2C), 154.4 (C_q), 154.5 (C_q), 155.3 (C_q), 155.7 (C_q, 2C);MS (ESI$^+$): *m/z* (%) 446.3 [M + H]$^+$ (100).

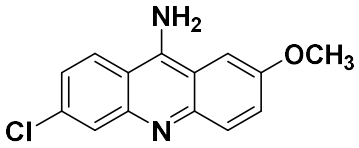

43

6-Chloro-2-methoxyacridin-9-amine (43):[159,176] 6,9-dichloro-2-methoxyacridine (1 g, 3.59 mmol) were mixed with PhOH (3 g , 31.80 mmol) under an Ar atmosphere and the reaction was heated at 70 °C for a period of 1 h. Then, $(NH_4)_2CO_3$ (700 mg, 7.28 mmol) was added and the temperature was increased to 110 °C for 3 h. The reaction was cooled, the precipitated washed with NaOH 10 % (3 x 20 mL), H_2O (2 x 20 mL), DCM (2 x 10 mL), acetone (1 x 10 mL) and then dried over P_2O_5 to yield compound **43** (750 mg 2.89 mmol, 81%) as a yellow solid. ^{1}H NMR (DMSO-d_6, 300 MHz): δ 3.91 (s, 3H), 7.30 (dd, *J* = 9.2, 1.3 Hz, 1H),7.37 (dd, *J* = 9.3,1.9 Hz, 1H), 7.67 (d, *J* = 1.9 Hz, 1H), 7.70 (s, 2H), 7.8 (d, *J* = 1.3 Hz, 1H), 8.30 (d, *J* = 9.2 Hz, 1H); ^{13}C NMR (DMSO-d_6, 75 MHz): δ 55.7 (CH_3), 100.3 (CH), 111.2 (C_q), 113.2 (C_q), 122.0 (CH), 124.4 (CH), 125.3 (CH), 126.9 (CH), 130.5 (CH), 133.5 (C_q), 145.9 (C_q), 147.7 (C_q), 148.7 (C_q), 154.6 (C_q); MS (ESI$^+$): *m/z* (%): 259.0 (100) [*M* + H]$^+$; purity (HPLC): 98%.

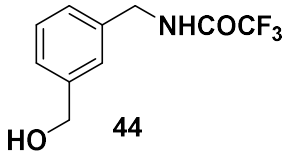

44

2,2,2-Trifluoro-*N*-(3-(hydroxymethyl)benzyl)acetamide (44):[37] The amino alcohol **24** (885 mg, 6.45 mmol) was dissolved in 10 mL of dry MeOH under an Ar atmosphere. TEA (6.45 mmol, 653 mg, 896 µL) was added, the reaction mixture was cooled to 0 °C, and ethyl trifluoroacetate (8.38 mmol, 1.19 g, 998 µL) was added dropwise. The reaction mixture was allowed to return to room temperature while stirring for 1 h. After removal of MeOH in vacuum, the crude product was dissolved in AcOEt (10 mL) and washed with H_2O (1 x 10 mL). The aqueous layer was extracted with AcOEt (3 × 20 mL), the organic layers were pooled, dried over Na_2SO_4, filtered and concentrated under vacuum. The product was purified by flash chromatography (SiO_2, eluent: Cyclohexane / AcOEt, 2:1; R_f = 0.25), to give **2** (1.00 g, 4.28 mmol, 67%) as a white solid. ^{1}H NMR ($CDCl_3$, 300 MHz): δ 1.93 (s, 1H), 4.53 (d, *J* = 5.7 Hz, 2H), 4.69 (s, 2H), 6.69 (s, 1H), 7.21–7.40 (m, 4H); ^{13}C NMR, ($CDCl_3$, 75 MHz): δ 43.9 (CH_2), 64.9 (CH_2), 118.0 (C_q, *J* = 287 Hz), 126.5 (CH), 126.9 (CH), 127.2 (CH), 129.3 (CH), 136.1 (C_q), 141.8 (C_q), 157.1 (C_q), 157.2 (C_q, *J* = 37 Hz); MS (ESI$^+$): *m/z* (%) 257.1 (5) [*M* + Na]$^+$, 216.2 (100) [*M* - OH]$^+$.

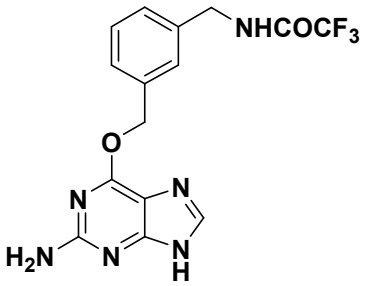

45

***N*-(3-(((2-amino-9*H*-purin-6-yl)oxy)methyl)benzyl)-2,2,2-trifluoroacetamide (45)**:[37] Under an Ar atmosphere, **44** (415 mg, 1.78 mmol) was dissolved dry DMF (5 mL) together with *t*-BuOK (1.02 g, 9.14 mmol) and the mixture was stirred for 30 minutes at room temperature for after the addition of **26**(228 mg, 0.89 mmol). The mixture was stirred for 5 h at room temperature. The solvent removed and the crude was purified by flash chromatography (SiO_2, eluent: DCM / EtOH gradient, 95:5 to 90:10; R_f = 0.15) to yield **4** (304 mg, 0.82 mmol, 48%) as a white solid. ^{1}H NMR (DMSO-d_6, 300 MHz): δ 4.41 (d, *J* = 5.8 Hz, 2H), 5.48 (s, 2H), 6.29 (s, 2H), 7.24-7.42 (m, 4H), 7.81 (s, 1H), 10.03 (t, *J* = 5.8 Hz 1H), 12.42 (s, 1H); MS (ESI$^+$): *m/z* (%) 367.1 (100) [*M* + H]$^+$.

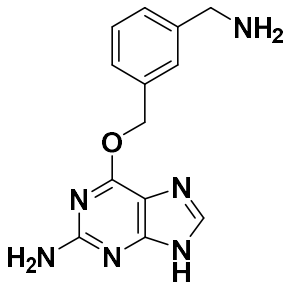

46

6-((3-(Aminomethyl)benzyl)oxy)-9H-purin-2-amine (46):[37] **6-((3-(Aminomethyl)benzyl)oxy)-9*H*-purin-2-amine (5):**[37] Method A: In a mixture of MeOH (26 mL) and H_2O (800 µL), compound **4** (366 mg, 0.72 mmol) and K_2CO_3 (500 mg, 3.6 mmol) were resuspended and the mixture was refluxed for 4 h until the disappearance of the starting material (TLC). The solvent was removed and the crude product was purified by flash chromatography (SiO_2, eluent: DCM / MeOH / TEA, 80:20:1, R_f = 0.2) to give **46** (108 mg, 0.39 mmol, 51%) as a white solid. ^{1}H NMR (DMSO-d_6, 300 MHz): δ 3.74 (s, 2H), 5.46 (s, 2H), 6.28 (s, 2H), 7.31–7.33 (m, 3H), 7.47 (s, 1H), 7.83 (s, 1H); ^{13}C NMR (DMSO-d_6, 75 MHz): δ 45.4 (CH_2), 66.9 (CH_2), 126.5 (CH), 126.8 (CH), 127.3 (CH), 128.2 (CH), 136.4 (C_q), 138.2 (CH), 144.0 (C_q), 159.5 (C_q); MS (ESI$^+$): *m*/z (%) 271.2 (100) [*M* + H]$^+$.

Method B: In an Ar atmosphere, compound **44** (2.19 g, 9.39 mmol) was dissolved in dry pyridine (30 mL) and *t*-BuOK (2.12 g, 18.93 mmol) were added, the reaction was stirred for 20–30 min at room temperature, followed by the addition of salt (1.20 g, 4.71 mmol). After 6 h, more *t*-BuOK (2.12 g,

18.93 mmol) was added and the reaction was stirred overnight. Then, **26** (2.19 g, 2.39 mmol) was added to the mixture, which was finally stirred for 24 h more. Finally, H_2O (6 mL) was added and the mixture refluxed for 2 h. The solvents were removed under vacuum and the crude purified as described above to yield **46** (1.03 g, 3.80 mmol, 77%); the spectroscopic data were identical with those given above.

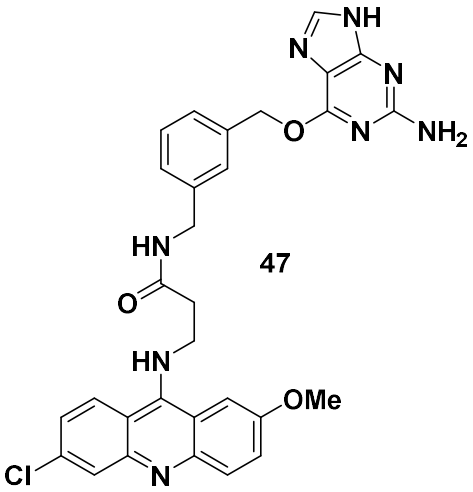

47

Synthesis of *N*-(3-(((2-amino-9*H*-purin-6-yl)oxy)methyl)benzyl)-3-((6-chloro-2-methoxyacridin-9-yl)amino)propanamide (47): Compound **36** (159 mg, 0.48 mmol) was dissolved in dry DMF (10 mL), under an Ar atmosphere together with DIPEA (195 mg, 1.51 mmol, 249 μL), HBTU (364, 0.96 mmol) and HOBt (13 mg, 0.09 mmol). The mixture was stirred for 30 minutes and then **46** (143 mg, 0.52 mmol) was added to the mixture. The reaction was stirred for 24 h at room temperature, when H_2O (10 mL) was added and the crude was extracted with a mixture of DCM / MeOH (9:1, 4 x 50 mL). The organic layers were pooled and dried over Na_2SO_4. The reaction was purified two times by flash chromatography (DCM / MeOH / TEA, 95:5:1, R_f = 0.12) to yield **47** (76 mg, 0.13 mmol, 34%) as a yellow solid. ^{1}H NMR (DMSO-d_6, 300 MHz, recorded at 40 °C): δ 1.24 (s, 1H), 2.64 (m, 2H), 3.91 (s, 3H), 4.05 (m, 2H), 4.26 (m, 2H), 5.42 (s,2H), 9.18 (s, 2H), 7.15-7.45 (m, 6H), 7.80-7.86 (4H), 8.37-8.44 (m, 2H), 12.36 (bp, 1H); ^{13}C NMR (APT, DMSO-d_6, 75 MHz, recorded at 40 °C): δ 35.9 (CH_2), 41.9 (CH_2), 45.9 (CH_2), 55.5 (CH_3), 66.5 (CH_2), 101.4 (CH), 109.7 (CH), 114.4 (C_q), 117.1 (CH), 118.4(CH), 122.8 (CH), 123.9 (CH), 124.4 (CH), 126.7 (CH), 126.8 (CH), 127.1 (CH), 128.2 (CH), 134.8 (C_q), 136.6 (C_q), 139.4 (C_q), 144.2 (Observed by HMBC), 146.3 (C_q), 150.9 (C_q), 155.1 (2C, C_q), 159.5 (C_q), 170.3 (C_q); MS (ESI$^+$): *m/z* (%) 292.2 (100) [*M* + 2H]$^+$, 583.3 (10) [*M* + H]$^+$, purity (HPLC): 97%; HRMS (TOF ES$^+$): calcd. for $C_{30}H_{28}ClN_8O_3$ [*M*+ H]$^+$: 583.1973, found: 583.1993.

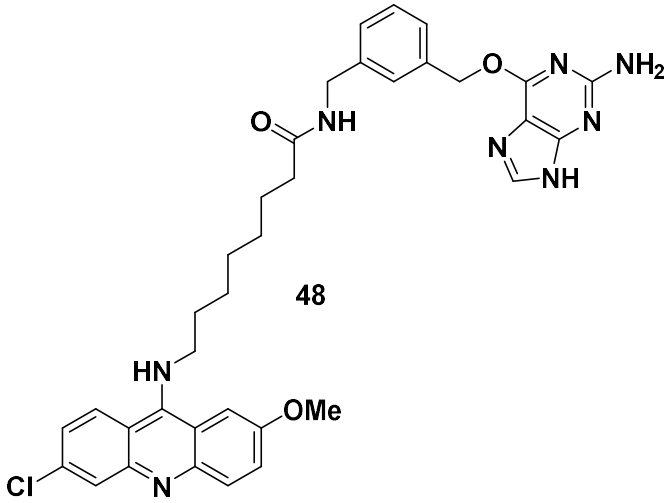

Synthesis of *N*-(3-(((2-amino-9*H*-purin-6-yl)oxy)methyl)benzyl)-8-((6-chloro-2-methoxyacridin-9-yl)amino)octanamide (48): Compound **38** (100 mg, 0.25 mmol) was dissolved in dry DMF (10 mL) under an Ar atmosphere together with DIPEA (97 mg ,0.75 mmol, 124 μL), HBTU (114 mg, 0.30 mmol) and HOBT (7 mg, 0.05 mmol). The mixture was stirred for 30 minutes approximately and **46** (101 mg, 0.38 mmol) was added. The reaction was stirred for 24 h at room temperature. To quench the reaction, H_2O (10 mL) was added and the crude was extracted with a mixture of DCM / MeOH (9:1, 5 x 50 mL). The organic layers were pooled, washed with H_2O and brine (1 x 30 mL each), and dried over Na_2SO_4. The reaction was purified two times by flash chromatography (SiO_2, eluent: DCM / MeOH / TEA, 95:5:1, R_f = 0.12) to yield compound **48** (106 mg, 0.16 mmol, 62%) as a yellow solid. ^{1}H NMR (CD_3OD, 300 MHz) : δ 1.27-1.31 (m, 8H), 1.52-1.57 (m, 2H), 1.72-1.77 (m, 2H), 2.16 (t, *J* = 7.3 Hz, 2H), 3.80 (t, *J* = 7.2 Hz, 2H), 3.93 (s, 3H), 4.34 (s, 2H), 5.46 (s, 2H), 7.19-7.44 (m, 6H), 7.53 (d, *J* = 2.6 Hz, 1H), 7.77-7.82 (m, 3H), 8.24 (d, *J* = 9.4 Hz, 1H); ^{13}C NMR (APT, CD_3OD, 75 MHz): δ 25.3 (CH_2), 26.3 (CH_2), 28.5 (CH_2), 30.5 (CH_2), 35.5 (CH_2), 42.5 (CH_2), 49.5 (CH_2), 54.9 (CH_3), 67.4 (CH_2), 100.1 (CH), 113.9 (C_q), 116.6 (C_q), 122.9 (CH), 125.0 (CH), 126.7 (CH), 126.9 (CH), 127.0 (CH), 128.2 (CH), 135.6 (C_q), 136.7 (C_q), 138.6 (CH), 139.1 (C_q), 152.3 (C_q), 155.9 (C_q), 172.1 (C_q), 174.5 (C_q); MS (ESI$^+$): *m/z* (%): 653.5 (5) [*M* + H]$^+$, 327.4 (100) [*M* + 2H]$^+$; purity (HPLC): 97%; HRMS (TOF ESI$^+$): calcd. for $C_{35}H_{38}ClN_8O_3$ [*M* + H]$^+$: 653.2570, found: 657.2782.

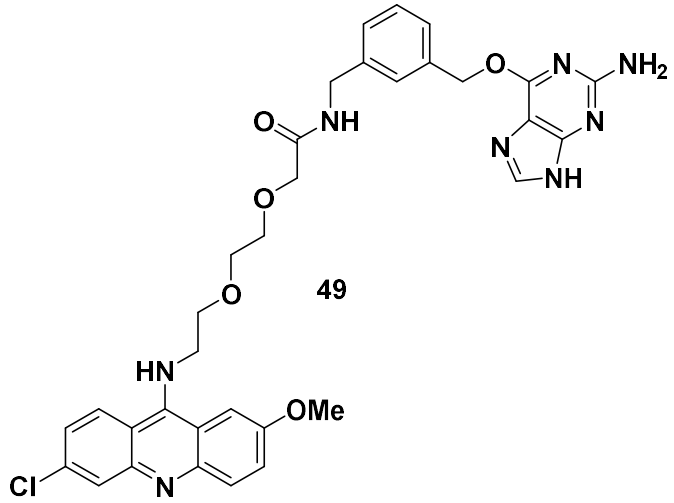

49

***N*-(3-(((2-amino-9*H*-purin-6-yl)oxy)methyl)benzyl)-8-((6-chloro-2-methoxyacridin-9-yl)-amino)octanamide (49):** Compound **40** (80 mg, 0.19 mmol) was dissolved in dry DMF (8 mL) under an Ar atmosphere together with DIPEA 577 mg, 0.59 mmol, 98 μL), HBTU (90 mg, 0.23 mmol), and HOBt (5 mg, 0.04 mmol). The mixture was stirred for 30 min and then **46** (80 mg, 0.29 mmol) was added. The reaction was stirred for 24 h at room temperature. After addition of H_2O (10 mL), the crude was extracted with a mixture of DCM / MeOH (9:1, 5 × 50 mL). The organic layers were pooled, washed with H_2O and brine (1× 30 mL each), dried over Na_2SO_4, filtrated and concentrated under vacuum The reaction was purified two times by flash chromatography (SiO_2, eluent: DCM / MEOH / TEA, 95:5:1, R_f = 0.14). Compound **49** (85 mg, 0.12 mmol, 65%) was obtained as a yellow solid. ^{1}H NMR (CD_3OD 300 MHz): δ 3.64 (s, 4H), 3.77 (t, *J* = 5.1 Hz, 2H), 3.89 (s, 3H), 3.96-3.97 (m, 5H), 4.21 (s, 2H), 5.28 (s, 2H), 7.02 (d, *J* = 7.4 Hz, 1H), 7.12 (t, *J* = 7.5 Hz, 1H), 7.19 (d, *J* = 7.4 H, 1H), 7.24–7.29 (m, 2H), 7.45 (d, *J* = 9.3 Hz, 1H), 7.55 (m, 1H), 7.70-7.73 (m, 2H), 7.80 (s, 1H), 8.26 (d, *J* = 9.3 Hz, 1H); ^{13}C NMR (APT, CD_3OD, 75 MHz): δ 43.2 (CH_2), 49.6 (CH_2), 56.4 (CH_3), 68.6 (CH_2), 70.8 (CH_2), 71.1 (CH_2), 71.2 (CH_2, 2C), 72.0 (CH_2), 102.5 (CH), 114.4 (C_q), 117.5 (C_q), 123.3 (CH), 124.9 (CH), 126.5 (CH), 127.3 (CH), 127.8 (CH), 128.0 (CH), 128.1 (CH), 129.6 (CH), 138.0 (C_q), 138.8 (C_q), 139.7 (C_q), 139.9 (CH), 142.2 (C_q), 145.5 (C_q), 155.3 (C_q), 157.6 (C_q), 161.2 (C_q), 161.6 (C_q), 172.5 (C_q); MS (ESI$^+$): *m/z* (%) 657.4 (5) [*M* + H]$^+$, 329.3 (100) [*M* + 2H]$^+$,; purity (HPLC): 97%; HRMS (TOF ESI$^+$): calcd. for $C_{33}H_{34}ClN_8O_5$ [*M* + H]$^+$: 657.2335, found: 657.2364.

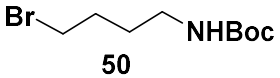

50

***tert*-Butyl (4-bromobutyl)carbamate (50):**[237] Under an Ar atmosphere, 500 mg (2.02 mmol) of 4-bromobutan-1-amine hydrobromide (500 mg, 2.02 mmol) was dissolved in dry THF (10 mL) at 0 °C together with$(Boc)_2O$ (519 mg, 2.37 mmol) and TEA (262 mg,2.59 mmol, 360 μL). After reaching room temperature the mixture was stirred for 24 h. Solvent was removed by vacuum and the sample diluted DCM (50 mL). The organic layer is washed with aq. HCl (5%, 1 x 15 mL) and H_2O (1 x 15 mL), dried over

Na_2SO_4, filtered and concentrated under vacuum to yield **29** (537 mg, 2.37 mmol, 100 %) as a transparent oil that solidifies upon freezing. ^{1}H NMR ($CDCl_3$, 300 MHz): δ 1.44 (s, 9H), 1.65 (m, 1H), 1.92 (m, 2H), 3.16 (q, *J* = 6.6 Hz, 2H) 3.31 (m, 1H), 3.41 (t, *J* = 6.6 Hz, 2H), 4.54 (s, 1H).

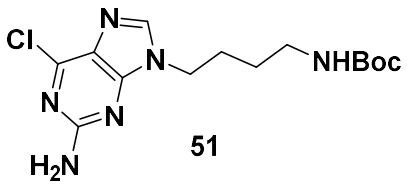

51

***Tert*-butyl (4-(2-amino-6-chloro-9H-purin-9-yl)butyl)carbamate (51):** Compound Under an Ar atmosphere 2-amino-6-chlorpurine (327 mg, 1.93 mmol) was resuspended in dry DMF (5 mL) with Cs_2CO_3 (1.43 g, 4.38 mmol) and stirred for 15 minutes. Then **50** (663 mg, 2.63 mmol) was added to the mixture and stirred for 24 h at room temperature. Reaction was quenched by adding H_2O (5 mL) and the mixture was extracted with AcOEt (4 x 50 mL). The organic layers were pooled, dried over Na_2SO_4, filtered and concentrated under vacuum. The crude was purified by flash chromatography (DCM / EtOH, 98 :2 system. R_f = 0.34) to yield **51** (262 mg, 0.77 mmol, 40%) as a white solid. ^{1}H NMR ($CDCl_3$, 300 MHz), δ (ppm): 1.45 (s, 9H), 1.52 (m, 2H), 1.77 (m, 2H), 3.21 (q, *J* = 6.4 Hz, 2H), 4.12 (t, *J* = 7.2 Hz, 2H), 4.84 (s, 1H), 5.20 (s, 2H), 7.77 (s, 1H); ^{13}C NMR ($CDCl_3$, 75 MHz): δ 27.1 (CH_2), 28.5 (CH_3 and CH_2), 39.7 (CH_2), 43.1 (CH_2), 77.3 (C_q), 79.6 (C_q), 119.6 (C_q), 125.4 (C_q), 142.4 (CH), 151.5 (C_q), 153.9 (C_q), 156.2 (C_q), 159.0 (C_q); MS (ESI$^+$): *m/z* (%): 341.3 (15) [*M* + H]$_+$, 285.2 (100) [*M* - C_4H_9]$^+$.

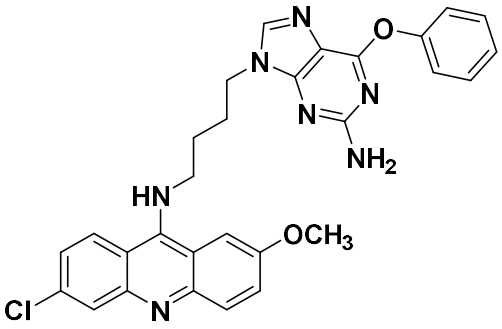

52

***N*-(4-(2-amino-6-phenoxy-9H-purin-9-yl)butyl)-6-chloro-2-methoxyacridin-9-amine (52):** Compound **51** (171 mg, 0.50 mmol)) was dissolved in dry dioxane (4 mL) the reaction was cooled on an ice bath, where HCl (4M in dioxane, 3.2 mmol, 800 μL) was added and the ice bath immediately removed once the reaction reached room temperature it was gently stirred for 6 h. The solvent was removed under vacuum and was washed with MeOH (10 mL). Then, 6,9-dichloro-2-methoxyacridine (152 mg, 0.45 mmol) and PhOH (800 mg, 10.00 mmol) were added and the mixture was heated for 6 h at 110 °C and then stirred at room temperature for 18 h. The reaction was dissolved in MeOH (1 mL) and Et_2O (10 mL) was added. An orange precipitated was formed, filtered and purified by flash chromatography

(DCM / MeOH, 95:5, R_f = 0.1) to yield **13** (65 mg, 0.12 mmol, 24%) as an orange solid. ^{1}H NMR (DMSO-d_6, 300 MHz) : δ 1.79-1.89 (m, 4H), 3.91-4.05 (m, 5H), 4.08 (t, *J* = 5.3 Hz, 2H), 6.35 (s, 2H), 7.21-7.27 (m, 3H), 7.41-7.44 (m, 3H), 7.55 (d, *J* = 7.5 Hz, 1H), 7.75 (s, 1H), 7.73 (d, *J* = 9.3 Hz, 1H), 7.89 (s, 1H), 7.96 (s, 1H), 8.38 (d, *J* = 9.3 Hz, 1H); ^{13}C NMR (DMSO-d_6,75 MHz): δ 26.5 (CH_2), 26.9 (CH_2), 42.4 (CH_2), 48.5 (CH_2), 55.9 (CH_3), 102.3 (CH), 113.4 (C_q), 121.6 (CH, 3C), 122.9 (CH), 125.0 (CH),125.6 (CH), 127.6 (CH), 129.5 (CH, 2C), 140.8 (CH), 152.3 (C_q), 155.2 (C_q), 155.4 (C_q), 159.6 (C_q); MS (ESI$^+$): *m/z* (%): 540.4 (20) [*M* + H]$^+$, 270.2 (100) [*M* + 2H] $^{2+}$; purity (HPLC): 97%; HRMS (TOF ESI$^+$): calcd for $C_{29}H_{27}ClN_7O_2$ [*M* + H]$^+$: 540.1915, found: 540.1897.

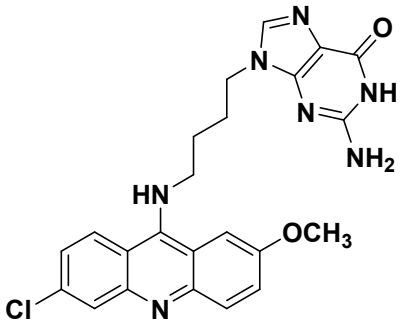

53

2-Amino-9-(4-((6-chloro-2-methoxyacridin-9-yl)amino)butyl)-1,9-dihydro-6H-purin-6-one (53): Compound **54** (159 mg, 0.38 mmol), was dissolved in dry dioxane (5 mL) under an Ar atmosphere and the reaction was cooled on an ice bath when HCl (4M in dioxane,2.00 mmol, 500 mL) was added, the ice bath was immediately removed and the reaction was stirred for 2.5 h until the disappearance of the starting material. The solvent was removed and PhOH (700 mg, 9.09 mmol) and 6,9-dichloro-2-methoxyacridine were added. The reaction was heated for 4 h at 110 °C and then stirred at room temperature for a total of 24 h. The reaction was cooled and Et_2O (50 mL) was added, the orange precipitate was filtered. The crude was purified by flash chromatography (DCM / MeOH / TEA, 95:5:1, R_f = 0.1). Compound **53** (90 mg, 0.19 mmol, Y = 50%) was obtained as an orange solid. ^{1}H NMR (300 MHz, DMSO-d_6): δ 1.69-1.80 (m, 4H), 3.79 (t, *J* = 6.9 Hz, 2H), 3.75-3.96 (m, 5H), 6.40 (s, 2H), 7.06 (bp, 1H), 7.33 (dd, *J* = 9.3, 1.5 Hz, 1H), 7.43 (dd, *J* = 9.3, 2.0 Hz), 7.60 (d, *J* = 2.3 Hz, 1H), 7.65 (s, 1H), 7.81-7.87 (m, 3H), 8.30 (d, *J* = 9.3 Hz, 1H), 10.53 (s, 1H); ^{13}C NMR (DMSO-d_6, 75 MHz): δ 26.5 (CH_2), 28.0 (CH_2), 42.3 (CH_2), 49.0 (CH_2), 55.6 (CH_3), 116.6 (CH), 117.0 (C_q), 119.2 (CH); 122.7 (CH), 124.3 (CH), 126.5 (CH), 133.8 (CH), 137.4 (C_q), 150.7 (C_q), 151.1 (C_q), 155.4 (C_q), 155.1 (C_q),156.7 (C_q);MS (ESI$^+$): *m/z* (%): 232.7 (100), [*M* + 2H] $^{2+}$, 464.4 (15) [*M* + H]$^+$, purity (HPLC): 98%; HRMS (ESI$^+$ TOF) calcd for $C_{23}H_{23}ClN_7O_2$ [*M* + H]$^+$: 464.1602, found: 464.1577.

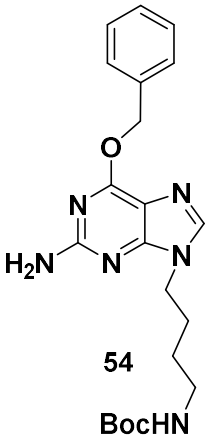

54

***Tert*-butyl (4-(2-amino-6-(benzyloxy)-9H-purin-9-yl)butyl)carbamate (54):** O^6BG (315 mg, 1.31 mmol) was resuspended with Cs_2CO_3 (851, 2.61 mmol) in dry DMF (10 mL) and stirred under an Ar atmosphere for 10 minutes. Then, **50** (395 mg, 1.56 mmol) was added and the mixture was stirred for 24 h at room temperature. To quench the reaction, 15 mL of H_2O (15 mL) was added and the mixture was extracted with AcOEt (4 x 25 mL). The organic layers were pooled, dried over Na_2SO_4, filtered and concentrated under vacuum. The crude was purified by flash chromatography (DCM / MeOH gradient, 100:0 to 98:2, R_f = 0.3) to yield **54** (247 mg, 0.60 mmol, 46%) as a transparent oil that solidifies in the fridge ^{1}H NMR ($CDCl_3$, 300 MHz): δ 1.45 (s, 9H), 1.50 (m, 2H), 1.89 (m, 2H), 3.20 (dd, *J* = 8.5, 6.7 H , 2H), 4.07(t, *J* = 6.8 Hz, 2H), 4.90 (s, 2H), 5.06 (s, 1H), 5.57 (s, 2H), 7.26-7.52 (m, 5H), 7.59 (s, 1H); ^{13}C NMR ($CDCl_3$, 75 MHz): δ 26.6 (CH_2), 27.3 (CH_2), 28.5 (CH_3) , 39.7 (CH_2), 42.8 (CH_2), 68.0 (CH_2), 79.0 (CH_2), 80.3 (C_q), 115.6 (C_q), 127.9 (C_q), 128.2 (CH_2), 128.3 (CH_2), 136.6 (C_q), 154.1 (C_q), 156.1 (C_q), 159.2 (C_q), 161.0 (C_q); HRMS (TOF ESI$^+$): calcd for $C_{21}H_{30}N_6O_3$ [*M* + H]$^+$: 413.2296, found: 413.2277.

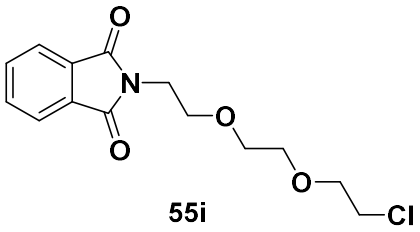

55i

Synthesis of 2-(2-(2-(2-chloroethoxy)ethoxy)ethyl)isoindoline-1,3-dione (55i):[180] Potassium phtalimide (1.0 g, 5.40 mmol) was resuspended in 1,2-bis(2-chloroethoxy)ethane (8.5 mL, 10.1 g, 54.0 mmol) under an Ar atmosphere and the mixture was heated at 130 °C for 48 h. The crude was cooled and purified by flash chromatography (Cyclohexane / AcOEt, 8:2 to 6:4, R_f = 0.2 in 6;4) to yield the **57** (957 mg, 3.3 mmol, 61%) as a transparent oil ^{1}H NMR ($CDCl_3$, 300 MHz): δ 3.54 (t, *J* = 5.4 Hz, 2H), 3.56-3.70 (m, 6H), 3.75 (t, *J* = 5.6 Hz,2H), 3.91 (t, *J* = 5.6 Hz, 2H), 7.73-7.75 (m, 2H), 7.84-7.86 (m, 2H); ^{13}C NMR (APT, $CDCl_3$, 75 MHz): δ 37.3 (CH_2), 42.7 (CH_2), 68.0 (CH_2), 70.1 (CH_2), 70.6 (CH_2), 71.4 (CH_2), 123.3 (CH), 132.1 (CH), 133.9 (C_q), 168.2 (C_q); MS (ESI$^+$): *m/z* (%): 298.3 (10) [*M* + H]$^+$, 174.2 (100) [*M* - $C_4H_8ClO_2$] $^+$.

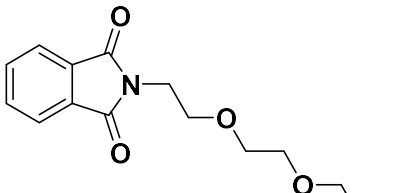

55

Synthesis of 2-(2-(2-(2-Iodoethoxy)ethoxy)ethyl)isoindoline-1,3-dione (55):[180] Compound **55i** (200 mg, 0.67 mmol) and NaI (252 mg, 2.67 mmol) were dissolved in dry MeCN (4 mL) under an Ar atmosphere and refluxed for 24 h. The reaction was quenched by addition of H_2O (10 mL) and the mixture was extracted with AcOEt (4 x 10 mL). The organic layer were pooled, dried over Na_2SO_4, filtered and concentrated under vacuum to yield compound **55** (251 mg, 0.64 mmol, 96%) as a yellow oil . ^{1}H NMR ($CDCl_3$, 300 MHz): δ 3.17 (t, *J* = 6.9 Hz, 2H), 3.60-3.68 (m, 6H), 3.76 (t, *J* = 5.7 Hz, 2H), 3.91 (t, *J* =5.7 Hz, 2H), 7.71- 7.73 (m, 2H), 7.83-7.87 (m, 2H); ^{13}C NMR ($CDCl_3$, 75 MHz): δ 3.0 (CH_2), 37.4 (CH_2), 68.1 (CH_2), 70.2 (CH_2), 70.3 (CH_2), 72.1 (CH_2), 123.4 (CH), 132.3 (CH), 134.1 (C_q), 168.4 (C_q); MS (ESI$^+$): *m/z* (%) 412.2 (5) [*M* + Na]$^+$, 390.2 (30) [*M* + H]$^+$, 362.1 (40) [*M* - I]$^+$, 174.2 (100) [*M* - $C_4H_8IO_2$] $^+$

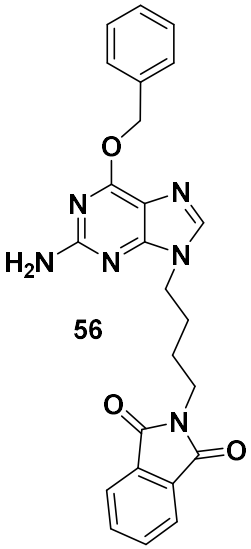

56

Synthesis of 2-(4-(2-amino-6-(benzyloxy)-9*H*-purin-9-yl)butyl)isoindoline-1,3-dione, (59): O^6BG (1.5 g, 6.24 mmol) and Cs_2CO_3 (3.0 g, 9.30 mmol) were resuspended in dry DMF (20 mL) under an Ar atmosphere and the mixture was stirred for 10 minutes. 2-(4-bromobutyl)isoindoline-1,3-dione – (1.9 g, 6.81 mmol) was added and the reaction was stirred at room temperature for 24 h. The reaction was quenched by addition of H_2O (10 mL) and extracted with AcOEt (3 x 100 mL), the organic layers were pooled, dried over Na_2SO_4, filtered and concentrated under vacuum. The crude was purified by flash chromatography (DCM / MeOH, 98:2, R_f = 0.14) to obtain **56** (1.9 g, 4.22 mmol, 68%) as a white solid. ^{1}H NMR ($CDCl_3$, 300 MHz): δ 1.72 (m, 2H), 1.90 (m, 2H), 3.75 (t, *J* = 7.3 Hz, 2H), 4.11 (t, *J* = 7.0 Hz,2H), 4.84 (s, 2H), 5.56 (s, 2H), 7.29-7.35 (m, 3H), 7.50 (m, 2H), 7.60 (s, 1H), 7.72 (dd, *J*= 5.4, 3.0 Hz, 2H), 7.83 dd, *J* = 5.4, 3.0 Hz, 2H); ^{13}C NMR ($CDCl_3$, 75 MHz): δ : 25.6 (CH_2), 27.2 (CH_2), 37.0 (CH_2), 42.8 (CH_2),

67.9 (CH_2), 115.6 (C_q), 123.3 (CH, 2C), 127.9 (CH), 128.2 (CH), 128.4 (CH), 132.0 (CH), 134.0 (CH), 136.5 (C_q), 139.4 (CH), 154.1 (C_q), 159.1 (C_q), 161.0 (C_q), 168.4 (C_q); MS (ESI^+): *m/z* (%) 443.3 (100) [*M* + H]$^+$;purity (HPLC): 96%; HRMS (ESI^+ TOF) calcd for $C_{24}H_{23}N_6O_3$ [*M* + H]$^+$: 443.1832, found: 443.1819.

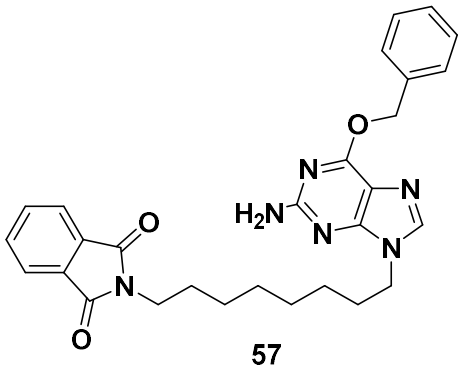

57

2-(8-(2-Amino-6-(benzyloxy)-9H-purin-9-yl)octyl)isoindoline-1,3-dione (57): O^6BG (1.0 g, 4.14 mmol) was dissolved in dry DMF (20 mL) under an Ar atmosphere and the reaction was cooled to 0 °C. Cs_2CO_3 (2.0 g, 6.14 mmol) and 2-(8-bromooctyl)isoindoline-1,3-dione (1.7 g, 4.91 mmol) were added portion wise. The reaction was kept on an ice bath for 8 hours and then it stirred for a total of 24 h. The reaction was quenched by the addition of H_2O (40 mL), extracted with AcOEt (6 x 40 mL), the organic layers were pooled, dried over Na_2SO_4, filtered and rotovaporated. The crude was purified by flash chromatography (DCM / EtOH, 99:1 to 97:3, R_f = 0.36 and 0.28 in 95:5 for each isomer respectively. Isomers N^9 and N^7 were assigned according to HMBC experiments. Isomer N^9 (998 mg, 2.01 mmol, 48 %) was obtained as a white solid. ^{1}H NMR ($CDCl_3$,300 MHz): δ : 1.32 (m, 8H), 1.66 (m, 2H), 1.82 (m, 2H), 3.67 (t, *J* = 7.2 Hz, 2H), 4.03 (t, *J* = 7.2 Hz, 2H), 4.86 (s, 2H), 5.56 (s, 2H), 7.32-7.37 (m, 3H), 7.50-7.52 (m, 2H), 7.59 (s, 1H),7.69 -7.72 (2H), 7.81-7.85 (m, 2H); ^{13}C NMR ($CDCl_3$, 75 MHz): δ 26.6 (CH_2), 26.8 (CH_2), 28.6 (CH_2), 28.9 (CH_2), 29.0 (CH_2), 29.9 (CH_2), 38.1 (CH_2), 43.6 (CH_2), 68.1 (CH_2), 115.8 (CH), 123.3 (CH), 128.0 (CH), 128.4 (CH), 128.5 (CH), 132.2 (C_q), 133.9 (CH), 136.7 (C_q), 139.6 (CH),154.3 (C_q), 159.2 (C_q), 161.1 (C_q), 168.6 (C_q); MS (ESI^+): *m/z* (%): 499.4 (100) [*M* + H]$^+$ (100).Isomer N^7 (608 mg, 1.21 mmol, 24%) was obtained as a white solid. ^{1}H NMR ($CDCl_3$, 300 MHz): δ 1.18-1.22 (m, 4H), 1.23-1.25 (m, 4H), 1.64 (dd, *J* = 7.3 Hz, 6.7 Hz, 2H), 1.75 (dd, *J* = 7.3, 7.1 Hz, 2H), 3.66 (t, *J* = 7.3 Hz, 2H), 4.12 (t, *J* = 7.3 Hz, 2H), 4.98 (s, 2H), 5.5 (s, 2H), 7.35-7.45 (m, 5H), 7.39-7.71 (dd, *J* = 5.4 Hz, 3.1 Hz, 2H), 7.74 (s, 1H), 7.82 (dd, *J* = 5.4 Hz, 3.1 Hz, 2H); ^{13}C NMR ($CDCl_3$, 75 MHz): δ 26.3 (CH), 26.7 (CH_2), 28.5 (CH_2), 28.8 (CH_2), 28.9 (CH_2), 31.3 (CH_2), 37.9 (CH_2), 47.6 (CH_2), 68.1 (CH_2), 107.1 (C_q), 123.2 (CH) 128.2 (CH), 128.4 (CH), 128.7 (CH), 132.2 (C_q), 133.9 (CH), 136.1 (C_q), 144.6 (CH), 157.1 (C_q), 159.2 (C_q), 164.1 (C_q), 164.4, (C_q);MS (ESI^+): *m/z* (%): 499.4 (100) [*M* + H]$^+$ (100).

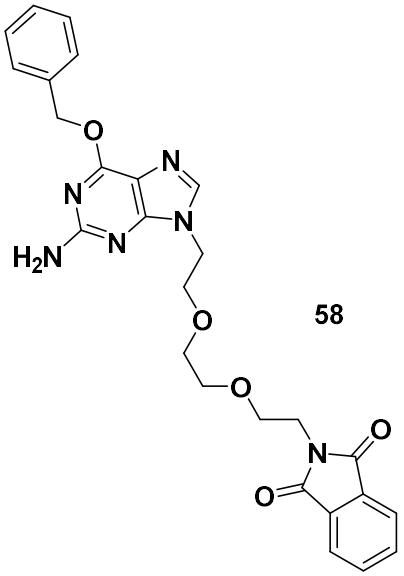

58

2-(2-(2-(2-(2-Amino-6-(benzyloxy)-9*H*-purin-9-yl)ethoxy)ethoxy)ethyl)isoindoline-1,3-dione, (58): O^6BG (366 mg, 1.52 mmol) was dissolved in dry DMF (14 mL) under an Ar atmosphere. The reaction was cooled to 0 °C on an ice bath and Cs_2CO_3 (731 mg, 1.52 mmol) and compound **55** (708 mg, 1.82 mmol, in 6 mL of DMF) were added portion wise. The reaction mixture was stirred at 0°C for 8 h and then at room temperature for a total of 24 h. The reaction was quenched by adding H_2O (40 mL) and the mixture was extracted with AcOEt (6 x 40 mL). The organic layers were pooled, dried over Na_2SO_4, filtered and concentrated under vacuum. The crude was purified by flash chromatography (DCM / EtOH, 99:1 to 96:4 , R_f = 0.4 and 0.17 in 98:2 for both isomers respectively. N^9 isomer (277 mg, 0.55 mmol, 36 %) was obtained as a sticky oil. ^{1}H NMR ($CDCl_3$, 300 MHz) : δ 3.53 (m, 2H), 3.58 (m, 2H), 3.70 (m, 4H), 3.88 (t *J* = 5.6 Hz, 2H), 4.16 (t, *J* = 4.9 Hz, 2H), 4.85 (s, 2H), 5.56 (s, 2H), 7.26-7.29 (m, 3H), 7.49-7.52 (m, 2H), 7.69-7.772 (m, 3H), 7.82-7.85 (m, 2H); ^{13}C NMR ($CDCl_3$, 75 MHz): δ 37.2 (CH_2), 43.3 (CH_2), 68.0 (CH_2), 68.1 (CH_2), 69.3(CH_2), 70.0 (CH_2), 70.6 (CH_2), 115.4 (C_q) 123.3 (CH, 2C), 127.9 (CH), 128.3 (CH), 128.4 (CH), 132.1 (C_q), 136.6 (C_q), 140.6 (CH), 154.1 (C_q), 159.1 (C_q), 160.9 (C_q), 168.3 (C_q); MS (ESI^+): m/z (%): 503.4 (100) $[M + H]^+$. Isomer N^7 (280 mg, 0.56 mmol, 37%) was obtained as a sticky oil. ^{1}H NMR ($CDCl_3$, 300 MHz): δ 3.41 (dd, *J* =5.6 Hz, 3.0 Hz, 2H), 3.5 (dd, *J* =5.6 Hz, 3.0 Hz, 2H), 3.68 (m, 4H), 3.84 (t, *J* = 5.4 Hz, 2H), 4.29 (t, *J* = 5.7 Hz, 2H), 4.9 (s, 2H), 5.5 (s, 2H), 7.35-7.44 (m, 5H), 7.67-7.69 (m, 2H),7.79-7.83 (m, 2H), 7.85 (s, 1H); ^{13}C NMR ($CDCl_3$, 75 MHz): δ 37.2 (CH_2), 47.2 (CH_2), 68.0 (CH_2), 69.8 (CH_2), 69.9 (CH_2), 70.6 (CH_2, 2C), 106.8 (C_q), 123.2 (CH), 128.1 (CH), 128.3 (C_q), 128.6 (CH),132.1 (CH), 133.9 (CH), 136.2 (C_q), 145.9 (CH), 157.1 (C_q), 159.1 (C_q), 164.1 (C_q), 166.8 (C_q); MS (ESI^+): *m/z* (%) 503.4 (100) $[M + H]^+$.

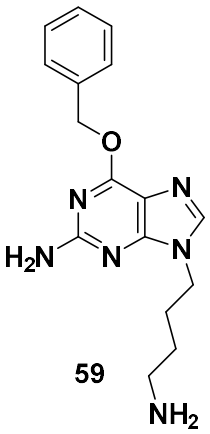

59

Synthesis of 9-(4-aminobutyl)-6-(benzyloxy)-9*H*-purin-2-amine (59): Compound **56** (1.42 g, 3.19 mmol) was dissolved in EtOH (80 mL) together with hydrazine hydrate (1.59 g, 31.89 mmol, 1.55 mL). The mixture was heated at 65 °C for 2.5 h. The reaction cooled and filtrated. Dissolved in DCM (20 mL) and re filtrated. Then re purified by flash chromatography (DCM / MeOH / TEA, 85:15:1, R_f = 0.11) to yield compound **59** (815 mg, 2.61 mmol, 82%) as a white solid were which was immediately stored under Ar at – 20 °C. ^{1}H NMR ($CDCl_3$, 300 MHz): δ 1.42-1.52 (m, 2H), 1.84-1.95 (m, 4H), 2.73 (t, *J* = 6.9 Hz, 2H), 4.07 (t, *J* = 7.2 Hz, 2H), 4.90 (s, 2H), 5.56 (s, 2H), 7.30-7.52 (m, 5H), 7.59 (s, 1H). ^{13}C NMR ($CDCl_3$, 75 MHz): δ 27.7 (CH_2), 30.4 (CH_2), 41.5 (CH_2), 43.4 (CH_2), 68.0 (CH_2), 115.6 (C_q), 127.9 (CH), 128.8 (CH), 128.4 (CH), 136.5 (C_q), 139.4 (CH), 154.2 (C_q), 159.0 (C_q), 161.0 (C_q); MS (ESI$^+$): *m/z* (%): 313.2 (60) [*M* + H]$^+$, 152.2 (100) [M -$C_{10}H_{16}N_1$]$^+$; purity (HPLC): 100%; HRMS (ES$^+$ TOF) calcd for $C_{16}H_{21}N_6O$ [*M* + H]$^+$: 313.1777, found: 317.1786.

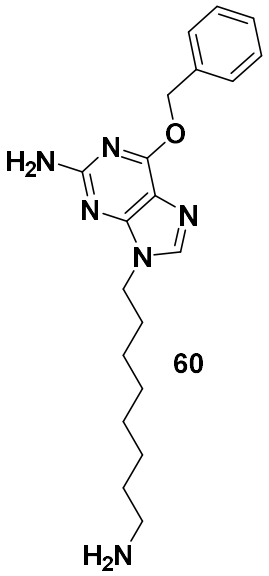

60

9-(8-Aminooctyl)-6-(benzyloxy)-9*H*-purin-2-amine (60): Compound **57** (400 mg, 0.80 mmol) was dissolved in EtOH (10 mL) together with hydrazine hydrate (400 mg, 0.80 mmol, 382 μL). The mixture was at 65 °C for 1 h and cooled down. The white solid was filtered and washed with DCM (2 x 10 mL).

The eluate was concentrated under vacuum, the corresponding eluate was re suspended in DCM (20 mL) filtered, washed with DCM again (2 x 10 mL) and concentrated under vacuum to yield compound **60** (278 mg, 0.75 mmol, 94%) as a sticky yellow oil. ^{1}H NMR ($CDCl_3$, 300 MHz): δ 1.26 (m, 8H), 1.38-1.40 (m, 2H), 1.78-1.83 (m, 2H), 2.09 (bp, 2H), 2.63 (t, *J* = 7.0 Hz, 2H), 4.01 (t, *J* = 7.2 Hz, 2H), 5.14 (s, 2H), 5.55 (s, 2H), 7.23-7.31 (m, 3H), 7.48-7.50 (m, 2H), 7.58 (s, 1H), ^{13}C NMR (APT, $CDCl_3$, 75 MHz) : δ 26.4 (CH_2), 26.6 (CH_2),28.9 (CH_2), 29.1 (CH_2), 29.7 (CH_2), 33.4 (CH_2), 41.9 (CH_2), 43.4 (CH_2), 67.9 (CH_2) ,115.5 (C_q), 127.9 (CH), 128.1 (CH), 128.3 (CH), 136.5 (C_q), 139.4 (CH), 154.1 (C_q), 159.2 (C_q), 160.9 (C_q), MS (ESI^+): *m/z* (%): 369.2 (100) $[M + H]^+$.

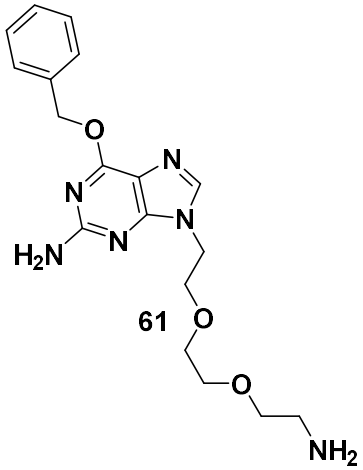

9-(2-(2-(2-aminoethoxy)ethoxy)ethyl)-6-(benzyloxy)-9*H*-purin-2-amine, (61): Compound **58** was dissolved (277 mg, 0.55 mmol) in EtOH (8 mL) together with hydrazine hydrate (315 mg, 6.1 mmol, 300 μL). The reaction was heated for 1 h at 65 °C and cooled to room temperature. The white solid was filtered and washed with DCM (2 x 10 mL). The eluate was concentrated under vacuum and re suspended in DCM (20 mL) filtered, washed with DCM again (2 x 10 mL) and concentrated under vacum to yield compound **61** (195 mg,0.52 mmol, 95%) as a sticky oil. ^{1}H NMR ($CDCl_3$, 300 MHz): δ 2.11 (bp, 2H), 2.84 (t, *J* = 5.2 Hz, 2H), 3.38 (t, *J* = 5.2 Hz, 2H), 3.5 (m, 4H), 3.79 (t, *J* = 5.1 Hz, 2H), 4.24 (t, *J* = 5.1 Hz, 2H), 4.94 (s, 2H), 5.56 (s, 2H), 7.30-7.33 (m, 3H), 7.49-7.52 (m, 2H), 7.76 (s, 1); ^{13}C NMR APT ($CDCl_3$, 75 MHz): δ 41.7 (CH_2), 43.4 (CH_2), 68.1 (CH_2), 69.4 (CH_2), 70.3 (CH_2), 70. (CH_2), 73.3 (CH_2), 115.4 (C_q), 128.0 (CH), 128.4 (CH), 128.5 (CH), 136.6 (CH), 140.6 (C_q), 154.2 (C_q), 159.1 (C_q), 161.0 (C_q); MS (ESI^+): *m/z* (%) 373.3 (100) $[M + H]^+$.

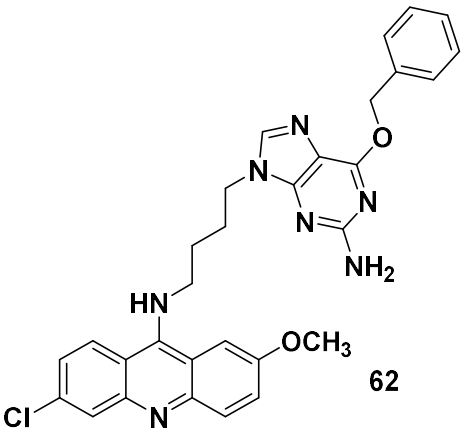

62

***N*-(4-(2-amino-6-(benzyloxy)-9*H*-purin-9-yl)butyl)-6-chloro-2-methoxyacridin-9-amine (62):** Compound **59** (200 mg, 0.64 mmol) and **28** (195 mg, 0.58 mmol) were dissolved in dry pyridine (5 mL) under an Ar atmosphere and the mixture was refluxed for 24 h. The solvent removed and the crude was purified three times flash chromatography (DCM / MeOH, 99:1 to 93:7, R_f = 0.12 in 93:7) to yield compound **62** (200 mg, 0.36 mmol, 56%) as an orange solid. ^{1}H NMR ($CDCl_3$, 300 MHz): δ 1.26 (s, 1H), 1.82 (m, 2H), 1.98 (m, 2H), 3.79 (m, 2H), 3.88 (s, 3H), 4.12 (t, *J* = 6.7 Hz, 1H), 4.87 (s, 2H), 5.56 (s, 2H), 7.23-7.35 (m, 6H), 7.51 (m, 2H), 7.5 (s, 1H), 7.97 (m, 2H), 8.0 (d, *J* = 1.3 Hz, 1H); ^{13}C NMR (APT, $CDCl_3$, 75 MHz): δ 27.5 (CH_2), 28.7 (CH_2), 43.1 (CH_2), 50.0 (CH_2), 68.1 (CH_3), 68.1 (CH_2), 99.2 (CH), 115.8 (C_q), 116.2 (C_q), 118.4 (C_q), 124.1 (CH), 124.7 (CH), 124.9 (CH), 128.2 (CH), 128.4 (CH), 128.5 (CH), 131.2 (CH), 135.1 (C_q), 136.5 (C_q), 139.3 (CH), 143.6 (C_q), 149.7 (C_q),154.2 (C_q),156.3 (C_q), 159.3 (C_q) ,161.3 (C_q,); MS (ESI$^+$): *m/z* (%) 554.3 (60) [*M* + H]$^+$, 464.2 (100) [*M* - Bn]$^+$, purity (HPLC): 95%; HRMS (ESI$^+$ TOF) calcd for $C_{30}H_{29}ClN_7O_2$ [*M* + H]$^+$: 554.2071, found: 554.2060.

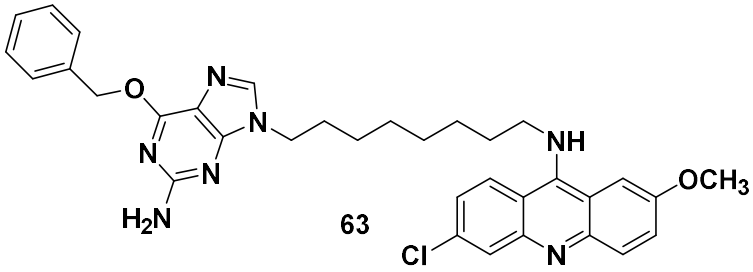

63

***N*-(8-(2-amino-6-(benzyloxy)-9*H*-purin-9-yl)octyl)-6-chloro-2-methoxyacridin-9-amine (63):** Compound **60** (278 mg, 0.75 mmol) and compound **28** (295 mg, 0.89 mmol) were dissolved in dry pyridine (10 mL) under an Ar atmosphere and the sample was refluxed for 24 h. The solvent was removed and the crude purified two times by flash chromatography (DCM / MeOH, 98:2 to 95:5, R_f = 0.16 in 95: 5) to yield compound **63** (123 mg, 0.20 mmol, 25%) as an orange solid. ^{1}H NMR (CD_3OD, 300 MHz): δ 1.15-1.30 (m, 10 H), 1.72-7.76 (m, 4H), 3.79 (t, *J* = 7.1 Hz, 2H), 3.93 (s, 3H), 4.02 (t, *J* = 7.1 Hz, 2H), 5.5 (s, 2H), 7.25-7.35 (m, 4H), 7.40 (dd, *J* = 2.6, 9.2 Hz, 1H), 7.46-7.48 (m, 2H), 7.5 (d, *J* = 2.6 Hz, 1H), 7.76-7.81 (m, 3H), 8.23 (d, *J* = 9.2 Hz, 1H); ^{13}C NMR (APT, CD_3OD ,75 MHz): δ : 27.3 (CH_2), 27.7 (CH_2), 29.9 (CH_2), 30.0 (CH_2), 30.6 (CH_2), 31.8 (CH_2), 44.5 (CH_2), 56.2 (CH_3), 68.9 (CH_2), 101.6 (CH), 115.2

(C_q), 117.9 (C_q), 125.3 (CH), 125.7 (CH), 128.8 (CH), 126.4 (CH), 127.4 (CH), 129.0 (CH), 129.3 (CH), 129.4 (CH), 137.2 (C_q), 137.9 (C_q), 141.2 (CH), 145.4 (C_q), 148.2 (C_q), 153.7 (C_q), 155.1 (C_q), 157.3 (C_q), 161.6 (C_q), 162.0 (C_q). MS (ESI^+): *m/z* (%) 610.4 (40) $[M + H]^+$, 520.4 (100) $[M - Bn]^+$; purity (HPLC): 98%; HRMS (ESI^+ TOF) calcd for $C_{34}H_{37}ClN_7O_2$ $[M + H]^+$: 610.2697, found: 610.2725.

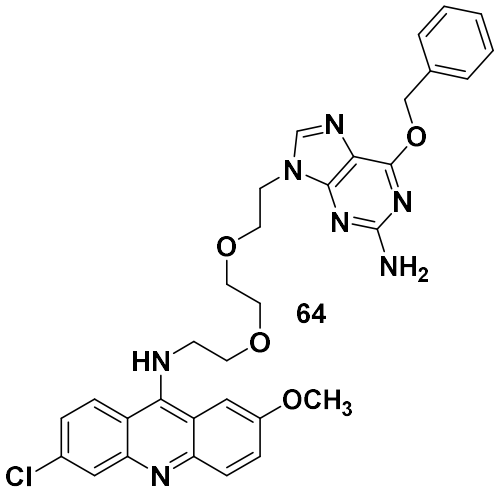

***N*-(2-(2-(2-(2-amino-6-(benzyloxy)-9H-purin-9-yl)ethoxy)ethoxy)ethyl)-6-chloro-2-methoxyacridin-9-amine (64):** Compound **61** (195 mg, 0.52 mmol) and compound **28** (180 mg, 0.54 mmol) were dissolved in dry pyridine (8 mL) under an Ar atmosphere and the mixture was refluxed for 24 h. The solvent was removed and the crude purified two times by flash chromatography (DCM / MeOH, 98:2 to 95:5, R_f = 0.19 in 90:10) to yield compound **64** (91 mg, 0.15 mmol, 27%) as an orange solid. ^{1}H NMR (CD_3OD, 300 MHz): δ 3.55 (s, 4H), 3.63 (t, *J* = 5.1 Hz, 2H), 3.74 (t, *J* = 4.9 Hz, 2H), 3.85-7.87 (m, 5H), 4.43 (t, *J* = 4.9 Hz, 2H), 5.28 (s, 2H), 7.19-7.33 (m, 6H), 7.37-7.40 (m, 2H), 7.71-7.76 (m, 3H), 8.14 (d, *J* = 8.1 Hz, 1H). ^{13}C NMR (APT, CD3OD, 75 MHz) : δ 42.7 (CH_2), 49.1 (CH_2), 54.9 (CH_3), 67.5 (CH_2), 68.4 (CH_2), 69.8 (CH_2), 69.9 (CH_2,2C), 100.4 (CH), 113.4 (C_q), 114.4 (C_q), 117.1 (C_q), 123.4 (CH), 123.9 (CH), 125.3 (CH), 125.8 (CH), 127.2 (CH), 127.6 (CH) , 127.8 (CH), 127.9 (CH,), 136.1 (C_q), 136.3 (C_q), 140.4 (CH), 143.4 (C_q), 145.8 (C_q), 152.6 (C_q), 153.6 (C_q), 156.0 (C_q), 160.1 (C_q), 160.4; MS (ESI^+): *m/z* (%) 614.3 (50) $[M + H]^+$, 524.3 (100) $[M – Bn]^+$ (100); purity (HPLC): 96%; HRMS (ESI^+ TOF) calcd for $C_{34}H_{37}ClN_7O_2$ $[M + H]^+$: 614.2283, found: 614.2341.

7.1.3 Photocaged molecules

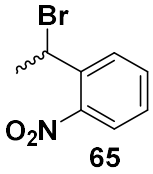

65

Synthesis of 1-(1-bromoethyl)-2-nitrobenzene (65):[222] In cyclohexane (35 mL), 1-ethyl-2-nitrobenzene (1.00 g, 6.60 mmol, 891 µL) was refluxed with BPO (16 mg, 0.06 mmol) and NBS (1.49 g, 8.37 mmol) for 6 h. The reaction was cooled and filtrated, the eluate concentrated under vacuum and

purified by flash cromatograph (SiO_2, eluent: Cyclohexane, R_f = 0.3) to yield compound **65**(218 mg, 0.95 mmol, 14%) as a brown liquid. ^{1}H NMR ($CDCl_3$, 300 MHz): δ 2.1 (d, *J* = 6.8 Hz, 3H), 5.81 (q, *J* = 6.8 Hz, 1H), 7.40 (dd, *J* = 8.3 Hz, 1.2 Hz, 1H), 7.62 (dd, *J* = 7.3 Hz, 1.1 Hz, 1H), 7.83 (dd, *J* = 8.3 Hz, 1.2 Hz, 1H), 7.88 (dd, *J* = 7.3 Hz, 1.1 Hz, 1H).

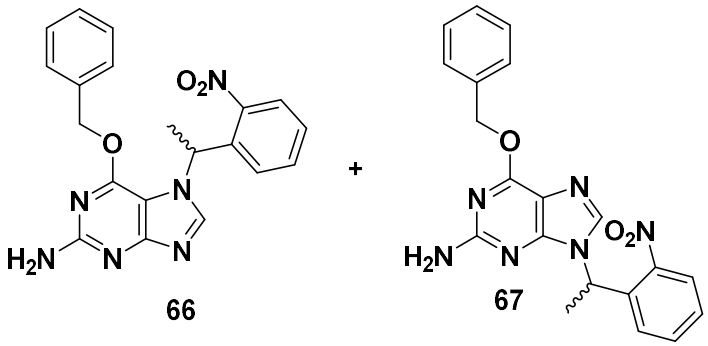

Synthesis of 6-(benzyloxy)-7-(1-(2-nitrophenyl)ethyl)-7*H*-purin-2-amine (66) and 6-(benzyloxy)-7-(1-(2-nitrophenyl)ethyl)-9*H*-purin-2-amine (67) and: Under an Ar atmosphere O^6BG (175 mg, 0.72 mmol and K_2CO_3 (300 mg, 2.17 mmol) were re suspended in dry DMF (0.5 mL) and stirred for 10 minutes. Compound **72** (200 mg, 0.87 mmol) was dissolved in dry DMF (2 mL) and added to the mixture and the reaction was stirred at room temperature for 24 h. Then H_2O (50 mL) was added and the reaction was extracted with AcOEt (3 x 40 mL). The organic layers were pooled over Na_2SO_4, filtered and concentrated under vacuum. The crude was purified by flash chromatography (SiO_2, eluent: DCM / EtOH, 100:0 to 90:10, R_f= 0.5 and 0.25 for N^9 and N^7 isomers in a 90:10 system respectively).. Isomer N^7, compound **66**, was obtained (88 mg, 0.22 mmol, 31%) as a white solid. ^{1}H NMR ($CDCl_3$, 300 MHz): δ 2.0 (d, *J* = 6.9 Hz, 2H), 4.84 (s, 2H), 5.25 (dd, *J* = 19.0, 12.0 Hz, 2H), 6.43 (d, *J* = 6.9 Hz, 2H), 6.81 (dd, *J* = 7.6, 1.1 Hz, 1H), 7.10-7.13 (m, 2H), 7.25-7.27 (m, 3H), 7.35 (dt, *J* = 7.8, 1.2 Hz, 1H), 7.45 (dt,J = 7.6 Hz, 1.1 Hz, 1H) 7.88 (dd, *J* = 7.6 Hz, 1.1 Hz, 1H), 8.11 (s, 1H);^{13}C NMR: 20.1 (CH_3), 53.4 (CH) , 67.6 (CH_2), 107.2 (C_q) , 125.0 (CH), 126.6 (CH), 128.2 (CH), 128.4 (CH), 128.5 (CH), 128.6 (CH), 134.1 (CH), 135.8 (C_q),137.9 (C_q), 142.2 (CH), 147.3 (C_q), 157.1 (C_q), 159.2 (C_q), 164.3 (C_q); MS (ESI$^+$): *m/z* (%) 391.2 (100) [*M* + H]$^+$; Purity (HPLC): 98%. Isomer N^9, compound **67**, was obtained (119 mg, 0.30 mmol, 42%) as a white solid. ^{1}H NMR ($CDCl_3$, 300 MHz): δ 2.02 (d, *J* = 7.1 Hz, 3H), 4.76 (s, 2H), 5.53 (dd, *J* = 12.4, 1.9 Hz, 2H), 6.33 (q, *J* =7.1 Hz, 1H), 7.25-7.51 (m, 8H), 7.85 (s, 1H), 7.98 (dd, *J* = 1.2, 8.0 Hz, 1H); ^{13}C NMR ($CDCl_3$, 75 MHz): δ: 20.4 (CH_3), 49.5 (CH) , 68.0 (CH_2), 115.9 (C_q), 124.9 (CH), 127.5 (CH), 128.0 (CH) ,128.3 (CH), 128.4 (CH), 128.7 (CH), 133.7 (CH), 136.3 (CH), 136.5 (C_q, 2C), 137.0 (CH), 147.4 (C_q), 154.0 (C_q), 159.1 (C_q), 160.9 (C_q); MS (ESI$^+$): *m/z* (%) 391.2 (100) [*M* + H]$^+$; purity (HPLC): 98%.

7.1.4 MGMT.abasic sites hybrids

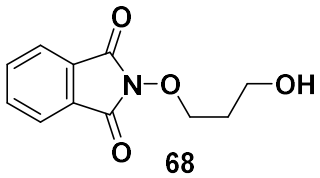

68

Synthesis of 2-(3-hydroxypropoxy)isoindoline-1,3-dione (68):[228] 1,3 propanediol (1.00 g, 13.14 mmol, 951 µL), *N*-hydroxyphtalimide (714 mg, 4.34 mmol) and PPh_3 (1.20 g, 4.57 mmol) were dissolved under an Ar atmosphere in dry THF (20 mL) and the reaction was cooled to 0 °C and DIAD (979 mg, 4.84 mmol, 960 µL) were added dropwise. The reaction was stirred at room temperature for 48 h, solvent was removed under vacuum and the excess of TPPO was removed as described.[238] The crude was purified by flash chromatography (SiO_2, eluent: Cyclohexane / AcOEt, 50:50, R_f = 0.5) to yield compound **68** (570 mg, 2.58 mmol, 26%) as a white sticky solid. ^{1}H NMR ($CDCl_3$, 300 MHz) δ: 2.17 (m, 2H), 4.29-4.36 (m, 4H), 7.75-7.80 (m, 4H); ^{13}C NMR ($CDCl_3$, 75 MHz) δ: 29.6 (CH_2), 60.7 (CH_2), 75.0 (CH_2), 123 (CH), 129.1 (C_q), 134.7 (CH), 163.9 (C_q); MS (ESI$^+$): *m/z* (%) 222.2 (100) [*M* + H]$^+$, 204.2 (60) [*M* – OH]$^+$.

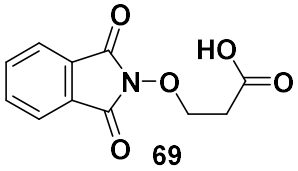

69

Synthesis 3-((1,3-dioxoisoindolin-2-yl)oxy)propanoic acid (69): Method A[228]: Compound **68**(483 mg, 2.18 mg) were dissolved in a mixture of MeCN / H_2O (5:1, 12 mL) and cooled to 0 °C. TEMPO (68 mg, 0.44 mmol) and BAIB (1.72 g, 5.34 mmol) were added portion wise and the reaction was stirred for 48 h at room temperature. Then DCM (10 mL) was added and the organic layers were extracted with aq. $NaHCO_3$ (10% , 2 x 30 mL). The aqueous layers were acidified with aq HCl (5%) to pH 2 and extracted with DCM (3 x 20 mL). The organic layers were pooled, dried over Na_2SO_4, filtered and concentrated under vacuum to yield compound **69** as a white solid (77 mg, 0.33 mmol, 15%). ^{1}H NMR (D_2O, 300 MHz): δ 2.87 (t, *J* = 5.3 Hz, 2H), 4.50 (t, *J* = 5.3 Hz, 2H), 7.85 (s, 4H);^{13}C NMR (D_2O, 75 MHz): δ 33.3 (CH_2), 73.6 (CH_2), 123.7 (CH), 128.4 (C_q), 135.1 (CH), 146.7 (C_q); MS (ESI$^+$) *m/z* (%) 258.3 (5) (*M* + Na]$^+$, 236.2 [*M* + H]$^+$, 218.1 (100) [*M* – OH]$^+$. Method B: A mixture of $NaIO_4$ (70 mg, 0.327 mmol) and $RuCl_3$ (2 mg, 0.06 mmol) in MeCN / H_2O (0.6:1.4, 2 mL) was stirred vigorously for 1 h at room temperature. The mixture was added to a solution at 0 °C of **68** (50 mg, 0.227 mmol) in MeCN (1 mL) and the reaction stirred for 5 h at room temperature. The reaction was diluted with AcOEt (15 mL) and extracted with aq. $NH_4Cl_{(sat)}$ (2 x 40 mL). The aqueous layers were extracted with AcOEt (1 x 15 mL), the organic layers were pooled and dried over Na_2SO_4 and filtrated two times through a pad of celite to yield compound **69** (42 mg, 0.179 mmol, 80%).

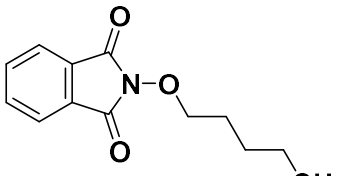

71

Synthesis of 2-(4-hydroxybutoxy)isoindoline-1,3-dione (71): 1,4 butanol (1.00 g, 11.10 mmol, 990 μL, *N*-hydroxyphtalimide (600 mg, 3.68 mmol) and PPh_3 (1.06 g, 4.04 mmol) were dissolved under an Ar atmosphere in dry THF (20 mL) and the reaction was cooled to 0 °C. DIAD (877 mg, 4.34 mmol, 860 μL) were added dropwise. The reaction was stirred at room temperature for 18 h, solvent was removed under vacuum and the excess of TPPO was removed as described.[238] The crude was purified by flash chromatography (SiO_2, eluent: Cyclohexane / AcOEt, 50:50, R_f = 0.5) to yield compound **71** (860 mg, 3.67 mmol, 33%) as a white sticky solid. ^{1}H NMR ($CDCl_3$, 300 MHz): δ 1.58 (bp, 1H), 1.74-1.73 (m, 4H), 3.69 (t, *J* = 5.8 Hz, 2H), 4.20 (t, *J* = 5.8 Hz, 2 H), 7.67-7.71 (m, 2H), 7.775-7.79 (m, 2H); MS (ESI$^+$): *m/z* (%) 236.1 (20) [*M* + H]$^+$, 218.2 (50) [*M* – OH]$^+$.

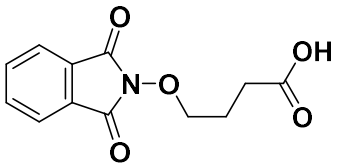

72

Synthesis of 4-((1,3-dioxoisoindolin-2-yl)oxy)butanoic acid (72): A mixture of $NaIO_4$ (1.60 g, 7.48 mmol) and $RuCl_3$ (30 mg, 0.14 mmol) in MeCN : H_2O (1:1.5, 25 mL) was stirred vigorously for 1 h at room temperature. The mixture was added to 0 °c solution of **71** (1.2 g, 5.10 mmol) in MeCN (15 mL), stirred for 3 h, when $RuCl_3$ (20 mg, 0.10 mmol) and $NaIO_4$ (1.00 g, 4.68 mmol) were added and the reaction was stirred for 3 h more at room temperature. The reaction was diluted with AcOEt (20 mL) and extracted with a mixture $NaHCO_3$:$Na_2S_2O_3$ (1:10, 40 mL). The aqueous layers were acidified with aq. HCl (5 %) to pH 2 and extracted with AcOEt (4 x 30 mL). The organic layers were pooled, dried over Na_2SO_4, filtered through a pad of celite and concentrated under vacuum to yield compound **72** (347 mg, 1.39 mmol, 27%). ^{1}H NMR ($CDCl_3$, 300 MHz): δ 2.11 (m, 2H), 2.64 (m, 2H), 4.20 (m, 2H), 7.76-7.84 (m, 4H); ^{13}C NMR ($CDCl_3$, 75 MHz): δ 23.4 (CH_2), 29.7 (CH_2), 60.3 (CH_2), 123.3 (CH), 129.6 (C_q), 137.5 (CH), 157.5 (C_q).

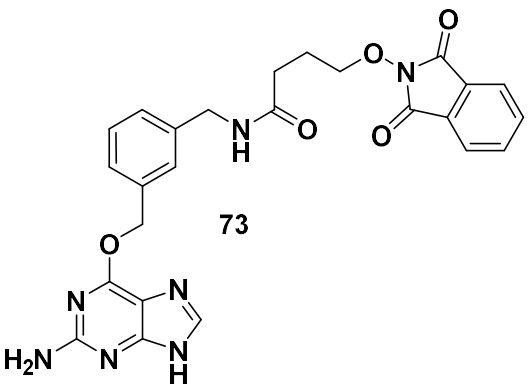

73

Synthesis of *N*-(3-(((2-amino-9H-purin-6-yl)oxy)methyl)benzyl)-4-((1,3-dioxoisoindolin-2-yl)oxy)butanamide (**73**): Compound **72** (150 mg, 0.60 mmol) was dissolved with HBTU (227 mg, 1.76 mmol) and HOBt (8 mg, 0.12 mmol) in dry DMF (3 mL) under an Ar atmosphere at 0°C. Compound **46** (135 mg, 0.50 mmol) was added and the mixture was stirred at room temperature of the acid with HBTU and HOBt under an Ar atmosphere at 0 °C. After 5 minutes aprox I add the amine and stirred at room temperature for 24 h. H_2O (15 mL) was added to the reaction and extracted with DCM / MeOH (90:10, 4 x 20 mL), washed with $K_2CO_{3\ (sat)}$ (1 x 10 mL) and H_2O (1 x 10 mL) dried over Na_2SO_4, filter and rotovap. The crude was purified by flash chromatography (SiO2, eluent : DCM:MeOH, 95:5 to 90:10). Compound **73** (45 mg, 0.09 mmol, Y = 15%) was obtained as a white solid. ^{1}H NMR (CD_3OD, 300 MHz): δ 1.30 (m, 1H), 2.05 (m, 2H), 2.53 (t, *J* = 7.2 Hz, 2H), 3.31 (s, 2H), 4.19 (t, *J* = 6.1 Hz, 2H), 4.41 (s, 2H), 5.49 (s, 2H), 7.24-7.35 (m, 3H), 7.44 (s, 1H), 7.51-7.90 (m, 5H); ^{13}C NMR (CD_3OD, 72 MHz): δ 25.5 (CH_2), 33.0 (CH_2);33.9 (CH_2); 43.9 (CH_2); 68.7 (CH_2); 68.8 (CH_2); 124.1 (CH); 128.1 (CH); 128.4 (C_q); 129.5 (CH); 129.6 (CH); 129.7 (CH); 131.2 (CH); 133.4 (CH); 135.7 (C_q); 140.4 (C_q); 161.3 (C_q); 165.1 (C_q); 175.1 (C_q); 175.4 (C_q); MS (ESI$^+$): *m/z* (%)502.3 (100) $[M+H]^+$, 1003.8. (5) $[2M+H]^+$.

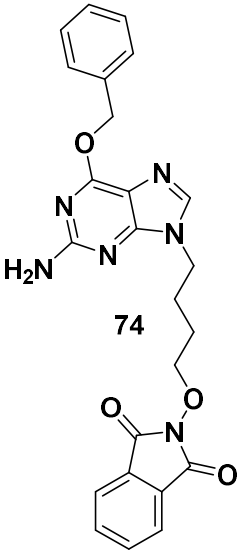

74

Synthesis of 2-(4-(2-amino-6-(benzyloxy)-9*H*-purin-9-yl)butoxy)isoindoline-1,3-dione (74): Under an Ar atmosphere O^6BG (500 mg, 2.07 mmol) and Cs_2CO_3 (1.00 g, 3.09 mmol) were re suspended in dry DMF (10 mL), the reaction was cooled to 0 °C and stirred for 10 minutes when 2-(4-bromobutoxy)isoindoline-1,3-dione (740 mg, 2.48 mmol) was added portion wise and the reaction as stirred at room temperature for 20 h. H_2O (10 mL) was added and the reaction was extracted with AcOEt (4 x 20mL), the organic layers were pooled, dried over Na_2SO_4 and concentrated under vacuum. The crude was purified by flash chromatography (SiO_2, eluent: DCM / EtOH, R_f = 0.2) to obtain the N^9 isomer **74** (258 mg, 0.56 mmol, 27%) as a white solid. ^{1}H NMR ($CDCl_3$, 300 MHz): δ (1.80 m, 2H) , 2.15 (m, 2H), 4.19 (t, *J* = 7.1 Hz, 2H), 4.26 (t, *J* = 6.1 Hz, 2H), 5.56 (s, 2H), 5.56 (s, 2H), 7.29-7.38 (m, 3H), 7.49-7.52 (m, 2H), 7.67 (s, 1H), 7.73-7.76 (m, 2H), 7.81-7.85 (m, 1H); ^{13}C NMR ($CDCl_3$, 75 MHz): δ 25.2 (CH_2), 26.5 (CH_2), 42.9 (CH_2), 67.9 (CH_2), 77.6 (CH_2), 115.7 (C_q), 123.6 (CH) 127.9 (CH), 128.2 (CH), 128.4 (CH), 128.9 (C_q), 134.6 (CH_2), 136.6 (C_q), 139.5 (CH), 154.3 (C_q), 159.2 (C_q), 161.0 (C_q), 163.6 (C_q); MS (ESI^+): *m/z* (%) 459.4 (100) $[M + H]^+$.

7.2 *In vitro* experiments

UV absorbance experiments

For **Chapter 2**, absorption spectras were recorded with a Cary 300 Bio double-beam spectrophotometer in quartz cells (1000 µL, 4 cm x 1 cm), scan rates of 300 nm/min and in compounds concentration concentrations ranging from 2-10 µM while DNA concentration was maintained constant at 10 µM, DMSO concentration was 1 % (v/v).

For **Chapter 3**, either for UV absorbance or of varied-temperature experiments were carried on a Cary 300 Bio double-beam spectrophotometers in quartz cells (1000 µL, 4 cm x 1 cm), scan rates of 300 nm/min and the concentration range of 10 µM with a maximum of 0.2% of DMSO**.** Otherwise, spectras

were recorded a Hitachi U2900 double-beam spectrophotometer, using scan speed of 100-200 nm/min using quartz cuvettes (1000 μL, 4 cm x 1 cm), scan rates of 100-300 nm/min on a range of 230-550 nm in different solvents. Compound concentration was 10 μM, DMSO concentration was 0.2 % (v/v). Hypochromism (*H*, %) values were determined as Equation (**3**)[181]:

$$H\ (\%) = 100*[1- (f\ Hybrid/(f\ O^6BG+ f\ Acr)] \quad (\mathbf{3})$$

being ƒ the oscillator strength values in the 260-315 nm region

pKa determination

Compounds were diluted in the Britton-Robbinson Buffer[105] (NaOAc, H_3PO_4, H_3BO_3 at 40 mM, pH 6.86) at 10 μM and were titrated by adding aq. HCl (2M, with compound at 10 μM to avoid dilution) or aq. NaOH (2M, with compound at 10 μM to avoid dilution). UV spectras were recorded with with a Cary 300 Bio double-beam spectrophotometer as described before. pKa was determined by plotting the pH *vs.* absorbance at λ = 334 nm and 300 nm for **14** or **15** respectively and calculated by a biphasic non-linear fitting curve (equation **4**) using GraphPad Prism 6:

Span=Top-Bottom (**4**)

Section1=Span*Frac/(1+10^((LogEC50_1-X)*nH1))

Section2=Span*(1-Frac)/(1+10^((LogEC50_2-X)*nH2))

Y=Bottom + Section1 +Section2

Bottom and **Top** are the plateaus at the left and right ends of the curve, in the same units as Y.

LogEC50_1 and **LogEC50_2** are the concentrations that give half-maximal stimulatory and inhibitory effects in the same units as X.

nH1 and **nH2** are the unitless slope factors or Hill slopes. Consider constraining these to equal 1.0 (stimulation) and -1 (inhibition).

Frac is the proportion of maximal response due to the more potent phase

DNA UV melting experiments

Single strand oligonucleotides (lyophillized, RP-HPLC grade) containing 17 base pairs (17 bp) were purchased from Eurogentec (Seraign, Belgium) as lyophilized powder and reconstituted in sterilized water to a final concentration of 100 μM according to the manufacturer's indications, and stored at –20 °C when not in use.

For **Chapter 2**, the sequence of each single strand is denoted below and are written from their 5' to its 3' ending

1. 17 bp TXG: GGG-TTA-CTO^{6}MeG-CGA-ACT-GG, X = X = THF, A, C and N = A, C, T, G, O^{6}MeG
2. 17 bp GCA: CCA-GTT-CGC-AGT-AAC-CC

Here single strands of the oligonucleotides were dissolved in buffer (10 mM Potassium Cacodylate pH 7.2, 10 mM KNO_3), and annealed by heating 5 minutes at 90 °C and then let reach room temperature for 3 h. Compounds of a 20 mM stock solution in DMSO are added and the solutions are mixed, then sonicated for 5 min in degas mode and then transferred to the cuvettes (400 μL, 4 cm x 1 cm). The experiments were carried on a 10 μM duplex concentration, with 0 to 300 μM of compounds, 6 μM for BrEt, DMSO concentration was 6 % (v/v).
Thermal denaturation profiles were recorded with a Cary 300 Bio spectrophotometer (Agilent) equipped with a thermoelectric temperature controller. The samples, containing oligonucleotides in the absence or in the presence of compounds were heated from 20 to 80 °C at a rate of 0.2 deg/min while the absorbance was monitored at 260/270 nm. The temperatures of DNA melting transitions were determined from the first-derivative plots of absorbance versus temperature.

For **Chapter 4**, (CT DNA, Invitrogen, 10 mg / mL) was diluted in ≈ 4-fold in buffer (10 mM Li Cacodylate, pH 7.2) and the precise was diluted and the precise concentration (4.2 mM base pairs, bp) was determined through A_{260} nm measurement using the extinction coefficient value of 12,824 $(cm.M)^{-1}$ concentration. Compounds of a 2 mM stock solution in DMSO are added and the solutions are mixed, then sonicated for 10 min in degas mode and then transferred to the cuvettes (1000 μL, 4 cm x 1 cm). The experiments were carried on a 12.5 μM CT DNA concentration, with 0 to 6.25 μM of ligand, DMSO concentration was 0.6 % (v/v). The temperatures of DNA melting transitions were determined from the first-derivative plots of absorbance versus temperature

DNA binding studies

Calf thymus DNA was diluted ≈ 5-fold in buffer (10 mM Li Cacodylate, 100 mM KCl , pH 7.2) and the precise concentration (3 mM base pairs, bp) was determined as before UV/Vis titrations were performed by titrating compound solutions (concentration 20 μM in the same buffer mentioned above, DMSO concentration 0.2 %) with solutions of CT DNA (3 mM) supplemented with 20 μM of the respective compound to avoid the dilution effects). After 5 min equilibration at room temperature,

spectra were recorded in the 350–500 nm range and binding isotherms were plotted as A / A_0 at 410 nm vs. c(CT DNA) and fitted to a One Site Binding model (equation **5**) in GraphPad Prism:

$$Y=B_{max} \times X / (Kd + X) \quad (\mathbf{5})$$

where X = c(CT DNA) and Kd is the equilibrium dissociation constant. The results represent the Kd values ± SD from three to five replicates.

Circular dichroism spectroscopy

CD spectra were recorded on a JASCO J-1500 spectropolarimeter. A 3 mL solution containing the compounds **Acr** or **62** (50 μM) and CT DNA (500 μM bp) in 10 mM $LiAsO_2Me_2$, 100 mM KCl buffer, pH 7.2, was prepared and spectra were recorded in quartz cuvettes (1 cm path length) in a 300–500 nm range (bandwidth: 2 nm, scanning speed: 100 nm min −1 , 8 scans per sample) at room temperature. Spectra were corrected by blank substraction

Fluorescence experiments

For **Chapter 2**, fluorescence spectras were recorded with a Cary Eclipse Spectrofluorimeter (Agilent) fluorimeter in quartz cells, slith widths of 5 nm and a scan rate of 120-600 nm/min with and the PMT was 550 V for the quantum yield determinations and the simple emission spectra and 800 V for the fluorescence titration. The excitation wavelength was between 280 and 380 nm and the concentration of the compound ranged from 2-10 μM while DNA concentration was maintained constant at 10 μM, DMSO concentration was 1 % (v/v).

For **Chapter 3** fluorescence spectras were recorder in a HORIBA JobinYvon Fluoromax-3 spectrofluorimeter using quartz cells at 1 μM compound concentration, λ_{exc} = 424 nm, IT 0.5 s, slith exc/em = 5 nm, DMSO concentration was 0.2% (v/v).

Quantum yields

For **Chapter 2**, quantum yields were determined as described before using Quinine Sulfate in 0.5 M H_2SO_4 (φ = 0.54),[183] in six different concentrations by triplicate on a range of 2 – 10 μM, DMSO concentration was 1 % (v/v), with the absorbance was maintained below 0.15.

For **Chapter 3**, quantum yield values were determined as described before using Coumarin 153 in EtOH (φ = 0.38) as a standard,[183] using a single point concentration at 10 μM of absorbance while the fluorescence was determined at 1 μM concentration for the compounds. DMSO concentration was 0.2 % (v/v).

Values were determined by plotting the Absorbance values *vs*. the integral of the emission spectra and using the equation (**6**):[239]

$$\varphi x = \varphi std(Gradx/Gradstd).(nx/nstd)^2 \qquad (\mathbf{6})$$

Where φx and φstd represent the quantum yields, Gradx and Gradstd the slopes of the plots and n the respective refractive index of each solvent for the compound (x) and the standard (std).

Ethidium bromide (BrEt) displacement assay:

Experiments were performed based on the already described protocols.[103] Briefly, BrEt solution in 10 mM $LiAsO_2Me_2$, 100 mM KCl buffer, pH 7.2 (1.13 µM, 44 µL), CT DNA solution in the same buffer (20 µM bp, 5 µL) and compound solution in DMSO (0–1 mM, 1 µL) were mixed in a 96-well half area black, flat-bottom NBS microplate (Corning 3993) and incubated for 30 min at room temperature in the dark. Fluorescence was measured on a microplate reader (CLARIOstarPlus , BMG Labtech) using excitation at 545 nm (bandwidth: 15 nm) and emission at 595 nm (bandwidth: 20 nm). Fluorescence intensity, corrected for the background fluorescence of BrEt in the absence of DNA, was plotted as a function of compound concentration. Results are the means from 3 to 5 independent titrations with their corresponding standard deviations

MGMT inhibition assays

DNA and protein stock solutions

Single strand oligonucleotides were purchased and reconstituted as before. The sequence of each single strand is denoted below and are written from their 5' to its 3' ending, in the corresponding case, a Cy3 fluorophore is attached on the 5' ending.

S1	Cy3-TAAAAGACTTC(O^6MeG)AAAAATTTTTAAAA
S2	TTTTAAAAATTTTTCGAAGTCTTTTA
S1'	Cy3-TAAAAGACTTCGAAAAATTTTTAAAA
Q1	GGGTTACT(O^6MeG)CGAACTGG
Q2	CCAGTTCGCAGTAACCC

For preparation of the O^6MeG-bearing substrate (S) or the non-methylated control (S') duplexes, the Cy3-labelled 26-mers S1 or S1' respectively (final concentration: 6.4 µM) were mixed with a slight excess of the unlabeled complementary strand S2 (final concentration: 7.0 µM) in a 10 mM Tris-HCl, 100 mM NaCl buffer (pH 8.5). For preparation of the unlabeled quencher (Q), the complementary 17-

mers Q1 and Q2 were mixed in the same buffer to give the final concentration of each strand of 15 µM. The duplexes were annealed as described before. CT DNA (10 mg/ mL) was diluted 20-fold with the same buffer and the precise concentration (700 µM, bp) was determined as before. Except from single stranded DNA, all solution were stored at + 4 °C covered from light.

MGMT protein synthesis

Recombinant human MGMT was produced and purified following a modification of the published protocol.[240] Human MGMT cDNA was digested with restriction endonucleases BamHI and XhoI and ligated into pET24 vector. *E. coli* STAR BL 21 pRare cells were transformed and grown at 37 °C in 1 L of Terrific Broth. Overexpression was induced with 0.25% arabinose and 0.5 mM IPTG at 20 °C overnight. The cells were harvested by centrifugation at 4000 × *g*, 4 °C for 15 min. The pellets were suspended in lysis buffer (glycerophosphate pH 7.6 50 mM, NaCl 80 mM, β-mercaptoethanol 8 mM, $MgCl_2$ 1 mM, *S. marcescens* nuclease (benzonase) 170 U μl^{-1}, 1X complete EDTA-free protease inhibitor cocktail). Cells were disrupted by passage through a T75 cell disruptor (Constant Systems, CellD). The resulting cell lysate was centrifuged at 43,000 × *g*, 4 °C for 1 h. Solid ammonium sulfate was added to the supernatant fraction to a final concentration of 25%. The mixture was stirred on ice for 15 min and left to stand on ice for 30 min. The precipitate was removed by centrifugation at 20,000 × *g*, 4 °C for 20 min. Additional ammonium sulfate was added to the supernatant to a final concentration of 55%. After a second centrifugation, the precipitate was redissolved in Buffer A (Tris-HCl pH 8.4 50 mM, EDTA 1 mM, β-mercaptoethanol 2 mM) and subjected to affinity chromatography on Toyopearl AF-Red (Tosoh Bioscience). The proteins were eluted in a buffer composed in Buffer A and NaCl (2 M). After an overnight dialysis (Spectra/Por 3, MWCO 3.5 kDa) against Buffer C (Tris-HCl 50 mM pH 8, EDTA 1 mM, glycerol 10%, DTT 1 mM, NaCl 20 mM), the eluate was loaded onto a Capto SP ImpRes ion exchange column (Cytiva) and eluted with a continuous gradient of NaCl (0.02 to 1 M) in the same buffer. The fractions containing MGMT were pooled, dialyzed and concentrated (Macrosep Pall, MWCO 3 kDa) with a buffer C (Tris-HCl 50 mM pH 8, EDTA 1 mM, glycerol 10%, DTT 1 mM, NaCl 500 mM) to a volume of about 3 mL, loaded onto a size exclusion chromatography column (HiLoad Superdex 75 pg, 26 × 600, Cytiva) and eluted with buffer C. The fractions containing the protein were collected. The purity of the protein was visualized on a 4–20% SDS-PAGE. The protein concentration (8 µM) was determined by $OD_{280\ nm}$ measurement. The enzyme was stored at –80 °C.

Coupled enzymatic assay

Stock solutions of compounds were prepared in DMSO at a 10 mM concentration. DNA solutions were prepared daily in a 10 mM Tris-HCl, 100 mM NaCl buffer (pH 8.5) and supplemented with DTT (final concentration: 1 mM). For the competition assay, compounds solutions (diluted with buffer to 25 µM, 3 µL) or DMSO control (1:400 in buffer) were mixed with the substrate S (1.2 µM, 1 µL), placed in a thermostat at 37 °C, and MGMT (2.4 µM, 2 µL) was added. Final assay concentrations were as following: ligands, 12.5 µM; S, 200 nM; MGMT, 800 nM (excess enzyme was required to account for the incomplete activity); DMSO, 0.125% (v/v), in a total reaction volume of 6 µL. After 5 min at 37 °C, 1.5 µL of reaction mixtures were transferred to ice-cooled Eppendorf vials containing the unlabeled reaction quencher Q (15 µM, 2.5 µL). Then, dH2O (2 µL), 5X TANGO buffer (2 µL) and Bsp119I (Thermo Scientific, 2 U/mL, 2 µL) were added to each vial, and the vials were incubated at 37 °C for 1 h. The reactions were quenched by addition of formamide / 5 M aq. Na_2EDTA solution (80:20, 5 µL). Aliquots (10 µL) of each reaction were loaded into a 0.75-mm denaturing gel (15% polyacrylamide, 7 M urea) and separated at ambient temperature during 35 min (~1200 V, 20 W). Gels were visualized with a Typhoon 5 imager (GE Healthcare) using standard settings for Cy3 detection and quantified with ImageQuant TL software (GE Healthcare). Inhibition efficiency (%) was determined using equation **7**:

$$\text{Inhibition (\%)} = 100 \times 1 - R_{comp}/R_{control} \quad (\mathbf{7})$$

where R_{comp} and $R_{control}$ are relative amounts of the 10-mer reaction product (relative to the sum of the bands of the product and the 26-mer substrate, as determined by densitometry analysis of electrophoresis gels) for the compound and DMSO control, respectively.

Endonuclease inhibition assay

The methylated substrate S was substituted by S', and MGMT and Q where substituted by equal volumes of the Tris / DTT buffer; the experiments were performed and analyzed as above.

Competitive assay

Compound solutions (diluted with buffer to 50 µM, 1.5 µL) or DMSO control (2:400 in buffer) were mixed with CT DNA (160 µM bp, 1.5 µL) and incubated at room temperature for 10 min, followed by the addition of the substrate S (1.2 µM, 1 µL). The reaction vials were placed in a thermostat at 37 °C, and MGMT (2.4 µM, 2 µL) was added. The subsequent reaction (5 min), quenching and analysis steps were performed as described above.

Uncompetitive assays

Solutions of MGMT (2.4 µM, 2 µL) and the compounds (25 µM, 3 µL) were preincubated for 30 min at room temperature, then placed in the thermostat (37 °C) and the substrate S (1.2 µM, 1 µL) was added. The subsequent reaction (5 min), quenching and analysis steps were performed as described above.

7.3 *In cellulo* experiments

Cell culture experiments

General remarks: T98G human glioblastoma cell line was purchased from American Type Culture Collection (ATCC). Adherent cells were grown in Minimum Essential Medium (MEM 1X + GlutaMAX™, Life Technologies) supplemented with 1% penicillin/streptomycin (Life Technologies), 10% fetal bovine serum (Biowest) and 1% MEM Non Essential Amino Acids (MEM NEAA (100X), Life Technologies), kept in humidified atmosphere with 5% CO_2 in air at 37 °C and subcultured twice a week by dispersal with TrypLE™ Express Enzyme (Life Technologies).

Growth inhibition (GI_{50}) determination

Cells were seeded at (0.125–0.25) × 10^5 cells / mL in a T25 cm^2 flask between 3–4 days before the experiment in the conditions mentioned above. After reaching this time, the medium was removed and the cells were washed with 5 mL of sterile PBS. For each flask, 1 mL of TrypLE™ Express Enzyme (Life Technologies) were added to the flask for 5–10 minutes at 37 °C, followed by 9 mL of medium. Cells were counted using a MaxiZ™ counter (Orflo, Ketchum) and resuspended in media at a 0.125 × 10^5 cells / mL concentration. 200 µL of this suspension was added into each well of a 96-well plate (Costar). After 4 h, 1 µL of solution of compounds in DMSO were added such as to obtain the final drug concentration in a range from 0.015 to 25 µM (final concentration of DMSO in each well: 0.5% v/v) and mixed. The cells were incubated for 96 h in the conditions mentioned above. Cell viability was assessed by using CellTiter Glo® Luminescent Cell Viability Assay (Promega) following the kit instructions. Cells viability (V, %) was determined as the ratio of the luminescent signal of the cells treated with the compound(s) and the vehicle (DMSO, 0.5% v/v). Each condition was assayed at least three times with two technical replicates per plate.

For determination of viability through cell counting, the following protocol was employed: T98G cells were plated in 24-well tissue culture plates (TPP®) at 0.25 × 10^5 cells / mL in 1 mL medium, and 4 h later treated with varied concentrations of each compound and incubated for 96 h at 37 °C and 5% CO_2. After washing with 500 µL of PBS, 100 µL of TrypLE™ Express Enzyme (Life Technologies) was added to the cells for 5 min at 37 °C, followed by 900 µL of medium. Cells were counted as described

before. Cells viability (%) were defined as the ratio between the concentration of cells treated with compound and the vehicle, where each condition was tested at least one time.

Drug combination experiments: Cells were seeded in a white 96-well tissue culture plate (Costar®) and the compounds were added as DMSO solutions and incubated for 2 h. After this time, TMZ was added as a DMSO solution, such as the final concentration of DMSO in each well was 0.5% v/v. The cells were grown for a total of 96 h and the experimental viability (V_{Exp}[A(a) + B[b)]) was determined using CellTiter Glo® kit as described before. For the analysis in terms of Bliss Independence model,[118–120] the theoretical viability of cells treated with a combination of drugs A and B (V_{Theo}[A(a) + B[b)] was calculated using equation (**8**):

$$V_{Theo}[A(a) + B[b)] = V_{Exp,A(a)} \times V_{Exp,B(b)} \quad (\mathbf{8})$$

where $V_{Exp,A(a)}$ and $V_{Exp,B(b)}$are the viabilities of cells treated individually with compounds A and B, at concentrations a and b respectively, at the same concentrations as in the combination experiment. The corresponding SD (σ) values were calculated using the error propagation formula, equation (**9**):

$$\sigma^2 = (V_{theo,AB})^2 \times \left(\frac{\sigma_{V_A}{}^2}{V_{A(a)}{}^2} + \frac{\sigma_{V_B}{}^2}{V_{B(b)}{}^2}\right), \quad (\mathbf{9})$$

where σ_{VA} and σ_{VB} are the SD values for the experimental viabilities $V_{Exp,A(a)}$and $V_{Exp,B(b)}$, respectively.

For Combination Index (CI) determination, the Chou–Talalay method was used by employing CompuSyn software as per software manual (https://www.combosyn.com/).[121,122]

Live cell imaging

T98G cells were cultured as described above and plated in an 8-well plate (ibidi®)at 0.25×10^5 cells/ mL in 0.3 mL of medium, and 4 h later treated with compound **62** (final concentration: 1.1 µM) and incubated for 96 h at 37 °C and 5% CO_2. Medium was removed and the cells were washed with PBS (300 µL). Medium was replenished, DRAQ5™ (Invitrogen) was added as a nuclear dye (final concentration: 20 µM) and cells were incubated for 20 minutes at room temperature, protected from light. Finally, medium was removed; cells were washed and medium was added as before. Images were acquired on TIRF Spinning Disk Microscope (Gataca systems - TiE Nikon), with a 100X oil magnification using a 488 nm laser (525 / 25 nm filter) and a 642 nm laser (700 / 75 nm filter). Pixel size was 0.11 µm and the Z step size was 0.5 µm over a Z range of 10 µm.

γH2AX immunostaining

T98G cells were plated in a 8-well plate Lab-Tek®II Chamber Slide™ at 0.125 × 10^5 cells/ mL concentration for DMSO and TMZ treatment and at 0.25 × 10^5 cells / mL for the rest of the conditions in 0.4 mL of medium and treated 4 h later with DMSO, O^6BG and **62** for 2 h at 37 °C and 5% CO_2. Then, TMZ was added and cells were incubated in the same conditions for 94 h more. Medium was removed, and cells were washed with PBS (2 x 400 µL) and fixed with PFA (2 % in PBS, 400 µL) for 10 min at rt, and then washed with PBS (3 x 400 µL). Cells were permeabilized with Triton X-100 (0.2 % in PBS, 400 µL) for 10 min at rt and then washed trice with PBS (400 µL). Cells were incubated with goat serum (Abcam, 10 % in PBS, 250 µL) for 1 h at room temperature, washed once with PBS (400 µL) and incubated overnight with γ-H2AX antibody (MerckMillipore, Antiphospho-Histone H2A.X (Ser139), clone JBW301,1:500 in BSA 1%, 250 µL) at 4 °C. Cells were washed with PBS (5 x 400 µL, intercalating 5 minutes between washing) and incubated with the secondary andibody (Life Technologies, AlexaFluor™ 555 goat anti-mouse IgG1 (γ1), 1:600 in BSA 1 %) for 30 min at rt. Cells were washed with PBS (5 x 400 µL, intercalating 5 minutes between washing) and slides were finally mounted with Vectashield® Mounting Medium for Fluorescence containing DAPI as nuclear dye (Vector Laboratories) and a coverglass (N° 1.5, VWR). Images were acquired on a 63X oil magnification with a Widefield Microscope (Leica) and processed using ImageJ software. Data presents the results of two individual replicate were a minimum of 150 cells were analyzed per condition.

Apoptosis and Necrosis determination

T98G cells were incubated in a 6-well plate (TPP®) in a 5 mL final volume, at 0.35 x 10^5 cells / mL for DMSO and TMZ treatment and at 0.7 x 10^5 cells / mL for the rest of the conditions for the 48 h experiment, 0.25 x 10^5 cells / mL for DMSO and TMZ treatment, 0.5 x 10^5 cells / mL for **62** and O^6BG and 1 x 10^5 cells / mL for the combination experiments for at 96 h. Treated 4 h later with the compounds as DMSO solution, incubated for 2 h at 37°C and 5 % CO_2 when TMZ was added and incubated to complete 48 or 96 h of incubation. After this time, medium was removed and washed with PBS (2 mL), cells were trypsinized and counted. Medium was removed by centrifugation (5 min, 1500 g at 4°C) and cells were washed again (2 X 2 mL) and analyzed using FITC Annexin V Apoptosis Detection Kit (BD PharmagenTM) according to kit instructions. Cells were analyzed with a BD FACSCanto II cytometer equipped with a 488 nm laser. The data presented were an average of three to five individual experiments per condition

Caspase 3/7 activation assay

In a 96-well plate, T98G cells were seeded at 1 × 10^4 cells / mL for **62** and **62** / TMZ combination experiment and 0.5 × 10^4 cells / mL for DMSO and TMZ experiments. Compounds were added as for the combination assay experiments at the corresponding concentrations, namely DMSO (0.5% v/v), TMZ (94 μM), **62** (1.1 μM) and **62** / TMZ combination (1.1 and 94 μM, respectively). Cells were incubated with compounds for 96 h and caspase 3/7 activity was measured using the Caspase-Glo® 3/7 kit (Promega) as per kit instructions.[206,207] Values were normalized with respect to the DMSO control and the amount of total protein (considered proportional to the cell number). The results represent means ± S.D. from three independent biological replicates.

Inactivation of cellular MGMT

T98G cells were seeded at 0.125 × 10^5 cell / mL in 30 mL of media in T75 flasks and incubated as described before. After four days, media was removed, the flasks were washed with PBS (10 mL) and filled with fresh media containing DMSO (0.5% v/v) or the compounds (2 μM) and incubated for 2 h at 37 °C. Media was removed, and cells were washed with PBS (2 × 10 mL) and trypsinized collecting about 1 × 10^7 cells per treatment. The cells were pelleted and N^2-frozen for storing at −80 °C. The pellets were resuspended in the reaction buffer (50 mM Tris-HCl, 50 mM NaCl, 1 mM EDTA, 5% glycerol, pH 8.0) supplemented with DTT (1 mM) and 1X HaltTM protease cocktail (Thermo Scientific). The suspension was pulse-sonicated 5 times (5 s each, 30 s between pulses) at 4 °C and then centrifuged for 30 min at 4 °C and 14000 g; the supernatant was transferred to a clean tube and kept on ice. Protein concentration, measured using PierceTM BCA protein assay kit (Thermo Scientific), was 4–8 mg / mL. Reactions were performed in 150 μL of reaction mixture containing the protein extract (147.5 μL, 100–500 μg of protein similar to what is reported in the literature) [200,241,242] and DNA substrate S (2.5 μL of a 240 nM solution, final concentration: 4 nM) and incubated 2 h at 37 °C. DNA was extracted using phenol : chloroform : isoamyl alcohol (25:24:1, Sigma) saturated with 10 mM Tris and 1 mM EDTA, pH 8.0 (150 μL). 100 μL of the DNA-containing phase were employed to precipitate the DNA using 50 μL of NaOAc (3 M), 900 μL of cold abs. EtOH, 1 μL of glycogen (20 μg/μL, Invitrogen) and then stored at −20 °C overnight. The samples were centrifuged (2 h, 4 °C, 16,000 g) and the supernatant was carefully removed. The pellet was washed with 150 μL of cold 70% EtOH and re-centrifuged (10 min, 4 °C, 16,000 g). The supernatant was removed and the DNA was dried by speed vacuum, then dissolved in a total of 10 μL of solution containing H_2O (6 μL), 2 μL of 5X TANGO (2μL) and Bsp119I (2 U/mL, 2 μL). Gel electrophoresis analysis was carried as before and the activity was calculated by dividing the MGMT activity by the amount of total protein used for the assay. The results represent the mean ± S.D. of three independent biological experiments.

Chapter 8
References

8 References

(1) Tykocki, T.; Eltayeb, M. Ten-Year Survival in Glioblastoma. A Systematic Review. *J. Clin. Neurosci.* **2018**, *54*, 7–13. https://doi.org/10.1016/j.jocn.2018.05.002.

(2) Hanif, F.; Muzaffar, K.; Perveen, K.; Malhi, S. M.; Simjee, S. U. Glioblastoma Multiforme: A Review of Its Epidemiology and Pathogenesis through Clinical Presentation and Treatment. *Asian Pacific J. Cancer Prev.* **2017**, *18* (1), 3–9. https://doi.org/10.22034/APJCP.2017.18.1.3.

(3) Tan, A. C.; Ashley, D. M.; López, G. Y.; Malinzak, M.; Friedman, H. S.; Khasraw, M. Management of Glioblastoma: State of the Art and Future Directions. *CA. Cancer J. Clin.* **2020**, *70* (4), 299–312. https://doi.org/10.3322/caac.21613.

(4) Davis, M. E. Glioblastoma: Overview of Disease and Treatment. *Clin. J. Oncol. Nurs.* **2016**, *20* (5), 1–8. https://doi.org/10.1188/16.CJON.S1.2-8.

(5) Zhang, J.; F.G. Stevens, M.; D. Bradshaw, T. Temozolomide: Mechanisms of Action, Repair and Resistance. *Curr. Mol. Pharmacol.* **2012**, *5* (1), 102–114. https://doi.org/10.2174/1874467211205010102.

(6) Chua, J.; Nafziger, E.; Leung, D. Evidence-Based Practice: Temozolomide Beyond Glioblastoma. *Curr. Oncol. Rep.* **2019**, *21* (4), 1–9. https://doi.org/10.1007/s11912-019-0783-5.

(7) Lee, S. Y. Temozolomide Resistance in Glioblastoma Multiforme. *Genes Dis.* **2016**, *3* (3), 198–210. https://doi.org/10.1016/j.gendis.2016.04.007.

(8) Travers, A.; Muskhelishvili, G. DNA Structure and Function. *FEBS J.* **2015**, *282* (12), 2279–2295. https://doi.org/10.1111/febs.13307.

(9) Chatterjee, N.; Walker, G. C. Mechanisms of DNA Damage, Repair, and Mutagenesis. *Environ. Mol. Mutagen.* **2017**, *58* (5), 235–263. https://doi.org/10.1002/em.22087.

(10) Yuriko, Y.; Kohda, K.; Tomita, K. Nucleic Acids Research. *Nucleic Acids Res.* **1988**, *16* (19), 9307–9321. https://doi.org/10.1093/nar/16.19.9307.

(11) Gaffney, B. L.; Jones, R. A. Thermodynamic Comparison of the Base Pairs Formed by the Carcinogenic Lesion O6-Methylguanine with Reference Both to Watson-Crick Pairs and to Mismatched Pairs. *Biochemistry* **1989**, *28* (14), 5881–5889. https://doi.org/10.1021/bi00440a026.

(12) Warren, J. J.; Forsberg, L. J.; Beese, L. S. The Structural Basis for the Mutagenicity of O6-Methyl-Guanine Lesions. *Proc. Natl. Acad. Sci. U. S. A.* **2006**, *103* (52), 19701–19706. https://doi.org/10.1073/pnas.0609580103.

(13) Koag, M. C.; Lee, S. Metal-Dependent Conformational Activation Explains Highly Promutagenic Replication across O6-Methylguanine by Human DNA Polymerase β. *J. Am. Chem. Soc.* **2014**, *136* (15), 5709–5721. https://doi.org/10.1021/ja500172d.

(14) Carusillo, A.; Mussolino, C. DNA Damage: From Threat to Treatment. *Cells* **2020**, *9* (7), 1–20. https://doi.org/10.3390/cells9071665.

(15) Fu, D.; Calvo, J. A.; Samson, L. D. Balancing Repair and Tolerance of DNA Damage Caused by Alkylating Agents. *Nat. Rev. Cancer* **2012**, *12* (2), 104–120. https://doi.org/10.1038/nrc3185.

(16) Tsao, N.; Schärer, O. D.; Mosammaparast, N. The Complexity and Regulation of Repair of Alkylation Damage to Nucleic Acids. *Crit. Rev. Biochem. Mol. Biol.* **2021**, *56* (2), 125–136. https://doi.org/10.1080/10409238.2020.1869173.

(17) Fu, D.; Calvo, J. A.; Samson, L. D. Balancing Repair and Tolerance of DNA Damage Caused by Alkylating Agents. *Nat. Rev. Cancer* **2012**, *12* (2), 104–120. https://doi.org/10.1038/nrc3185.

(18) Roos, W. P.; Thomas, A. D.; Kaina, B. DNA Damage and the Balance between Survival and Death in Cancer Biology. *Nat. Rev. Cancer* **2016**, *16* (1), 20–33. https://doi.org/10.1038/nrc.2015.2.

(19) Lim, A.; Li, B. F. L. The Nuclear Targeting and Nuclear Retention Properties of a Human DNA Repair Protein O6-Methylguanine-DNA Methyltransferase Are Both Required for Its Nuclear Localization: The Possible Implications. *EMBO J.* **1996**, *15* (15), 4050–4060.

https://doi.org/10.1002/j.1460-2075.1996.tb00778.x.
(20) Zang, H.; Fang, Q.; Pegg, A. E.; Guengerich, F. P. Kinetic Analysis of Steps in the Repair of Damaged DNA by Human O 6-Alkylguanine-DNA Alkyltransferase. *J. Biol. Chem.* **2005**, *280* (35), 30873–30881. https://doi.org/10.1074/jbc.M505283200.
(21) Daniels, D. S.; Woo, T. T.; Luu, K. X.; Noll, D. M.; Clarke, N. D.; Pegg, A. E.; Tainer, J. A. DNA Binding and Nucleotide Flipping by the Human DNA Repair Protein AGT. *Nat. Struct. Mol. Biol.* **2004**, *11* (8), 714–720. https://doi.org/10.1038/nsmb791.
(22) Jiapaer, S.; Furuta, T.; Tanaka, S.; Kitabayashi, T.; Nakada, M. Potential Strategies Overcoming the Temozolomide Resistance for Glioblastoma. *Neurol. Med. Chir. (Tokyo).* **2018**, *58* (10), 405–421. https://doi.org/10.2176/nmc.ra.2018-0141.
(23) Fan, C. H.; Liu, W. L.; Cao, H.; Wen, C.; Chen, L.; Jiang, G. O6-Methylguanine DNA Methyltransferase as a Promising Target for the Treatment of Temozolomide-Resistant Gliomas. *Cell Death Dis.* **2013**, *4* (10), e876-8. https://doi.org/10.1038/cddis.2013.388.
(24) Cabrini, G.; Fabbri, E.; Lo Nigro, C.; Dechecchi, M. C.; Gambari, R. Regulation of Expression of O6-Methylguanine-DNA Methyltransferase and the Treatment of Glioblastoma (Review). *Int. J. Oncol.* **2015**, *47* (2), 417–428. https://doi.org/10.3892/ijo.2015.3026.
(25) Yu, W.; Zhang, L.; Wei, Q.; Shao, A. O6-Methylguanine-DNA Methyltransferase (MGMT): Challenges and New Opportunities in Glioma Chemotherapy. *Front. Oncol.* **2020**, *9* (January), 1–11. https://doi.org/10.3389/fonc.2019.01547.
(26) Bocangel, D.; Sengupta, S.; Mitra, S.; Bhakat, K. K. P53-Mediated down-Regulation of the Human DNA Repair Gene O 6-Methylguanine-DNA Methyltransferase (MGMT) via Interaction with Sp1 Transcription Factor. *Anticancer Res.* **2009**, *29* (10), 3741–3750.
(27) Alves, A. L. V.; Gomes, I. N. F.; Carloni, A. C.; Rosa, M. N.; da Silva, L. S.; Evangelista, A. F.; Reis, R. M.; Silva, V. A. O. Role of Glioblastoma Stem Cells in Cancer Therapeutic Resistance: A Perspective on Antineoplastic Agents from Natural Sources and Chemical Derivatives. *Stem Cell Res. Ther.* **2021**, *12* (1), 1–22. https://doi.org/10.1186/s13287-021-02231-x.
(28) Rodríguez-Hernández, I.; Garcia, J. L.; Santos-Briz, A.; Hernández-Laín, A.; González-Valero, J. M.; Gómez-Moreta, J. A.; Toldos-González, O.; Cruz, J. J.; Martin-Vallejo, J.; González-Sarmiento, R. Integrated Analysis of Mismatch Repair System in Malignant Astrocytomas. *PLoS One* **2013**, *8* (9), 1–10. https://doi.org/10.1371/journal.pone.0076401.
(29) Tomaszowski, K. H.; Schirrmacher, R.; Kaina, B. Multidrug Efflux Pumps Attenuate the Effect of MGMT Inhibitors. *Mol. Pharm.* **2015**, *12* (11), 3924–3934. https://doi.org/10.1021/acs.molpharmaceut.5b00341.
(30) Mohri, M.; Nitta, H.; Yamashita, J. Expression of Multidrug Resistance-Associated Protein (MRP) in Human Gliomas. *J. Neurooncol.* **2000**, *49* (2), 105–115. https://doi.org/10.1023/A:1026528926482.
(31) Singh, N.; Miner, A.; Hennis, L.; Mittal, S. Mechanisms of Temozolomide Resistance in Glioblastoma - a Comprehensive Review. *Cancer Drug Resist.* **2020**, *4* (1), 17–43. https://doi.org/10.20517/cdr.2020.79.
(32) Zhang, Y.; Dube, C.; Gibert, M.; Cruickshanks, N.; Wang, B.; Coughlan, M.; Yang, Y.; Setiady, I.; Deveau, C.; Saoud, K.; et al. The P53 Pathway in Glioblastoma. *Cancers (Basel).* **2018**, *10* (9). https://doi.org/10.3390/cancers10090297.
(33) Sun, G.; Fan, T.; Zhang, N.; Ren, T.; Zhao, L.; Zhong, R. Identification of the Structural Features of Guanine Derivatives as Mgmt Inhibitors Using 3d-Qsar Modeling Combined with Molecular Docking. *Molecules* **2016**, *21* (7). https://doi.org/10.3390/molecules21070823.
(34) Chae, M. Y.; Swenn, K.; Kanugula, S.; Dolan, M. E.; Pegg, A. E.; Moschel, R. C. 8-Substituted O6-Benzylguanine, Substituted 6(4)-(Benzyloxy)Pyrimidine, and Related Derivatives as Inactivators of Human O6-Alkylguanine-DNA Alkyltransfer Ase. *J. Med. Chem.* **1995**, *38* (2), 359–365. https://doi.org/10.1021/jm00002a018.
(35) Moschel, R. C.; McDougall, M. G.; Dolan, M. E.; Stine, L.; Pegg, A. E. Structural Features of Substituted Purine Derivatives Compatible with Depletion of Human O6-Alkylguanine-DNA

Alkyltransferase. *J. Med. Chem.* **1992**, *35* (23), 4486–4491. https://doi.org/10.1021/jm00101a028.
(36) Dolan, M. E.; Moschel, R. C.; Pegg, A. E. Depletion of Mammalian O6-Alkylguanine-DNA Alkyltransferase Activity by O6-Benzylguanine Provides a Means to Evaluate the Role of This Protein in Protection against Carcinogenic and Therapeutic Alkylating Agents. *Proc. Natl. Acad. Sci. U. S. A.* **1990**, *87* (14), 5368–5372. https://doi.org/10.1073/pnas.87.14.5368.
(37) Pauly, G. T.; Loktionova, N. A.; Fang, Q.; Vankayala, S. L.; Guida, W. C.; Pegg, A. E. Substitution of Aminomethyl at the Meta-Position Enhances the Inactivation of O6-Alkylguanine-DNA Alkyltransferase by O6- Benzylguanine. *J. Med. Chem.* **2008**, *51* (22), 7144–7153. https://doi.org/10.1021/jm800675p.
(38) Moschel, R. C.; Pegg, A. E. Effect of O6-Benzylguanine Analogues on Sensitivity of Human Tumor Cells to the Cytotoxic Effects of Alkylating Agents. *Cancer Res.* **1991**, *51* (13), 3367–3372.
(39) Kaina, B.; Mühlhausen, U.; Piee-Staffa, A.; Christmann, M.; Boy, R. G.; Rösch, F.; Schirrmacher, R. Inhibition of O6-Methylguanine-DNA Methyltransferase by Glucose-Conjugated Inhibitors: Comparison with Nonconjugated Inhibitors and Effect on Fotemustine and Temozolomide-Induced Cell Death. *J. Pharmacol. Exp. Ther.* **2004**, *311* (2), 585–593. https://doi.org/10.1124/jpet.104.071316.
(40) Chae, M. Y.; McDougall, M. G.; Dolan, M. E.; Swenn, K.; Pegg, A. E.; Moschel, R. C. Substituted O6-Benzylguanine Derivatives and Their Inactivation of Human O6-Alkylguanine-DNA Alkyltransferase. *J. Med. Chem.* **1994**, *37* (3), 342–347. https://doi.org/10.1021/jm00029a005.
(41) McMurry, T. B. H. MGMT Inhibitors-The Trinity College-Paterson Institute Experience, a Chemist's Perception. *DNA Repair (Amst).* **2007**, *6* (8), 1161–1169. https://doi.org/10.1016/j.dnarep.2007.03.015.
(42) Javanmard, S.; Loktionova, N. A.; Fang, Q.; Pauly, G. T.; Pegg, A. E.; Moschel, R. C. Inactivation of O6-Alkylguanine-DNA Alkyltransferase by Folate Esters of O6-Benzyl-2'-Deoxyguanosine and of O 6-[4-(Hydroxymethyl)Benzyl]Guanine. *J. Med. Chem.* **2007**, *50* (21), 5193–5201. https://doi.org/10.1021/jm0705859.
(43) Wang, C.; Abegg, D.; Hoch, D. G.; Adibekian, A. Chemoproteomics-Enabled Discovery of a Potent and Selective Inhibitor of the DNA Repair Protein MGMT. *Angew. Chemie - Int. Ed.* **2016**, *55* (8), 2911–2915. https://doi.org/10.1002/anie.201511301.
(44) Clemons, M.; Kelly, J.; Watson, A. J.; Howell, A.; McElhinney, R. S.; McMurry, T. B. H.; Margison, G. P. O6-(4-Bromothenyl)Guanine Reverses Temozolomide Resistance in Human Breast Tumour MCF-7 Cells and Xenografts. *Br. J. Cancer* **2005**, *93* (10), 1152–1156. https://doi.org/10.1038/sj.bjc.6602833.
(45) Quinn, J. A.; Jiang, S. X.; Reardon, D. A.; Desjardins, A.; Vredenburgh, J. J.; Rich, J. N.; Gururangan, S.; Friedman, A. H.; Signer, D. D.; Sampson, J. H.; et al. Phase II Trial of Temozolomide Plus O6-Benzylguanine in Adults with Recurrent, Temozolomide-Resistant Malignant Glioma. *J. Clin. Oncol.* **2009**, *27* (8), 1262–1267. https://doi.org/10.1200/JCO.2008.18.8417.
(46) Watson, A. J.; Middleton, M. R.; McGown, G.; Thorncroft, M.; Ranson, M.; Hersey, P.; McArthur, G.; Davis, I. D.; Thomson, D.; Beith, J.; et al. O6-Methylguanine-DNA Methyltransferase Depletion and DNA Damage in Patients with Melanoma Treated with Temozolomide Alone or with Lomeguatrib. *Br. J. Cancer* **2009**, *100* (8), 1250–1256. https://doi.org/10.1038/sj.bjc.6605015.
(47) Tawbi, H. A.; Villaruz, L.; Tarhini, A.; Moschos, S.; Sulecki, M.; Viverette, F.; Shipe-Spotloe, J.; Radkowski, R.; Kirkwood, J. M. Inhibition of DNA Repair with MGMT Pseudosubstrates: Phase i Study of Lomeguatrib in Combination with Dacarbazine in Patients with Advanced Melanoma and Other Solid Tumours. *Br. J. Cancer* **2011**, *105* (6), 773–777. https://doi.org/10.1038/bjc.2011.285.

(48) Watson, A. J.; Sabharwal, A.; Thorncroft, M.; McGown, G.; Kerr, R.; Bojanic, S.; Soonawalla, Z.; King, A.; Miller, A.; Waller, S.; et al. Tumor O6-Methylguanine-DNA Methyltransferase Inactivation by Oral Lomeguatrib. *Clin. Cancer Res.* **2010**, *16* (2), 743–749. https://doi.org/10.1158/1078-0432.CCR-09-1389.

(49) Coyne, G. O. S.; Kummar, S.; Meehan, R. S.; Do, K.; Collins, J. M.; Anderson, L.; Ishii, K.; Takebe, N.; Zlott, J.; Juwara, L.; et al. Phase I Trial of TRC102 (Methoxyamine HCl) in Combination with Temozolomide in Patients with Relapsed Solid Tumors and Lymphomas. *Oncotarget* **2020**, *11* (44), 3959–3971. https://doi.org/10.18632/oncotarget.27784.

(50) Adams, D. M.; Zhou, T.; Berg, S. L.; Bernstein, M.; Neville, K.; Blaney, S. M. Phase 1 Trial of O 6 -Benzylguanine and BCNU in Children with CNS Tumors: A Children's Oncology Group Study. *Pediatr. Blood Cancer* **2008**, *50* (3), 549–553. https://doi.org/10.1002/pbc.21362.

(51) Caston, R. A.; Gampala, S.; Armstrong, L.; Messmann, R. A.; Fishel, M. L.; Kelley, M. R. The Multifunctional APE1 DNA Repair–Redox Signaling Protein as a Drug Target in Human Disease. *Drug Discov. Today* **2021**, *26* (1), 218–228. https://doi.org/10.1016/j.drudis.2020.10.015.

(52) Higuchi, F.; Nagashima, H.; Ning, J.; Koerner, M. V. A.; Wakimoto, H.; Cahill, D. P. Restoration of Temozolomide Sensitivity by PARP Inhibitors in Mismatch Repair Deficient Glioblastoma Is Independent of Base Excision Repair. *Clin. Cancer Res.* **2020**, *26* (7), 1690–1699. https://doi.org/10.1158/1078-0432.CCR-19-2000.

(53) Ferri, A.; Stagni, V.; Barilà, D. Targeting the DNA Damage Response to Overcome Cancer Drug Resistance in Glioblastoma. *Int. J. Mol. Sci.* **2020**, *21* (14), 1–19. https://doi.org/10.3390/ijms21144910.

(54) Mégnin-Chanet, F.; Bollet, M. A.; Hall, J. Targeting Poly (ADP-Ribose) Polymerase Activity for Cancer Therapy. *Cell. Mol. Life Sci.* **2010**, *67*, 3649–3662. https://doi.org/10.1007/s00018-010-0490-8.

(55) Hussain, M.; Carducci, M. A.; Slovin, S.; Cetnar, J.; Qian, J.; McKeegan, E. M.; Refici-Buhr, M.; Chyla, B.; Shepherd, S. P.; Giranda, V. L.; et al. Targeting DNA Repair with Combination Veliparib (ABT-888) and Temozolomide in Patients with Metastatic Castration-Resistant Prostate Cancer. *Invest. New Drugs* **2014**, *32* (5), 904–912. https://doi.org/10.1007/s10637-014-0099-0.

(56) Baxter, P. A.; Su, J. M.; Onar-Thomas, A.; Billups, C. A.; Li, X.-N.; Poussaint, T. Y.; Smith, E. R.; Thompson, P.; Adesina, A.; Ansell, P.; et al. A Phase I/II Study of Veliparib (ABT-888) with Radiation and Temozolomide in Newly Diagnosed Diffuse Pontine Glioma: A Pediatric Brain Tumor Consortium Study. *Neuro. Oncol.* **2020**, *22* (6), 875–885. https://doi.org/10.1093/neuonc/noaa016.

(57) Gupta, S. K.; Kizilbash, S. H.; Carlson, B. L.; Mladek, A. C.; Boakye-Agyeman, F.; Bakken, K. K.; Pokorny, J. L.; Schroeder, M. A.; Decker, P. A.; Cen, L.; et al. Delineation of MGMT Hypermethylation as a Biomarker for Veliparib-Mediated Temozolomide-Sensitizing Therapy of Glioblastoma. *J. Natl. Cancer Inst.* **2016**, *108* (5), 1–10. https://doi.org/10.1093/jnci/djv369.

(58) Hanna, C.; Kurian, K. M.; Williams, K.; Watts, C.; Jackson, A.; Carruthers, R.; Strathdee, K.; Cruickshank, G.; Dunn, L.; Erridge, S.; et al. Pharmacokinetics, Safety, and Tolerability of Olaparib and Temozolomide for Recurrent Glioblastoma: Results of the Phase i OPARATIC Trial. *Neuro. Oncol.* **2020**, *22* (12), 1840–1850. https://doi.org/10.1093/neuonc/noaa104.

(59) Blumenthal, D. T.; Rankin, C.; Stelzer, K. J.; Spence, A. M.; Sloan, A. E.; Moore, D. F.; Padula, G. D. A.; Schulman, S. B.; Wade, M. L.; Rushing, E. J. A Phase III Study of Radiation Therapy (RT) and O6-Benzylguanine + BCNU versus RT and BCNU Alone and Methylation Status in Newly Diagnosed Glioblastoma and Gliosarcoma: Southwest Oncology Group (SWOG) Study S0001. *Int. J. Clin. Oncol.* **2015**, *20* (4), 650–658. https://doi.org/10.1007/s10147-014-0769-0.

(60) Quinn, J. A.; Jiang, S. X.; Carter, J.; Reardon, D. A.; Desjardins, A.; Vredenburgh, J. J.; Rich, J. N.; Gururangan, S.; Friedman, A. H.; Bigner, D. D.; et al. Phase II Trial of Gliadel plus O 6-

Benzylguanine in Adults with Recurrent Glioblastoma Multiforme. *Clin. Cancer Res.* **2009**, *15* (3), 1064–1068. https://doi.org/10.1158/1078-0432.CCR-08-2130.
(61) Herrlinger, U.; Tzaridis, T.; Mack, F.; Steinbach, J. P.; Schlegel, U.; Sabel, M.; Hau, P.; Kortmann, R. D.; Krex, D.; Grauer, O.; et al. Lomustine-Temozolomide Combination Therapy versus Standard Temozolomide Therapy in Patients with Newly Diagnosed Glioblastoma with Methylated MGMT Promoter (CeTeG/NOA–09): A Randomised, Open-Label, Phase 3 Trial. *Lancet* **2019**, *393* (10172), 678–688. https://doi.org/10.1016/S0140-6736(18)31791-4.
(62) Kodadek, T. Inhibition of Proteolysis and Other Posttranslational Modifications with Substrate-Targeted Inhibitors. *Biopolym. - Pept. Sci. Sect.* **2002**, *66* (2), 134–140. https://doi.org/10.1002/bip.10233.
(63) Robin, T.; Reuveni, S.; Urbakh, M. Single-Molecule Theory of Enzymatic Inhibition. *Nat. Commun.* **2018**, *9* (1), 779. https://doi.org/10.1038/s41467-018-02995-6.
(64) Kukar, T. L.; Ladd, T. B.; Bann, M. A.; Fraering, P. C.; Narlawar, R.; Maharvi, G. M.; Healy, B.; Chapman, R.; Welzel, A. T.; Price, R. W.; et al. Substrate-Targeting γ-Secretase Modulators. *Nature* **2008**, *453* (7197), 925–929. https://doi.org/10.1038/nature07055.
(65) Eads, J. R.; Krishnamurthi, S. S.; Saltzman, J.; Bokar, J. A.; Savvides, P.; Meropol, N. J.; Gibbons, J.; Koon, H.; Sharma, N.; Rogers, L.; et al. Phase I Clinical Trial of Temozolomide and Methoxyamine (TRC-102), an Inhibitor of Base Excision Repair, in Patients with Advanced Solid Tumors. *Invest. New Drugs* **2020**. https://doi.org/10.1007/s10637-020-00962-x.
(66) Alarcon, K.; Demeunynck, M.; Lhomme, J.; Carrez, D.; Croisy, A. Potentiation of BCNU Cytotoxicity by Molecules Targeting Abasic Lesions in DNA. *Bioorganic Med. Chem.* **2001**, *9* (7), 1901–1910. https://doi.org/10.1016/S0968-0896(01)00097-9.
(67) Alarcon, K.; Demeunynck, M.; Lhomme, J.; Carrez, D.; Croisy, A. Diaminopurine-Acridine Heterodimers for Specific Recognition of Abasic Site Containing DNA. Influence on the Biological Activity of the Position of the Linker on the Purine Ring. *Bioorg. Med. Chem. Lett.* **2001**, *11* (14), 1855–1858. https://doi.org/10.1016/S0960-894X(01)00310-9.
(68) Barret, J. M.; Étiévant, C.; Fahy, J.; Lhomme, J.; Hill, B. T. Novel Artificial Endonucleases Inhibit Base Excision Repair and Potentiate the Cytotoxicity of DNA-Damaging Agents on L1210 Cells. *Anti-Cancer Drugs*. 1999, pp 55–65. https://doi.org/10.1097/00001813-199901000-00008.
(69) Belmont, P.; Jourdan, M.; Demeunynck, M.; Constant, J. F.; Garcia, J.; Lhomme, J.; Carez, D.; Croisy, A. Abasic Site Recognition in DNA as a New Strategy to Potentiate the Action of Anticancer Alkylating Drugs? *J. Med. Chem.* **1999**, *42* (25), 5153–5159. https://doi.org/10.1021/jm9901428.
(70) Lhomme, J.; Constant, J. F.; Demeunynck, M. Abasic DNA Structure, Reactivity, and Recognition. *Biopolymers*. 1999, pp 65–83. https://doi.org/10.1002/1097-0282(1999)52:2<65::AID-BIP1>3.0.CO;2-U.
(71) Kotera, N.; Poyer, F.; Granzhan, A.; Teulade-Fichou, M. P. Efficient Inhibition of Human AP Endonuclease 1 (APE1) via Substrate Masking by Abasic Site-Binding Macrocyclic Ligands. *Chem. Commun.* **2015**, *51* (88), 15948–15951. https://doi.org/10.1039/c5cc06084b.
(72) Caron, C.; Duong, X. N. T.; Guillot, R.; Bombard, S.; Granzhan, A. Interaction of Functionalized Naphthalenophanes with Abasic Sites in DNA: DNA Cleavage, DNA Cleavage Inhibition, and Formation of Ligand–DNA Adducts. *Chem. - A Eur. J.* **2019**, *25* (8), 1949–1962. https://doi.org/10.1002/chem.201805555.
(73) Caron, C. Macrocyclics Ligands of Abasic Sites as Inhibitors of DNA Reparation: Synthesis, Biochemical and Biological Studies, Université Paris Saclay, 2018.
(74) Rajendar, B.; Rajendran, A.; Ye, Z.; Kanai, E.; Sato, Y.; Nishizawa, S.; Sikorski, M.; Teramae, N. Effect of Substituents of Alloxazine Derivatives on the Selectivity and Affinity for Adenine in AP-Site-Containing DNA Duplexes. *Org. Biomol. Chem.* **2010**, *8* (21), 4949–4959. https://doi.org/10.1039/c0ob00057d.
(75) Rajendar, B.; Nishizawa, S.; Teramae, N. Alloxazine as a Ligand for Selective Binding to Adenine Opposite AP Sites in DNA Duplexes and Analysis of Single-Nucleotide

Polymorphisms. *Org. Biomol. Chem.* **2008**, *6* (4), 670–673. https://doi.org/10.1039/b719786a.
(76) Ye, Z.; Rajendar, B.; Qing, D.; Nishizawa, S.; Teramae, N. 6,7-Dimethyllumazine as a Potential Ligand for Selective Recognition of Adenine Opposite an Abasic Site in DNA Duplexes. *Chem. Commun.* **2008**, No. 48, 6588–6590. https://doi.org/10.1039/b816876h.
(77) Rajendar, B.; Rajendran, A.; Sato, Y.; Nishizawa, S.; Teramae, N. Effect of Methyl Substitution in a Ligand on the Selectivity and Binding Affinity for a Nucleobase: A Case Study with Isoxanthopterin and Its Derivatives. *Bioorganic Med. Chem.* **2009**, *17* (1), 351–359. https://doi.org/10.1016/j.bmc.2008.10.062.
(78) Pang, Y.; Xu, Z.; Sato, Y.; Nishizawa, S.; Teramae, N. Base Pairing at the Abasic Site in DNA Duplexes and Its Application in Adenosine Aptasensors. *ChemBioChem* **2012**, *13* (3), 436–442. https://doi.org/10.1002/cbic.201100666.
(79) Marsoner, T.; Schmidt, O. P.; Triemer, T.; Luedtke, N. W. DNA-Targeted Inhibition of MGMT. *ChemBioChem* **2017**, *18* (10), 894–898. https://doi.org/10.1002/cbic.201600652.
(80) Song, H.; Kaiser, J. T.; Barton, J. K. Crystal Structure of Δ-[Ru(Bpy)2dppz]2+ Bound to Mismatched DNA Reveals Side-by-Side Metalloinsertion and Intercalation. *Nat. Chem.* **2012**, *4* (8), 615–620. https://doi.org/10.1038/nchem.1375.
(81) Yang, Z.; Chen, F.; Alvarado, J. B.; Benner, S. A. Amplification, Mutation, and Sequencing of a Six-Letter Synthetic Genetic System. *J. Am. Chem. Soc.* **2011**, *133* (38), 15105–15112. https://doi.org/10.1021/ja204910n.
(82) Angelov, T.; Dahlmann, H. A.; Sturla, S. J. Oligonucleotide Probes Containing Pyrimidine Analogs Reveal Diminished Hydrogen Bonding Capacity of the DNA Adduct O6-Methyl-G in DNA Duplexes. *Bioorganic Med. Chem.* **2013**, *21* (20), 6212–6216. https://doi.org/10.1016/j.bmc.2013.07.036.
(83) Gahlon, H. L.; Sturla, S. J. Hydrogen Bonding or Stacking Interactions in Differentiating Duplex Stability in Oligonucleotides Containing Synthetic Nucleoside Probes for Alkylated DNA. *Chem. - A Eur. J.* **2013**, *19* (33), 11062–11067. https://doi.org/10.1002/chem.201204593.
(84) McKeague, M.; Otto, C.; Räz, M. H.; Angelov, T.; Sturla, S. J. The Base Pairing Partner Modulates Alkylguanine Alkyltransferase. *ACS Chem. Biol.* **2018**, *13* (9), 2534–2541. https://doi.org/10.1021/acschembio.8b00446.
(85) Dahlmann, H. A.; Berger, F. D.; Kung, R. W.; Wyss, L. A.; Gubler, I.; McKeague, M.; Wetmore, S. D.; Sturla, S. J. Fluorescent Nucleobase Analogues with Extended Pi Surfaces Stabilize DNA Duplexes Containing O6-Alkylguanine Adducts. *Helv. Chim. Acta* **2018**, *101* (7). https://doi.org/10.1002/hlca.201800066.
(86) Trantakis, I. A.; Nilforoushan, A.; Dahlmann, H. A.; Stäuble, C. K.; Sturla, S. J. In-Gene Quantification of O6-Methylguanine with Elongated Nucleoside Analogues on Gold Nanoprobes. *J. Am. Chem. Soc.* **2016**, *138* (27), 8497–8504. https://doi.org/10.1021/jacs.6b03599.
(87) Onizuka, K.; Nishioka, T.; Li, Z.; Jitsuzaki, D.; Taniguchi, Y.; Sasaki, S. An Efficient and Simple Method for Site-Selective Modification of O6-Methyl-2'-Deoxyguanosine in DNA. *Chem. Commun.* **2012**, *48* (33), 3969. https://doi.org/10.1039/c2cc17621a.
(88) Turner, J. A. A General Approach to the Synthesis of 1,6-, 1,7-, and 1,8-Naphthyridines. *J. Org. Chem.* **1990**, *55* (15), 4744–4750. https://doi.org/10.1021/jo00302a049.
(89) Chang, W. C.; Chang, C. W.; Sigrist, M.; Hua, S. A.; Liu, T. J.; Lee, G. H.; Jin, B. Y.; Chen, C. H.; Peng, S. M. Nonhelical Heterometallic [Mo2M(Npo)4(NCS)2] String Complexes (M = Fe, Co, Ni) with High Single-Molecule Conductance. *Chem. Commun.* **2017**, *53* (63), 8886–8889. https://doi.org/10.1039/c7cc05449a.
(90) Ge, H.; Liu, Q. Palladium-Catalyzed Suzuki Coupling towards 2-Amino-1,8-Naphthyridines. *Heterocycles* **2015**, *91* (5), 1001–1006. https://doi.org/10.3987/COM-14-13140.
(91) Baladi, T.; Granzhan, A.; Piguel, S. Microwave-Assisted C-2 Direct Alkenylation of Imidazo[4,5-b]Pyridines: Access to Fluorescent Purine Isosteres with Remarkably Large Stokes Shifts. *European J. Org. Chem.* **2016**, *2016* (14), 2421–2434.

https://doi.org/10.1002/ejoc.201600166.
(92) Mata, G.; Luedtke, N. W. Synthesis and Solvatochromic Fluorescence of Biaryl Pyrimidine Nucleosides. *Org. Lett.* **2013**, *15* (10), 2462–2465. https://doi.org/10.1021/ol400930s.
(93) Zhang, H.; Kwong, F. Y.; Tian, Y.; Chan, K. S. Base and Cation Effects on the Suzuki Cross-Coupling of Bulky Arylboronic Acid with Halopyridines: Synthesis of Pyridylphenols. *J. Org. Chem.* **1998**, *63* (20), 6886–6890. https://doi.org/10.1021/jo980646y.
(94) Pohl, R.; Socha, O.; Šála, M.; Rejman, D.; Dračínský, M. The Control of the Tautomeric Equilibrium of Isocytosine by Intermolecular Interactions. *European J. Org. Chem.* **2018**, *2018* (37), 5128–5135. https://doi.org/10.1002/ejoc.201800506.
(95) Müller, C. E. Synthesis of 3-Substituted 6-Aminouracils. *Tetrahedron Lett.* **1991**, *32* (45), 6539–6540. https://doi.org/10.1016/0040-4039(91)80214-Q.
(96) De Cian, A.; Guittat, L.; Kaiser, M.; Saccà, B.; Amrane, S.; Bourdoncle, A.; Alberti, P.; Teulade-Fichou, M. P.; Lacroix, L.; Mergny, J. L. Fluorescence-Based Melting Assays for Studying Quadruplex Ligands. *Methods* **2007**, *42* (2), 183–195. https://doi.org/10.1016/j.ymeth.2006.10.004.
(97) Renčiuk, D.; Zhou, J.; Beaurepaire, L.; Guédin, A.; Bourdoncle, A.; Mergny, J. L. A FRET-Based Screening Assay for Nucleic Acid Ligands. *Methods* **2012**, *57* (1), 122–128. https://doi.org/10.1016/j.ymeth.2012.03.020.
(98) Mergny, J.-L.; Lacroix, L. Analysis of Thermal Melting Curves. *Oligonucleotides* **2004**, *13* (6), 515–537. https://doi.org/10.1089/154545703322860825.
(99) Abe, Y.; Nakagawa, O.; Yamaguchi, R.; Sasaki, S. Synthesis and Binding Properties of New Selective Ligands for the Nucleobase Opposite the AP Site. *Bioorganic Med. Chem.* **2012**, *20* (11), 3470–3479. https://doi.org/10.1016/j.bmc.2012.04.009.
(100) Ono, A.; Cao, S.; Togashi, H.; Tashiro, M.; Fujimoto, T.; MacHinami, T.; Oda, S.; Miyake, Y.; Okamoto, I.; Tanaka, Y. Specific Interactions between Silver(i) Ions and Cytosine-Cytosine Pairs in DNA Duplexes. *Chem. Commun.* **2008**, No. 39, 4825–4827. https://doi.org/10.1039/b808686a.
(101) Guo, X.; Leonard, P.; Ingale, S. A.; Liu, J.; Mei, H.; Sieg, M.; Seela, F. 5-Aza-7-Deaza-2'-Deoxyguanosine and 2'-Deoxycytidine Form Programmable Silver-Mediated Base Pairs with Metal Ions in the Core of the DNA Double Helix. *Chem. - A Eur. J.* **2018**, *24* (35), 8883–8892. https://doi.org/10.1002/chem.201801273.
(102) Iwitzki, F.; Schlepegrell, R.; Eichhorn, U.; Kaina, B.; Beyersmann, D.; Hartwig, A. Nickel(II) Inhibits the Repair of O6-Methylguanine in Mammalian Cells. *Arch. Toxicol.* **1998**, *72* (11), 681–689. https://doi.org/10.1007/s002040050561.
(103) Tse, W. C.; Boger, D. L. A Fluorescent Intercalator Displacement Assay for Establishing DNA Binding Selectivity and Affinity. *Acc. Chem. Res.* **2004**, *37* (1), 61–69. https://doi.org/10.1021/ar030113y.
(104) Ramakrishnan, S.; Krainer, G.; Grundmeier, G.; Schlierf, M.; Keller, A. Structural Stability of DNA Origami Nanostructures in the Presence of Chaotropic Agents. *Nanoscale* **2016**, *8* (19), 10398–10405. https://doi.org/10.1039/c6nr00835f.
(105) Schäfer, K.; Ihmels, H.; Bohne, C.; Valente, K. P.; Granzhan, A. Hydroxybenzo[b]Quinolizinium Ions: Water-Soluble and Solvatochromic Photoacids. *J. Org. Chem.* **2016**, *81* (22), 10942–10954. https://doi.org/10.1021/acs.joc.6b01991.
(106) ChemAxon. Marvin 17.21.0.
(107) Grabowski, Z. R.; Rubaszewska, W. Generalised Förster Cycle. Thermodynamic and Extrathermodynamic Relationships between Proton Transfer, Electron Transfer and Electronic Excitation. *J. Chem. Soc. Faraday Trans. 1 Phys. Chem. Condens. Phases* **1977**, *73*, 11. https://doi.org/10.1039/f19777300011.
(108) Hagihara, S.; Kumasawa, H.; Goto, Y.; Hayashi, G.; Kobori, A.; Saito, I.; Nakatani, K. Detection of Guanine-Adenine Mismatches by Surface Plasmon Resonance Sensor Carrying Naphthyridine-Azaquinolone Hybrid on the Surface. *Nucleic Acids Res.* **2004**, *32* (1), 278–286.

https://doi.org/10.1093/nar/gkh171.
(109) Nakatani, K.; Hagihara, S.; Goto, Y.; Kobori, A.; Hagihara, M.; Hayashi, G.; Kyo, M.; Nomura, M.; Mishima, M.; Kojima, C. Small-Molecule Ligand Induces Nucleotide Flipping in (CAG)n Trinucleotide Repeats. *Nat. Chem. Biol.* **2005**, *1* (1), 39–43. https://doi.org/10.1038/nchembio708.
(110) Stein, G. H. T98G: An Anchorage-independent Human Tumor Cell Line That Exhibits Stationary Phase G1 Arrest in Vitro. *J. Cell. Physiol.* **1979**, *99* (1), 43–54.
(111) Bobola, M. S.; Tseng, S. H.; Blank, A.; Berger, M. S.; Silber, J. Role of O6-Methylguanine-DNA Methyltransferase in Resistance of Human Brain Tumor Cell Lines to the Clinically Relevant Methylating Agents Temozolomide and Streptozotocin. *Clin. Cancer Res.* **1996**, *2* (April), 735–741.
(112) Weller, M.; Rieger, J.; Grimmel, C.; Van Meir, E. G.; De Tribolet, N.; Krajewski, S.; Reed, J. C.; Von Deimling, A.; Dichgans, J. Predicting Chemoresistance in Human Malignant Glioma Cells: The Role of Molecular Genetic Analyses. *Int. J. Cancer* **1998**, *79* (6), 640–644. https://doi.org/10.1002/(SICI)1097-0215(19981218)79:6<640::AID-IJC15>3.0.CO;2-Z.
(113) Hermisson, M.; Klumpp, A.; Wick, W.; Wischhusen, J.; Nagel, G.; Roos, W.; Kaina, B.; Weller, M. O6-Methylguanine DNA Methyltransferase and P53 Status Predict Temozolomide Sensitivity in Human Malignant Glioma Cells. *J. Neurochem.* **2006**, *96* (3), 766–776. https://doi.org/10.1111/j.1471-4159.2005.03583.x.
(114) Barciszewska, A. M.; Gurda, D.; Głodowicz, P.; Nowak, S.; Naskręt-Barciszewska, M. Z. A New Epigenetic Mechanism of Temozolomide Action in Glioma Cells. *PLoS One* **2015**, *10* (8). https://doi.org/10.1371/journal.pone.0136669.
(115) Promega Corporation. CellTiter-Glo® Luminescent Cell Viability Assay. 2016, pp 1–14.
(116) Göbel, A.; Zinna, V. M.; Dell'Endice, S.; Jaschke, N.; Kuhlmann, J. D.; Wimberger, P.; Rachner, T. D. Anti-Tumor Effects of Mevalonate Pathway Inhibition in Ovarian Cancer. *BMC Cancer* **2020**, *20* (1), 1–17. https://doi.org/10.1186/s12885-020-07164-x.
(117) Pan, C. H.; Otsuka, Y.; Sridharan, B. P.; Woo, M.; Leiton, C. V.; Babu, S.; Torrente Gonçalves, M.; Kawalerski, R. R.; Ji, J. D.; Chang, D. K.; et al. An Unbiased High-Throughput Drug Screen Reveals a Potential Therapeutic Vulnerability in the Most Lethal Molecular Subtype of Pancreatic Cancer. *Mol. Oncol.* **2020**, *14* (8), 1800–1816. https://doi.org/10.1002/1878-0261.12743.
(118) Demidenko, E.; Miller, T. W. Statistical Determination of Synergy Based on Bliss Definition of Drugs Independence. *PLoS One* **2019**, *14* (11), 1–22. https://doi.org/10.1371/journal.pone.0224137.
(119) Roell, K. R.; Reif, D. M.; Motsinger-Reif, A. A. An Introduction to Terminology and Methodology of Chemical Synergy-Perspectives from across Disciplines. *Front. Pharmacol.* **2017**, *8* (APR), 1–11. https://doi.org/10.3389/fphar.2017.00158.
(120) Foucquier, J.; Guedj, M. Analysis of Drug Combinations: Current Methodological Landscape. *Pharmacol. Res. Perspect.* **2015**, *3* (3). https://doi.org/10.1002/prp2.149.
(121) Chou, T. C. Theoretical Basis, Experimental Design, and Computerized Simulation of Synergism and Antagonism in Drug Combination Studies. *Pharmacol. Rev.* **2006**, *58* (3), 621–681. https://doi.org/10.1124/pr.58.3.10.
(122) Chou, T. C. Drug Combination Studies and Their Synergy Quantification Using the Chou-Talalay Method. *Cancer Res.* **2010**, *70* (2), 440–446. https://doi.org/10.1158/0008-5472.CAN-09-1947.
(123) Varkuti, B. H.; Liu, Z.; Kepiro, M.; Pacifico, R.; Gai, Y.; Kameneka, T.; Davis, R. L. High-Throughput Small Molecule Screen Identifies Modulators of Mitochondrial Function in Neurons. *iScience* **2020**, *23* (3), 100931. https://doi.org/10.1016/j.isci.2020.100931.
(124) Montague, C. R.; Fitzmaurice, A.; Hover, B. M.; Salazar, N. A.; Fey, J. P. Screen for Small Molecules Increasing the Mitochondrial Membrane Potential. *J. Biomol. Screen.* **2014**, *19* (3), 387–398. https://doi.org/10.1177/1087057113495295.

(125) Sittampalam, G.; Coussens, N.; Arkin, M.; Auld, D.; Austin, C.; Bejcek, B.; Glicksman, M.; Inglese, J.; Iversen, P.; Mcgee, J.; et al. *Assay Guidance Manual*; 2016.
(126) Żyro, D.; Śliwińska, A.; Szymczak-Pajor, I.; Stręk, M.; Ochocki, J. Light Stability, pro-Apoptotic and Genotoxic Properties of Silver (I) Complexes of Metronidazole and 4-Hydroxymethylpyridine against Pancreatic Cancer Cells in Vitro. *Cancers (Basel).* **2020**, *12* (12), 1–17. https://doi.org/10.3390/cancers12123848.
(127) Liang, P.; Shi, H.; Zhu, W.; Gui, Q.; Xu, Y.; Meng, J.; Guo, X.; Gong, Z.; Chen, H. Silver Nanoparticles Enhance the Sensitivity of Temozolomide on Human Glioma Cells. *Oncotarget* **2017**, *8* (5), 7533–7539. https://doi.org/10.18632/oncotarget.13503.
(128) Daina, A.; Michielin, O.; Zoete, V. SwissADME: A Free Web Tool to Evaluate Pharmacokinetics, Drug-Likeness and Medicinal Chemistry Friendliness of Small Molecules. *Sci. Rep.* **2017**, *7* (October 2016), 1–13. https://doi.org/10.1038/srep42717.
(129) Decker, M. *Design of Hybrid Molecules for Drug Development*, First.; Decker, M., Ed.; Elsevier: Amsterdam, Netherlands, 2017.
(130) Saha, T.; Makar, S.; Swetha, R.; Gutti, G.; Singh, S. K. Estrogen Signaling: An Emanating Therapeutic Target for Breast Cancer Treatment. *Eur. J. Med. Chem.* **2019**, *177*, 116–143. https://doi.org/10.1016/j.ejmech.2019.05.023.
(131) Saha, P.; Debnath, C.; Bérubé, G. Steroid-Linked Nitrogen Mustards as Potential Anticancer Therapeutics: A Review. *J. Steroid Biochem. Mol. Biol.* **2013**, *137*, 271–300. https://doi.org/10.1016/j.jsbmb.2013.05.004.
(132) Bello, E.; Taraboletti, G.; Colella, G.; Zucchetti, M.; Forestieri, D.; Licandro, S. A.; Berndt, A.; Richter, P.; D'Incalci, M.; Cavalletti, E.; et al. The Tyrosine Kinase Inhibitor E-3810 Combined with Paclitaxel Inhibits the Growth of Advanced-Stage Triple-Negative Breast Cancer Xenografts. *Mol. Cancer Ther.* **2013**, *12* (2), 131–140. https://doi.org/10.1158/1535-7163.MCT-12-0275-T.
(133) Bold, G.; Schnell, C.; Furet, P.; McSheehy, P.; Brüggen, J.; Mestan, J.; Manley, P. W.; Drückes, P.; Burglin, M.; Dürler, U.; et al. A Novel Potent Oral Series of VEGFR2 Inhibitors Abrogate Tumor Growth by Inhibiting Angiogenesis. *J. Med. Chem.* **2016**, *59* (1), 132–146. https://doi.org/10.1021/acs.jmedchem.5b01582.
(134) Dolly, S. O.; Wagner, A. J.; Bendell, J. C.; Kindler, H. L.; Krug, L. M.; Seiwert, T. Y.; Zauderer, M. G.; Lolkema, M. P.; Apt, D.; Yeh, R. F.; et al. Phase I Study of Apitolisib (GDC-0980), Dual Phosphatidylinositol-3-Kinase and Mammalian Target of Rapamycin Kinase Inhibitor, in Patients with Advanced Solid Tumors. *Clin. Cancer Res.* **2016**, *22* (12), 2874–2884. https://doi.org/10.1158/1078-0432.CCR-15-2225.
(135) Lim, K. M.; Park, Y. H. Development of PAC-14028, a Novel Transient Receptor Potential Vanilloid Type 1 (TRPV1) Channel Antagonist as a New Drug for Refractory Skin Diseases. *Arch. Pharm. Res.* **2012**, *35* (3), 393–396. https://doi.org/10.1007/s12272-012-0321-6.
(136) Dermawan, J. K. T.; Hitomi, M.; Silver, D. J.; Wu, Q.; Sandlesh, P.; Sloan, A. E.; Purmal, A. A.; Gurova, K. V.; Rich, J. N.; Lathia, J. D.; et al. Pharmacological Targeting of the Histone Chaperone Complex FACT Preferentially Eliminates Glioblastoma Stem Cells and Prolongs Survival in Preclinical Models. *Cancer Res.* **2016**, *76* (8), 2432–2442. https://doi.org/10.1158/0008-5472.CAN-15-2162.
(137) Rupp, M.; Mouhri, Z. S.; Williams, C.; Jean-Claude, B. J. Molecular Analysis of the Dual Targeting of the Epidermal Growth Factor Receptor and the O6-Methylguanine-DNA Methyltransferase with a Double Arm Hybrid Molecule. *Oncotarget* **2018**, *9* (80), 35041–35055. https://doi.org/10.18632/oncotarget.25120.
(138) Sun, G.; Zhang, N.; Zhao, L.; Fan, T.; Zhang, S.; Zhong, R. Synthesis and Antitumor Activity Evaluation of a Novel Combi-Nitrosourea Prodrug: Designed to Release a DNA Cross-Linking Agent and an Inhibitor of O6-Alkylguanine-DNA Alkyltransferase. *Bioorganic Med. Chem.* **2016**, *24* (9), 2097–2107. https://doi.org/10.1016/j.bmc.2016.03.041.
(139) Wang, Y.; Ren, T.; Lai, X.; Sun, G.; Zhao, L.; Zhang, N.; Zhong, R. Synthesis and Antitumor

Activity Evaluation of a Novel Combi-Nitrosourea Prodrug: BGCNU. *ACS Med. Chem. Lett.* **2017**, *8* (2), 174–178. https://doi.org/10.1021/acsmedchemlett.6b00358.
(140) Wanner, M. J.; Koch, M.; Koomen, G. J. Synthesis and Antitumor Activity of Methyltriazene Prodrugs Simultaneously Releasing DNA-Methylating Agents and the Antiresistance Drug O 6-Benzylguanine. *J. Med. Chem.* **2004**, *47* (27), 6875–6883. https://doi.org/10.1021/jm049556d.
(141) Palchaudhuri, R.; Hergenrother, P. J. DNA as a Target for Anticancer Compounds: Methods to Determine the Mode of Binding and the Mechanism of Action. *Current Opinion in Biotechnology*. 2007, pp 497–503. https://doi.org/10.1016/j.copbio.2007.09.006.
(142) Ali, A.; Bhattacharya, S. DNA Binders in Clinical Trials and Chemotherapy. *Bioorganic and Medicinal Chemistry*. Elsevier Ltd August 2014, pp 4506–4521. https://doi.org/10.1016/j.bmc.2014.05.030.
(143) Gurova, K. New Hopes from Old Drugs: Revisiting DNA-Binding Small. *Futur. Oncol.* **2010**, *5* (10), 1–28. https://doi.org/10.2217/fon.09.127.New.
(144) Gurova, K. New Hopes from Old Drugs: Revisiting DNA-Binding Small Molecules as Anticancer Agents. *Future Oncology*. December 2009, pp 1685–1704. https://doi.org/10.2217/fon.09.127.
(145) Ehsanian, R.; Van Waes, C.; Feller, S. M. Beyond DNA Binding - A Review of the Potential Mechanisms Mediating Quinacrine's Therapeutic Activities in Parasitic Infections, Inflammation, and Cancers. *Cell Commun. Signal.* **2011**, *9*, 1–18. https://doi.org/10.1186/1478-811X-9-13.
(146) Preet, R.; Mohapatra, P.; Mohanty, S.; Sahu, S. K.; Choudhuri, T.; Wyatt, M. D.; Kundu, C. N. Quinacrine Has Anticancer Activity in Breast Cancer Cells through Inhibition of Topoisomerase Activity. *Int. J. Cancer* **2012**, *130* (7), 1660–1670. https://doi.org/10.1002/ijc.26158.
(147) Oien, D. B.; Pathoulas, C. L.; Ray, U.; Thirusangu, P.; Kalogera, E.; Shridhar, V. Repurposing Quinacrine for Treatment-Refractory Cancer. *Semin. Cancer Biol.* **2021**, *68*, 21–30. https://doi.org/10.1016/j.semcancer.2019.09.021.
(148) Gurova, K. V.; Hill, J. E.; Guo, C.; Prokvolit, A.; Burdelya, L. G.; Samoylova, E.; Khodyakova, A. V.; Ganapathi, R.; Ganapathi, M.; Tararova, N. D.; et al. Small Molecules That Reactivate P53 in Renal Cell Carcinoma Reveal a NF-KB-Dependent Mechanism of P53 Suppression in Tumors. *Proc. Natl. Acad. Sci. U. S. A.* **2005**, *102* (48), 17448–17453. https://doi.org/10.1073/pnas.0508888102.
(149) Guo, C.; Gasparian, A. V.; Zhuang, Z.; Bosykh, D. A.; Komar, A. A.; Gudkov, A. V.; Gurova, K. V. 9-Aminoacridine-Based Anticancer Drugs Target the PI3K/AKT/MTOR, NF-KB and P53 Pathways. *Oncogene* **2009**, *28* (8), 1151–1161. https://doi.org/10.1038/onc.2008.460.
(150) Jani, T. S.; DeVecchio, J.; Mazumdar, T.; Agyeman, A.; Houghton, J. A. Inhibition of NF-KB Signaling by Quinacrine Is Cytotoxic to Human Colon Carcinoma Cell Lines and Is Synergistic in Combination with Tumor Necrosis Factor-Related Apoptosis-Inducing Ligand (TRAIL) or Oxaliplatin. *J. Biol. Chem.* **2010**, *285* (25), 19162–19172. https://doi.org/10.1074/jbc.M109.091645.
(151) Dermawan, J. K. T.; Gurova, K.; Pink, J.; Dowlati, A.; De, S.; Narla, G.; Sharma, N.; Stark, G. R. Quinacrine Overcomes Resistance to Erlotinib by Inhibiting FACT, NF-KB, and Cell-Cycle Progression in Non–Small Cell Lung Cancer. *Mol. Cancer Ther.* **2014**, *13* (9), 2203–2214. https://doi.org/10.1158/1535-7163.MCT-14-0013.
(152) Gasparian, A. V.; Burkhart, C. A.; Purmal, A. A.; Brodsky, L.; Pal, M.; Saranadasa, M.; Bosykh, D. A.; Commane, M.; Guryanova, O. A.; Pal, S.; et al. Curaxins: Anticancer Compounds That Simultaneously Suppress NF- B and Activate P53 by Targeting FACT. *Sci. Transl. Med.* **2011**, *3* (95), 95ra74. https://doi.org/10.1126/scitranslmed.3002530.
(153) Oien, D. B.; Pathoulas, C. L.; Ray, U.; Thirusangu, P.; Kalogera, E.; Shridhar, V. Repurposing Quinacrine for Treatment-Refractory Cancer. *Seminars in Cancer Biology*. Elsevier Ltd January 2021, pp 21–30. https://doi.org/10.1016/j.semcancer.2019.09.021.
(154) Barone, T. A.; Burkhart, C. A.; Safina, A.; Haderski, G.; Gurova, K. V.; Purmal, A. A.; Gudkov, A.

V.; Plunkett, R. J. Anticancer Drug Candidate CBL0137, Which Inhibits Histone Chaperone FACT, Is Efficacious in Preclinical Orthotopic Models of Temozolomide-Responsive and -Resistant Glioblastoma. *Neuro. Oncol.* **2017**, *19* (2), 186–196. https://doi.org/10.1093/neuonc/now141.

(155) Winer, A.; Denlinger, C. S.; Vijayvergia, N.; Cohen, S. J.; Astaturov, I.; Dotan, E.; Gallant, J. N.; Wang, E. W.; Kunkel, M.; Lim, B.; et al. First-in-Human Phase 1b Trial of Quinacrine Plus Capecitabine in Patients With Refractory Metastatic Colorectal Cancer. *Clin. Colorectal Cancer* **2021**, *20* (1), e43–e52. https://doi.org/10.1016/j.clcc.2020.08.003.

(156) Bhateja, P.; Dowlati, A.; Sharma, N. Phase I Study of the Combination of Quinacrine and Erlotinib in Patients with Locally Advanced or Metastatic Non Small Cell Lung Cancer. *Invest. New Drugs* **2018**, *36* (3), 435–441. https://doi.org/10.1007/s10637-017-0515-3.

(157) Prasher, P.; Sharma, M. Medicinal Chemistry of Acridine and Its Analogues. *MedChemComm*. Royal Society of Chemistry 2018, pp 1589–1618. https://doi.org/10.1039/C8MD00384J.

(158) Belmont, P.; Boudali, A.; Constant, J. F.; Demeunynck, M.; Fkyerat, A.; Michon, P.; Serratrice, G.; Lhomme, J. Efficient and Versatile Chemical Tools for Cleavage of Abasic Sites in DNA. *New J. Chem.* **1997**, *21* (1), 47–54.

(159) Dana, S.; Keshri, S. K.; Shukla, J.; Vikramdeo, K. S.; Mondal, N.; Mukhopadhyay, P.; Dhar, S. K. Design, Synthesis and Evaluation of Bifunctional Acridinine Naphthalenediimide Redox-Active Conjugates as Antimalarials. *ACS Omega* **2016**, *1* (3), 318–333. https://doi.org/10.1021/acsomega.6b00060.

(160) Joubert, J. P.; Smit, F. J.; Du Plessis, L.; Smith, P. J.; N'da, D. D. Synthesis and in Vitro Biological Evaluation of Aminoacridines and Artemisinin-Acridine Hybrids. *Eur. J. Pharm. Sci.* **2014**, *56* (1), 16–27. https://doi.org/10.1016/j.ejps.2014.01.014.

(161) Zimmerman, S. C.; Luu, L. M.; Nguyen, L.; Jahromi, A. H.; Miller, K. A.; Fu, Y.; Baranger, A. M. Developing Bivalent Ligands to Target CUG Triplet Repeats, the Causative Agent of Myotonic Dystrophy Type 1. *J. Med. Chem.* **2013**, *56* (23), 9471–9481. https://doi.org/10.1021/jm400794z.

(162) Arambula, J. F.; Ramisetty, S. R.; Baranger, A. M.; Zimmerman, S. C. A Simple Ligand That Selectively Targets CUG Trinucleotide Repeats and Inhibits MBNL Protein Binding. *Proc. Natl. Acad. Sci.* **2009**, *106* (38), 16068–16073. https://doi.org/10.1073/pnas.0901824106.

(163) Jahromi, A. H.; Nguyen, L.; Fu, Y.; Miller, K. A.; Baranger, A. M.; Zimmerman, S. C. A Novel CUGexp·MBNL1 Inhibitor with Therapeutic Potential for Myotonic Dystrophy Type 1. *ACS Chem. Biol.* **2013**, *8* (5), 1037–1043. https://doi.org/10.1021/cb400046u.

(164) Ding, S.; Qiao, X.; Kucera, G. L.; Bierbach, U. Design of a Platinum-Acridine-Endoxifen Conjugate Targeted at Hormone-Dependent Breast Cancer. *Chem. Commun.* **2013**, *49* (24), 2415–2417. https://doi.org/10.1039/c3cc38957j.

(165) Ding, S.; Qiao, X.; Kucera, G. L.; Bierbach, U. Using a Build-and-Click Approach for Producing Structural and Functional Diversity in DNA-Targeted Hybrid Anticancer Agents. *J. Med. Chem.* **2012**, *55* (22), 10198–10203. https://doi.org/10.1021/jm301278c.

(166) Wong, C. H.; Fu, Y.; Ramisetty, S. R.; Baranger, A. M.; Zimmerman, S. C. Selective Inhibition of MBNL1-CCUG Interaction by Small Molecules toward Potential Therapeutic Agents for Myotonic Dystrophy Type 2 (DM2). *Nucleic Acids Res.* **2011**, *39* (20), 8881–8890. https://doi.org/10.1093/nar/gkr415.

(167) Pignataro, L.; Boghi, M.; Civera, M.; Carboni, S.; Piarulli, U.; Gennari, C. Rhodium-Catalyzed Asymmetric Hydrogenation of Olefins with PhthalaPhos, a New Class of Chiral Supramolecular Ligands. *Chem. - A Eur. J.* **2012**, *18* (5), 1383–1400. https://doi.org/10.1002/chem.201102018.

(168) Kumar, P.; Jiang, T.; Li, S.; Zainul, O.; Laughlin, S. T. Caged Cyclopropenes for Controlling Bioorthogonal Reactivity. *Org. Biomol. Chem.* **2018**, *16* (22), 4081–4085. https://doi.org/10.1039/C8OB01076E.

(169) Keppler, A.; Gendreizig, S.; Gronemeyer, T.; Pick, H.; Vogel, H.; Johnsson, K. A General

Method for the Covalent Labeling of Fusion Proteins with Small Molecules in Vivo. *Nat. Biotechnol.* **2003**, *21* (1), 86–89. https://doi.org/10.1038/nbt765.
(170) Ross, S. A.; Pitié, M.; Meunier, B. Synthesis of Two Acridine Conjugates of the Bis(Phenanthroline) Ligand "Clip-Phen" and Evaluation of the Nuclease Activity of the Corresponding Copper Complexes. *Eur. J. Inorg. Chem.* **1999**, No. 3, 557–563. https://doi.org/10.1002/(SICI)1099-0682(199903)1999:3<557::AID-EJIC557>3.0.CO;2-Y.
(171) Ferlin, M. G.; Marzano, C.; Chiarelotto, G.; Baccichetti, F.; Bordin, F. Synthesis and Antiproliferative Activity of Some Variously Substituted Acridine and Azacridine Derivatives. *Eur. J. Med. Chem.* **2000**, *35* (9), 827–837. https://doi.org/10.1016/S0223-5234(00)00170-7.
(172) Zhang, X. X.; Prata, C. A. H.; McIntosh, T. J.; Barthélémy, P.; Grinstaff, M. W. The Effect of Charge-Reversal Amphiphile Spacer Composition on DNA and SiRNA Delivery. *Bioconjug. Chem.* **2010**, *21* (5), 988–993. https://doi.org/10.1021/bc9005464.
(173) Combourieu, B.; Besse, P.; Sancelme, M.; Veschambre, H.; Delort, A. M.; Poupin, P.; Truffaut, N. Morpholine Degradation Pathway of Mycobacterium Aurum MO1: Direct Evidence of Intermediates by in Situ 1H Nuclear Magnetic Resonance. *Appl. Environ. Microbiol.* **1998**, *64* (1), 153–158.
(174) Singla, P.; Dalal, P.; Kaur, M.; Arya, G.; Nimesh, S.; Singh, R.; Salunke, D. B. Bile Acid Oligomers and Their Combination with Antibiotics to Combat Bacterial Infections. *J. Med. Chem.* **2018**, *61* (22), 10265–10275. https://doi.org/10.1021/acs.jmedchem.8b01433.
(175) Surrey, A. R.; Suter, C. M.; Buck, J. S. New Anthelmintics. The Synthesis of Some 9-Hydroxyalkyl- and Dihydroxylalkyl-Aminoalkylaminoacridines. *J. Am. Chem. Soc.* **1952**, *74* (16), 4102–4103. https://doi.org/10.1021/ja01136a041.
(176) Bonse, S.; Santelli-Rouvier, C.; Barbe, J.; Krauth-Siegel, R. L. Inhibition of Trypanosoma Cruzi Trypanothione Reductase by Acridines: Kinetic Studies and Structure-Activity Relationships. *J. Med. Chem.* **1999**, *42* (26), 5448–5454. https://doi.org/10.1021/jm990386s.
(177) Wuts, P. G. M.; Greene, T. W. *Greene's Protective Groups in Organic Synthesis*; John Wiley & Sons, Inc.: Hoboken, NJ, USA, 2006; Vol. 9. https://doi.org/10.1002/0470053488.
(178) Li, H.; Yoo, J. C.; Kim, E.; Hong, J. H. Synthesis of Novel Difluoro-Cyclopropyl Guanine Nucleosides and Their Phosphonate Analogues as Potent Antiviral Agents. *Nucleosides, Nucleotides and Nucleic Acids* **2011**, *30* (11), 945–960. https://doi.org/10.1080/15257770.2011.625374.
(179) Shaw, S. A.; Vokits, B. P.; Dilger, A. K.; Viet, A.; Clark, C. G.; Abell, L. M.; Locke, G. A.; Duke, G.; Kopcho, L. M.; Dongre, A.; et al. Discovery and Structure Activity Relationships of 7-Benzyl Triazolopyridines as Stable, Selective, and Reversible Inhibitors of Myeloperoxidase. *Bioorganic Med. Chem.* **2020**, *28* (22), 115723. https://doi.org/10.1016/j.bmc.2020.115723.
(180) Lukyanenko, N. G.; Kirichenko, T. I.; Scherbakov, S. V. Novel Cryptands Containing Thiourea Units as a Part of the Macrocyclic Framework. *J. Chem. Soc. Perkin 1* **2002**, *2* (21), 2347–2351. https://doi.org/10.1039/b207902j.
(181) Constant, J. F.; Laügaa, P.; Roques, B. P.; Lhommee, J. Heterodimeric Molecules Including Nucleic Acid Bases and 9-Aminoacridine: Spectroscopic Studies, Conformations, and Interactions with DNA. *Biochemistry* **1988**, *27* (11), 3997–4003. https://doi.org/10.1021/bi00411a016.
(182) Bolte, J.; Demuynck, C.; Lhomme, M. F.; Lhomme, J.; Barbet, J.; Roques, B. P. Synthetic Models Related to DNA Intercalating Molecules: Comparison between Quinacrine and Chloroquine in Their Ring-Ring Interaction with Adenine and Thymine. *J. Am. Chem. Soc.* **1982**, *104* (3), 760–765. https://doi.org/10.1021/ja00367a019.
(183) Brouwer, A. M. Standards for Photoluminescence Quantum Yield Measurements in Solution (IUPAC Technical Report). *Pure Appl. Chem.* **2011**, *83* (12), 2213–2228. https://doi.org/10.1351/pac-rep-10-09-31.
(184) Constant, J. F.; Laügaa, P.; Roques, B. P.; Lhommee, J. Heterodimeric Molecules Including Nucleic Acid Bases and 9-Aminoacridine: Spectroscopic Studies, Conformations, and

Interactions with DNA. *Biochemistry* **1988**, *27* (11), 3997–4003. https://doi.org/10.1021/bi00411a016.
(185) Ihmels, H.; Faulhaber, K.; Viola, G.; Schmuck, C. Evaluation of the DNA-Binding Properties of Cationic Dyes by Absorption and Emission Spectroscopy. In *Highlights in Bioorganic Chemistry: Methods and Applications*; Schmuck, C., Wennemers, H., Eds.; Wiley-VCH Verlag GmbH & Co. KGaA: Weinheim, 2004; pp 172–190. https://doi.org/10.1002/3527603727.ch2e.
(186) Eriksson, M.; Nordén, B. Linear and Circular Dichroism of Drug-Nucleic Acid Complexes. *Methods Enzymol.* **2001**, *340* (X), 68–98. https://doi.org/10.1016/S0076-6879(01)40418-6.
(187) Garbett, N. C.; Ragazzon, P. A.; Chaires, J. O. B. Circular Dichroism to Determine Binding Mode and Affinity of Ligand-Dna Interactions. *Nat. Protoc.* **2007**, *2* (12), 3166–3172. https://doi.org/10.1038/nprot.2007.475.
(188) Bolte, J.; Demuynck, C.; Lhomme, M. F.; Lhomme, J.; Barbet, J.; Roques, B. P. Synthetic Models Related to DNA Intercalating Molecules: Comparison between Quinacrine and Chloroquine in Their Ring-Ring Interaction with Adenine and Thymine. *J. Am. Chem. Soc.* **1982**, *104* (3), 760–765. https://doi.org/10.1021/ja00367a019.
(189) Benner, K.; Granzhan, A.; Ihmels, H.; Viola, G. Targeting Abasic Sites in DNA by Aminoalkyl-Substituted Carboxamidoacridizinium Derivatives and Acridizinium-Adenine Conjugates. *European J. Org. Chem.* **2007**, *2007* (28), 4721–4730. https://doi.org/10.1002/ejoc.200700207.
(190) Kreklau, E. L.; Limp-Foster, M.; Liu, N.; Xu, Y.; Kelley, M. R.; Erickson, L. C. A Novel Fluorometric Oligonucleotide Assay to Measure O6-Methylguanine DNA Methyltransferase, Methylpurine DNA Glycosylase, 8-Oxoguanine DNA Glycosylase and Abasic Endonuclease Activities: DNA Repair Status in Human Breast Carcinoma Cells Overexpressing M. *Nucleic Acids Res.* **2001**, *29* (12), 2558–2566. https://doi.org/10.1093/nar/29.12.2558.
(191) Qi, Q.; He, K.; Yoo, M. H.; Chan, C. B.; Liu, X.; Zhang, Z.; Olson, J. J.; Xiao, G.; Wang, L.; Mao, H.; et al. Acridine Yellow G Blocks Glioblastoma Growth via Dual Inhibition of Epidermal Growth Factor Receptor and Protein Kinase C Kinases. *J. Biol. Chem.* **2012**, *287* (9), 6113–6127. https://doi.org/10.1074/jbc.M111.293605.
(192) McGovern, S. L.; Helfand, B. T.; Feng, B.; Shoichet, B. K. A Specific Mechanism of Nonspecific Inhibition. *J. Med. Chem.* **2003**, *46* (20), 4265–4272. https://doi.org/10.1021/jm030266r.
(193) Pegg, A. E.; Chung, L.; Moschel, R. C. Effect of DNA on the Inactivation of O6-Alkylguanine-DNA Alkyltransferase by 9-Substituted O6-Benzylguanine Derivatives. *Biochem. Pharmacol.* **1997**, *53* (10), 1559–1564. https://doi.org/10.1016/S0006-2952(97)00060-9.
(194) Chakravarty, M.; Ganguli, P.; Murahari, M.; Sarkar, R. R.; Peters, G. J.; Mayur, Y. C. Study of Combinatorial Drug Synergy of Novel Acridone Derivatives With Temozolomide Using In-Silico and in-Vitro Methods in the Treatment of Drug-Resistant Glioma. *Front. Oncol.* **2021**, *11* (March), 1–19. https://doi.org/10.3389/fonc.2021.625899.
(195) Melikishvili, M.; Rodgers, D. W.; Fried, M. G. 6-Carboxyfluorescein and Structurally Similar Molecules Inhibit DNA Binding and Repair by O 6-Alkylguanine DNA Alkyltransferase. *DNA Repair (Amst).* **2011**, *10* (12), 1193–1202. https://doi.org/10.1016/j.dnarep.2011.09.007.
(196) Bhaduri, S.; Ranjan, N.; Arya, D. P. An Overview of Recent Advances in Duplex DNA Recognition by Small Molecules. *Beilstein J. Org. Chem.* **2018**, *14*, 1051–1086. https://doi.org/10.3762/bjoc.14.93.
(197) Richards, R.; Schwartz, H. R.; Honeywell, M. E.; Stewart, M. S.; Cruz-Gordillo, P.; Joyce, A. J.; Landry, B. D.; Lee, M. J. Drug Antagonism and Single-Agent Dominance Result from Differences in Death Kinetics. *Nat. Chem. Biol.* **2020**, *16* (7), 791–800. https://doi.org/10.1038/s41589-020-0510-4.
(198) Escher, B. I.; Henneberger, L.; König, M.; Schlichting, R.; Fischer, F. C. Cytotoxicity Burst? Differentiating Specific from Nonspecific Effects in Tox21 in Vitro Reporter Gene Assays. *Environ. Health Perspect.* **2020**, *128* (7), 077007. https://doi.org/10.1289/EHP6664.
(199) Felip-León, C.; Martínez-Arroyo, O.; Díaz-Oltra, S.; Miravet, J. F.; Apostolova, N.; Galindo, F.

Synthesis, Spectroscopic Studies and Biological Evaluation of Acridine Derivatives: The Role of Aggregation on the Photodynamic Efficiency. *Bioorg. Med. Chem. Lett.* **2018**, *28* (5), 869–874. https://doi.org/10.1016/j.bmcl.2018.02.005.

(200) Beharry, A. A.; Nagel, Z. D.; Samson, L. D.; Kool, E. T. K. Fluorogenic Real-Time Reporters of DNA Repair by MGMT, a Clinical Predictor of Antitumor Drug Response. *PLoS One* **2016**, *11* (4), 1–15. https://doi.org/10.1371/journal.pone.0152684.

(201) Belanich, M.; Randall, T.; Pastor, M. A.; Kibitel, J. T.; Alas, L. G.; Dolan, M. E.; Schold, S. C.; Gander, M.; Lejeune, F. J.; Li, B. F. L.; et al. Intracellular Localization and Intercellular Heterogeneity of the Human DNA Repair Protein O6-Methylguanine-DNA Methyltransferase. *Cancer Chemother. Pharmacol.* **1996**, *37* (6), 547–555. https://doi.org/10.1007/s002800050427.

(202) Bonner, W. M.; Redon, C. E.; Dickey, J. S.; Nakamura, A. J.; Sedelnikova, O. A.; Solier, S.; Pommier, Y. ΓH2AX and Cancer. *Nat. Rev. Cancer* **2008**, *8* (12), 957–967. https://doi.org/10.1038/nrc2523.

(203) Jackson, C. B.; Noorbakhsh, S. I.; Sundaram, R. K.; Kalathil, A. N.; Ganesa, S.; Jia, L.; Breslin, H.; Burgenske, D. M.; Gilad, O.; Sarkaria, J. N.; et al. Temozolomide Sensitizes MGMT-Deficient Tumor Cells to ATR Inhibitors. *Cancer Res.* **2019**, *79* (17), 4331–4338. https://doi.org/10.1158/0008-5472.CAN-18-3394.

(204) Yang, Z.; Wei, D.; Dai, X.; Stevens, M. F. G.; Bradshaw, T. D.; Luo, Y.; Zhang, J. C8-Substituted Imidazotetrazine Analogs Overcome Temozolomide Resistance by Inducing DNA Adducts and DNA Damage. *Front. Oncol.* **2019**, *9* (JUN), 485. https://doi.org/10.3389/fonc.2019.00485.

(205) Sato, Y.; Kurose, A.; Ogawa, A.; Ogasawara, K.; Traganos, F.; Darzynkiewicz, Z.; Sawai, T. Diversity of DNA Damage Response of Astrocytes and Glioblastoma Cell Lines with Various P53 Status to Treatment with Etoposide and Temozolomide. *Cancer Biol. Ther.* **2009**, *8* (5), 452–457. https://doi.org/10.4161/cbt.8.5.7740.

(206) Promega Corporation. *Caspase-Glo ® 3/7 Assay*; 2015.

(207) Xu, T.; Niu, C.; Zhang, X.; Dong, M. β-Ecdysterone Protects SH-SY5Y Cells against β-Amyloid-Induced Apoptosis via c-Jun N-Terminal Kinase-and Akt-Associated Complementary Pathways. *Lab. Investig.* **2018**, *98* (4), 489–499. https://doi.org/10.1038/s41374-017-0009-0.

(208) Johannessen, T.; Hasan-Olive, M. M.; Zhu, H.; Denisova, O.; Grudic, A.; Latif, M. A.; Saed, H.; Varughese, J. K.; Røsland, G. V.; Yang, N.; et al. Thioridazine Inhibits Autophagy and Sensitizes Glioblastoma Cells to Temozolomide. *Int. J. Cancer* **2019**, *144* (7), 1735–1745. https://doi.org/10.1002/ijc.31912.

(209) Daina, A.; Michielin, O.; Zoete, V. SwissADME: A Free Web Tool to Evaluate Pharmacokinetics, Drug-Likeness and Medicinal Chemistry Friendliness of Small Molecules. *Sci. Rep.* **2017**, *7* (March), 1–13. https://doi.org/10.1038/srep42717.

(210) Liu, H.; Wang, L.; Lv, M.; Pei, R.; Li, P.; Pei, Z.; Wang, Y.; Su, W.; Xie, X.-Q. AlzPlatform: An Alzheimer's Disease Domain-Specific Chemogenomics Knowledgebase for Polypharmacology and Target Identification Research. *J. Chem. Inf. Model.* **2014**, *54* (4), 1050–1060. https://doi.org/10.1021/ci500004h.

(211) Arvanitis, C. D.; Ferraro, G. B.; Jain, R. K. The Blood–Brain Barrier and Blood–Tumour Barrier in Brain Tumours and Metastases. *Nat. Rev. Cancer* **2020**, *20* (1), 26–41. https://doi.org/10.1038/s41568-019-0205-x.

(212) Belykh, E.; Shaffer, K. V.; Lin, C.; Byvaltsev, V. A.; Preul, M. C.; Chen, L. Blood-Brain Barrier, Blood-Brain Tumor Barrier, and Fluorescence-Guided Neurosurgical Oncology: Delivering Optical Labels to Brain Tumors. *Front. Oncol.* **2020**, *10* (June), 1–27. https://doi.org/10.3389/fonc.2020.00739.

(213) Silva, J. M.; Silva, E.; Reis, R. L. Light-Triggered Release of Photocaged Therapeutics - Where Are We Now? *J. Control. Release* **2019**, *298* (October 2018), 154–176. https://doi.org/10.1016/j.jconrel.2019.02.006.

(214) Klán, P.; Šolomek, T.; Bochet, C. G.; Blanc, A.; Givens, R.; Rubina, M.; Popik, V.; Kostikov, A.;

Wirz, J. Photoremovable Protecting Groups in Chemistry and Biology: Reaction Mechanisms and Efficacy. *Chem. Rev.* **2013**, *113* (1), 119–191. https://doi.org/10.1021/cr300177k.
(215) Mayer, G.; Hechel, A. Biologically Active Molecules with a "Light Switch." *Angew. Chemie - Int. Ed.* **2006**, *45* (30), 4900–4921. https://doi.org/10.1002/anie.200600387.
(216) Banala, S.; Maurel, D.; Manley, S.; Johnsson, K. A Caged, Localizable Rhodamine Derivative for Superresolution Microscopy. *ACS Chem. Biol.* **2012**, *7* (2), 289–293. https://doi.org/10.1021/cb2002889.
(217) Maurel, D.; Banala, S.; Laroche, T.; Johnsson, K. Photoactivatable and Photoconvertible Fluorescent Probes for Protein Labeling. *ACS Chem. Biol.* **2010**, *5* (5), 507–516. https://doi.org/10.1021/cb1000229.
(218) Fan, N. C.; Cheng, F. Y.; Ho, J. A. A.; Yeh, C. S. Photocontrolled Targeted Drug Delivery: Photocaged Biologically Active Folic Acid as a Light-Responsive Tumor-Targeting Molecule. *Angew. Chemie - Int. Ed.* **2012**, *51* (35), 8806–8810. https://doi.org/10.1002/anie.201203339.
(219) Horbert, R.; Pinchuk, B.; Davies, P.; Alessi, D.; Peifer, C. Photoactivatable Prodrugs of Antimelanoma Agent Vemurafenib. *ACS Chem. Biol.* **2015**, *10* (9), 2099–2107. https://doi.org/10.1021/acschembio.5b00174.
(220) Shin, W. S.; Han, J.; Kumar, R.; Lee, G. G.; Sessler, J. L.; Kim, J. H.; Kim, J. S. Programmed Activation of Cancer Cell Apoptosis: A Tumor-Targeted Phototherapeutic Topoisomerase I Inhibitor. *Sci. Rep.* **2016**, *6* (April), 1–11. https://doi.org/10.1038/srep29018.
(221) Döbber, A.; Phoa, A. F.; Abbassi, R. H.; Stringer, B. W.; Day, B. W.; Johns, T. G.; Abadleh, M.; Peifer, C.; Munoz, L. Development and Biological Evaluation of a Photoactivatable Small Molecule Microtubule-Targeting Agent. *ACS Med. Chem. Lett.* **2017**, *8* (4), 395–400. https://doi.org/10.1021/acsmedchemlett.6b00483.
(222) Banala, S.; Arnold, A.; Johnsson, K. Caged Substrates for Protein Labeling and Immobilization. *ChemBioChem* **2008**, *9* (1), 38–41. https://doi.org/10.1002/cbic.200700472.
(223) Hanswillemenke, A.; Stafforst, T. *Protocols for the Generation of Caged GuideRNAs for Light-Triggered RNA-Targeting with SNAP-ADARs*, 1st ed.; Elsevier Inc., 2019; Vol. 624. https://doi.org/10.1016/bs.mie.2019.06.004.
(224) Hanswillemenke, A.; Kuzdere, T.; Vogel, P.; Jékely, G.; Stafforst, T. Site-Directed RNA Editing in Vivo Can Be Triggered by the Light-Driven Assembly of an Artificial Riboprotein. *J. Am. Chem. Soc.* **2015**, *137* (50), 15875–15881. https://doi.org/10.1021/jacs.5b10216.
(225) Bodagh, R. Activatable Probes for Anti-Cancer Therapy, University of Toronto, 2019.
(226) Liu, E. K.; Sulman, E. P.; Wen, P. Y.; Kurz, S. C. Novel Therapies for Glioblastoma. *Curr. Neurol. Neurosci. Rep.* **2020**, *20* (7). https://doi.org/10.1007/s11910-020-01042-6.
(227) Wilson, D. L.; Kool, E. T. Ultrafast Oxime Formation Enables Efficient Fluorescence Light-up Measurement of DNA Base Excision. *J. Am. Chem. Soc.* **2019**, jacs.9b09812. https://doi.org/10.1021/jacs.9b09812.
(228) Chen, F.; Song, K. S.; Wu, Y. D.; Yang, D. Synthesis and Conformational Studies of γ-Aminoxy Peptides. *J. Am. Chem. Soc.* **2008**, *130* (2), 743–755. https://doi.org/10.1021/ja0772750.
(229) Turner, J. A. Regiospecific Electrophilic Substitution of Aminopyridines: Ortho Lithiation of 2-, 3-, and 4-(Pivaloylamino)Pyridines. *J. Org. Chem.* **1983**, *48* (20), 3401–3408. https://doi.org/10.1021/jo00168a007.
(230) Moriya, M.; Kishino, H.; Sakuraba, S.; Sakamoto, T.; Suga, T.; Takahashi, H.; Suzuki, T.; Ito, M.; Ito, J.; Moriya, R.; et al. Identification of 2-Aminobenzimidazoles as Potent Melanin-Concentrating Hormone 1-Receptor (MCH1R) Antagonists. *Bioorganic Med. Chem. Lett.* **2009**, *19* (13), 3568–3572. https://doi.org/10.1016/j.bmcl.2009.04.147.
(231) Kompella, A.; Gampa, V. K.; Ganganamoni, S.; Sirigireddy, B. R.; ADIBHATLA, K. S. B. R.; Nannapaneni, V. C. WO2015/186137, 2015.
(232) Bahman Jahromi, E.; Mehranpour, A. A Novel Synthesis of New 1,8-Naphthyridine Derivatives Using the Reaction of Vinamidinium Salts With 2,6-Diaminopyridine. *J. Heterocycl. Chem.* **2017**, *54* (2), 1210–1214. https://doi.org/10.1002/jhet.2694.

(233) Qian, C. G.; Zhu, S.; Feng, P. J.; Chen, Y. L.; Yu, J. C.; Tang, X.; Liu, Y.; Shen, Q. D. Conjugated Polymer Nanoparticles for Fluorescence Imaging and Sensing of Neurotransmitter Dopamine in Living Cells and the Brains of Zebrafish Larvae. *ACS Appl. Mater. Interfaces* **2015**, *7* (33), 18581–18589. https://doi.org/10.1021/acsami.5b04987.

(234) Murata, T.; Saito, G.; Nakamura, K.; Maesato, M.; Hiramatsu, T.; Yoshida, Y. Exploration of Charge-Transfer Solids Utilizing Nucleobases: Nanoarchitectures by Hydrogen-Bonds in the Ionic Assemblies of Guanine and TCNQ Derivatives. *Cryst. Growth Des.* **2013**, *13* (7), 2778–2792. https://doi.org/10.1021/cg400059h.

(235) McComas, W.; Kyungjin, K. Chemoselective High-Throughput Purification Mediated by Solid-Supported Reagents Its Application to the First 6,9-Disubstituted Purine Library Synthesis. *Combinatorial Chemistry & High Throughput Screening*. 2000, pp 125–129. https://doi.org/http://dx.doi.org/10.2174/1386207003331779.

(236) Hockemeyer, J.; Burbiel, J. C.; Müller, C. E. Multigram-Scale Syntheses, Stability, and Photoreactions of A2A Adenosine Receptor Antagonists with 8-Styrylxanthine Structure: Potential Drugs for Parkinson's Disease. *J. Org. Chem.* **2004**, *69* (10), 3308–3318. https://doi.org/10.1021/jo0358574.

(237) Ward, C. C.; Kleinman, J. I.; Brittain, S. M.; Lee, P. S.; Chung, C. Y. S.; Kim, K.; Petri, Y.; Thomas, J. R.; Tallarico, J. A.; McKenna, J. M.; et al. Covalent Ligand Screening Uncovers a RNF4 E3 Ligase Recruiter for Targeted Protein Degradation Applications. *ACS Chem. Biol.* **2019**, *14* (11), 2430–2440. https://doi.org/10.1021/acschembio.8b01083.

(238) Batesky, D. C.; Goldfogel, M. J.; Weix, D. J. Removal of Triphenylphosphine Oxide by Precipitation with Zinc Chloride in Polar Solvents. *J. Org. Chem.* **2017**, *82* (19), 9931–9936. https://doi.org/10.1021/acs.joc.7b00459.

(239) HORIBA Jobin Yvon. A Guide to Recording Fluorescence Quantum Yields http://www.horiba.com/fileadmin/uploads/Scientific/Documents/Fluorescence/quantumyieldstrad.pdf (accessed Apr 18, 2020).

(240) Chan, C. L.; Wu, Z. N.; Ciardelli, T.; Eastman, A.; Bresnick, E. Kinetic and DNA-Binding Properties of Recombinant Human O6-Methylguanine-DNA Methyltransferase. *Arch. Biochem. Biophys.* **1993**, *300* (1), 193–200. https://doi.org/10.1006/abbi.1993.1027.

(241) Nagel, Z. D.; Beharry, A. A.; Mazzucato, P.; Kitange, G. J.; Sarkaria, J. N.; Kool, E. T.; Samson, L. D. Fluorescent Reporter Assays Provide Direct, Accurate, Quantitative Measurements of MGMT Status in Human Cells. *PLoS One* **2019**, *14* (2), 1–13. https://doi.org/10.1371/journal.pone.0208341.

(242) Kreklau, E. L.; Limp-Foster, M.; Liu, N.; Xu, Y.; Kelley, M. R.; Erickson, L. C. A Novel Fluorometric Oligonucleotide Assay to Measure O(6)-Methylguanine DNA Methyltransferase, Methylpurine DNA Glycosylase, 8-Oxoguanine DNA Glycosylase and Abasic Endonuclease Activities: DNA Repair Status in Human Breast Carcinoma Cells Overexpressin. *Nucleic Acids Res* **2001**, *29* (12), 2558–2566. https://doi.org/10.1093/nar/29.12.2558.